Decoding the metabolic mechanism of L-glyceraldehyde as an anti-cancer therapeutic

Inaugural-Dissertation

to obtain the academic degree

Doctor rerum naturalium (Dr. rer. nat.)

submitted to the

Department of Biology, Chemistry, Pharmacy

of

Freie Universität Berlin

by

MARTIN ROBERT FORBES

Berlin, 2021

This thesis was carried out under the supervision of Dr. Stefan Kempa from December 2016 until February 2021 at the Max Delbrück Zentrum für Molekulare Medizin, Berlin, Germany.

1st Reviewer: Dr. Stefan Kempa

2nd Reviewer: Prof. Dr. Oliver Daumke

Date of Disputation: 30.04.2021

Summary

Glyceraldehyde (GA) is a 3-carbon monosaccharide that is present in cells as byproduct of fructose metabolism. The phosphorylated form, glyceraldehyde-3-phosphate is a key metabolite in central carbon metabolism. Bruno Mendel and Otto Warburg proved that the application of glyceraldehyde to cancer cells inhibits glycolysis and their growth. This phenomenon was extensively studied up until the 1970's. The consensus reached was that the L-isomer of glyceraldehyde is a more effective glycolytic inhibitor than the D-isomer. However, the mechanism by which this occurred was not clarified.

This thesis describes a novel mechanism by which L-GA inhibits cancer cell growth. The work describes how L-GA induces significant changes in the metabolic profile and hinders nucleotide biosynthesis. Gas chromatography–mass spectrometry and ^{13}C-labelling was employed to measure the flow of carbon through glycolytic intermediates under L-GA treatment. The data in this thesis recapitulated previous research on the inhibitory efficacy of L-GA and D-GA. It was found that L-GA is a more potent inhibitor of glycolysis due to its targeting of NADH-dependent reactions, leading to a redox crisis in the cancer cell. Through proteomics analysis it was confirmed that redox mechanisms were modulated via L-GA. This elucidated a specific subset of proteins harbouring oxidoreductase and anti-oxidant activity. Further bioinformatic and molecular biology analysis suggested that the generation of reactive oxygen species via L-GA activates the KEAP1-NRF2 pathway, to drive the expression of anti-oxidant proteins.

Analysis of nucleotide pools in L-GA treated cells depicted a remarkable and previously unreported phenotype. Nucleotide biosynthesis in neuroblastoma cells is significantly inhibited upon L-GA treatment, yet the D-isomer showed minimal inhibition. Critically, this evidence could be linked to findings in the proteome and metabolome. Through the application of the antioxidant N-acetyl-cysteine in conjunction with L-GA, inhibition was relieved. This work presents significant novel evidence for the mechanism of L-GA action in neuroblastoma cells. Specifically, a simple sugar that inhibits the growth of cancer via dysregulating the fragile homeostatic environment inherent to the nature of the cancerous cell.

Zusammenfassung

Glyzerinaldehyd (GA) ist ein Dreifachzucker und entsteht als Nebenprodukt im zellulären Fruktosestoffwechsel. Die phosphorylierte Form, Glyzerinaldehyd-3-Phosphat, ist ein zentraler Metabolit in der Glykolyse. Bruno Mendel und Otto Warburg konnten nachweisen, dass Glyzerinaldehyd das Wachstum und die Glykolyse in Krebszellen hemmen kann. Forschungen zu dieser Fragestellung gab es bis in die 70er Jahre des 20. Jahrhunderts. Es konnte zweifelsfrei nachgewiesen werden, dass die L-Konformation des Glyzerinaldehyds den Stoffwechsel und das Wachstum von Krebszellen effektiver inhibiert als die D-Konformation, die Gründe hierfür blieben aber unaufgeklärt.

Im Rahmen dieser Arbeit wird ein neuer Mechanismus beschrieben, auf welche Weise L-Glyzerinaldehyd (L-GA) das Wachstum von Krebszellen inhibiert. Die Arbeit beschreibt, wie L-GA signifikante Änderungen im zellulären Stoffwechsel herbeiführt und die Nukleotidbiosynthese beeinflusst. Mittels GC-MS basierten Isotopen-unterstützten Stoffwechselanalysen konnten die Änderungen des Kohlenstoffflusses in der Glykolyse bestimmt werden. Die Daten, welche in dieser Arbeit gezeigt werden, spiegeln bisher veröffentlichte Daten über die Wirkung von L-GA wider. Weiterführend wurde gezeigt, dass L-GA ein stärkerer Inhibitor der Glykolyse ist als D-GA, weil ein dominanter Einfluss auf NADH abhängige Reaktionen vorliegt. Schließlich wird eine Änderung des zellulären RedOx Zustandes in der Zelle provoziert. Dies konnte mit Hilfe von ungerichteten Proteomanalysen bestätigt werden. Weitergehende bioinformatische und molekularbiologische Analysen deuten darauf hin, dass die Entstehung von freien Radikalen durch L-GA Behandlung den KEAP1-NRF2 Signalweg beeinflusst.

Die Analyse der zellulären Nukleotidmengen unter L-GA Behandlung zeigte bemerkenswerte und bis dahin unbekannte Änderungen des Nukleotidstoffwechsels. Die Neusynthese von Nukleotiden wird durch Behandlung mit L-GA stark inhibiert. D-GA provozierte dem gegenüber nur eine mäßige Veränderung in den Nukleotidmengen. Das konnte durch die gefundenen Änderungen im Metabolome und Proteom bestätigt werden.

In dieser Arbeit werden neue Aspekte der Wirkweise von L-GA in Neuroblastomzellen aufgezeigt. Letztendlich kann ein einfacher Zucker das Wachstum von Krebszellen vermindern, indem das fragile zelluläre Gleichgewicht von Krebszellen gezielt gestört wird.

Acknowledgements

Education is not trivial. I consider myself unbelievably fortunate to be in a position to realise that this statement is true. This thesis is in fact the culmination of many years of guidance, support, error and trial. Those who have educated and supported me are just as much an author of this thesis as I am.

Imogen and Ross Forbes deserve the highest of credit in raising a mind, indeed three minds, which have the resources to do things that lads from Stanley weren't expected to do. The environment that was created by Imogen and Ross has had a wide and significant influence on the young minds that were faced with a challenging path. This may only be a thesis, but I hope it is realised that all of the support that the Forbes family have provided, has been worth it.

Families are a curious construct. You can't choose them but they can be created at unlikely and unexpected times. One may compare this to a working environment. Science requires patience, understanding, teamwork and the occasional argument to develop ideas. Working in the Kempa lab has provided all of these qualities. I am very grateful to all of the team for their continued friendship and unity in attempting to answer extremely complex questions. Particular gratitude must go to Jenny Grobe. Without Jenny the Kempa lab would not function. Jenny, I apologise for all the times I have made life more difficult than it needs to be. Safak has been a great friend and I have had the best of times working with her. Thank you Safak for all the help you have given me, particularly the many arduous pSIRMs. Similarly, Guido has been a constant source of information, help with protocols and great Italian coffee. Thank you for all the advice and keeping my brain on its toes. I certainly owe you a whisky, or two. To Sabrina and Guido, thank you both for reading over my thesis and giving great feedback. Many thanks must go to Matthias, for the help with the metabolomics analysis and helping me make sense of it all. I have also had the fortune of working with two great students, Richard and Jonas, both of whom I wish all the best for the future. I would also like to acknowledge and thank previous lab mates for their support and advice: Birte, Christin, Fardad and Nadine. To all lab members past or present, I hope that I can work with people like you for the rest of my scientific career.

Dr. Stefan Kempa has been a great mentor, I feel very fortunate to have been given the opportunity to research this PhD in his lab. On many occasions Stefan has given me confidence in this work, when I had lost all of it. The conversations, scientific or political, have always been enlightening and often full of humour. Thank you for taking the chance on me and your continued support over the past 4 years. I would also like to thank PD Dr. med. Hedwig Deubzer and Prof. Dr. Oliver Daumke for their support and supervision in this work.

There have been many great times but also incredible stressful times during the writing of this thesis. This makes one difficult to be around and to manage. Céline, you have been a rock and I owe you an enormous amount for all the love and support you have given. Thank you will never be enough.

"Nature's imagination is so much greater than man's, she's never going to let us relax"
Richard Feynman

Contents

List of figures **iii**

List of tables **v**

List of Abbreviations **vi**

1 Introduction **1**
1.1 An introduction to glyceraldehyde as a cancer therapeutic . . . 1
1.2 The origins and development of cancer . . . 2
1.3 Metabolism in Cancer . . . 3
1.3.1 Overview: Glycolysis . . . 4
1.3.2 Overview: The TCA cycle and Glutamine Metabolism . . . 5
1.3.3 Nucleotide Metabolism . . . 6
1.4 Metabolic reprogramming in cancer . . . 8
1.5 Maintaining Cellular Homeostasis . . . 10
1.5.1 The generation and function of ROS in cancer . . . 10
1.5.2 Mechanisms of ROS regulation and cell fate . . . 12
1.5.3 Targeting mechanisms of ROS reduction for cancer therapy . . . 13
1.6 Metabolism as a therapeutic target . . . 13
1.6.1 Glyceraldehyde . . . 14
1.6.2 2-D-deoxyglucose . . . 15
1.6.3 3-Bromopyruvate . . . 16
1.6.4 Oxythiamine . . . 16
1.7 Methods for measuring metabolism . . . 16
1.7.1 GC-MS and Time-resolved metabolomics . . . 17
1.7.2 LC-MS and DI-MS-MS in proteomic and nucleotide analysis . . . 18
1.8 Neuroblastoma . . . 19
1.9 Objectives of the thesis . . . 20

2 Materials **21**
2.1 Cellular biology methods . . . 21
2.1.1 Cell lines and Cell Culture . . . 21
2.1.2 Cell freezing and thawing . . . 21
2.1.3 Cell number determination and harvesting . . . 22
2.1.4 Cell staining and imaging . . . 22
2.1.5 Cell Cycle Analysis . . . 22

2.1.6 iCelligence cell growth analysis . . . 23
2.1.7 Reactive oxygen species quantification . . . 23
2.2 Biochemical methods . . . 23
2.2.1 Preparation of whole cell lysates . . . 23
2.2.2 Quantification of proteins . . . 24
2.2.3 SDS-PAGE . . . 24
2.2.4 Western blot . . . 24
2.3 Proteomics . . . 25
2.3.1 Sample preparation of protein lysates and digests . . . 25
2.3.2 Analysis of peptides via liquid-chromatography mass spectrometry (LC-MS) . . . 25
2.3.3 Data analysis of LC-MS derived proteomics data . . . 26
2.4 Metabolomic analysis . . . 26
2.4.1 Cell culture for pSIRM analysis . . . 26
2.4.2 Extraction of metabolites . . . 27
2.4.3 Measurements of metabolites via GC-MS . . . 27
Sample preparation for GC-MS . . . 27
GC-MS measurements . . . 27
Analysis of GC-MS data . . . 27
2.5 Measurement of nucleotides via DI-MS-MS . . . 28
2.5.1 Sample preparation for DI-MS-MS . . . 28
2.5.2 DI-MS-MS acquisition . . . 28
2.5.3 Analysis of direct infusion MS data . . . 28
2.6 Statistics . . . 29

3 Results **30**
3.1 Glyceraldehyde Inhibits the Growth of Neuroblastoma Cells . . . 30
3.1.1 L-GA inhibits neuroblastoma cell growth in a concentration dependent manner . . . 30
3.1.2 L-GA is a fast acting and potent inhibitor of neuroblastoma cell proliferation . . . 32
3.1.3 L-GA is a more potent inhibitor of neuroblastoma cell growth than D-GA 34
3.2 L-GA causes morphological and cytoskeletal aberrations . . . 35
3.2.1 Actin polymerisation is dysregulated upon L-GA treatment . . . 35
3.3 L-GA causes cell cycle arrest . . . 38
3.3.1 Cell cycle arrest is a common phenotype in L-GA treated cells . . . 38
3.4 Glyceraldehyde causes a depletion of nucleotide pools . . . 40
3.4.1 L-GA depletes nucleotide pools following 24 hrs incubation . . . 40
3.4.2 Nucleotide depletion in neuroblastoma cells is dependent on the concentration of L-GA . . . 44
3.4.3 L-GA induces stress on redox co-factors and reduces the phosphorylation potential of neuroblastoma cells . . . 46
3.4.4 L-GA causes rapid depletion of nucleotides . . . 48

3.4.5 L-GA is a more potent inhibitor of nucleotide synthesis than D-GA or DL-GA in neuroblastoma cells . . . 49
3.4.6 Alternate modes of glycolytic inhibition is not as effective as L-GA at depleting nucleotide pools . . . 50
3.5 Glyceraldehyde inhibits glycolysis and induces metabolic reprogramming in neuroblastoma cells . . . 52
3.5.1 L-GA and D-GA inhibit glycolysis downstream of aldolase . . . 52
3.5.2 L-GA causes a metabolic switch to glutaminolysis . . . 59
3.6 Proteomic Analysis of L-GA treated Cells . . . 62
3.7 L-GA induces oxidative stress in neuroblastoma cells . . . 66
3.7.1 L-GA induces oxidative stress . . . 67
3.7.2 L-GA induces the NRF2 pathway which is rescued by NAC . . . 68
3.7.3 Cell growth is partially restored by NAC in L-GA treated cells . . . 70
3.7.4 Oxidative stress reduces nucleotide pools which is rescued via NAC . . . 71
3.7.5 NAC restores metabolic function of L-GA treated cells . . . 73
3.7.6 Serine and Glycine metabolism is not affected by L-GA . . . 75

4 Discussion **78**
4.1 Growth inhibition and cell cycle arrest . . . 78
4.1.1 Neuroblastoma cells produce a heterogeneous cell cycle response to L-GA 79
4.2 L-GA targets nucleotide biosynthesis causing severe depletion of pools . . . 81
4.2.1 L-GA targets specific nucleotide intermediates . . . 83
4.3 The impact of L-GA on the metabolic profile of neuroblastoma cells . . . 84
4.3.1 L-GA targets NAD+/NADH cycling . . . 84
4.3.2 L-GA induces increased glutaminolysis . . . 86
4.4 L-GA induces perturbations in the proteome . . . 87
4.4.1 Up-regulation of the oxidoreductase enzyme class . . . 87
4.4.2 Apoptotic signalling pathways are initiated in response to L-GA . . . 88
4.4.3 Cell cycle specific proteins correlate to cell cycle analysis . . . 88
4.5 Oxidative stress is a hallmark of L-GA treatment . . . 89
4.5.1 Nucleotide biosynthesis is a ROS sensitive process . . . 89
4.5.2 Application of NAC restores NAD+/NADH cycling inhibited by L-GA . 91
4.5.3 The fate of glyceraldehyde . . . 92
4.6 Conclusions and limitations . . . 92
4.6.1 Outlook . . . 95

5 Supplementary Data **112**
5.1 Materials . . . 112
5.1.1 Nucleotides . . . 115
5.1.2 Metabolomics . . . 117
5.2 Additional results . . . 119
5.2.1 Cell biology and Western blotting . . . 119
5.2.2 Metabolomics . . . 120
5.2.3 Proteomics . . . 123

List of Figures

1.1 Central carbon metabolism - Central Carbon Metabolism - Glycolysis and the TCA cycle . . . 5
1.2 Pathways of nucleotide metabolism . . . 7
1.3 The role of increasing ROS levels in cells . . . 11
1.4 Regulators of glycolysis . . . 14
1.5 Pulsed stable isotope resolved metabolomics . . . 18

3.1 Inhibition of neuroblastoma cell growth is dependent on L-GA concentration . . . 31
3.2 L-GA causes detachment of neuroblastoma cells from plates and causes morphological changes in VH-7 cells. . . . 32
3.3 L-Glyceraldehyde is a Fast Acting Growth Inhibitor . . . 33
3.4 Inhibition of neuroblastoma cell growth by glyceraldehyde enantiomers . . . 35
3.5 L-GA causes dysregulation of actin polymerisation . . . 37
3.6 L-GA causes cell cycle arrest in neuroblastoma cells . . . 39
3.7 L-GA depletes nucleotide pools in neuroblastoma cells after 24 hrs . . . 41
3.8 L-GA depletes deoxyribonucleotides and ribonucleotides to different degrees in neuroblastoma cells after 24 hrs. . . . 42
3.9 L-GA depletes purine and pyrimidine, and their phosphorylation states, derived nucleotides to different degrees. . . . 43
3.10 Nucleotide depletion in neuroblastoma cells is dependent on the concentration of L-GA . . . 44
3.11 L-GA selectively depletes nucleotide precursor pools in neuroblastoma cells . . . 45
3.12 L-GA alters redox and energy state of the cell . . . 46
3.13 L-GA depletes adenosine derived nucleotide pools as a function of their phosphorylation state . . . 47
3.14 L-GA depletes nucleotide pools in neuroblastoma cells within 24 hrs . . . 48
3.15 L-GA depletes nucleotide intermediates within 24 hrs . . . 49
3.16 L-GA is a more potent inhibitor than D-GA or DL-GA . . . 50
3.17 Glycolytic inhibition depletes nucleotide pools . . . 51
3.18 Effects of L-GA on glycolysis intermediates in IMR-32 and SH-SY5Y cells . . . 53
3.19 Effects of L- and D-GA on glycolysis intermediates in IMR-32 cells . . . 54
3.20 Effects of L- and D-GA on glycolysis intermediates in SH-SY5Y cells . . . 56
3.21 Effects of L-GA on the NAD+ and NADH pools . . . 58
3.22 Effects of L- and D-GA on TCA cycle intermediates in IMR-32 cells . . . 60
3.23 Effects of L- and D-GA on TCA cycle intermediates in SH-SY5Y cells . . . 61
3.24 L-GA induces a change in the proteomic landscape . . . 63

3.25 L-GA induces a change in the proteomic landscape 64
3.26 Elements of the oxidoreductase pathway is over-expressed in L-GA treated cells 66
3.27 Quantification of reactive oxygen species following L-GA treatment 68
3.28 The KEAP1-NRF2 pathway is induced upon L-GA treatment in IMR-32 cells . . . 69
3.29 L-GA reduces cell growth in neuroblastoma cells which is recovered via NAC . . 70
3.30 H_2O_2 and L-GA reduces nucleotide pools which are rescued by NAC treatment . 72
3.31 H_2O_2 and L-GA affects the cell status which is rescued by NAC treatment 73
3.32 Effects of L-GA and NAC on glycolysis intermediates in IMR-32 and SH-SY5Y cells 74
3.33 L-GA does not effect synthesis of serine and glycine 76
3.34 The fate of glyceraldehyde metabolism in the presence of NAC 77

4.1 Oxythiamine does not affect cell growth of IMR-32 cells 83
4.2 Ratio of nucleotide intermediates following ROS exposure 90
4.3 Proposed mechanism of the action of L-GA 93

5.1 L-GA causes multi nucleation of neuroblastoma cells 119
5.2 AMPK-phopshorylation in L-GA treated cells 119
5.3 pSIRM analysis of L-GA and D-GA treated cells. 120
5.4 pSIRM analysis of L-GA and D-GA treated cells. 121
5.5 pSIRM analysis of L-GA and NAC treated cells. 122
5.6 Metabolomics analysis of L-GA treated cells. 122
5.7 Nucleotide depletion in neuroblastoma cells is dependent on the concentration of L-GA 123

List of Tables

1.1 Risk stratification of neuroblastoma from INRG, table adapted from (Cohn et al., 2009) . . . 19

4.1 An example of therapeutic inhibitors of nucleotide metabolism (Thompson Coon, 2010; Siebert et al., 2020) . . . 82

5.1 Cell culture reagents and supplements . . . 112
5.2 Chemicals . . . 112
5.3 SDS-PAGE gel preparation . . . 113
5.4 Commercial kits . . . 114
5.5 Antibodies . . . 114
5.6 Consumables . . . 114
5.7 Equipment . . . 114
5.8 Software . . . 115
5.9 Direct infusion MS transition parameter . . . 115
5.10 GC-MS masses used for quantification . . . 117
5.11 GC-MS fragment ranges used for determination of stable isotope incorporation . . . 118
5.12 Proteins of interest with -log(pvalue) >1.3 and difference between PBS/LGA >1 and <-1 . . . 123

List of Abbreviations

General abbreviations

CCM	Central carbon metabolism
GC	Gas chromatography
LC	Liquid chromatography
MS	Mass spectrometry
OXPHOS	Oxidative phosphorylation
pSIRM	Pulsed stable isotope-resolved metabolomics
ROS	Reactive oxygen species
PPP	pentose phosphate pathway
TCA	Tricarboxylic acid cylce

Enzymes

6PGD	6-phosphogluconate dehydrogenase
ALDO	Aldolase
ACYL	ATP citrate lyase
ADK	Adenylate kinase
AMPK	5′ Adenosine monophosphate-activated protein kinase
APC	Anaphase promoting complex
CCNA2	Cyclin A2
ENO1	Enolase1
G6PD	Glucose 6-phosphate dehydrogenase
GAPDH	Glyceraldehyde-3-phosphate dehydrogenase
GLS	Glutaminase
GLUD	Glutamate dehydrogenase
GLUL	Glutamine synthase
GLUT	Glucose transporter
GPDH	Glycerol-3-phosphate dehydrogenase
HK2	Hexokinase 2
KEAP1	Kelch-like ECH-associated protein 1
IMPDH2	Inosine-5-monophosphate dehydrogenase 2
LDHA	Lactate dehydrogenase A
NME1	Nucleoside diphosphate kinase A
NRF2	Nuclear factor erythroid 2-related factor 2
NQO1	NAD(P)H dehydrogenase 1
PAICS	Phosphoribosylaminoimidazole carboxylase
PFK1	Phosphofructo kinase 1
PGK1	Phosphoglycerate kinase 1
PHGDH	Phosphoglycerate dehydrogenase
PKA	Protein kinase A
PKFM	Phosphofructokinase
PKM	Pyruvate kinase M
PPAT	Phosphoribosyl pyrophosphate amidotransferase

PRPS2	Phosphoribosyl pyrophosphate synthetase 2
PSAT	Phosphoserine aminotransferase
RRM2	Ribonucleoside-diphosphate reductase
SCF	Skp, Cullin, F-box containing complex
SHMT2	Serine hydroxymethyltransferase
TALDO	Transaldolase
TKT	Transketolase
TPI	Triosephosphate isomerase
TYMS	Thymidylate synthase

Metabolites

3-PGA	Glyceric acid-3-phosphate
2-DG	2-deoxyglucose
Acetyl-CoA	Acetyl coenzyme A
AICAR	5-Aminoimidazole-4-carboxamide ribonucleotide
AIR	5-Aminoimidazole ribonucleotide
α-KG	α-Ketoglutarate
Ala	Alanine
Asn	Asparagine
Asp	Aspartate
BrPyr	3-Bromopyruvate
CAIR	4-carboxy-5-aminoimidazole ribonucleotide
cAMP	Cyclic AMP
Cys	Cysteine
Cit	Citrate
D-GA	D-Glycerladehyde
DL-GA	DL-Glyceraldehyde
DHAP	Dihydroxyacetone phosphate
F6P	Fructose-6-phosphate
F16BP	Fructose-1,6-bisphosphate
FAICAR	N-Formylaminoimidazole 4-carboxamide ribonucleotide
FGAM	Formylglycineamidine ribonucleotide
FGAR	Formylglycineamide ribonucleotide
Fum	Fumarate
GAR	Glycineamide ribonucleotide
Glc	Glucose
G6P	Glucose-phosphate
Glyc3P	Glycerol-3-phosphate
Gln	Glutamine
Glu	Glutamate
IMP	Inosine monophosphate
Lac	Lactate
L-GA	L-glyceraldehyde
Mal	Malate
NAD	Nicotinic acid adenine dinucleotide
OAA	Oxaloacetate
OMP	Orotidine 5-monophosphate
PRPP	Phosphoribosyl pyrophosphate
Pyr	Pyruvate
R5P	Ribose-5-phosphate
SAICAR	N-succinylo-5-aminoimidazole-4-carboxamide ribonucleotide
Suc	Succinate

Chapter 1

Introduction

1.1 An introduction to glyceraldehyde as a cancer therapeutic

The nature of cancer cells is that they exhibit an addiction to glucose and show high glycolytic activity. This observation was described by Otto Warburg in 1924 (Warburg et al., 1924). Warburg deduced that this process was akin to fermentation, the process by which glucose is metabolised to lactic acid. Yet, cancer cells perform this fermentation metabolism even in the presence of oxygen, whereas normal cells convert glucose to CO_2 via respiration. Indeed, this was the first description of cancer cells harbouring a metabolic adaptation to support their high rates of proliferation.

Five years after Warburg's postulation, Bruno Mendel made the discovery that glycolysis can be inhibited in Jensen sarcoma tumour cells by a simple sugar, namely glyceraldehyde. Glyceraldehyde is a three carbon monosaccharide, ubiquitous in nature and existing as a racemic molecule of D- and L- isomers. Crucial to Mendel's experiments is that glyceraldehyde inhibited tumour growth without affecting normal tissue (Mendel, 1929). Following Mendel's discovery in 1929 and the synthesis of pure L-glyceraldehyde it was found that the D- isomer showed less inhibitory action on glycolysis than the L- isomer of glyceraldehyde (Needham and Lehmann, 1937; Mendel et al., 1938). This prompted the seminal research led by Warburg, showing that glyceraldehyde was effective at curing ascites cancer in all 75 mice that were treated (Warburg et al., 1963). Warburg found that the D-isomer was more effective *in vivo* than the L-isomer. It was reported that all animals that were injected with tumour cells and treated with D-glyceraldehyde survived the duration of the treatment. Although, this research was not without controversy. Brock and Niekamp found that 80% of animals died from peritonitis following D-glyceraldehyde treatment (Brock and Niekamp, 1965). One of the last published experiments of the efficacy of DL-glyceraldehyde *in vivo* showed that neuroblastoma cells were sensitive to DL-glyceraldehyde and exhibited inhibited glycolysis and cell proliferation. Furthermore, neuroblastoma cell growth was inhibited to a greater degree than the non cancerous chinese hamster ovary cells, albeit this being a questionable control when comparing murine to human cells (Prasad, 1972).

Glyceraldehyde as a therapeutic went largely out of fashion following these competing data. A revival of the use of glyceraldehyde occurred in the 1970's, in the context of stimulating

insulin secretion in pancreatic cells (Schauder et al., 1977). In the following decades, glyceraldehyde was only researched in relevance to its action as an insulin secretagogue (Taniguchi et al., 2000; MacDonald et al., 2006).

It is here where this thesis resumes the research interest into glyceraldehyde as an anti-cancer therapeutic. Most recently it has been shown that L-glyceraldehyde is effective against hepatocellular carcinoma cell growth, *in vitro* and *in vivo* (Pietzke, Unpublished). Including recent research in the Kempa laboratory, the question of glyceraldehyde has been dominated by attempting to understand the mechanism by which glyceraldehyde inhibits glycolysis and ultimately prevents the proliferation of tumour cells (Stickland, 1941; Weinhouse et al., 1956; Warburg et al., 1963). With novel technology, and a broader scope of question, the data herein shows that glyceraldehyde challenges cancer cell growth by previously unexplored pathways. This thesis presents a novel mechanism which exploits the metabolic fragility inherent to cancer cells outside of glycolytic dependency.

1.2 The origins and development of cancer

Over the course of history from Hippocrates to Virchow to Warburg, defining the mechanisms of cancer occurred through definitive milestones in medical and technological advancements (Warburg, 1955; Papavramidou et al., 2010).

The origins of cancer are disputed. The consensus is that multiple mutations occur during cancer development. Armitage and Doll (1954) stated that the epidemiology of cancer would be consistent with sequential mutations acquired through one's lifetime. Hanahan and Weinberg (2011) recapitulated this in a seminal review, positing that six essential alterations occur during the transition from a non-cancerous to a cancerous cell state. In support of this, it may be stated that cancer occurs through a process of 'somatic evolution'. Here genetic mutations confer global cellular alterations resulting in a Darwinian selective advantage of the clonal tumour cell population over the normal cell environment (Nowell, 1976). This 'cell centric' theory is criticised when applied to a tissue environment, where the communication between cells and their extracellular environment is critical to the understanding of cancer development (Sonnenschein and Soto, 2013). As stated by Sonnenschein and Soto (2018), cancer is development gone awry. In the context of this thesis, neuroblastoma is characterised by mutations in the MYC, ALK and ATRX genes causing devastating effects in early childhood cellular development (Matthay et al., 2016).

The description of the development of cancer is largely dominated by the characterisation of genetic alterations. The cancerous state of the cell can be profiled on multiple levels including: DNA, RNA, proteins, and metabolites; all of which can be attributed to specific hallmarks in relation to cancer (De Berardinis and Chandel, 2016). The metabolism of a cancer cell is regarded significantly different to that of a non-cancerous cell and has been a topic of study for almost 100 years (Warburg et al., 1924). Specifically, the genetic mutations that are acquired result in change in the regulation of metabolic networks conferring an advantage to the proliferation of the cancer cell. The interplay between genetic mutations and the resulting net metabolic change is the core principle to the metabolic reprogramming of the cancer cell into a malignant

state. This thesis aims to explore what is a pathological metabolic state and whether this state has targetable nodes to hinder cancer development.

1.3 Metabolism in Cancer

Warburg claimed that the origin of cancer cells is to be understood through the lens of metabolism. Warburg stated that cancer cells can be classified by their metabolic profile. It is specifically through their preference of aerobic glycolysis over respiration to generate adenosine triphosphate (ATP) - the molecular currency of energy in the cell (Warburg, 1955).

This finding, termed the 'Warburg Effect', is common place as an opening line in literature relating to the metabolism of cancer. The phenomenon by which Warburg described the metabolic state of the cancer cell is attributed to the production of ATP via lactate through glycolysis, even in replete oxygen conditions. The preference for the production of ATP via lactate rather than oxidative phosphorylation seems counter-intuitive; 2 moles of ATP are generated per mole of glucose via lactate, whereas oxidative phosphorylation provides 36 moles of ATP. Warburg stated that this occurred due to the fact that mitochondria of the cancer cell have impaired or injured respiration. In order to compensate for the lack of ATP generated by oxidative phosphorylation, cancer cells exhibit a high rate of aerobic glycolytic activity. Warburg's findings showed that the quotient of ATP produced via lactate was approximately 60-fold higher in ascites tumour cells relative to the liver and kidney (Warburg et al., 1924, 1926).

Although the 'Warburg Effect' is a widely reported and a ubiquitously accepted theory, the hypothesis that all cancer cells exhibit rates of aerobic glycolysis significantly above that of non-cancerous cells has been challenged. In 1956, and readdressed in 1976, Weinhouse states that Warburg's studies do not explicitly show evidence that cancerous cells have impaired respiration. Weinhouse showed via isotope labelled substrates that: (a) that slices of mouse and rat tumours oxidised glucose to CO_2 at rates within the ranges exhibited by various normal tissue slices; (b) that long and short chain fatty acids are oxidised to CO_2 to varying extents by slices of rat and mouse hepatomas at rates ranging from very low to rates comparable with those displayed by host livers; and (c) that citric acid was an intermediate of glucose and fatty acid oxidation in tumours as it is in normal tissues. These observations combined, negate the assumption that mitochondrial respiration is impaired under the Warburg hypothesis (Weinhouse, 1976; Weinhouse et al., 1956). Weinhouse and colleagues continue, stating that high aerobic glycolysis is a function of 'instability in the normally rigid mechanisms of gene regulation leading to profound alterations of isozyme composition' (Weinhouse, 1951). Zu and Guppy (2004) state that there is a lack of either: observations for the oxygen consumption of cancer cells, or there is a lack of observations for alternative fuel sources for the production of total ATP. They define a minimum energy budget, which permits the calculation of the proportion of ATP derived from glycolysis to the total ATP produced. They summarise that: 'The mean values for the glycolytic contribution to total ATP production are 20% for normal cells and 17% for cancer cells. So the actual mean for the cancer cells is numerically lower, but the means are not different (unpaired t test, p=0.46). Admittedly, this data is derived from isolated cells and grown *in vitro* therefore may not represent whole tissue (Zu and Guppy, 2004).

With this, we come back to the origins of cancer. We can interpret Weinhouse's statement as the instability of the mechanisms of gene regulation as a hypothesis predating the technological requirements for theorising the metabolic reprogramming of the cancer cell. Zu and Guppy (2004) concluded cancers follow the Pasteur Effect rather than the Warburg Effect, noting they are glycolytic but only under hypoxic conditions. It is widely recognised that cancer cells prefer, and maximise, their ATP production through glycolysis rather than mitochondrial oxidative phosphorylation. Even in hypoxic environments a significant fraction of ATP production is derived from oxidative phosphorylation (OXPHOS). It is more precise to state that the cancer cell metabolism is reprogrammed in favour of glycolysis for anabolic precursors (Ward and Thompson, 2012).

1.3.1 Overview: Glycolysis

As summarised by Berg, Jeremy et al. (2015) and figure 1.1, the metabolism of glucose branches into multiple pathways: glycolysis, pentose phosphate pathway (PPP), TCA cycle, and amino acid metabolism. These pathways support the generation of biomass and ATP. The glycolysis pathway is comprised of seven reversible reactions and three irreversible enzymatic reactions. The first irreversible reaction is catalysed by hexokinases (HK) that consumes one mole of adenosine triphosphate (ATP) per mole of glucose. In turn, glucose is phosphorylated to glucose-6-phosphate (G6P), sequestering it in the cell. G6P is isomerised to fructose-6-phosphate (F6P) in a reversible reaction via phosphoglucose isomerase (GPI). F6P is irreversibly phosphorylated to fructose-1,6-bisphosphate (F1,6-BP) via phosphofructokinase (PFK1), consuming one mole of ATP. F1,6-BP is the terminal hexose in the preparatory phase of glycolysis, whereby ATP is consumed to generate two triose molecules. Aldolase cleaves F1,6-BP into glyceraldehyde-3-phosphate (GA3P) and dihydroxyacetone phosphate (DHAP) in a reversible reaction, triosephosphate isomerase (TPI) interconverts DHAP and GA3P. DHAP maybe converted to glycerol-3-phosphate for lipid synthesis, in a reduced nicotinamide adenine dinucleotide (NADH) dependent reaction. GA3P is the entry point of the pay-off phase in which 2 moles of ATP and 2 moles of NADH are produced. GA3P is phosphorylated and oxidised via glyceraldehyde-3-phosphate dehydrogenase (GAPDH) to 1,3-Bisphosphoglycerate (1,3-BPG) consuming 2 moles of NAD^+ and 2 moles of free phosphate (Pi), generating 2 NADH. The irreversible conversion of 1,3-BPG to 3-phosphoglycerate (3-PGA) via phosphoglycerate kinase (PGK) generates 2 moles of ATP. 3-PGA is isomerised to 2-phosphoglycerate (2-PGA) or converted to serine (Ser) for amino acid production. Subsequently, 2-PGA is isomerised to phosphoenolpyruvate (PEP) which is required for an irreversible reaction which produces pyruvate (Pyr) and 2 moles of ATP via enolase and pyruvate kinase (PK), respectively. This terminal step results in a net yield of 2 moles of ATP from glucose to pyruvate. In the absence of oxygen Pyr is reversibly reduced to lactate (Lac) via lactate dehydrogenase (LDH), consuming 2 moles of NADH. Under aerobic conditions Pyr is transported into the mitochondria to be oxidised to CO_2 in the tricaboxylic acid (TCA) cycle (Berg, Jeremy et al., 2015).

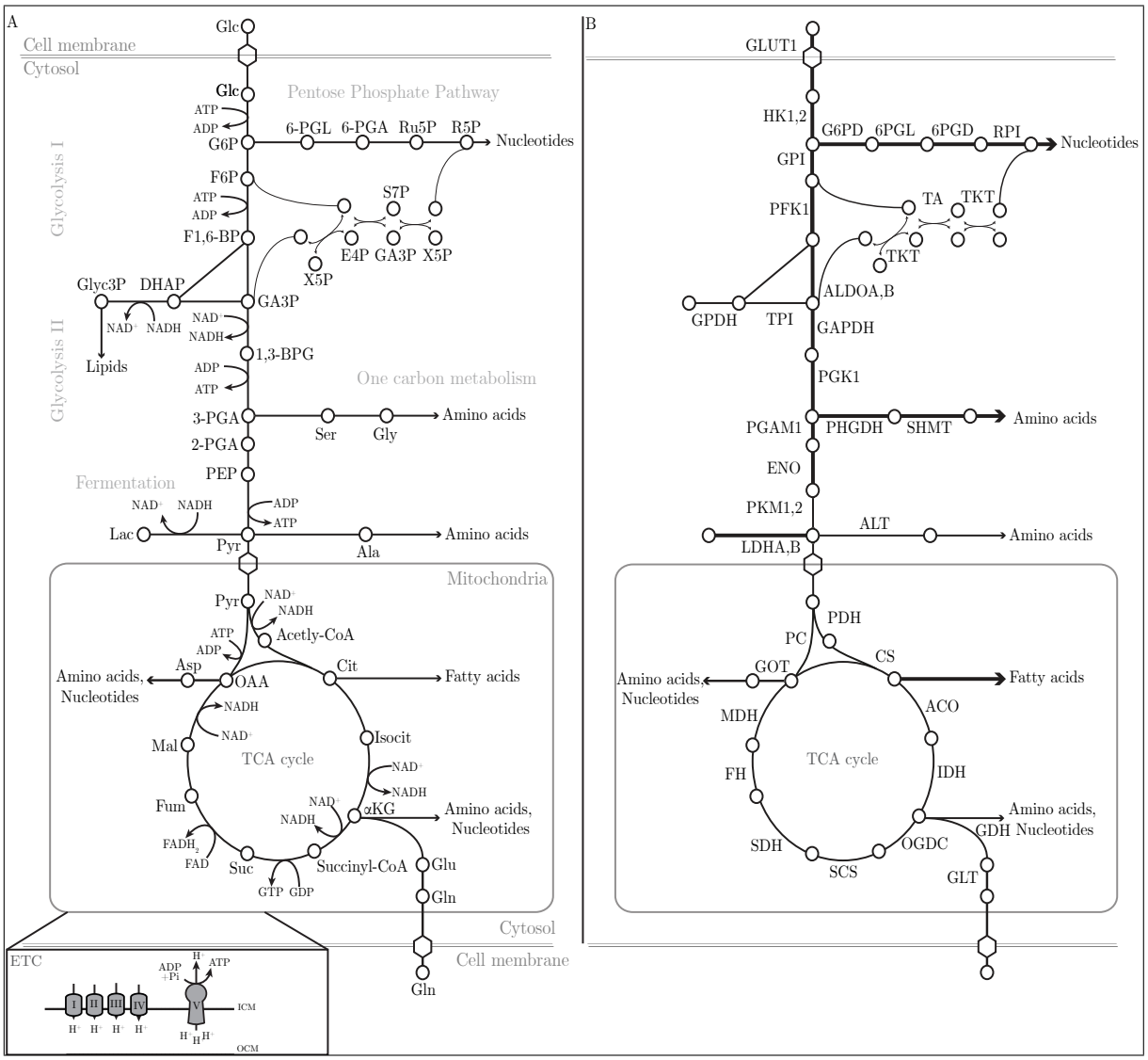

Figure 1.1: Central carbon metabolism - Glycolysis and TCA cycle
A: Schematic depicts the central carbon metabolism composed of Glycolysis and the TCA cycle. Glycolysis is initiated by the phosphorylation of glucose inside the cytoplasm, in a sequence of seven reversible reactions and three irreversible enzymatic reactions: 2 moles of pyruvate, ATP and NADH are generated. Glycolysis branches for the production of nucleotides, amino acids and lipids. Pyruvate enters the mitochondria and is condensed to acetyl-coA. The step-wise oxidation of acetyl-CoA into CO_2, generates 3 moles of NADH, 1 mole of GTP and 1 mole of $FADH_2$. ATP is generated via ATP synthethase and oxidative phosphorylation in the electron transport chain (ETC) employing a H^+ gradient fuelled by $FADH_2$ and NADH oxidation. B: Schematic of proteins associated with glycolysis and TCA cycle. Essential abbreviations provided in the list of abbreviations. Figure adapted from (Boroughs and Deberardinis, 2015).

1.3.2 Overview: The TCA cycle and Glutamine Metabolism

Pyruvate enters the TCA cycle and is decarboxylated via pyruvate decarboxylase (PDC) and condenses with co-enzyme A to form acetyl-CoA, requiring one mole of NAD^+. Citrate synthase (CS) condenses acetyl-CoA and oxaloacetate (OAA) to form the six-carbon citrate (Cit). Through a sequence of isomerisation, oxidative decarboxylation and hydration one molecule of acetyl-CoA yields three molecules of NADH, two molecules CO_2, and one molecule GTP and $FADH_2$. The total eight enzymatic reactions within the TCA cycle utilise isocitrate (Isocit), α-ketoglutarate (α-KG), succinate (Suc), fumarate (Fum) and malate (Mal).

A complete oxidative turn of the TCA cycle, originating from acetyl-CoA, generates two molecules of CO_2, reduces three molecules of NAD^+ and one molecule of FAD. The reduced electron carriers (NADH, $FADH_2$) are subsequently oxidised by the electron transport chain (ETC). The ETC consists of a series of four membrane proteins (complex I-IV), each protein facilitates the transfer of electrons from the reduced electron donors to electron acceptors, for example O_2 and Suc. This process generates a flux of protons across the inner mitochondrial membrane resulting in an electrical potential. This potential drives the phosphorylation of ADP to ATP via the ATPase, Protein complex V. Given that one molecule of glucose equates to 2 molecules of acetyl-CoA and two turns of the TCA cycle, 36 molecules of ATP are generated via OXPHOS (Berg, Jeremy et al., 2015).

In addition to glucose, the TCA cycle may be fuelled by glutamine. Glutamine provides a source of carbon and nitrogen for central carbon and nucleotide metabolism. As with pyruvate, aspartate and β-oxidation of fatty acids, glutamine can replenish intermediates of the TCA cycle via α-ketoglutarate through anaplerosis. Glutamine is initially irreversibly deaminated to glutamate via glutaminase (GLS), subsequently glutamate enters the TCA cycle by conversion to α-ketoglutarate via two possible enzymatic pathways. In one, transaminases transfer the amino group from glutamate to a ketoacid, producing α-ketoglutarate and an amino acid. In the other, glutamate is deaminated by glutamate dehydrogenase (GDH) producing α-ketoglutarate. However, under glucose-replete conditions the former pathway is predominant (DeBerardinis et al., 2011).

1.3.3 Nucleotide Metabolism

Nucleotide metabolism encompasses the pathways which synthesise the building blocks of DNA and RNA. Furthermore, essential redox co-factors and cell signalling molecules such as NADP+ and cAMP are synthesised during nucleotide metabolism. Glucose-6-phosphate (G6P) is at the convergence point of not only glycolysis but also the pentose phosphate pathway, the hexosamine pathway and glycogen synthesis (Hay, 2016; Lane and Fan, 2015). The pentose phosphate pathway (PPP) is the branching of glycolysis which provides the precursor for all nucleotides, R5P. R5P is generated as described in figure 1.2. In the oxidative PPP, G6P is oxidised to 6-phosphoglucolactone (6-PGL) utilising the co-enzyme NADP+ and Glucose 6-phosphate dehydrogenase (G6PD). 6-PGL is then hydrolysed to 6-phosphogluconic acid (6-PGA) which is oxidised to ribulose-5-phosphate (Ru5P). Ru5P is isomerised to R5P, until this point 2 moles of $NADPH_2$ are produced per mole of G6P.

The production of R5P through the non-oxidative PPP utilises fructose-6-phosphate (F6P) and glyceraldehyde-3-phosphate (GA3P). The 9-carbons compromising GA3P and F6P are cycled to R5P and Ru5P through a sequence of carbon exchanges. Firstly, transketolase (TKT) facilitates the cycling of carbons from GA3P and F6P to erythrose-6-phosphate (E6P) and xylulose-5-phosphate (X5P). Transaldolase (TALDO) cycles carbons from F6P and E6P to produce GA3P and sedoheptulose-7-phosphate (S7P). Finally TKT catalyses the production of R5P and X5P through cycling of carbons from S7P and GA3P. All reactions in the non-oxidative pathway are reversible and the rate of reaction depends on cellular demands. Specifically, the non-oxidative pathway is down-regulated when $NADPH_2$ requirements are high (Lane and Fan,

2015). R5P enters the nucleotide biosythesis pathway via its phosphorylation to phosphoribosyl pyrophosphate (PRPP), whereby PRPP-synthetase (PRPS) consumes 1 mole of ATP. PRPP is the root pentose intermediate common to both purine and pyrimidine synthesis.

De novo purine synthesis

Adenosine and guanosine derived nucleotides are synthesised from IMP which is synthesised from a complex set of reactions originating from PRPP. Initially, PRPP condenses with glutamine, forming 5-phosphoribosylamine. The enzyme catalysing this reaction, glutamine phosphoribosyl pyrophosphate amidotransferase, is inhibited by IMP, GMP, and AMP thereby acting as a rate-limiting entry point for purine synthesis. Glycinamide kinosynthase catalyses the synthesis of glycinamide ribonucleotide (GAR) which consumes 1 mole of ATP and glycine. In the synthesis of formylglycinamide ribonucleotide (FGAR) a formyl group is received from N^{10}-formyltetrahydrofolate (10-formyl THF) from the folate cycle. Through a sequence of reactions the intermediate FAICAR is produced, which consumes 1 mole of: ATP, 10-formyl THF, aspartate and glutamine. FAICAR is hydrolysed to IMP which is used to synthesise AMP and GMP in a glutamine, aspartate, NAD+ and ATP dependent reaction. The amino acids: aspartate, glutamate and glycine provide the nitrogen groups for the synthesis of the purine rings.

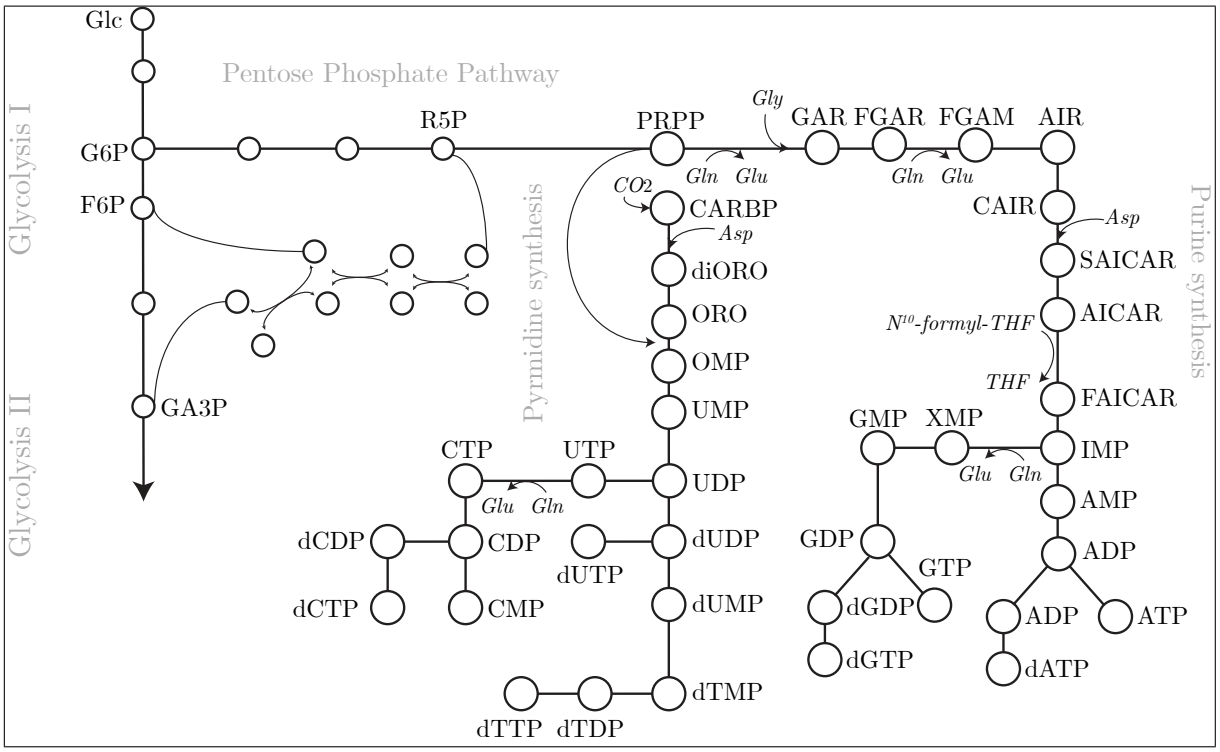

Figure 1.2: Pathways of nucleotide metabolism. *De novo* nucleotide biosynthesis is derived from glycolysis intermediates G6P, F6P and GA3P which produce R5P in two distinct pathways: the oxidative and non-oxidative pathways. R5P is phosphorylated to PRPP which splits the pathway into purine and pyrimidine synthesis. Purine synthesis requires diORO as the initial substrate to produce Cytosine, Thymidine and Uridine derived nucleotides. Pyrimidine synthesis occurs through a number of reactions to produce IMP which is the precursor to Adenosine and Guanosine derived nucleotides. Abbreviations can be found in the list of abbreviations. Figure adapted from (Lane and Fan, 2015)

De novo pyrimidine synthesis

In the first step of pyrimidine synthesis, carbamoyl phosphate and aspartate react to produce carbamoyl aspartate. Following dehydration of carbamoyl aspartate to dihydroorotic (diORO) it is oxidised to orotic acid (ORO) in an NAD+ dependent reaction. Orotic acid condenses with PRPP to produce orotidine-5-phosphate (OMP). OMP is decarboxylated to UMP. UMP is phosphorylated by 2 moles of ATP to UTP which is converted to cytidine triphosphate (CTP) by CTP-synthetase. Thymidine mono-phosphate (dTMP) is synthesised from reduced UMP (dUMP) via methylation of dUMP by thymidylate synthase (TYMS) consuming 1 mole of NADPH and 10-formyl THF.

As described, GA3P is a substrate in the synthesis of nucleotides. It is of particular interest that L-glyceraldehyde has been described only in the context of a glycolytic inhibitor. We must ask how does the metabolic reprogramming in a cancer cell contribute to nucleotide biosynthesis.

1.4 Metabolic reprogramming in cancer

Cells that are rapidly proliferating require sufficient rates of production of ATP, amino acids, lipids, proteins and nucleotides for subsequent daughter cell synthesis (Tennant et al., 2009). The complexity of metabolic reprogramming in cancer is not limited to the malignant cell but also the environment in which the cell resides, namely the tumour microenvironment (TME). Cells within the TME modulate surrounding cells to maintain the supply of nutrients required for cancer cell growth (Sonveaux et al., 2008; Nieman et al., 2011). Therefore metabolic reprogramming and the metabolites which are involved in the development of malignancy, must be viewed from both the 'cell-centric' and TME viewpoints. Despite this complexity, it has been suggested that malignancy arises from perturbations in a finite set of pathways involved in anabolism, catabolism and redox balance (De Berardinis and Chandel, 2016). The perturbations in these pathways serve to satisfy the demands generated by the metabolic reprogramming of the malignant cells. It would be excusable to state that by analysing these perturbations we would have a definitive 'hallmark of cancer'. Yet, we observe high phenotypic heterogeneity between cancer cells and within the TME, suggesting that no single model of cancer metabolism exists (Cantor and Sabatini, 2012).

For the scope of this thesis we will examine the reprogramming of glycolysis and nucleotide biosynthesis pathways. Mutations in oncogenes such as *c-MYC/MYCN*, AKT and p53 drive the up-regulation of signalling pathways influencing glycolysis (Boroughs and Deberardinis, 2015; Hay, 2016). Mutations in *c-MYC/MYCN* and the subsequent MYC pathway up-regulate or modulate a plethora of genes essential to biomass synthesis and glycolysis (Stine et al., 2015; Qing et al., 2010). For example, increased *MYC* expression results in the stabilisation of HIF1α. Subsequently, hexokinase synthesis increases resulting in increased glucose phosphorylation and up-regulated glycolysis (Doe et al., 2012; Dang, 2013). Furthermore, *MYC* mutations induce up-regulated nucleotide biosynthesis. MYC can enhance glycolytic flux from 3-phosphoglycerate (3-PGA) to the synthesis of serine and glycine, which are essential nitrogen donors for nucleotide biosynthesis (Vazquez et al., 2011).

In addition to MYC, another canonical regulator of cancer metabolism is the PI3K/AKT/mTOR signalling pathways. PI3K directly interacts with enzymes of glycolysis. On stimulation of PI3K from growth factors, PI3K releases aldolase from the cytoskeleton to increase glycolysis. (Hu et al., 2016). Downstream of PI3K are the signalling molecules AKT and mTOR. Upon enhanced PI3K activation, AKT and mTOR activity is up-regulated. Both AKT and mTOR have broad effects on glycolysis. For example AKT regulates fructose 2,6-bisphosphatase (PFKFB2) expression and enhances phase I glycolysis (Sun et al., 2011). In another example, activation of mTOR increases pyruvate production through the activation of pyruvate kinase (PKM2) (Dando et al., 2016). In summary, the activation of the PI3K/AKT/mTOR pathway coordinates broad changes in cellular metabolism.

A significant hallmark of the cancer cell is its ability to evade cell cycle checkpoints, thereby promoting aberrant cell division. The cell cycle is an energetically demanding process which requires synthesis of proteins, lipids and nucleic acids. Anabolism of these molecules are highly dependent on the flux of carbon and nitrogen metabolism. The appropriate signalling pathways confer their availability to cell cycle regulators. The cell cycle occurs in precise phases, namely: the G_0/G_1 and phase when cells grow and synthesise biomass, the S-phase during which DNA is replicated, and the G_2/M phase when cells observe mitosis and cytokinesis (Kalucka et al., 2015). Each phase is regulated by a complex network of cyclin-dependent kinases (CDKs) and E3 ubiquitin ligases. The major Cdks regulate the cell cycle in the following fashion: cyclin D–CDK 4/6 regulates G_1/S, cyclin E–CDK2 regulates S-phase, and cyclin B–CDK1 regulates G_2/M phase transition (Salazar-Roa and Malumbres, 2017). CDKs and E3 ubiquitin ligases modulate glycolysis and oxidative phosphorylation at discrete stages in the cell cycle. For example, in the late G_1 phase 6-phosphofructo-1-kinase (PFK1) and Hexokinase (HK) are activated by the ligase anaphase-promoting complex or cyclosome (APC/C) and 6-phosphofructo-2-kinase/fructose-2,6-bisphosphatase, isoform 3 (PFKFB3). These enzymes coordinate to induce an up-regulation in glycolytic flux. Conversely, in the S-phase glycolysis is inhibited by the Skp1–Cul1–F-box protein (SCF) by degrading PFKFB3 and glutaminolysis is increased by glutaminase 1 (GLS1) activation (Kalucka et al., 2015).

In addition to the cell cycle regulating glycolysis, glycolytic enzymes and metabolites also regulate the cell cycle. Glyceraldehyde-3-phosphate dehydrogenase (GAPDH) has been shown to regulate the G_2/M transition by directly inducing cyclin B/CDK1 activity (Carujo et al., 2006). Furthermore, the glycolytic enzyme, PKM2 is known to interact with a wealth of cell cycle regulators such as MYC, ERK1/2 and CCND1 (Keller et al., 2014). Ratios of the metabolites AMP/ATP and NAD+/NADH are known to be indicators of cellular energy and redox states. The ratio of AMP/ATP is registered by AMP-activated protein kinase (AMPK). Upon high AMP levels AMPK is activated thereby reducing metabolic processes, promoting oxidative phosphorylation and phosphorylating p53 to induce cell cycle arrest. Furthermore, AMPK is known to regulate nucleotide biosynthesis by negatively regulating PRSP, which converts R5P to PRPP (Qian et al., 2018). In addition, the ratio NAD+/NADH is essential to maintaining cellular homeostasis. Upon NADH depletion and oxidative stress the NAD-dependent deacetylase sirtuin-1 (SIRT1) protein activates a range of cell cycle proteins, including p53, E2F and FOXO3. The coordination of these proteins generate a cell cycle arrest and up-regulate

anti-oxidant mechanisms (Mandal et al., 2010).

It is apparent that the cross talk between the energy state of the cell - inferred by the level of ATP and NAD+/NADH ratio - and the cell cycle is tightly linked. Mutations in the cell cycle machinery are common given that cancer cells exhibit a unique energy demand. Furthermore, the cell must be able to maintain its homeostasis to enable the evasion of cell cycle checkpoints in order to support proliferation.

1.5 Maintaining Cellular Homeostasis

Rapid but inefficient production of ATP via glycolysis comes at the cost of an increased oxidative state (Kroemer and Pouyssegur, 2008). Cancer cells in proliferative states require a metabolic adaptation to accommodate the increase of reductive and oxidative cellular processes (redox). Specifically, reactive oxygen species (ROS) accumulate due to the increase in metabolic processes. The cancer cell therefore requires mechanisms to detoxify the cell of ROS and maintain a homeostatic redox balance. This system is finely tuned for cancer cell growth and presents opportunities for therapeutic targets.

1.5.1 The generation and function of ROS in cancer

Central to the generation and function of ROS generation is that its cellular function is dependent on the concentration within the cell, with increasing ROS concentrations becoming more toxic as described in figure 1.3 (Galadari et al., 2017; Vučetić et al., 2017). Low levels of ROS modify protein structure and function by reversibly oxidising thiol groups. This post-translational modification of proteins can act as a signalling mechanism (Schumacker, 2015). As ROS concentrations increase oxidative damage occurs at the DNA, protein and lipid levels resulting in growth inhibition, genomic instability and cell death. To alleviate oxidative damage, cells initiate oxidative stress responses through metabolic reprogramming and transcription of stress response genes (Liou and Storz, 2010; Circu and Aw, 2010).

The majority of ROS are generated during mitochondrial OXPHOS, yet they are also generated in response to xenobiotics, cytokines, and bacterial invasion. During OXPHOS in the mitochondria, ATP is produced via electron transport chain (ETC) generating H^+ which reduces O_2 to water. Although this is a highly efficient process, ROS are generated upon partial reduction of O_2. The possible reactive species produced in this partial reduction include: superoxide anion ($O_2^{\cdot}$), hydrogen peroxide (H_2O_2), and hydroxyl radical (OH•) (Kamata and Hirata, 1999). This occurs due to the mitochondria being a redox hub at the ETC complex, which in part leaks electrons to molecular oxygen thereby generating ROS (Kardeh et al., 2014).

ROS may act as cell signalling molecules to drive activation of growth pathways including mitogen activated protein kinases (MAPK), phosphatidylinositol 3-kinase (PI3/K) and phospholipase C gamma (PLCgamma). Through a phosphorylation cascade and translocation of transcription factors to the nucleus, ROS stimulates gene expression of growth promoting genes (Kamata and Hirata, 1999; Cadenas and Boveris, 2005). However as ROS concentrations reach

their toxicity thresholds, apoptotic responses are initiated. As the scales slide against the clearance of ROS by antioxidants, pro-apoptotic signalling molecules, such as ASK1, JNK, p53 and p38 are activated (Kardeh et al., 2014; Yang et al., 2018). Therefore we arrive at the crossroad of how cancer cells, relating to the ROS concentration, evade cell death via oxidation.

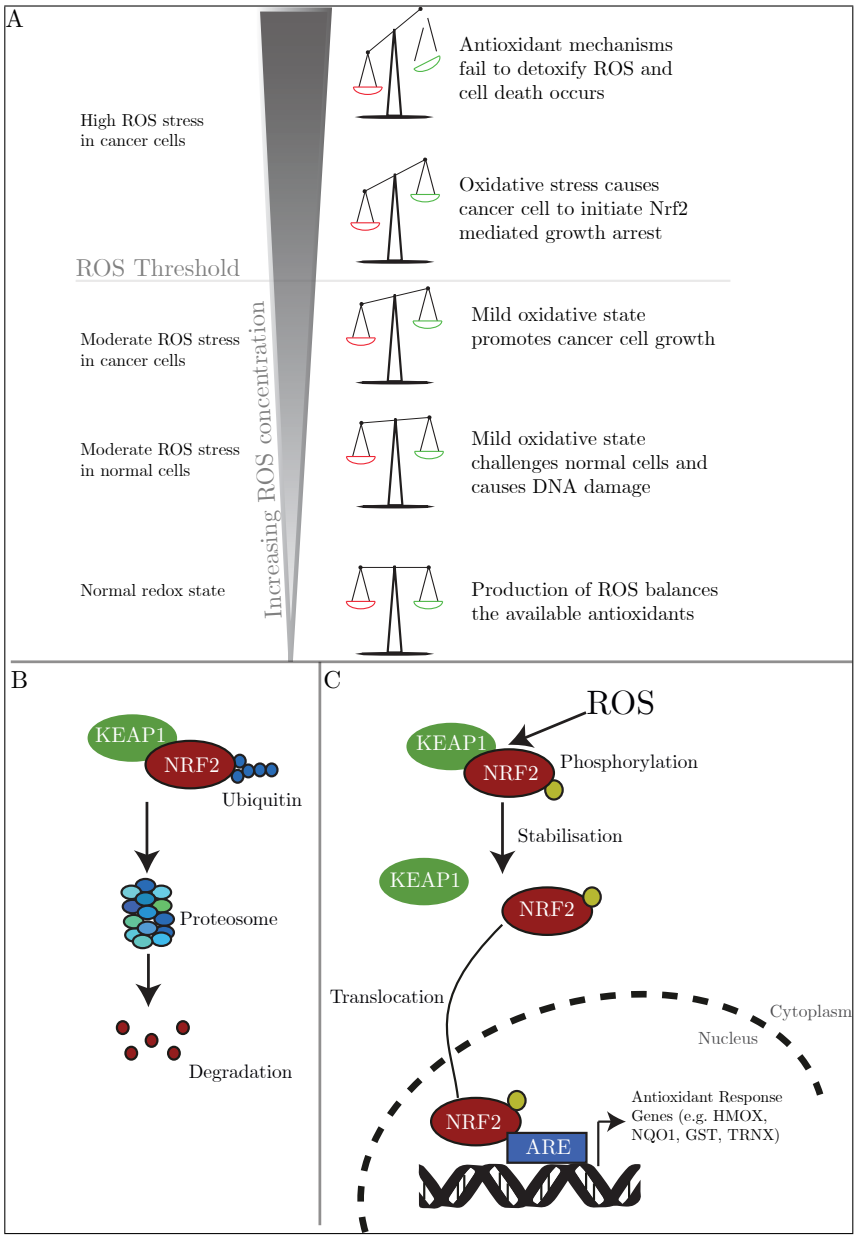

Figure 1.3: The role of increasing ROS levels in cells. A: As ROS levels increase in cells they induce DNA damage and oxidation of lipids and proteins. In normal cells, increased ROS levels induce antioxidant response pathways to balance ROS levels (green and red scales, respectively). Cancer cells employ a moderate state of ROS stress, greater than that of normal cells, favouring their survival. This state is still maintained due to mutations in antioxidant pathways, up-regulating ROS scavenging mechanisms. However, if ROS levels exceed the cells antioxidant capacity cells initiate programmed cell death. B: KEAP1 and NRF2 are maintained in a complex and is ubiquitinated under normal conditions and degraded by the proteosome. C: Upon stimulation by ROS, the KEAP1/NRF2 complex is untethered and NRF2 is stabilised. NRF2 translocates to the nucleus and act as a transcription factor for the anti-oxidant response element (ARE) to expression anti-oxidant response genes. Adapted from Vučetić et al. (2017)

1.5.2 Mechanisms of ROS regulation and cell fate

Generation of ROS induces metabolic reprogramming in cancer cells, inhibiting multiple glycolytic enzymes, including glyceraldehyde 3-phosphate dehydrogenase, pyruvate kinase M2, and phosphofructokinase (Mullarky and Cantley, 2015). To prevent the inhibition of glycolytic enzymes via ROS, the cell redirects glycolytic flux to produce antioxidants. Specifically, glycolytic inhibition promotes flux into the oxidative branch of the pentose phosphate pathway (PPP) to generate nicotinamide adenine dinucleotide phosphate (NADPH) via glucose-6-phosphate dehydrogenase (G6PD) and 6-phosphogluconate dehydrogenase (6PGD). NADPH is critically important, as it provides the reducing power that fuels the protein-based antioxidant systems (Ciccarese and Ciminale, 2017). NADPH is a co-factor for the ROS scavenging systems: thioredoxin/peroxiredoxin (TRX/PRX) and glutathione/glutathione peroxidase (GSH/GPX) which reduces H_2O_2 to H_2O. Specifically, thioredoxin and glutathione act as electron donors in the process of reducing oxidised molecules, NADPH is utilised by their relative reductases to restore reducing power. As stated, NADPH pools are maintained in the cytosol via the PPP. However, NADPH pools in the mitochondria must be maintained via alternate mechanisms as NADPH does not cross the mitochondrial membrane. NADPH is generated via six pathways utilising: (i) NADP+ transhydrogenation by nicotinamide nucleotide transhydrogenase (NNT); (ii) glutamate conversion to α-ketoglutarate by glutamate dehydrogenase 1 (GDH1); (iii) NADH phosphorylation by mitochondrial NAD kinase (NADK2); (iv) isocitrate dehydrogenase 2 (IDH2); (v) malic enzymes (ME2/3); and (vi) the mitochondrial folate cycle (Petrosillo et al., 2003).

The regulation of NADPH generation is tightly controlled via a number of pathways (Mitsuishi et al., 2012). A prime example is the regulation of the KEAP1-NRF2 pathway, a major regulator of cytoprotective response to ROS stress. In detail, the nuclear factor erythroid 2-related factor 2 (NRF2) binds to the antioxidant response element (ARE) and regulatory regions of KEAP1 (Kelch ECH associating protein 1), in response to ROS elevation. NRF2 is negatively regulated by KEAP1 via the ubiquitiation of the NRF2 and KEAP1 complex under normal conditions. As ROS levels increase, the structural conformation of the cysteine-rich KEAP1 protein is modified, releasing NRF2 and preventing its degradation. Upon translocation to the nucleus, NRF2 initiates the expression of a plethora of antioxidant enzymes such as: NAD(P)H quinone oxidoreductase 1 (NQO1), haemeoxygenase 1 (HMOX1), glutamate-cysteine ligase (GCL) and glutathione S transferases (GSTs) (Kansanen et al., 2013). In addition to stimulating ARE genes, NRF2 is also known to redirect glucose and glutamine to anabolic pathways via activation of the PI3K-AKT signalling pathway (Sporn and Liby, 2012).

Cancer cells often up-regulate or harbour mutations that confer constitutive expression of antioxidant dependent mechanisms (Sporn and Liby, 2012). NRF2 hyper-activation confers several advantages to cancer cell survival. The oncogenic properties of NRF2 can be exemplified by its targets NQO1 and GST, the overexpression of these proteins confer drug resistance in cancer cells (Meijerman et al., 2008). The consequence of NRF2 hyperactivity and its associated targets result in, but not limited to: angiogenesis, proliferation via metabolic reprogramming, chemoresistance and inhibition of apoptosis (Sporn and Liby, 2012).

1.5.3 Targeting mechanisms of ROS reduction for cancer therapy

As aforementioned, low levels of ROS production facilitates cancer cell growth through the activation of survival pathways and activating proliferation (Sena and Chandel, 2012). Mutations in oncogenes such as *c-MYC* have shown to not only promote ROS production but also stabilise NRF2 to activate antioxidant systems (Denicola et al., 2011). In addition, mutations in NRF2 liberate it from the control of KEAP1, thereby promoting cancer survival in high ROS conditions (Shibata et al., 2008). Given that cancer cells promote antioxidant pathways- and indeed depend on such pathways for survival- we may investigate whether these pathways offer therapeutic targets.

A number of studies have shown that inhibitors of antioxidant pathways are effective at limiting cancer cell growth. Glutathione (GSH) and thioredoxin (TXN) are crucial for antioxidant pathways. Inhibiting the pathways of GSH and TXN synthesis has been shown to cause synergistic cancer cell death (Harris et al., 2015). Furthermore, blocking the uptake of the GSH precursor via cysteine/glutamate antiporter significantly affects cancer cell survival (Lo et al., 2008). In a similar manner, providing the cell with an inactive glutathione mimetic (NOV-002) results in an increase in oxidative stress and cancer cell survival is decreased (Townsend et al., 2008). Interestingly, when cancer cells are treated with the thioredoxin inhibitor, auranofin, oxidative stress increases. This phenotype could be reversed with the ROS scavenger N-acetylcysteine, confirming that indeed oxidative stress is involved in cancer cell death (Sobhakumari et al., 2012).

The process of programmed cell death (PCD) is tightly linked to ROS generation and ROS-induced apoptosis. PCD encompasses apoptosis, autophagy and necrosis. With credit to the global cellular functions of ROS, it is not surprising that ROS act upon all three PCD modes. Briefly, ROS stimulates the caspase cascade to induce apoptosis; inhibits mTORC1 to induce autophagy and via RIP3 to stimulate necrosis (Zhang et al., 2009; Perillo et al., 2020).

In the context of this thesis, glyceraldehyde has been shown to dysregulate ROS production in pancreatic cells (Takahashi et al., 2004). Furthermore, *MYCN* amplified neuroblastoma cells were shown to have increased ROS production (Wang et al., 2018). Given that MYCN increases glutaminolysis and thereby increased ROS production, sensitivity to ROS is increased. Therefore, there is certainly scope to assess the function of glyceraldehyde in relation to ROS production.

1.6 Metabolism as a therapeutic target

Glycolysis may be regulated by metabolites, proteins and exogenous small molecules. ROS species inhibit glycolysis by attacking cysteine-rich enzymes such as GAPDH and PKM1,2. However, metabolites of glycolysis may also auto-inhibit their synthesis to maintain appropriate glycolytic levels. As described in figure 1.4, A, metabolites such as G6P, Lac, Cit, and PEP inhibit central glycolysis at the HK1,2 and PFK1 positions. Furthermore the pentose phosphate pathway may be inhibited by 3-PGA originating from glycolysis II (Hay, 2016). Conversely, F1,6-BP, Ser and SAICAR enhance the metabolism of Pyr at the PKM1,2 position. Exogenous

small molecules can be delivered to the cell to hijack these mechanisms of regulation (figure 1.4, B). These molecules are of particular therapeutic interest, given the dependency of the cancer cell on the glycolytic pathway (Granchi and Minutolo, 2012).

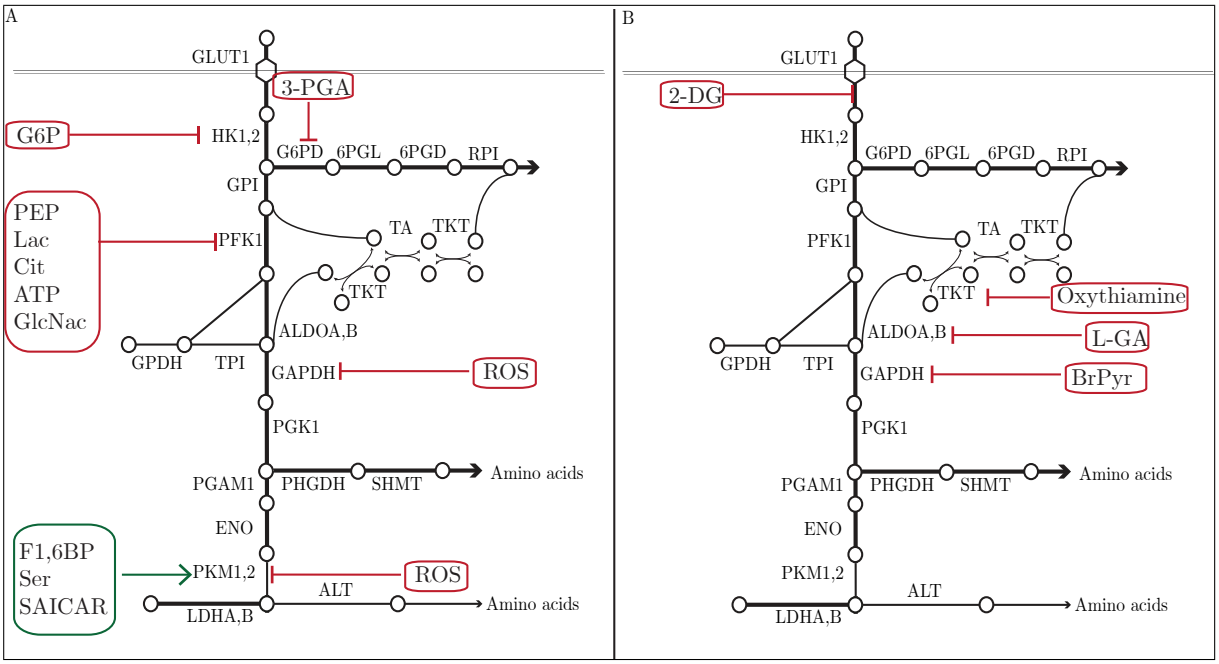

Figure 1.4: Regulators of glycolysis and points of therapeutic intervention A: Metabolites can either positively or negatively regulate glycolytic enzymes, modulating glycolytic flux. Reactive oxygen species (ROS) are known to oxidize and inhibit glyceraldehyde-3-phosphate dehydrogenase (GAPDH) and pyruvate kinase M2 (PKM2). Positive regulators are in green boxes and negative regulators are in red boxes. B: Anti-metabolites or small molecules can inhibit glycolysis as competitive inhibitors or by sequestering Pi. 2-DG sequesters Pi at the initial stage of glycolysis. L-GA is theorised to inhibit at the ALDOA,B position and may also inhibit the TKT. Oxythiamine inhibits TKT and BrPyr inhibits GAPDH. Abbreviations detailed in the list of abbreviations. Figure adapted from (Pietzke et al., 2014; Hay, 2016)

1.6.1 Glyceraldehyde

Following the preamble of this thesis, and indeed the central topic, glyceraldehyde is a triose monosaccharide existing as D- and L- isomers. Glyceraldehyde is formed through fructose and glycerol metabolism (Hagopian et al., 2008). As shown in figure 1.1 the phosphorylated form, GA3P is a substrate for the enzymes GAPDH, ALDO, TPI and TKT. Therefore, GA3P is a substrate for glycolysis, glycerol metabolism and nucleotide biosynthesis. Although there is significant amounts of data, dating back to the 1920's, the mechanisms of L-GA action is still not untangled. The metabolism of D-GA and L-GA via aldolase results in two distinct phosphorylated trioses, fructose-1-phosphate and sorbose-1-phosphate, respectively. Needham et al. (1951) found that sorbose-1-phosphate inhibited hexokinase, thereby preventing glucose phosphorylation. Interestingly, D- isomers of saccharides are common in nature, whereas L- isomers are rare. This may lend to the findings that L-GA has proven to be a more effective glycolytic inhibitor. Both D-GA and L-GA can be phosphorylated to D-GA3P and L-GA3P via triokinase, respectively. Whereas D-GA3P is the natural substrate for glycolysis, it is unknown whether L-GA3P is metabolised by GAPDH. However, it is understood that aldehyde dehydrogenase (ALDH) oxidises D-GA and L-GA to D- and L- glyceric acid. In turn glycerate kinase (GLYCTK)

phoshorylates glyceric acid to 3-PGA to be used in glycolysis (Antony et al.). In addition to inhibiting glycolysis, L-GA shows inhibitory effects on protein synthesis. Specifically L-GA was shown to inhibit leucine incorporation into proteins of normal and cancer tissues, although the mechanism was not described (Guidotti et al., 1964). Furthermore, no studies currently address the mechanism of L-GA in the role nucleotide biosynthesis, of which this thesis will attempt to explore.

L-Glyceraldehyde

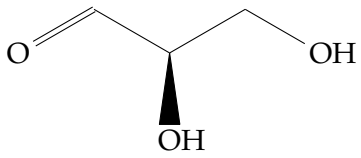

D-Glyceraldehyde

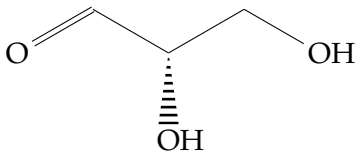

1.6.2 2-D-deoxyglucose

2-D-deoxyglucose (2-DG) was introduced as an anticancer therapeutic in the 1950's, promising results showed inhibition of tumour growth *in vivo* (Ely, 1954). However, competing evidence arose in the 1980's claiming that 2-DG showed no efficacy against murine tumour cells (Tannock et al., 1983). Further research elucidated the syngergistic effects of 2-DG. *In vivo*, 2-DG enhanced the anticancer activity of adriamycin and paclitaxel in xenograft mice with human osteosarcoma or non-small-cell lung cancer (Maschek et al., 2004). Within this study it was found that 2-DG alone does not show anti-cancer efficacy. *In vivo*, 2-DG is relatively well tolerated with dosages up to 250mg/kg being reported as tolerable in combination with radiation therapy (Singh et al., 2005). 2-DG has been extensively studied and has proved a valuable tool for analysing glycolytic inhibition and as a cancer diagnostic *in vitro*. The fluorine modified analogue 2-FDG, is sequestered in the cell facilitating positron emission tomography (PET) imaging of highly proliferative and glycolytic cells (Som et al., 1980).

2-DG is a synthetic glucose analog in which the 2-hydroxyl group is replaced by hydrogen. 2-DG is imported into the cell in the same manner as glucose, by GLUT1. In the cell 2-DG is phosphorylated to 2-DG-P, which is not a substrate for glucose-6-phosphate isomerase (GPI). Therefore, ATP is sequestered and glycolysis is halted as fructose-6-phosphate synthesis decreases. This mode of inhibition of glycolysis leads to cell cycle arrest, oxidative stress and cell death (Weindruch et al., 2001; Maher et al., 2004; Coleman et al., 2008).

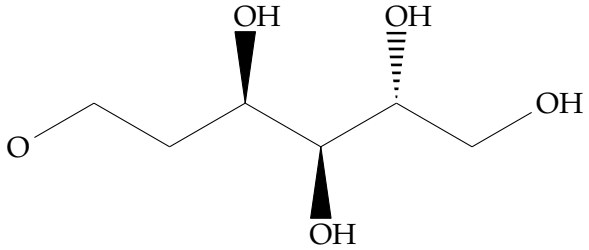

1.6.3 3-Bromopyruvate

3-Bromopyruvate (BrPyr) is a potent inhibitor of glycolysis which results in a severe depletion of ATP. BrPyr is effective at the concentration of 100 µM, which is more potent than 2-DG which requires millimolar concentrations (Pelicano et al., 2006).

BrPyr is a pyruvate analogue harbouring a bromine atom at the carbon 3- position. Studies point towards as a hexokinase inhibitor yet recent work in the Kempa lab showed that it is a potent GAPDH inhibitor (Pietzke, 2015; Cal et al., 2020; Gong et al., 2014). BrPyr causes rapid ATP depletion, oxidative stress, and in turn, the release of cytochrome c, leading to cell death (Pelicano et al., 2006; Ehrke et al., 2015). Animal studies showed that BrPyr has *in vivo* therapeutic activity against liver cancer when given by infusion (Geschwind et al., 2002). Nevertheless, BrPyr is known to present hepatotoxicity reducing its value as a therapeutic (Philippe et al., 2012).

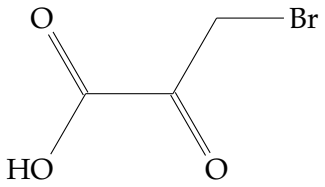

1.6.4 Oxythiamine

Oxythiamine (OT), an analogue of thiamine which is a co-factor in nucleotide biosyntheis. OT inhibits transketolase (TKT) of the the nonoxidative pentosee phosphate pathway and synthesis of ribose-5-phosphate (R5P). More recently, OT has been shown to inhibit transketolase-like 1 protein (TKTL1) (Mariadasse et al., 2016). OT has been shown to induce cell apoptosis and causes a G1 phase arrest *in vitro* and *in vivo* (Boros et al., 1997; Raïs et al., 1999). However, there is sparse evidence for OT being used as a clinical therapeutic. Yet, its use in elucidating the role of TKT and TKTL1 in redox maintenance and cancer cell signalling has proven successful (Wang et al., 2013; Tseng et al., 2018).

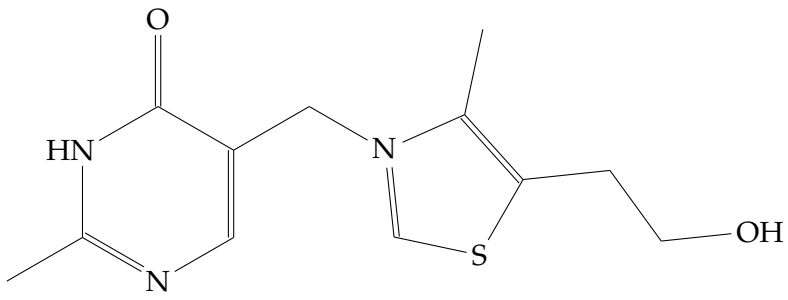

1.7 Methods for measuring metabolism

As described in 1.3.1 cancer cells have specific metabolic alterations which, in theory, describe their phenotype. Understanding and measuring these alterations require analytical methods to extract, quantify and analyse the components of the cell. The components of metabolism are not strictly limited to metabolites. For instance, we may measure changes in the metabolic profile on a metabolite, protein or gene based tier. The advent of the 'Omics' era is comprised

of genomics, transcriptomics, lipidomics, proteomics and metabolomics. Whist genomics and transcriptomics depend on DNA and RNA amplification and sequencing, the measurement of proteomics and metabolomics depend on mass spectrometry (MS) methods (Grimm et al., 2016). We will focus on the methods for measuring the proteomic and metabolic landscape.

1.7.1 GC-MS and Time-resolved metabolomics

Mass spectrometry methods often employ upstream chromatography for the separation of molecules based on their functional properties. In gas chromatography (GC) biological samples are extracted from the cell, separated into polar and non-polar fractions and the metabolites derivitised to add functional groups to the molecules. Compounds that contain functional groups such as OH, NH, CO_2H, and SH are difficult to analyse by GC as they are not sufficiently volatile or are thermally unstable. In order to increase volatility samples are derivitised to add silyl groups to the functional groups. Gas chromatography–mass spectrometry (GC–MS) is a versatile method to quantify metabolite abundance from cell extracts. GC-MS can efficiently distinguish between closely related isomers, for example fructose and glucose. This is essential for the molecules of the central carbon metabolism which observe many isomerisation events. When combined with metabolite labelling strategies, GC-MS can provide models of metabolic pathways as a function of time.

The metabolic profile of a cell will rapidly change upon treatment with a drug, response to external stimuli or intracellular stress. The redundancy of metabolic networks and systems act to remedy the metabolic profile to a homeostatic state. Therefore, methods are required to analyse the flux of metabolites in short periods of time, before the cell returns to a normal state (Pietzke et al., 2014). By applying stable isotope labelled substrates to the cell, the flux of carbons through downstream metabolites can be measured. Following the labelling one can infer both the abundance of the metabolite and the percentage of isotope incorporation (Zasada and Kempa, 2016). This principle is central to the pulsed stable isotope-resolved metabolomics (pSIRM) method (Pietzke et al., 2014).

pSIRM allows for dynamic analysis of the flux of labelled carbons into metabolites. By quenching labelling reactions in short intervals, or pulses, the incorporation of ^{13}C-labelled carbon can be resolved and traced through the metabolic network. This is in contrast to steady state labelling in which, the incorporation of the isotope label reaches a maximum and kinetics cannot be resolved. Simply put, when we apply a drug to the pSIRM labelling system, we wish observe perturbations in the rate of label incorporation and metabolite abundance. With this information we can derive the position in which the network is hindered (figure 1.5).

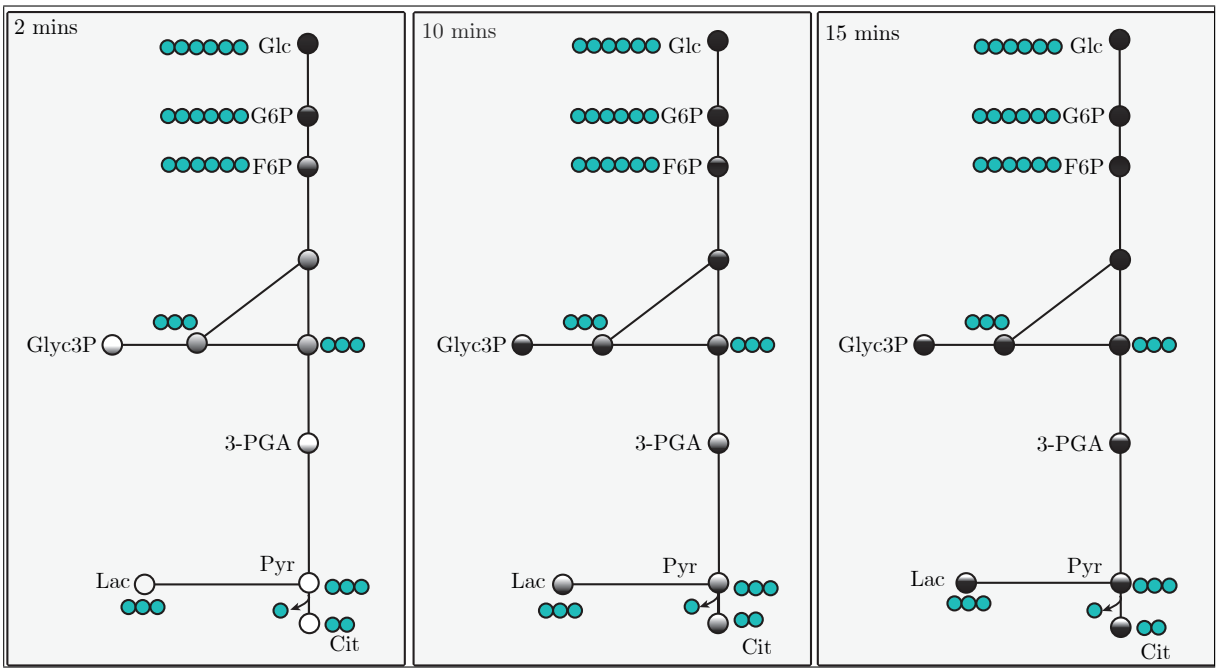

Figure 1.5: Pulsed stable isotope resolved metabolomics (pSIRM) Incorporation of U-^{13}-C-glucose is described through 2 mins, 10 mins and 15 mins of application to cells before label quenching. The proportion of (black) labelled metabolite relative to unlabelled (white) is indicated by the increasing level of black gradient. Blue circles represent the U-^{13}C-labelled carbons derived from U-^{13}C-glucose during glycolysis. The measurement of label incorporation and the relative metabolite pools via GC-MS allows for estimation of pertubations in glycolytic flux during drug treatments. Abbreviations – Cit: Citrate, F6P: Fructose-6-phosphate, Glc: Glucose, G6P: Glucose-6-phosphate, Glyc3P: Glycerol-3-phosphate, Lac: Lactate, Pyr: Pyruvate, 3-PGA: 3-phosphoglycerate.

1.7.2 LC-MS and DI-MS-MS in proteomic and nucleotide analysis

Understanding the metabolic network depends on the characterisation of both the metabolites and the enzymes, or proteins, responsible for their metabolism. Liquid chromatography (LC) operates by firstly flowing a sample over a column to which they bind, then flowing a solvent over the column. The molecules in the sample are separated by their relative affinity for the column and the solvent. Proteins are separated and quantified from cell extracts via LC coupled to mass spectrometry (LC-MS). By employing a shotgun proteomics: proteins are subjected to fragmentation, identified based upon unique peptide sequences, reassembled into full protein identifications and finally quantified. The identification of proteins from their unique peptide sequences requires both experimentally and *in silico* derived data (Zasada and Kempa, 2016). Proteomics is a valuable tool for classifying cells and tissues in disease states such as cancer. Furthermore, proteomic data aid in the understanding different biological mechanisms, which may be targets for drug development. As will become clear in this thesis, proteomic data allow for the discovery of pathways that are perturbed upon drug treatment. The integration of proteomic and metabolomic data in a systems biology approach gives deeper understanding of the dynamics of metabolic pathways. For example, proteomic data capture isoforms of proteins that confer advantages to the cancer cell. As described by Hsu and Hung (2018) the isoform of pyruvate kinase, PKM2, directly and strongly correlates with aggressiveness and glycolytic efficiency in cancer cells. By quantifying and classifying proteins and their isoforms cancer metabolism can be characterised on multiple tiers.

For nucleotide analysis, we may use direct infusion MS-MS (DI-MS-MS) (Banoub and Limbach, 2009). This method employs no chromatography but fragmentation of a selected parent ion to uniquely identify nucleotides with similar masses. Initially nucleotides are enriched from cell extracts and dissolved in methanol. This sample is directly injected into the mass spectrometer which selects the parent ion which in turn is fragmented to give the unique mass of the nucleotide. Both transitions, are used to quantify the amount of nucleotide in the sample (Quinn et al., 2013).

1.8 Neuroblastoma

Neuroblastoma is a paediatric solid tumour occurring in the developmental sympathetic nervous system. The neuroendocrine tumour arises from any neural crest element which results in the developments of tumours in the adrenal glands and/or sympathetic ganglia. Of all childhood cancers, neuroblastoma accounts for 15%, making it the most commonly diagnosed malignancy in the first years of life (Matthay et al., 2016). Approximately 90% of neuroblastoma tumours are diagnosed in children under the age of 10, with a median age of 18 months. Less than 5% of cases occur in adolescents (Cheung et al., 2012). Metastasis are frequently found in bone marrow, lymph node, skin and liver. Over 50% of cases show metastatic tumours (Whittle et al., 2017).

Neuroblastoma is stratified into a staging system of risk developed by the International Neuroblastoma Risk Group (INRG), as described in table 1.1.

Stage	Description
L1	Localised tumour which is confined to a body compartment. The tumour does not involve vital structures as defined by image-defined risk factors.
L2	Localised regional tumour with presence of one or more image-defined risk factors.
M	Distant metastatic disease.
MS	Metastatic disease in children younger than 18 months with metastases confined to skin, liver, and/or bone marrow

Table 1.1: Risk stratification of neuroblastoma from INRG, table adapted from (Cohn et al., 2009)

Neuroblastoma risk is further simplified into 3 risk categories based upon INRG staging, age, histologic category, grade of tumor differentiation, MYCN amplification, 11q aberration and ploidy to divide patients into pre-treatment risk groups. Very low risk is defined as an event-free survival of >85%, low risk is 75–85%, intermediate risk is 50–75% and high risk is <5% (Park et al., 2013). In the low and intermediate risk patients there is a high overall survival of greater than 90% with minimal invasive therapy. However in the high risk groups long-term survival is below 50%. Furthermore, the treatment regimens are severe and invasive with chemotherapy, surgery, radiation and stem cell transplantation (Baker et al., 2010; Whittle et al., 2017). Therapies for high risk groups are extremely invasive and often toxic to the patient. The premise of this thesis is to investigate whether L-GA has scope for as an alternative therapy

which shows low toxicity, is relatively cheap to synthesise and proven to be well tolerated *in vivo* (Mendel et al., 1938; Bennett and Connon, 1966).

1.9 Objectives of the thesis

The work in this thesis aimed to further understand the mechanism of L-glyceraldehyde (L-GA) as an anti-cancer therapeutic. L-GA is significantly researched as a glycolytic inhibitor. However, as will become clear, there are many unexplored avenues of the mechanism of L-GA. We hope that by achieving a deeper understanding of the action of L-GA its full therapeutic value will be recognised. It is expected that L-GA will not only have therapeutic value, but prove to be a useful analytical tool for probing metabolism. Advancements in systems biology and 'Omic' technology permits the analysis of the cell on multiple biological levels. We aim to exploit these technologies to understand the action of L-GA on the metabolome, proteome and the cell's molecular structure.

Initially, the objective was to characterise the efficacy of glyceraldehyde against neuroblastoma cells. In line with previous research (Pietzke, 2015) it was aimed to show that cell growth was inhibited and L-GA induced cell cycle arrest in neuroblastoma cells. Results elucidated morphological changes in the cell. Staining of the cytoskeleton resulted in the hypothesis that the glycolytic inhibition induces a dysregulation of cytoskeletal maintenance.

In the second part of the project, the aim was to measure nucleotide pools in neuroblastoma cells exposed to L-GA. By utilising DI-MS/MS it became apparent that ATP was not the only nucleotide derivative to be depleted upon L-GA treatment. This generated the hypothesis that glycolytic inhibition alone was not the sole source of cellular stress. A novel method was devised to measure nucleotide intermediates to gain a more comprehensive picture of L-GA action nucleotide biosynthesis. In conjunction with nucleotide analysis we aimed to characterise the metabolic profile of L-GA treated neuroblastoma cells. Through a ^{13}C-labelling strategy, we were able to measure the mechanism by which L-GA inhibited NADH-dependent reactions. This evidence provided a framework for experiments probing the effect of oxidative stress on neuroblastoma cells when exposed to L-GA.

In the final sections of the thesis, the effect of L-GA on cellular homeostasis was investigated. Nucleotide analysis, metabolomics, proteomics and fluorescence based techniques, were employed to provide evidence that L-GA generates oxidative stress in the cell through reactive oxygen species. The application of the anti-oxidant N-acetyl-cysteine was investigated to provide a mechanism by which L-GA treatment could be reversed.

Chapter 2

Materials

A list of chemicals, kits and equipment is listed in the supplementary material 5.1.

2.1 Cellular biology methods

2.1.1 Cell lines and Cell Culture

Cell lines were maintained in Dulbeccos modified Eagle Medium (DMEM (GIBCO), without glucose, glutamine, phenol red, and sodium pyruvate) supplemented with 10% fetal bovine serum (FBS, v/v), 2 mM glutamine, and 2.5 g/L glucose and cultivated at 37 °C, 5% CO_2, 21% O_2 and 85% relative humidity. To avoid contact inhibition, cells were passaged every 3-4 days. Adherent cells at a confluence of 60-80% were washed once with 2ml 1x phosphate buffered saline (PBS) and removed from the culture dish surface using TrypLE (Gibco). Following cell detachment, fresh medium was added to quench the trypsin reaction. The cell suspension was centrifuged at 350 xg, 4 min. The supernatant was discarded and the cell pellet was resuspended in fresh pre-warmed media. Cells were split to a ratio relative to the doubling time. The neuroblastoma cell lines: BE-2(C), CLB-GA, GI-ME-N, IMR-32, SH-SY5Y and SK-N-AS were purchased from ATCC and authenticated via the Multiplex human Cell line Authentication Test (Multiplexion). The active primary human foreskin fibroblasts from an infant donor (VH7) were a gift from Petra Boukamp (German Cancer Research Center (DKFZ), Heidelberg, Germany)

2.1.2 Cell freezing and thawing

Cells were harvested following the protocol described in section 2.1.1. The cell pellet was resuspended in chilled DMEM supplemented with 10% dimethyl sulfoxide (DMSO, v/v) to 1-3e+6 cells/mL. The cell pellet was transferred to a labelled cryovial and stored in a Mr. Frosty cooling chamber (Thermo Scientific) at $-80\,^{\circ}$C overnight to cool at almost exactly $-1\,^{\circ}$C per minute, the optimal speed for cell preservation. Frozen cells were stored in a $-80\,^{\circ}$C freezer. Prior to freezing, cells were routinely tested for mycoplasma infection using the Mycoplasma Detection Kit "MycoAlert™ " (Lonza) according to the manufacturers instructions. In order to thaw cells for seeding, cryovials were removed from the $-80\,^{\circ}$C freezer and placed in a 37 °C water bath. Following thawing, cells were resuspended in a 15ml falcon with 10ml pre-warmed

media. The cell suspension was centrifuged at (350 xg, 4 min), and the supernatant removed. Cells were plated into 10 cm plates with 10 ml of fresh media.

2.1.3 Cell number determination and harvesting

Cells were trypsinised and harvested as described in section 2.1.1. Numbers of viable cells were determined using trypan blue exclusion. A cell suspension was prepared with 50 µL 0.4% trypan blue solution (w/v) and 50 µL trypsinised cells. Following mixing 10 µL of the cell suspension was loaded into a cell counting slide. Viability and cell number were measured using the TC10 automated cell counter (Biorad). For protein analysis cells were harvested following section 2.1.1, immediately after trypsinisation cells were washed with 2ml ice-cold 1X PBS, centrifuged for 4 min, 400 xg, 1°C, then snap frozen in liquid nitrogen.

2.1.4 Cell staining and imaging

Cells were seeded on circular glass slides in 6-well plates at 1e+5 cells per well. Cells were allowed to settle for 24hrs. Media was exchanged for treatment with 1X PBS or 1 mM L-GA and incubated for 24 hrs. After treatment media was removed and glass slides were washed with 500 µL 1X PBS. PBS was aspirated and 500 µL of ice-cold acetone was added to each well containing the slides for 10 mins. Slides were then washed 3 times with PBS. 50 µL Cytopainter Phalloidin-iFluor 488 (10X) (ab176753, Abcam) and 50 µL of Deoxyribonuclease I, Alexa Fluor 594 (1mg/ml) (D12372, Thermofischer) was added to each well and incubated for 20 mins in the dark. Following the staining, glass slides were washed 3 times with PBS and stored at 4°C before scanning with a Keyence bz-x700 microscope at 594nm and 488nm filters. Images were processed with ImageJ 1.8.0 software. For unstained cells, cells were imaged via phase contrast microscopy at 10X magnification on a Nikon Eclipse TS2 microscope.

2.1.5 Cell Cycle Analysis

Cells were seeded at 1.5e+6 cells per 10 cm plate and allowed to settle for 24 hrs. Cells were treated with 1 mM L-GA or 1X PBS for 24 hrs or 72 hrs. Following treatment media was collected from the plate and dispensed into a 15ml Falcon tube. Cells were detached from the plate by washing once with 2ml PBS then adding 2ml TrypLE (Gibco). Cells were transferred to the associated Falcon tube and homogenised. Cells were counted as described in section 2.1.3. Cells were then centrifuged for 5min at 250xg, 4 °C. The supernatant was aspirated and discarded. The cell pellet was resuspended in 1ml ice-cold 1X PBS and transferred to a 1.5ml eppendorf tube before centrifuging for 5min at 250xg, 4 °C. The supernatant was aspirated and discarded. The cell pellet was then resuspended by adding 1 ml of ice-cold 70% ethanol in a drop-wise fashion while gently vortexing. The cell suspension was stored overnight at 4 °C to fix the cells. Following fixing, cells were centrifuged for 10 mins at 200xg, 4 °C. The supernatant was aspirated and discarded before washing with 1ml ice-cold 1X PBS. Cells were then centrifuged 5 mins at 250xg, 4 °C. The supernatant was discarded and the cell pellet was resuspened in 500 µL 1X PBS and 25 µL RNase A solution (10mg/ml) (Qiagen). Cells were incubated overnight at 4 °C. Following incubation, 15 µL of propidium iodide (PI) (1mg/ml)

(Thermoscientific) and incubated in the dark for 15 mins at 4 °C. PI Stained cells were transferred to fluorescence-activated cell sorting (FACS)-tubes (Sigma-Aldrich), for Fluorescence-activated cell sorting (FACS) on a BD LSR Fortessa II analyzer (Becton Dickinson) running BD FACSDIVA software v6.0 (BD Bioscience). Cell doublets were excluded by the evaluation of the propidium iodide area (PI-A) versus propidium iodide width (PI-W) density plot. Cell debris was excluded by analysing the forward scatter area and side scatter area (FSC-Area versus SSC-Area). The distinct cell cycle phases: sub-G1, G1/GO, S and G2/M, were determined in a propidium iodide histogram. Further data analysis was performed with the FlowJo-X software (BD Bioscience, v10.0.7r2).

2.1.6 iCelligence cell growth analysis

Cells were seeded at 1.5e+6 cells per 10 cm plate and allowed to settle for 24 hrs. Cells were optimised on the iCelligence™system for a seeding density which provided optimal log-phase growth after 24 hrs from seeding. For both IMR-32 and SH-SY5Y a cell seeding density of 1.5e+4 per plate was found to be optimal. To analyse cell growth, cells from a 10 cm plate were harvested and counted as described in section 2.1.3. The iCelligence™16-well plate was measured for background impedance and electrical contacts were checked. Cells were resuspended to a concentration of 1.5e+5 cells/ml in fresh media, 100 µL of cell suspension was added to each of the 16-wells of the iCelligence™plate. Each of the wells were then adjusted to 200 µL with fresh media. The plate was left for 30 mins at room temperature. The plate was then inserted into the iCelligence™device and cultivated in an incubator at 37 °C, 5% CO_2, 21% O_2 and 85% relative humidity. After 24 hrs media was exchanged in each well to correspond with treatments: L-GA, 1X PBS or Oxythiamine. Impedance readings were taken in triplicate from each well every 15 mins for 120 hrs. Data was analysed with iCelligence DA software (ACEA Biosciences, Inc.)

2.1.7 Reactive oxygen species quantification

Approximately 3-4e+6 cells were grown and harvested from 10cm plates before seeding at 2.5e+4 cells per well in a black-walled transparent bottom 96-well plate (Corning). Cells were allowed to attach overnight then washed once with 1X buffer provided with the DCFDA / H2DCFDA - Cellular ROS Assay Kit (ab113851). Cells were stained with 25 µL DCFDA in 1X Buffer for 45 mins at 37 °C in an incubator. Staining media was removed and media was replaced with the drug treatment program specified in section 3.7.1. Following 4 hrs incubation plates were scanned at Ex/Em: 485/535 nm on a Spectramax iD microplate reader (Molecular Devices). Relative fluorescence was determined relative change to control after background subtraction

2.2 Biochemical methods

2.2.1 Preparation of whole cell lysates

Cell pellets were acquired following the protocol in section 2.1.2. Cell pellets were thawed on ice and lysed with RIPA buffer. RIPA buffer composed of: 50 mM TrisHCl (pH 7.9), 140 mM

NaCl, 1 mM ETDA, 1% Triton x-100 (v/v), 0.1% Na-deoxycholate (v/v), 0.1% sodium dodecyl sulfate (SDS, w/v) and supplemented with 1X complete Easy protease inhibitor (Roche). Samples were sonicated for 25 s (Bandelin Sonorex Digitec DT 100) and vortexed for 10 s. This cycle was repeated 3 times with 10 mins incubation on ice between each round of sonication. Following sonication cells were centrifuged at 14,000 xg for 5 min, 4 °C). The protein concentration was determined with Pierce BCA Protein Assay Kit (Thermo Scientific) as described in section 2.2.2. Depending on the theoretical abundance of the target protein 15 to 30 µg of protein was diluted in 2x SDS sample buffer and stored at −20 °C for sodium dodecyl sulfate polyacrylamide gel electrophoresis (SDS-PAGE) analysis.

2.2.2 Quantification of proteins

The determination of protein concentration was performed with the colourimetric Pierce BCA Protein Assay Kit (Thermo Scientific). Two µL of cell lysate and bovine serum albumin (BSA) standard dilution (50-10,000 µg/mL, diluted in 1x PBS) were mixed with 100 µL of 75 µL ddH_2O and 25 µL of Bradford reagent incubated for 30 min at room temperature in the dark. The absorbance of each sample was read at a wavelength of 562 nm (Infinite 2000, Tecan). Each sample was measured in technical duplicates. A negative control of reagent without BSA or cell lysate was used to deduct the background signal.

2.2.3 SDS-PAGE

SDS-PAGE was performed according to Laemmli with modifications (Laemmli, 1970; Fritsche-Guenther et al., 2018). Fifteen to 30 µg of protein were diluted in 2x SDS sampling buffer (50 mM TrisBase (pH 6.8), 100 mM dithiothreitol (DTT), 2% SDS (w/v), 10% glycerol (v/v), 10 g/L bromphenol blue, diluted in ddH_2O) and denatured for 5 mins at 95 °C under constant agitation. Samples were kept ice, centrifuged at 14,000 xg for 5 min, 4 °C).and pipetted into a pre-casted SDS polyacrylamide gel. A PageRuler pre-stained protein ladder (Thermo Scientific) was used as a molecular marker. The discontinuous electrophoresis was carried out at 60-135 V in the Biorad Mini Protean system with 1x SDS running buffer (25 mM TrisBase, 190 mM glycine, 0.1% SDS (w/v), diluted in H_2O, pH 8.3).

2.2.4 Western blot

Following SDS-page as described in section 2.2.3, proteins were transferred to nitrocelluose or polyvinylidene difluoride (PVDF) membrane, as per the manufacturer's instructions for each antibody. Proteins were transferred to membranes in a semi-dry fashion using a Biorad Trans-Blot Turbo Transfer system for 30 min (25 V, 1 A). Nitroceullose membranes were prepared by incubation in blotting buffer (48 mM TrisBase, 40 mM glycine, 0.075% SDS (w/v), 20% MeOH (v/v) diluted in H_2O) prior to overlay of the membrane. PVDF membranes were activated in 100% MeOH for 25 s, then washed in H_2O for 2 mins and placed in blotting buffer before overlaying with gel. Gels removed from glass casings and placed in blotting buffer, as well as 6 sheets (3 per side of the gel) of Whatmann filter papers. Following blotting membranes were blocked with 5% milk or 1-5% BSA (w/v) in TBS-T (1x TBS (20 mM TrisBase, 137 mM NaCl, 0.1% Tween-20 (v/v)) for 60 mins at room temperature. Incubation of the primary antibody was

performed overnight at 4 °C under constant rolling in 50 ml Falcon tubes. Membranes were washed 3 times for 10 min in TBS-T and probed for 1 hr at room temperature with an HRP-coupled secondary antibody, corresponding to the primary antibody. Three 10 min washing steps were performed with TBS-T, before application of an 1:10 dilution of Amersham ECL Western Blotting detection solution (GE Healthcare). Membranes were exposed on a Fusion FX chemiluminescence microscope system (VILBER).

2.3 Proteomics

2.3.1 Sample preparation of protein lysates and digests

Cells were harvested by scratching cells in 2 ml ice-cold 1X PBS on ice and transferred to a 2 ml tube, cells were centrifuged at 14,000 xg for 5 mins, 4 °C. Cell pellets were lysed in 300 µL urea buffer (8 M Urea, 100 mM TrisHCl (pH 8.5). Samples were sonicated as described in section 2.2.1 and centrifuged at 14,000 xg for 5 mins, 4 °C. Lysates were incubated for 10 mins at 4 °C under constant agitation. Lysates were centrifuged at 14,000 xg for 5 mins, 4 °C, supernatants removed and protein concentration determined via the protocol described in section 2.2.2.
Proteins were alkylated and denatured by addition of 2 mM DTT for 30 min at 25 °C, followed by addition of 11 mM iodoacetamide for 15 min at room temperature in the dark. Following the calculation from the BCA assay 100 µg of protein was aliquoted and digested using Lys-C (Wako, 1:40 (w/w) and immobilised trypsin beads (Applied Biosystem, 5-10 µL, 4 hrs under rotation, 30 °C). Digested proteins were diluted with 50 mM ammonium bicarbonate before tryptic digestion. Digestion was halted with 5 µL of triflouracetic acid (TFA). Twenty µg of digested sample was then desalted and purified on in-house prepared stage tips, the remaining protein digest was stored at −20 °C. Stages tips were primed with 50 µL 100% methanol and 50 µL 0.5% acetic acid (v/v). Stage tips were centrifuged at 300 xg for 7 mins then digests were loaded into the tips and washed once with 50 µL 0.5% acetic acid (v/v). Peptides were eluted by addition of 10µL 0.5% acetic acid (v/v) in 80% acetonitrile. Eluates were dried by centrifugation under vacuum then resuspended in 10 µL 0.5% acetic acid (v/v) and sonicated at room temperature for 5 mins.

2.3.2 Analysis of peptides via liquid-chromatography mass spectrometry (LC-MS)

Peptide mixtures processed via the protocol described in section 2.3.1, were analysed by LC-MS following a shotgun proteomics method (Yates, 2013). LC-MS was performed on an automated high performance liquid-chromatograph (NanoLC 415, Eksigent) coupled to tandem mass spectrometry (Q Exactive HF, Thermo Fisher Sci- entific). Samples were pipetted into 5 µL aliquots into a 96-well plate to be acquired in two technical replicates. Samples were loaded on the column with a flow rate of 450 nL/min. Elution was performed with a flow rate of 400 nl/min using a 240 mins gradient ranging from 5% to 40% of buffer B (80% acetonitrile and 0.1% formic acid) in buffer A (5% acetonitrile in 0.1% formic acid). Chromatographic separation was performed on a 200 cm long MonoCap C18 HighResolution 2000 column (GL Scientific). The nanospray source of the Q Exactive HF was maintained at 2.4 kV and the downstream ion transfer tube at 260 °C. Data were acquired in data-dependent mode with one survey MS scan

(resolution: R=120,000 at m/z 200) followed by a maximum of ten MS/MS scans (resolution: R=30,000 at m/z 200, intensity threshold: 5,000) of the most intense ions.

2.3.3 Data analysis of LC-MS derived proteomics data

Raw data were analyzed using the MaxQuant proteomics pipeline (version 1.5.3.30) and the built in Andromeda search engine with the human Uniprot database (Tyanova et al., 2016). Carbamidomethylation was set as a fixed modification, oxidation of methionine as well as acetylation of N-terminus as variable modifications. The search engine peptide assignments were filtered at 1 % FDR. Peptides with a minimum length of seven amino acids and a maximum of two miscleavages were further processed. Peptides were matched between runs. Label-free quantification (LFQ) was performed for all samples, using razor peptides to define groups of peptides and unique proteins belonging to the razor peptides groups with the largest matches. The software Perseus (version 1.5.6.0) was used to collate LFQ data, perform imputation and $\log_2$ transformation of data prior to input of data into custom R script for further analysis.

2.4 Metabolomic analysis

As described in section 1.7.1, pSIRM permits the labelling of glycolytic intermediates in short time frames. The method, developed by Dr. Matthias Pietzke and Dr. Stefan Kempa, was used to acquire relative quantification of glycolytic intermediates, ^{13}C-incorporation and relative ^{13}C-labelled metabolite quantities (Pietzke et al., 2014). U-^{13}C-labelled glutamine and U-^{13}C-labelled - where U denotes all carbons labelled, glucose were used to probe the TCA cycle and glycolysis, respectively.

2.4.1 Cell culture for pSIRM analysis

Cells were seeded at 1.5e+6 cells 24 hrs prior to treatment and pSIRM. Three biological replicates were used per treatment and time-point. Fresh media was exchanged 4 hrs prior to initiating pSIRM to permit high glycolytic activity and remove potential inhibitors. Cell culture media was replaced by media containing U-^{13}C-glucose and incubated at 37 °C for 2, 5, 10 or 15 mins before quenching. In the case of U-^{13}C-glutamine labelling plates were incubated for 5, 15, 30 or 45 mins. Following incubation with the labelled substrate cells were quickly washed with a buffer consisting of 140 mM NaCl, 5 mM HEPES, pH 7.4, supplemented with the corresponding ^{13}C-substrate and drug of interest. Immediately after removal of the wash buffer, cell metabolism was quenched by the addition of 5 mL ice-cold 50% MeOH supplemented with 2 µg/mL cinnamic acid to the plate. Cinnamic acid served as an internal extraction standard. The cells were scratched on ice in the plate with a cell scraper and pipetted repeatedly to homogenise the cells. The cell suspension was transferred to a 15 mL Falcon tube containing 1 ml of 100% chloroform. Falcons were shaken to initiate metabolite extraction and placed into liquid nitrogen.

2.4.2 Extraction of metabolites

Falcons were removed from liquid nitrogen and shaken for 1 hr at 4 °C. Following shaking, the Falcon tubes were centrifuged at 14,000 xg for 10 min at 4 °C for extraction of polar metabolites into the methanol phase. 4.5 ml of methanol containing the polar phase was collected and transferred to a new 15 ml Falcon. Polar phases were dried down under vacuum in a speed vac. After complete evaporation of the methanol, metabolites were resuspended in 600 µL of 20% MeOH, shaken for 1 hr at 4 °C and then centrifuged 14,000 xg for 10 min. Polar metabolites were split into triplicate eppendorfs, dried down under vacuum and then stored at −20 °C until preparation for GC-MS.

2.4.3 Measurements of metabolites via GC-MS

Sample preparation for GC-MS

Polar metabolites, identification standards and a quantification dilution series dried down in a speed vac prior to derivatisation. Derivatisation was performed as per the following protocol described in Kempa et al. (2009). 20 µL of methoxyamine hydrochloride solution (40 mg/mL MeOx in 1 mL pyrimidine) were added to the samples followed by incubation in a heating block at 30 °C with constant agitation at 1400 rpm for 90 mins. Following incubation, 80 µL of N-methyl-N-[trimethylsilyl] trifluoroacetamide (MSTFA, supplemented with a C17 alkane mixture) was added to the each of the samples, standards and quantification mixes and shaken at 37°C or 60 mins. Excess alkalane/MSTFA solution was dispensed into a glass vial and used as a wash during GC-MS measurement. After incubation, samples were centrifuged at 14,000 xg for 10 mins. Supernatants were aspirated and split into duplicate glass vials for GC-MS measurement.

GC-MS measurements

Metabolite analysis was performed on a 1D gas chromatograph coupled to time of flight mass spectrometer (GC-ToF-MS, Pegasus IV-ToF-MS-System, LECO), samples were handled with an auto-sampler (MultiPurpose Sampler 2 XL, Gerstel). The samples were injected in split mode (split 1:5, injection volume 1 µL) in a temperature-controlled injector (CAS4, Gerstel) with a baffled glass liner (Gerstel). The following temperature program was applied during sample injection: initial temperature of 80 °C for 30 s followed by a ramp with 12 °C/min to 120 °C and a second ramp with 7 °C/min to 300 °C and final hold for 2 min. Gas chromatographic separation was performed on a Restek Rxi-5ms column (Restek, Bad Homburg Germany). Helium was used as carrier gas with a flow rate of 1.2 mL/min. Gas chromatography was performed with the following temperature gradient: 2 min heating at 70 °C, first temperature gradient with 5 °C/min up to 120 °C and hold for 30 s; subsequently, a second temperature increase of 7 °C/min up to 350 °C with a hold time of 2 min. The spectra were recorded in a mass range of m/z = 60 to 600 mass units with 20 spectra/s at a detector voltage of 1650 V.

Analysis of GC-MS data

The GC-MS chromatograms were processed with ChromaTOF software (LECO). To accommodate for the difference in retention times of metabolites between GC-MS runs and differing

column we applied a retention index (RI) method, aligned to each of the alkanes in the C17 mix (Kováts, 1958). Mass spectra data were extracted from the Chromatof software using proprietary methods and processed using the software tool MetMax[1] or the in-house software Maui-SILVIA (Kuich et al., 2015). Mass isotope distribution (MIDs) of unlabelled metabolites were used for the correction of the natural abundance of isotopes. The theory behind the calculation of label incorporation is described in detail in (Pietzke et al., 2014). Mass fragments were specified based upon individual metabolites and chosen to calculate the ^{13}C-incorporation which are listed in the supplementary material, 5.1.2.

2.5 Measurement of nucleotides via DI-MS-MS

2.5.1 Sample preparation for DI-MS-MS

Polar metabolites, including nucleotides, were extracted following the same protocol described in 2.4.1. Nucleotide enrichment followed the protocol described by (Lorkiewicz et al., 2012), with minor modifications. Initially, dried polar metabolites were resuspended in 5 mM hexylamine buffer A (5 mM hexylamine, pH adjusted to 6.3 with acetic acid) to give 3e+5 cells in 10 µL and kept on ice. Samples and nucleotide calibration standards (10 µM - 20 nM in 5 mM hexylamine buffer, pH 6.3) were centrifuged at 4 °C at 14,000 xg for 5 mins. ZipTips (Millipore) were conditioned by aspirating five times 10 µL of 100% MeOH and, five times 10 µL of buffer A. Samples were loaded onto the C18 solid phase of the ZipTip by 8 cycles of aspirating and dispensing 10 µL, followed by 4 cycles of washing with 10 µL of buffer A. Elution was performed by aspirating and dispensing 12 times with 10 µL of elution buffer (70% buffer A, 30% buffer B (90% MeOH, 10% NH_4AC, pH adjusted to 8.5 with NH_4OH)). The eluted nucleotides were diluted with 20 µL of MeOH before DI-MS-MS analysis.

2.5.2 DI-MS-MS acquisition

Measurement of nucleotides was performed by direct-infusion mass spectrometry on a TSQ Quantiva triple quadrupole mass spectrometer (Thermo Scientific) coupled to a Triversa Nanomate nanoESI ion source (spray voltage: 1.5 kV, head gas pressure: 0.5 psi) and argon used as collision gas (pressure: 1.5 mTorr). FWHM Resolution for both Q1 and Q3 was set at 0.7. Data acquisition was run for 3 min per sample, using a cycle time of 3.3 sec and total acquisition of 55 SRM scans for each nucleotide. The sum of the two transitions for each of the 40 nucleotides were measured in negative mode. All transitions and unique fragment sizes are documented in supplmentary material 5.1.1.

2.5.3 Analysis of direct infusion MS data

The software Xcalibur (Thermo Fisher Scientific) was used to manually check the quality of each measurement, scans which presented poor signal acquisition or stalling in scanning were omitted. Data was further processed with an OpenMS package, and using in-house developed R scripts.

[1] http://gmd.mpimp-golm.mpg.de/apps/metmax/

2.6 Statistics

Statistical analysis were performed using the RStudio Desktop software (version 1.1.383). All data are presented as mean ± SE (standard error of the mean) unless specified otherwise. Where data was assumed to be not normally distributed, for example nucleotide analysis, Wilcoxon statistical tests were employed using the untreated sample (PBS / 0 mM L-GA) as a reference group, unless specified otherwise. Holm post-hoc correction was included where multiple tests were performed. To test significance between multiple groups of parametric data, a pairwise-T-test with Holm post-hoc correction was applied. The significance levels were set at: ns $p \geq 0.05$; * $p \leq 0.05$; ** $p \leq 0.01$; *** $p \leq 0.001$; **** $p \leq 0.0001$

Chapter 3

Results

3.1 Glyceraldehyde Inhibits the Growth of Neuroblastoma Cells

Previous work in the Kempa lab (Pietzke, 2015) showed that low millimolar concentrations of L-glyceraldehyde (L-GA) inhibited the growth of T98G and HEK293 cells. Specifically, following 24 hrs incubation of L-GA an EC_{50} was found at 940 µM and 920 µM for T98G and HEK293 respectively. The aim was to find, if any, the EC_{50} of L-GA on neuroblastoma cells: IMR-32 and SH-SY5Y and a non cancerous control cell line VH7.

3.1.1 L-GA inhibits neuroblastoma cell growth in a concentration dependent manner

In the attempt to derive an EC_{50} concentration of L-GA for IMR-32, SH-SY5Y and VH7 cells were cultured in media containing increasing concentrations of L-GA (0-1.5 mM). Following 24 hrs of incubation, cells were trypsinised and viable cell counts were taken via the trypan blue exclusion assay (Figure 3.1). The EC_{50} was set at the point of which the ratio of viable cells counted relative to the 0.0 mM control was 0.5 or below. VH7 cells did not achieve an EC_{50} at the highest L-GA concentration used in this experiment. IMR-32 and SH-SY5Y both achieved a similar EC_{50} at L-GA concentrations: 0.76 mM and 0.55 mM respectively. Interestingly, these results are similar to the L-GA concentrations found to inhibit glycolysis during experiments conducted in the 1940s, whereby sub 1 mM L-GA inhibited production of lactic acid in muscle extracts (Stickland, 1941).

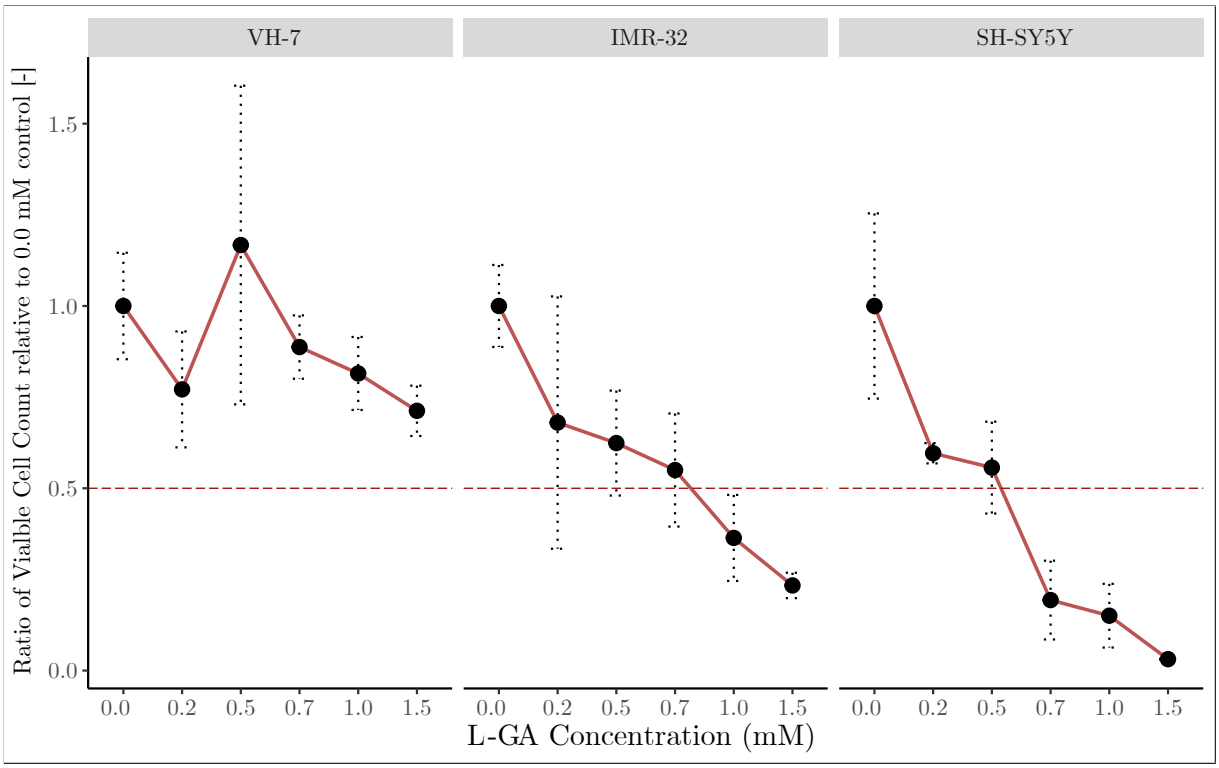

Figure 3.1: Inhibition of neuroblastoma cell growth is dependent on L-GA concentration. Cell lines VH-7, IMR-32 and SH-SY5Y cells were incubated with varying concentrations of L-GA for 24 hours after seeding at 1.5e+5 cells per well in a 6 well plate. Viable cell counts were taken for each L-GA concentration via the trypan exclusion method and normalised to 0.0 mM control. The EC_{50} is denoted by a dotted red line with errors bar representing the $\pm$ SD of the mean for three biological replicates.

In addition to measuring the cells present via trypan blue exclusion, cells were imaged via phase contrast microscopy (Figure 3.2). Following 24 hrs treatment of 1 mM LGA there was a significant reduction in the amount of cells adherent to the plates, in both SH-SY5Y and IMR-32 relative to the PBS control. However, it appeared that SH-SY5Y cells were slightly less sensitive. VH-7 showed an apparent change in morphology, yet cells remained adherent at 1 mM L-GA. As shown, neuroblastoma cells presented significant morphological changes and reduction in cell number following L-GA treatment. Therefore, the aim was to show that this is a rapid process by which cellular growth is inhibited within 24 hrs.

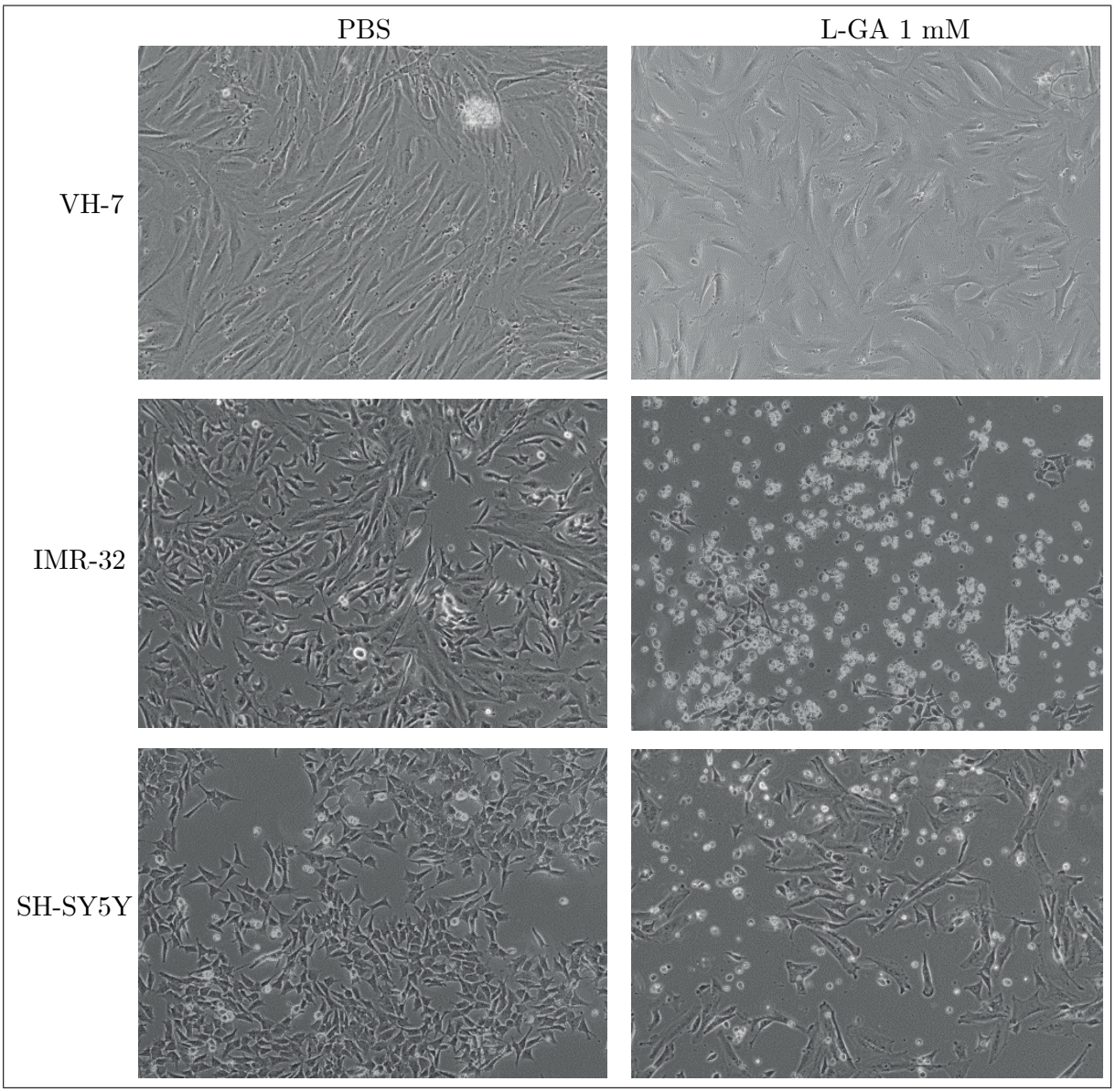

Figure 3.2: L-GA causes detachment of neuroblastoma cells from plates and morphological changes in VH-7 cells. Cell lines VH-7, IMR-32 and SH-SY5Y cells were incubated with 1 mM L-GA for 24 hours after seeding at 1.5e+5 cells per well in a 6 well plate. Cells were imaged via phase contrast microscopy at 10X magnification on a Nikon Eclipse TS2 microscope.

3.1.2 L-GA is a fast acting and potent inhibitor of neuroblastoma cell proliferation

As stated, the EC_{50} of L-GA for IMR-32 and SH-SY5Y was in the vicinity of 0.6 mM, when considering both cell lines. Given this, cells were treated with 1 mM glyceraldehyde for further experiments to achieve a consistently significant and observable response.

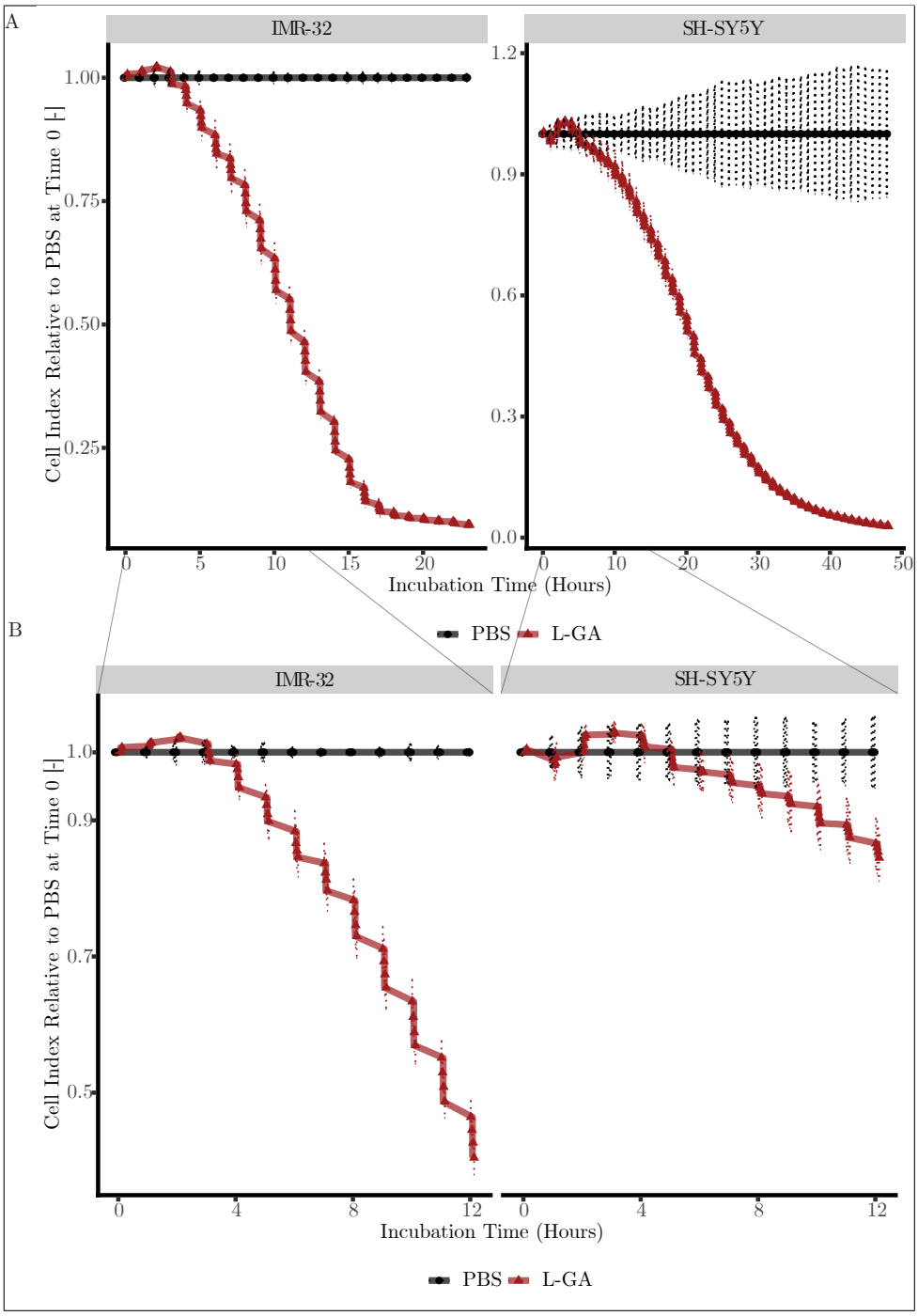

Figure 3.3: Inhibition of Growth by Glyceraldehyde. Cell lines IMR-32 and SH-SY5Y were seeded at a density of 1.5e+4 cells per well in a 16-well RTCA iCelligence™ chip. Three wells were used per cell line and treatment. Cells were treated with either PBS or 1 mM L-GA 24 hrs post seeding, defined as Time 0 hrs. A: Graphs represent the cell index normalised to the PBS control over a period of 24 hrs and 50 hrs for IMR-32 and SH-SY5Y respectively. Measurements were taken in triplicate every 15 minutes. Error bars represent ± SD of the mean. B: Graphs presented follow the format of those found in A. The X-axis has been curtailed to 12 hrs to show the relative efficacy of L-GA between IMR-32 and SH-SY5Y within this time period.

The RTCA iCelligence™ system allows for triplicate measurements in 15 minute intervals to characterise: cell adhesion, morphology and proliferation. Following the method described in Chapter 2.1.6, IMR-32 and SH-SY5Y were treated with 1 mM L-GA over a period of 72hrs (Figure 3.3, A). Both cell lines treated with L-GA showed significant reduction in the cell index - a measurement of the impedance in the conductivity of the iCelligence chip induced by adherent

cells. Relative to PBS treated cells, L-GA reduced the cell index by 50% approximately 12 and 20 hrs post application of the drug for IMR-32 and SH-SY5Y, respectively. It was found that IMR-32 approaches a baseline cell index post 20 hrs incubation. However SH-SY5Y required a significantly longer incubation time - in excess of 40 hrs - to approach a baseline cell index comparable to IMR-32. When examining the initial effects of L-GA, defined as sub 12 hrs, it was apparent that L-GA is a potent and fast acting inhibitor of neuroblastoma cell growth (Figure 3.3, B). Nevertheless, there was a heterogeneous response between IMR-32 and SH-SY5Y. Specifically, following 12 hrs incubation the cell index for IMR-32 was approximately halved whereas the cell index for SH-SY5Y was reduced to 0.85 to that of the control.

3.1.3 L-GA is a more potent inhibitor of neuroblastoma cell growth than D-GA

Following this experiment, the comparative efficacy of the enantiomer D-glyceraldehyde was assessed. Furthermore, the racemic mixture, DL-glyceraldehyde has been shown to be less effective at arresting cancer cell metabolism than the L- enantiomer (Warburg et al., 1963). A long-term treatment with D-, L- and DL-glyceraldehyde to define the relative effects on cell growth was conducted.

Cell lines IMR-32, SH-SY5Y and VH-7 were treated over a period of 72 hrs with 1 mM of L-, D-, or DL-GA to address the relative efficacy of each enantiomer. Viable cell counts were assessed at 24, 48, 72 and 96 hrs using trypan blue exclusion method and semi-automated cell counting. For IMR-32 and SH-SY5Y similar results are presented (Figure 3.4). Following 24 hrs of incubation with L- and DL-glyceraldehyde cell counts were below detectable levels when counted via the method described in section 2.1.3. Inhibition of cell growth persisted over the 72 hrs incubation. Interestingly, treatment with D-GA affected IMR-32 and SH-SY5Y in a similar manner, yet it did not ablate growth completely. The viable cell count for D-GA treated neuroblastoma cells was between 4- to 5-fold lower than PBS treated cells after 72 hrs.

The fibroblast cell line, VH-7, showed a less extreme response to GA treatment than the neuroblastoma cell lines. When addressing the 72 hrs incubation time point for VH-7, it was observed that L-GA caused the greatest reduction in viable cells compared to the PBS control. DL- and D-GA followed in relative levels of efficacy in reducing cell growth.

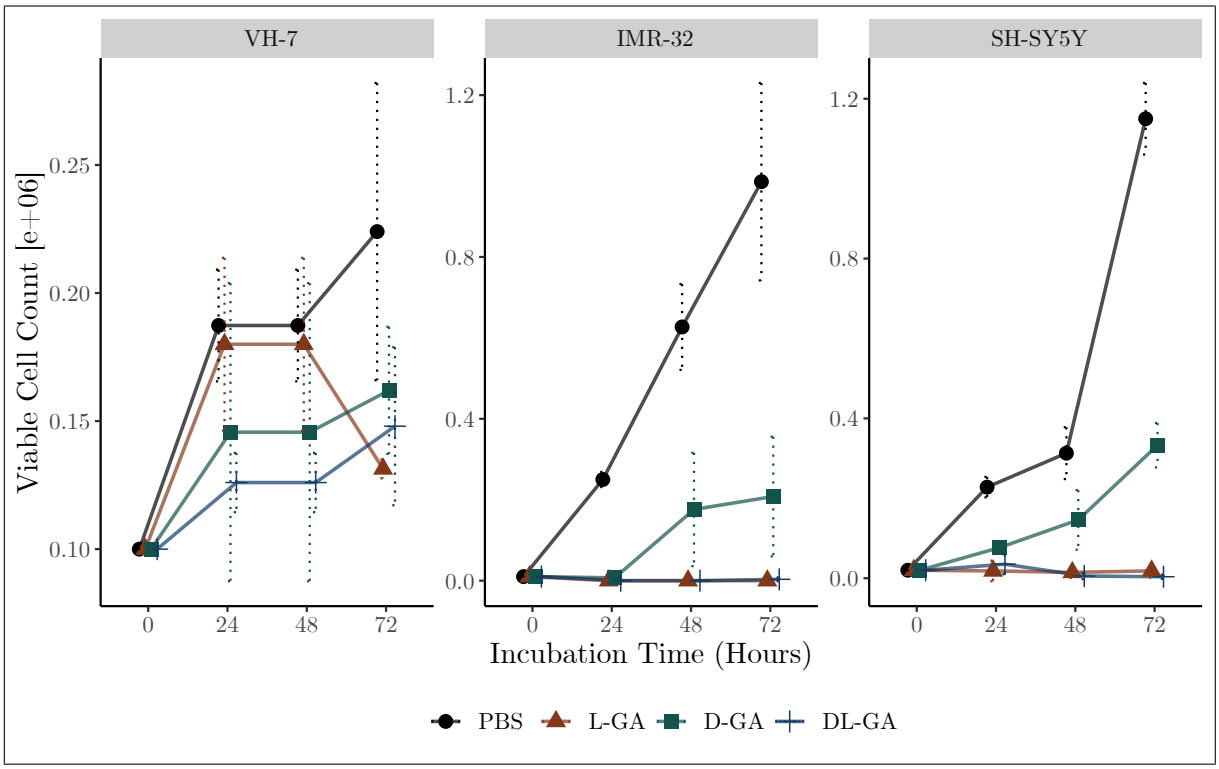

Figure 3.4: Inhibition of neuroblastoma cell growth by glyceraldehyde enantiomers. Cell lines VH-7, IMR-32 and SH-SY5Y cells were incubated with 1 mM L-GA (red), D-GA (green), DL-GA (blue), or PBS (black) for 72 hrs after seeding. VH-7 was seeded at 1.5e+4 cells; IMR-32 and SH-SY5Y were seeded at 1.5e+5 cells per well in a 6 well plate. Viable cell counts were taken every 24 hrs via the trypan exclusion method. Error bar representing the ± SD of the mean for three biological replicates.

When collating the results described so far it is postulated that L-GA causes: a rapid inhibition of neuroblastoma cell growth, detachment of cells from the culture plate surface and apparent morphological changes. Given this, the effect of L-GA on the structure and maintenance of the cytoskeleton was characterised.

3.2 L-GA causes morphological and cytoskeletal aberrations

Glyceraldehyde is widely considered to be an inhibitor of glycolysis, and an inhibitor of ATP synthesis (Stickland, 1941; Needham et al., 1951). It was hypothesised that the changes in cell morphology shown by phase-contrast microscopy is a result of the dysregulation in the maintenance of the ATP-dependent microfilaments of the cytoskeleton. A mature cytoskeletal microfilament is composed of globular monomeric subunits of actin (G-actin) polymerised into filamentous actin (F-actin). The maintenance of the F-actin polymer is an ATP-dependent reaction. Therefore, the inhibitory action of L-GA on glycolysis may perturb actin polymerisation.

3.2.1 Actin polymerisation is dysregulated upon L-GA treatment

In order to assess the effect of L-GA on the cytoskeleton, cells were stained with probes for F-actin and G-actin simultaneously for microscopic imaging. As described in more detail in 2.1.4, phalloidin and DNase I selectively bind to F- and G-actin, respectively. Using fluorophore

conjugated phalloidin and DNase I the cytoskeletal proteins were imaged via fluorescent microscopy. Briefly, cell lines: IMR-32, SH-SY5Y and VH-7 were treated with either PBS or 1 mM L-GA for 24 hrs. Following treatment, cells were fixed to glass slides and probed for F- and G-actin simultaneously. Slides were imaged via fluorescent excitation and emission (ex/em) 493/517 nm for phalloidin and 590/617 nm for DNase I (Figure 3.5, A). The total intensity of the fluorescence from each probe was then measured for 3 individual slides from each cell line and treatment condition. For neuroblastoma cells the fluorescence of DNase I 594 probe (G-actin) relative to phalloidin 488 probe (F-actin) was significantly increased upon L-GA treatment (Figure 3.5, B). This resulted in a decrease in the F- to G-actin ratio. For IMR-32 the ratio of F- to G-actin decreased to 0.43 ($\pm$ 0.03) upon L-GA treatment relative to PBS. SH-SY5Y presented a decrease to 0.67 ($\pm$ 0.02) upon L-GA treatment relative to the PBS control.

The fibroblast cell line VH-7 did not show a significant increase in G-actin upon L-GA treatment, or indeed a decrease in F-actin. Although it was not significant, there was a 1.30-fold ($\pm$ 0.06) increase in the F- to G-actin ratio upon L-GA treatment relative to PBS treated cells. This data suggests that L-GA causes a dysregulation in the F-actin structures of neuroblastoma cells, yet not in the fibroblast cell line. The increase in G-actin in conjunction with F-actin puncta is indicative of unpolymerised F-actin. This data gives weight to the argument that L-GA depletes available ATP for actin polyermisation. Given that cellular division is a process in which regulation of the cytoskeletal is essential, it was assessed whether cellular division is also compromised. Nuclei of cells can be stained and imaged using 4,6-diamidino-2-phenylindole (DAPI). The hypothesis was that by staining nuclei one would observe multiple nuclei per cell, if cellular division was hindered. Following the method stated above, cells were treated and fixed onto glass slides and nuclei stained with DAPI. To assist with defining cell boundaries the phalloidin 488 probe was also used to image fixed cells (supplementary material, Figure 5.1).

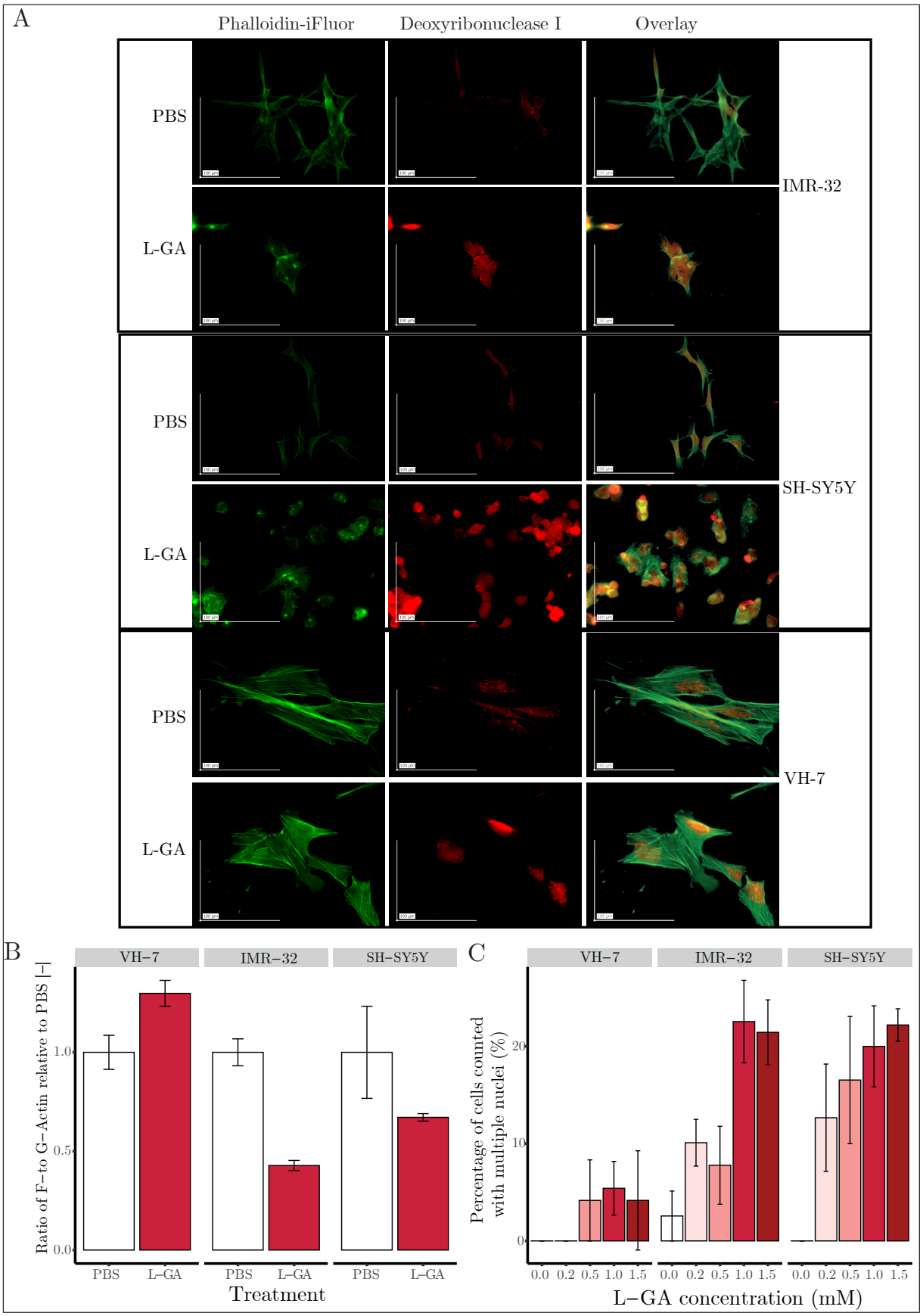

Figure 3.5: L-GA causes dysregulation of actin polymerisation. A: Cell lines VH-7, IMR-32 and SH-SY5Y were seeded at 1.5e+5 cells per well on glass slides in a 6-well plate. Following 24 hrs settling, cells treated for 24 hrs with 1 mM L-GA or PBS. Cells were then fixed to the glass slide with 100% acetone. Slides were incubated with Phallodin-iFluor(F-) or Deoxyribonuclease I (G-) actin probes then imaged at 60X mag, F- Actin: 1/25s exposure G-Actin 1/12s exposure using Keyence Bz-x700 microscope with 30% contrast enhancement. B: Intensities of probe fluorescence were measured for Phallodin-iFluor(F-) or Deoxyribonuclease I (G-) from 3 independent slides from each treatment condition. Ratios of F- to G- actin were calculated and normalised to PBS control. Error bars represent the ± SD of the mean for three biological replicates. *continued on next page*

Figure 3.5: (*Continued from previous page,*) C: Following the same method as in figure A, cells were treated with a range of L-GA concentrations (0-1.5 mM) and multiple nuclei were counted via staining with DAPI. Data represents the percentage of cells that were counted harbouring multiple nuclei (%). Three slides were counted per L-GA concentration. Error bars represent the ± SD of the mean.

Cell lines: VH-7, IMR-32 and SH-SY5Y were treated with a range of L-GA concentrations (0-1.5 mM). For each cell line nuclei from cells from 3 slides were counted, permitting the calculation for the percentage of cells that harboured multiple nuclei. The percentage of neuroblastoma cells with multiple nuclei increased as a function of L-GA concentration (figure 3.5, C). VH-7 exhibited less multi-nucleation events compared to neuroblastoma cells lines at equivalent L-GA concentrations. Neuroblastoma cell lines exhibited similar multi-nucleation values; IMR-32 cells treated with 1 mM L-GA showed 23% (± 4.2%) whereas SH-SY5Y presented 20% (± 4.1%).

The combination of the dysregulation of the cytoskeleton and multi-nucleation of cells leads to the hypothesis that cells undergo a cell cycle arrest. Indeed, it was shown in previous work at the Kempa lab that T98G and HEK293 cells enter an S-phase arrest when exposed to L-GA for 18 hrs (Pietzke, 2015). Therefore, the aim was to assess whether this occurs in neuroblastoma cells.

3.3 L-GA causes cell cycle arrest

Cellular division is an energetically demanding process, requiring synthesis of DNA, biomass and macromolecules. In proliferating cells the rate of glycolysis is high to meet these energy demands. The regulation of the cell cycle is a highly integrated and complex mechanism which binds the metabolic input to key cell cycle activators or repressors (Seyfried and Shelton, 2010; Buchakjian and Kornbluth, 2010).

In the event of glycolytic inhibition via L-GA the cell cycle may be arrested or dysregulated as the cell responds to a lack of nutrient availability. Continuing from the previous section, the aim was to gain further insight into the multi-nucleation phenotype observed and whether this is a function of cell cycle arrest.

3.3.1 Cell cycle arrest is a common phenotype in L-GA treated cells

In cooperation with the AG Deuzber Laboratory (Charité, Berlin), a panel of neuroblastoma cell lines, including the fibroblast control cell line VH-7, was chosen to assess whether L-GA causes a common cell cycle phenotype. Neuroblastoma cell lines: BE(2)-C, IMR5/75, SH-SY5Y and SK-N-AS, CLB-GA and GI-ME-N constituted the testing panel. Additionally VH-7, SH-SY5Y and IMR-32 was tested in our laboratory.

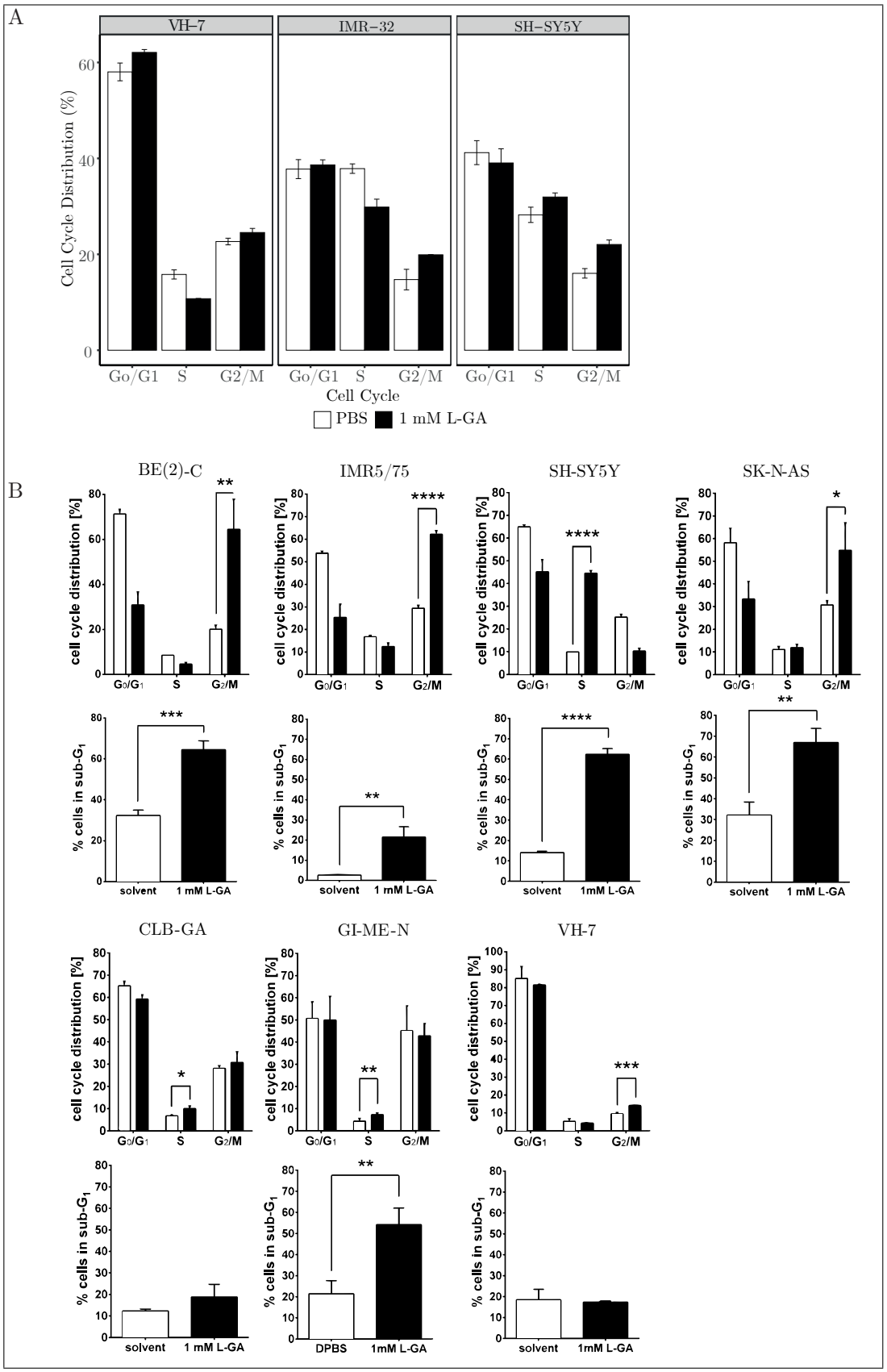

Figure 3.6: L-GA causes cell cycle arrest in neuroblastoma cells. A: SH-SY5Y, IMR-32 and VH-7 were treated with 1 mM L-GA or PBS for 24 hrs and subjected to flow cytometry analysis. Cells in the media and adherent to the plates were collected and stained with propidium iodide. Cells were subjected to flow cytometric analysis and gated for cell cycle phases: G_O/G_1, S and G_2/M. The mean of the percentage of cells in each phase was calculated from 3 biological replicates. Error bars represent $\pm$ SD of the mean. Cell lines: BE(2)-C, IMR5/75, SK-N-AS, SH-SY5Y CLB-GA, GI-ME-N and VH-7 were treated for 72 hrs with 1 mM L-GA or PBS. Cells were collected and stained as in A. Cells were subjected to flow cytometric analysis and gated for cell cycle phases: G_O/G_1, S and G_2/M. Sub-G_1 fractions were also calculated. The mean of the percentage of cells in each phase was calculated from 3 biological replicates. Error bars represent $\pm$ SD of the mean. P values shown: ns $p \geq 0.05$; * $p \leq 0.05$; ** $p \leq 0.01$; *** $p \leq 0.001$; **** $p \leq 0.0001$. All data provided in B, was carried out by Annika Sprüssel and Daniela Tiburtius at the AG Deuzber Laboratory (Charité, Berlin)

Following the method described in chapter 2.1.5, cells were treated with 1 mM L-GA for 24 hrs before harvesting the media and adherent cells to collect the complete cellular population. Cells were then stained with propidium iodide to stain for DNA and analysed by flow cytometric analysis. Cells were gated into G_O/G1, S or G_2/M cell cycle phases and the distribution was calculated in percentage. Cell lines: VH-7, IMR-32 and SH-SY5Y investigated as shown in (Figure 3.6, A). IMR-32 showed an 8.1% ($\pm$ 0.98%) decrease in cells in the S phase and an increase of 5.2% ($\pm$ 2.14%) for cells for in the G_2/M phase upon L-GA treatment. SH-SY5Y cells observed a 3.7% ($\pm$ 0.85%) increase in the S-phase upon L-GA treatment. A panel of neuroblastoma cell were treated for 72 hrs and subjected to flow cytometric analysis (Figure 3.6, B). Following 72 hrs incubation with 1 mM L-GA, neuroblastoma cell lines: BE(2)-C, IMR5/75, SK-N-AS showed a significant increase in the G_2/M phase. SH-SY5Y, CLB-GA and GI-M-EN presented significant increases in the S-phase upon L-GA treatment. It is to be noted that CLB-GA and GI-M-EN did not show a decrease in the G_O/G_1 phase which is discordant with other neuroblastoma cell lines. In VH-7 there was a minute yet significant increase in the G_2/M phase in response to L-GA. All neuroblastoma cell lines except CLB-GA presented a significant increase of cells in the sub-G_1 phase, suggestive of a strong apoptotic response. VH-7 did not show an increase in the sub-G_1 fraction in response to L-GA.

The cell cycle crisis that neuroblastoma cells experience lead to the hypothesis that essential nutrients aren't available to the cell. The regulation of the cell cycle is tightly controlled. Checkpoint kinases receive input from nutrient levels to initiate entry and exit from cell cycle phases. Consequently, the aim was to quantify nucleotide pools to assess whether L-GA reduces these essential cell cycle molecules.

3.4 Glyceraldehyde causes a depletion of nucleotide pools

The depletion of nucleotide pools results in a stalling of DNA synthesis and cell cycle arrest. Furthermore, the imbalance of purine and pyrimidine nucleotide pools induce pro-apoptotic pathways and inhibit cell proliferation (Messina et al., 2004; Camici et al., 2019). As described in 1.3.3, the *de novo* synthesis of nucleotides originates from the production of R5P derived from the oxidative or non-oxidative pentose phosphate pathway (PPP). The oxidative PPP synthesises R5P via G6P, 6-PGL, 6-PGA and Ru5P. Two moles of NADPH are generated via the decarboxlyation of 6-PGA to Ru5P, this process is essential to replenishing NADPH pools for redox mechanisms. The non-oxidative pathway produces R5P through the cycling of carbons from F6P and GA3P as described in figure 1.2. It is of particular interest that the non-oxidative pathway requires GA3P as a substrate. It was hypothesised that L-GA perturbs the synthesis of nucleotides via disruption of R5P synthesis, thereby inducing limited nucleotide availability for correct cell cycle maintenance.

3.4.1 L-GA depletes nucleotide pools following 24 hrs incubation

Initial experiments aimed to follow previous methodology, whereby IMR-32, SH-SY5Y and VH-7 were treated with 1 mM L-GA for 24 hrs. Cells were harvested, nucleotides enriched and measured as described in section 2.5. In neuroblastoma cells the average nucleotide pools were significantly depleted following 24 hrs incubation with 1 mM L-GA, (Figure 3.7). Specifically,

IMR-32 showed a mean fold change of 0.19 ($p \leq 0.0001$) relative to PBS, whereas SH-SY5Y presented a mean reduction of 0.21 ($p \leq 0.0001$). The fibroblast control cell line VH-7 showed significantly less reduction in nucleotide pools compared to the neuroblastoma cell lines 0.83 ($p \leq 0.05$).

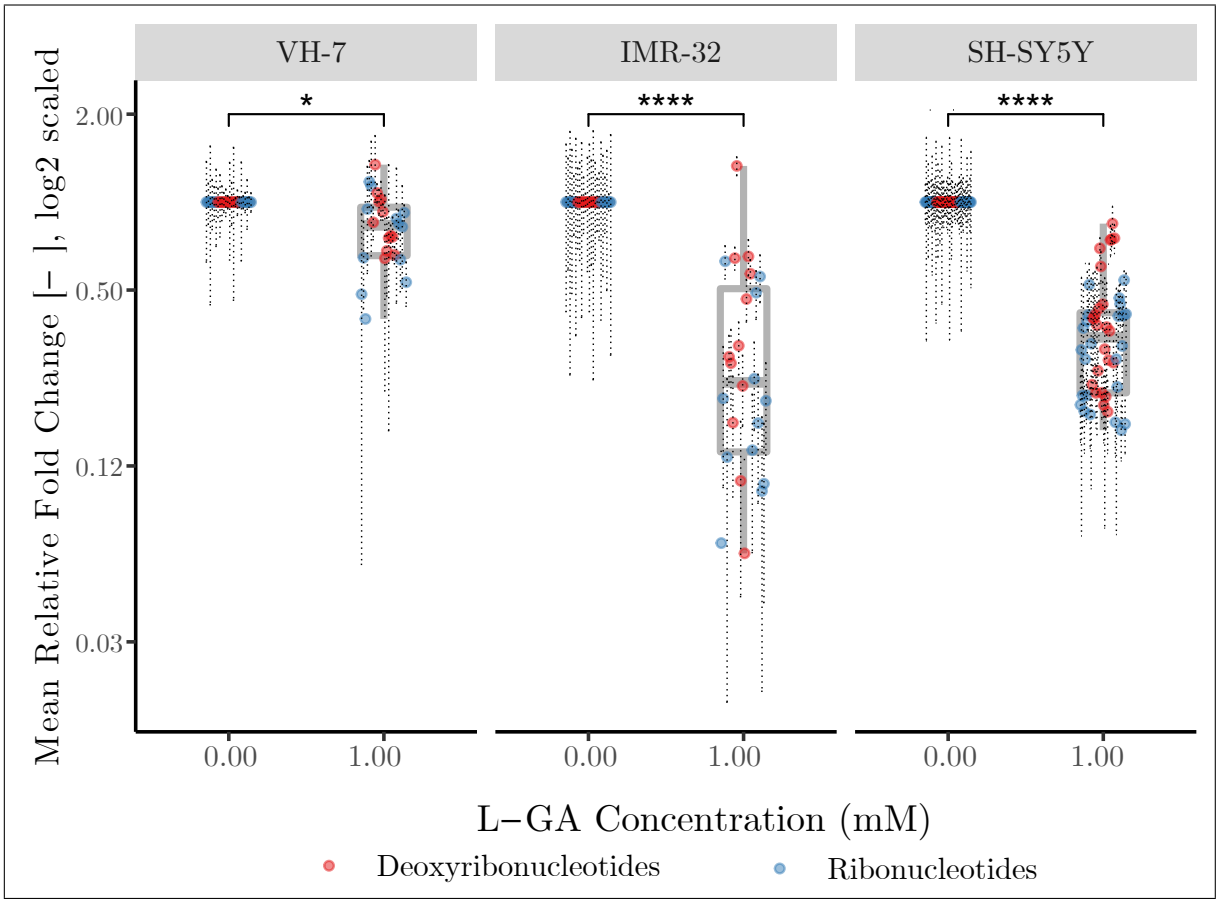

Figure 3.7: L-GA depletes nucleotide pools in neuroblastoma cells after 24 hrs. Cell lines VH-7, IMR-32 and SH-SY5Y were treated with 1.0 mM LGA or 0.0 mM L-GA for 24 hrs. Nucleotides were extracted from cell lysates and measured by DI-MS/MS. Boxplots present the mean fold change relative to 0.0 mM for ribonucleotide intensities measured in 4 biological and 3 technical replicates. Error bars represent ± SEM. P-values were calculated using Wilcoxon non-parametric test with 0 mM L-GA as the reference group, stars represent ns $p \geq 0.05$; * $p \leq 0.05$; ** $p \leq 0.01$; *** $p \leq 0.001$; **** $p \leq 0.0001$

When examining deoxy- and ribose derived nucleotides, ribonucleotides presented a greater reduction following L-GA treatment in general (Figure 3.8). IMR-32 and SH-SY5Y showed a reduction of 0.39 ($p \leq 0.01$) and 0.40 ($p \leq 0.0001$) for deoxyribonucleotides. Yet, there was a reduction of 0.38 ($p \leq 0.0001$) and 0.37 ($p \leq 0.0001$) for ribonucleotides in IMR-32 and SH-SY5Y, respectively. However, in VH-7 there was no difference in the reduction of ribo- or deoxyribonucleotides, On further analysis it was found that purines and pyrimidines respond differently to L-GA, (Figure 3.9, A). IMR-32 showed a 0.19 ($p \leq 0.001$) mean reduction in pyrimidine nucleotides relative to 0.17 ($p \leq 0.0001$) for purine nucleotides. Similar results were found with VH-7, pyrimidines were reduced by a mean of 0.93 ($p \geq 0.05$) and 0.64 ($p \leq 0.01$) for purines. SH-SY5Y showed marginal differences between pyrimidine and purine reductions, with 0.20 and 0.21, respectively.

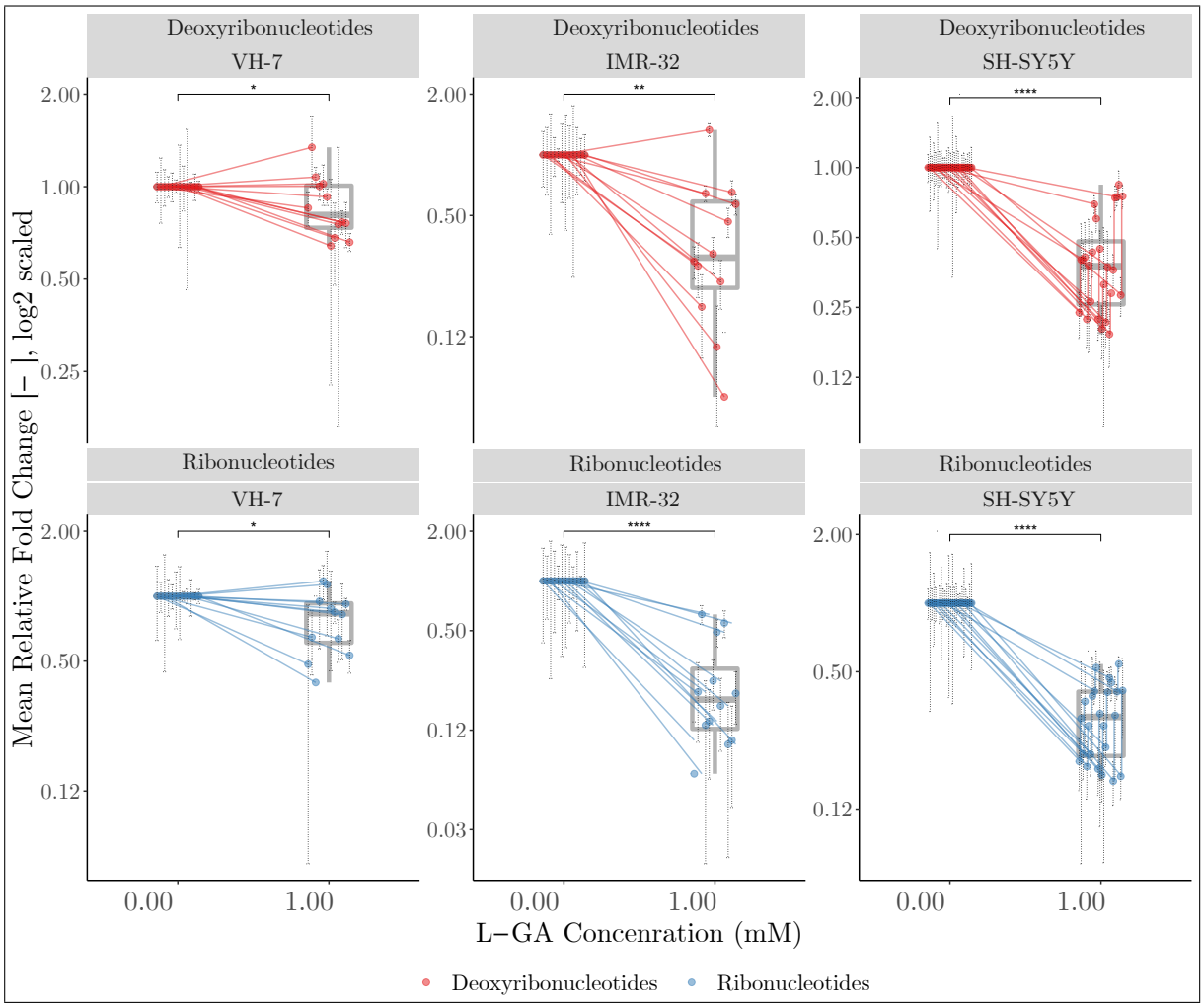

Figure 3.8: L-GA depletes deoxyribonucleotides and ribonucleotides to different degrees in neuroblastoma cells after 24 hrs. Cell lines VH-7, IMR-32 and SH-SY5Y were treated with 1.0 mM L-GA or 0.0 mM L-GA for 24 hrs. Nucleotides were extracted from cell lysates and measured by DI-MS/MS. Boxplots present the mean fold change in deoxy- and ribonucleotide intensities relative to 0.0 mM. Data shown represents n=4 with 3 technical replicates. Error bars represent ± SEM. P-values were calculated using Wilcoxon non-parametric test with 0.00 mM L-GA as the reference group, stars represent: ns $p \geq 0.05$; * $p \leq 0.05$; ** $p \leq 0.01$; *** $p \leq 0.001$; **** $p \leq 0.0001$.

In all cell lines it was observed that within the purines, adenosine derived nucleotides consistently showed greater reduction relative to guanosine derived nucleotides. Interestingly, there was no observable difference in the reduction between cytosine and uridine derived nucleotides. It was also found that as the phosphorylation that tri-phosphorylated nucleotides presented significantly more depletion than mono-phosphorylated nucleotides (Figure 3.9, B). IMR-32 presented a relative decrease of 0.4 to 0.1 from mono to tri-phosphoryated, whereas SH-SY5Y showed a decrease of 0.32 to 0.19. VH-7 showed a reduction from 0.85 to 0.58 from mono- to tri-phosphorylated nucleotides, although no statistical significance was found.

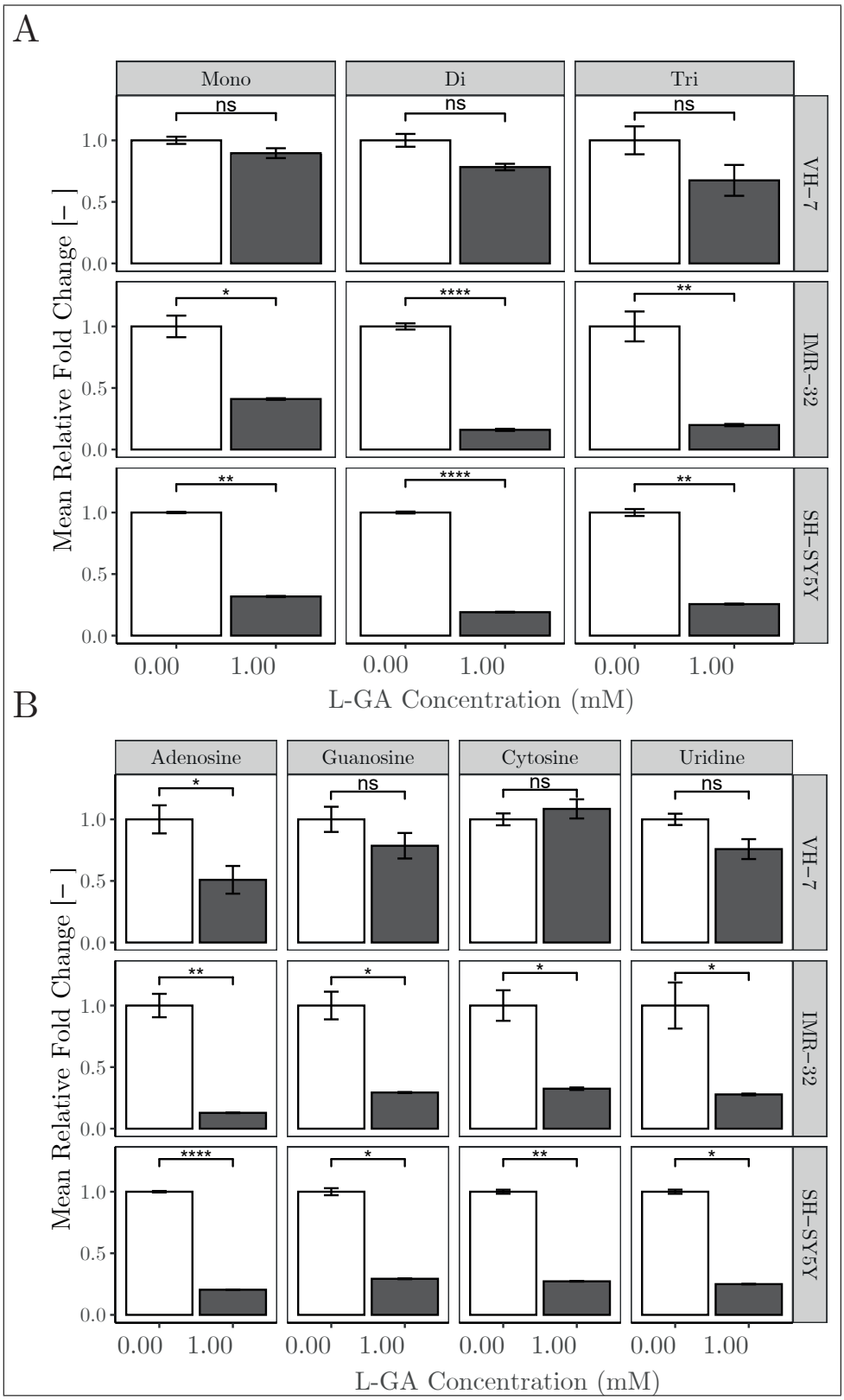

Figure 3.9: L-GA depletes purine and pyrimidine, and their phosphorylation states, nucleotides to different degrees. A: Cell lines VH-7, IMR-32 and SH-SY5Y were treated with 0.0 or 1 mM LGA for 24 hrs. Nucleotides were extracted from cell lysates and measured by DI-MS/MS. Bar plots present the mean fold change in Adenosine, Guanosine, Cytosine and Uridine ribonucleotides relative to 0.0 mM LGA . B: Data from A was taken to derive each mono-, di- and tri- phosphorylated nucleotide, bar plots present the mean fold change of all nucleotide phosphorylation states relative to 0.0 mM LGA treated cells. Data shown represents n=4 with 3 technical replicates. Error bars represent $\pm$ SEM. P-values were calculated using two-tailed T-test. Stars represent: ns $p \geq 0.05$; * $p \leq 0.05$; ** $p \leq 0.01$; *** $p \leq 0.001$; **** $p \leq 0.0001$.

3.4.2 Nucleotide depletion in neuroblastoma cells is dependent on the concentration of L-GA

In section 3.1.1 cell numbers were found to decrease at sub 1 mM L-GA concentrations. Therefore, the aim was to assess whether L-GA reduces nucleotide pools as a function of its concentration. A panel of neuroblastoma cell lines were treated with a range of concentrations (0-1 mM) for 24 hrs. VH-7 was omitted as at 1 mM L-GA there was minimal nucleotide depletion. Figure 3.10 shows the fold change in nucleotide pools relative to 0.0 mM. For IMR-32 there was a significant increase ($p \leq 0.0001$) in the fold change of nucleotide pools following 0.2 mM treatment with L-GA, conversely SH-SY5Y presented a significant decrease ($p \leq 0.001$) in nucleotide pools at 0.2 mM L-GA. At 0.5 mM IMR-32 presented a decrease in the fold change of nucleotides relative to 0.2 mM L-GA, yet the fold change is significantly higher relative to the 0.0 mM control ($p \leq 0.001$). SH-SY5Y showed a significant decrease in nucleotide pools at 0.5 mM relative to 0.0 mM L-GA ($p \leq 0.0001$). As concurrent with previous experiments at 1 mM L-GA, IMR-32 and SH-SY5Y displayed a significant decrease in nucleotide pools relative to the 0.0 mM control ($p \leq 0.0001$).

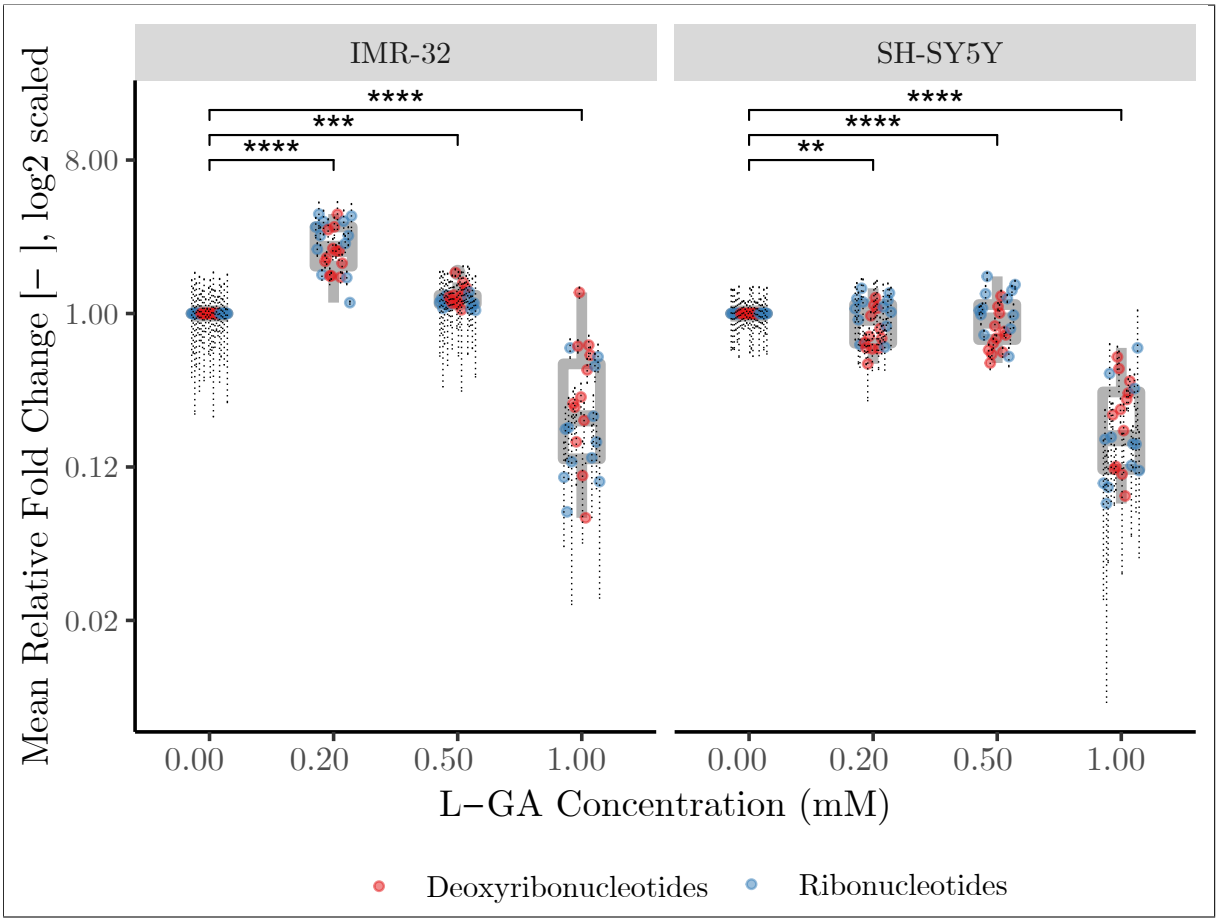

Figure 3.10: Nucleotide depletion in neuroblastoma cells is dependent on the concentration of L-GA. Cell lines IMR-32 and SH-SY5Y were treated with a range of L-GA concentrations (0-1.5 mM) for 24 hrs. Nucleotides were extracted from cell lysates and measured by DI-MS/MS. Boxplots present the mean fold change of nucleotide intensities relative to 0.0 mM L-GA for 24 nucleotides intensities measured in 4 biological and 3 technical replicates. Error bars represent ± SEM. P-values were calculated using Wilcoxon non-parametric test between concentrations of L-GA with 0.00 mM L-GA as the reference group and Holm post-hoc correction. Stars represent ns $p \geq 0.05$; * $p \leq 0.05$; ** $p \leq 0.01$; *** $p \leq 0.001$; **** $p \leq 0.0001$.

As stated previously in the prelim of this section, the synthesis of nucleotides originates from R5P. A protocol was devised to measure intermediates of nucleotide synthesis preceding adenosine, cytosine, uridine and guanosine derived nucleotides. Specifically, the intermediates: R5P, PRPP, SAICAR, AICAR, IMP and UMP were measured. All nucleotides require the intermediates, R5P and PRPP for synthesis, however SAICAR, AICAR and IMP are specifically required for purine synthesis. Figure 3.11 shows the intermediates of nucleotide synthesis following treatment of L-GA for 24 hrs. Upon initial analysis the data presented a difference in the response of the intermediates between cell lines at 1 mM L-GA. However, it was found that IMP - the precursor to purine synthesis- was consistently lower compared to UMP in the mean fold change relative to 0 mM L-GA, in both cell lines. This supports the evidence that purines are affected more than pyrimidines. Furthermore, the precursor to all nucleotides - R5P - was decreased after 1 mM L-GA treatment. It was also shown that SAICAR and AICAR are increased at low L-GA concentrations in SH-SY5Y and remain the least affected intermediates at 1 mM L-GA. Similarly SAICAR was the least affected intermediate in IMR-32 cells, although AICAR was strongly depleted. Interestingly, PRPP responded less to L-GA treatment than R5P in both cell lines. This would seem counter-intuitive as the conversion of R5P to PRPP is an ATP-dependent reaction. Therefore, it may be inferred that the depletion of nucleotides is not solely due to the inhibition of glycolysis derived ATP production via L-GA. It is likely that L-GA affects both the synthesis and the usage of nucleotide intermediates.

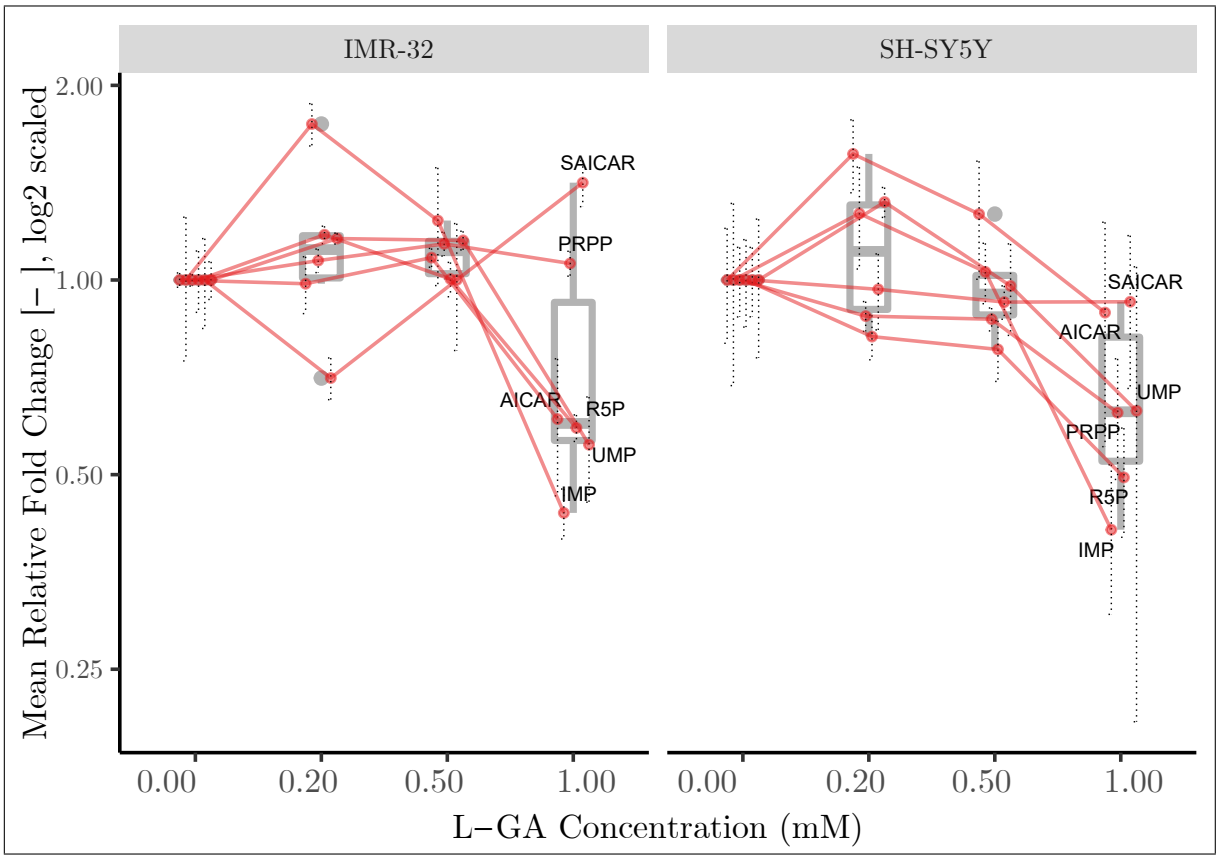

Figure 3.11: L-GA selectively depletes nucleotide precursor pools in neuroblastoma cells. Cell lines IMR-32 and SH-SY5Y were treated with a range of L-GA concentrations (0-1.5 mM) for 24 hrs. Nucleotides were extracted from cell lysates and measured by DI-MS/MS. Boxplots present the mean fold change relative to 0.0 mM L-GA of nucleotide precursors: SAICAR, AICAR, PRPP, R5P, IMP and UMP. Error bars represent ± SEM, n=4.

3.4.3 L-GA induces stress on redox co-factors and reduces the phosphorylation potential of neuroblastoma cells

Evidence from the previous section showed that L-GA depletes nucleotides and their intermediates above 0.5 mM. It was hypothesised that cells experience stress on redox and ATP dependent mechanisms upon L-GA treatment. In order to assess the cellular redox and phosphorylation state of the cell the following ratios were measured:

- $AMP/ATP\,ratio = \frac{[AMP]}{[ATP]}$
- $ATP/ADP\,ratio = \frac{[ATP]}{[ADP]}$
- $NADH\,ratio = \frac{[NAD+]}{[NADH]}$
- $NADPH\,ratio = \frac{[NADP+]}{[NADPH]}$
- $Phosphorylation\,potential = \frac{[ATP]+\times 0.5[ADP]}{[ATP]+[ADP]+[AMP]}$ (Atkinson and Walton, 1967)

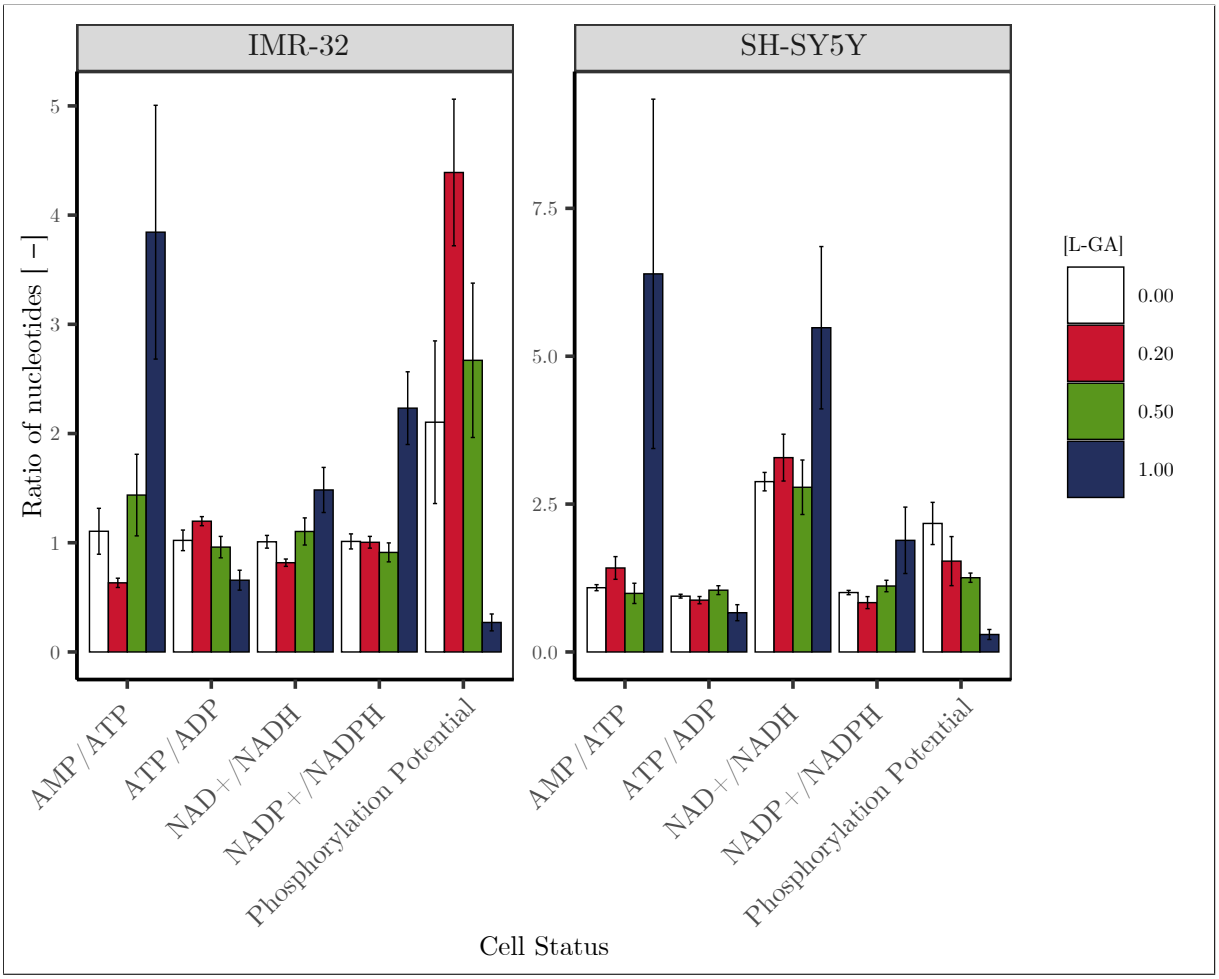

Figure 3.12: L-GA depletes nucleotide pools in neuroblastoma cells after 24 hrs. Cell lines IMR-32 and SH-SY5Y were treated with a range of L-GA concentrations (0-1.5 mM) 24 hrs. Nucleotides were extracted from cell lysates and measured by DI-MS/MS. Boxplots present the ratio of nucleotides from equations stated in 3.4.2. Data shown represents n=4 with 3 technical replicates.

Figure 3.12 shows the ratios of the nucleotides measured from the equations above. IMR-32

and and SH-SY5Y presented similar results across the cell status parameters. When addressing the ratio of AMP/ATP there was a trend of an increase as a function of L-GA concentration. In both cell lines there was on average, a 3.7-fold increase in the ratio of AMP to ATP following 1 mM L-GA treatment. The ATP/ADP ratio was found to be slightly reduced at 1 mM L-GA. The NAD+/NADH ratio tended to increase as a function of L-GA concentration, implying that NADH pools are decreased with increasing L-GA. This decrease in NADH hinders NADH-dependent enzymes and causes redox stress. The NADP+/NADPH ratio is indicative of the cells' response to mitigate oxidative stress. In both cell lines the NADP+/NADPH ratio increased at 1 mM L-GA, suggestive of a depletion in reducing potential of the cell. Lastly, the phosphorylation potential of the cell - defined as the fraction of free ATP to conduct adenosine nucleotide derived phosphorylation reactions - presented heterogeneity between cell lines. IMR-32 observed an increase in the phosphorylation potential at 0.2 and 0.5 mM L-GA. Yet at 1 mM the phosphorylation potential is drastically depleted. SH-SY5Y displayed a general trend of a reduction in phosphorylation potential as a function of L-GA concentration. In order to give supporting evidence for the reduction in phosphorylation potential, AMP, ADP and ATP were measured at varying L-GA concentrations (figure 3.13). In IMR-32 and SH-SY5Y there was a step-wise decrease in adenosine derived nucleotides relative to their phosphorylation state at 1 mM L-GA. IMR-32 increased adenosine derived nucleotides at 0.2 mM and both cell lines showed approximately no change at 0.5 mM. This data correlated to the phosphorylation potential data provided in figure 3.12.

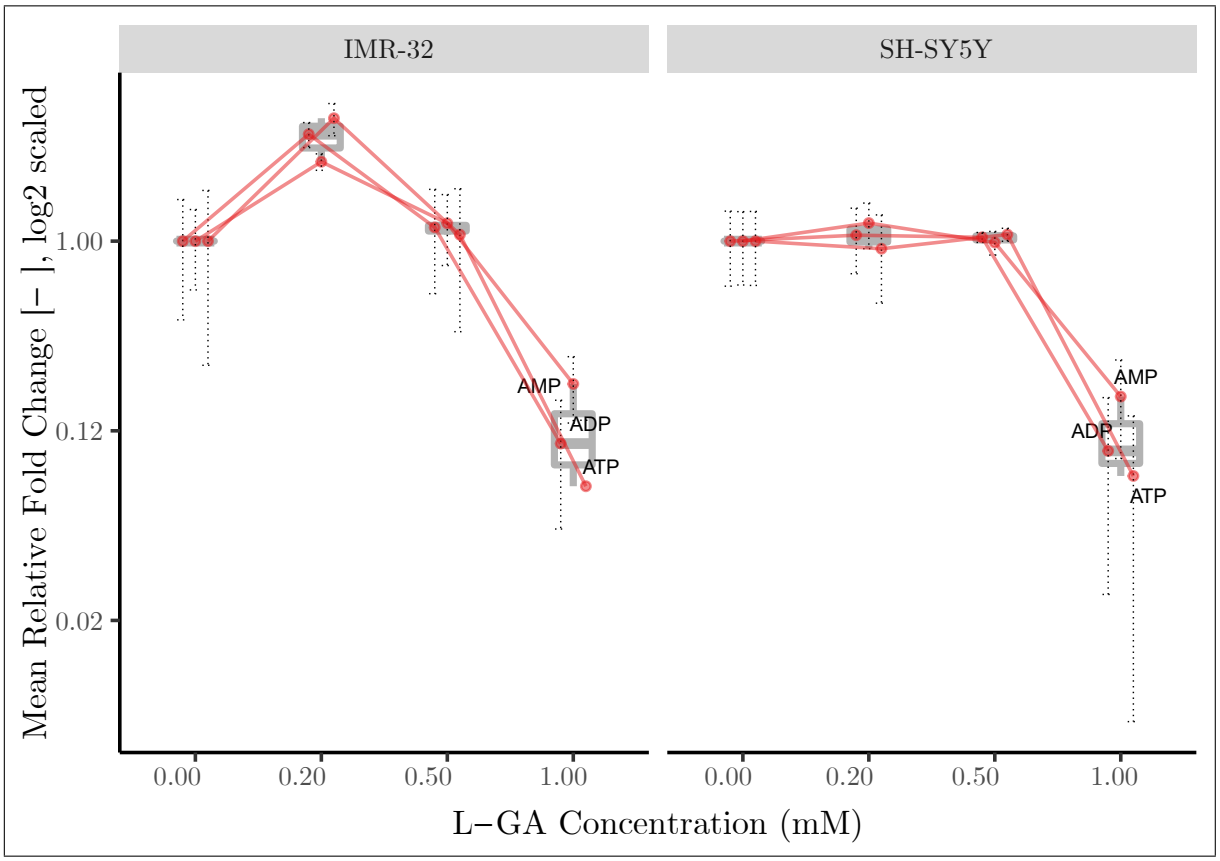

Figure 3.13: L-Glyceraldehyde depletes adenosine derived nucleotide pools as a function of their phosphorylation state. Cell lines IMR-32 and SH-SY5Y were treated with a range of L-GA concentrations (0-1.5 mM) for 24 hrs. Nucleotides were extracted from cell lysates and measured by DI-MS/MS. Boxplots present the mean fold change relative to 0 mM L-GA of adenosine derived nucleotides: AMP, ADP and ATP. Error bars represent ± SEM.

In summary, L-GA caused, in general, a concentration dependent increase in the: AMP/ATP, NAD+/NADH and NADP+/NADPH ratios. The phosphorylation potential of the cell is severely inhibited at 1 mM L-GA. Taken together, it is apparent that the cell experiences redox stress and a reduction in the ability to perform phosphorylation reactions which can be represented in the phosphorylation states of nucleotides.

3.4.4 L-GA causes rapid depletion of nucleotides

As shown in figure 3.3, cell growth of neuroblastoma cells was rapidly inhibited upon L-GA treatment. Given this evidence, the aim was to investigate whether the free nucleotide pool depletes in under 8 hrs. Cells lines IMR-32 and SH-SY5Y were treated with 1 mM L-GA for 1 and 8 hrs prior to harvesting and nucleotide measurements. Figure 3.14 shows that after 1 hr there was no significant change in nucleotide pools for IMR-32. SH-SY5Y increased nucleotides by a median of 1.22 ($p \leq 0.0001$). Following 8 hrs treatment there was a significant depletion of nucleotides in both cell lines. IMR-32 displayed a median reduction to 0.49 ($p \leq 0.0001$) and a median reduction of 0.63 ($p \leq 0.0001$) in SH-SY5Y. Identifying nucleotide intermediates which are affected to a greater degree may elucidate a metabolic mechanism for nucleotide depletion. As described in figure 3.15, it was found that after 8 hrs AICAR is the depleted to the greatest degree followed by UMP, IMP and R5P. Similarly, SH-SY5Y presented a greater depletion in R5P, UMP, AICAR and IMP relative to PRPP and SAICAR, albeit to a lesser degree than IMR-32.

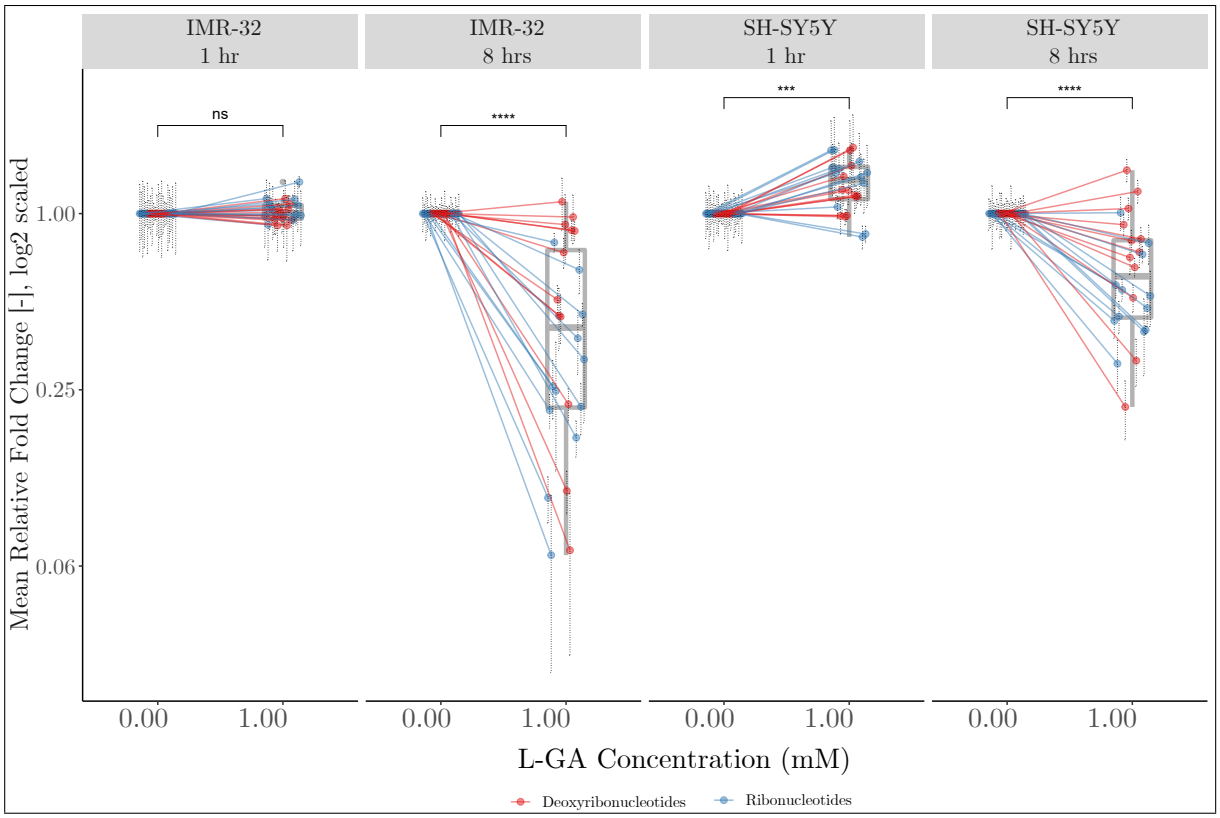

Figure 3.14: L-GA depletes nucleotide pools in neuroblastoma cells within 24 hrs. Cell lines IMR-32 and SH-SY5Y were treated with 1.00 mM L-GA or 0.00 mM L-GA for 1 hr and 8 hrs. Nucleotides were extracted from cell lysates and measured by DI-MS/MS. Box plots present the mean fold change in nucleotide intensity relative to 0.00 mM L-GA. Error bars represent ± SEM. P-values were calculated using Wilcoxon non-parametric test. Stars represent ns $p \geq 0.05$; * $p \leq 0.05$; ** $p \leq 0.01$; *** $p \leq 0.001$; **** $p \leq 0.0001$.

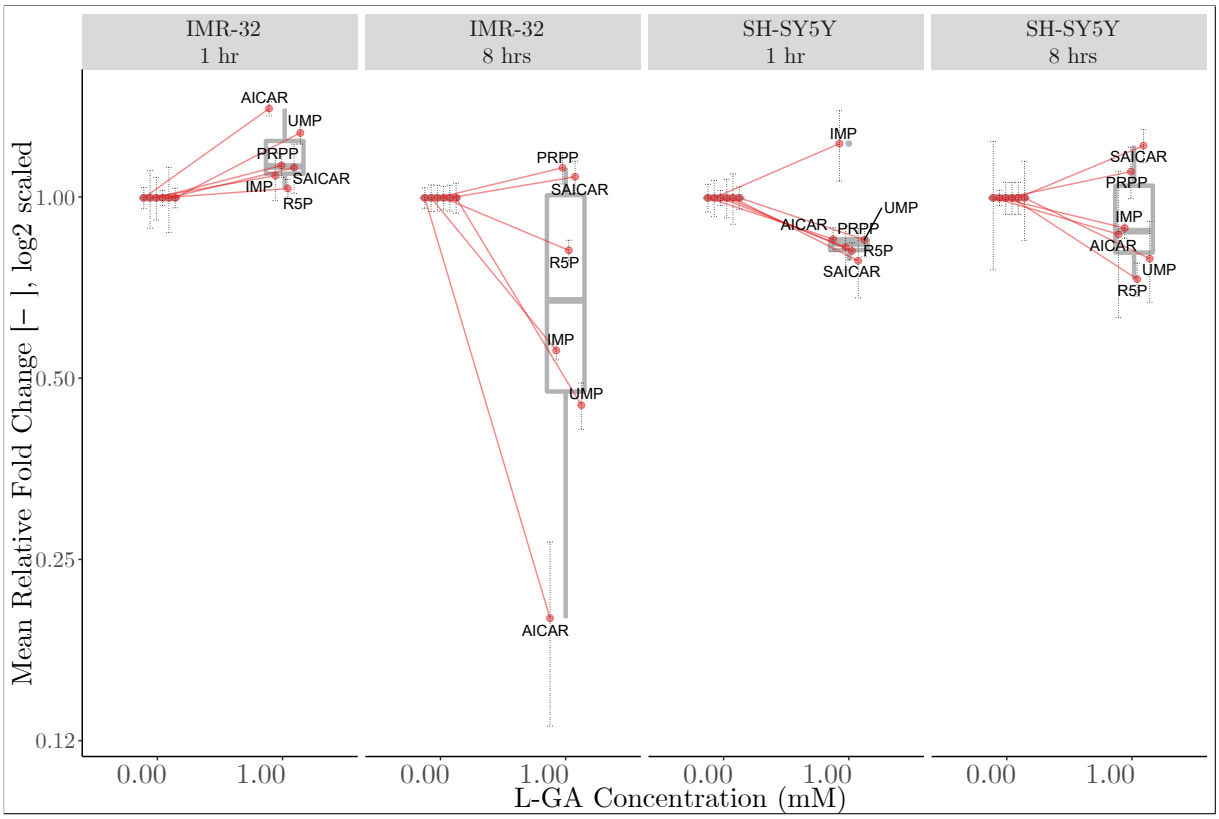

Figure 3.15: L-GA depletes nucleotide intermediates nucleotide intermediates within 8 hrs Cell lines IMR-32 and SH-SY5Y were treated with 1 mM L-GA for 1 hr and 8 hrs. Nucleotides were extracted from cell lysates and measured by DI-MS/MS. Box plots present the mean fold change in nucleotide intensity relative to 0.00 mM L-GA. Boxplots present the mean fold change relative to 0.00 mM of nucleotide precursors: SAICAR, AICAR, PRPP, R5P, IMP and UMP. Error bars represent ± SEM.

3.4.5 L-GA is a more potent inhibitor of nucleotide synthesis than D-GA or DL-GA in neuroblastoma cells

As shown in figure 3.4, L-GA inhibits neuroblastoma cell growth with greater efficacy than D- or DL-GA. Given this, the aim was to assess whether this is reflected in the depletion of nucleotides. Cell lines VH-7, IMR-32 and SH-SY5Y were treated with 1 mM D-, DL- or L-GA for 24 hrs.

Figure 3.16 shows the 24 nucleotides measured following x-GA treatment. As previously found, L-GA caused significant depletion in IMR-32, SH-SY5Y cell lines and moderate depletion in VH-7. The data showed median fold changes of 0.38 ($p \leq 0.0001$), 0.31 ($p \leq 0.0001$) and 0.84 ($p \leq 0.001$), respectively. D-GA caused a 1.16 ($p \leq 0.0001$) median increase in nucleotide pools in IMR-32. However, SH-SY5Y and VH-7 showed a 0.75 ($p \leq 0.0001$) and 0.53 ($p \leq 0.0001$) median decrease, respectively. Interestingly, there was a median decrease of 0.41 ($p \leq 0.0001$) and 0.25 ($p \leq 0.0001$) upon DL-GA treatment for IMR-32 and SH-SY5Y. It is apparent that D-GA treatment of VH-7 appears to be more effective at nucleotide depletion than L- or DL-GA. This appears to align with the growth curves in figure 3.16 showing L-GA to be less effective at hindering VH-7 growth.

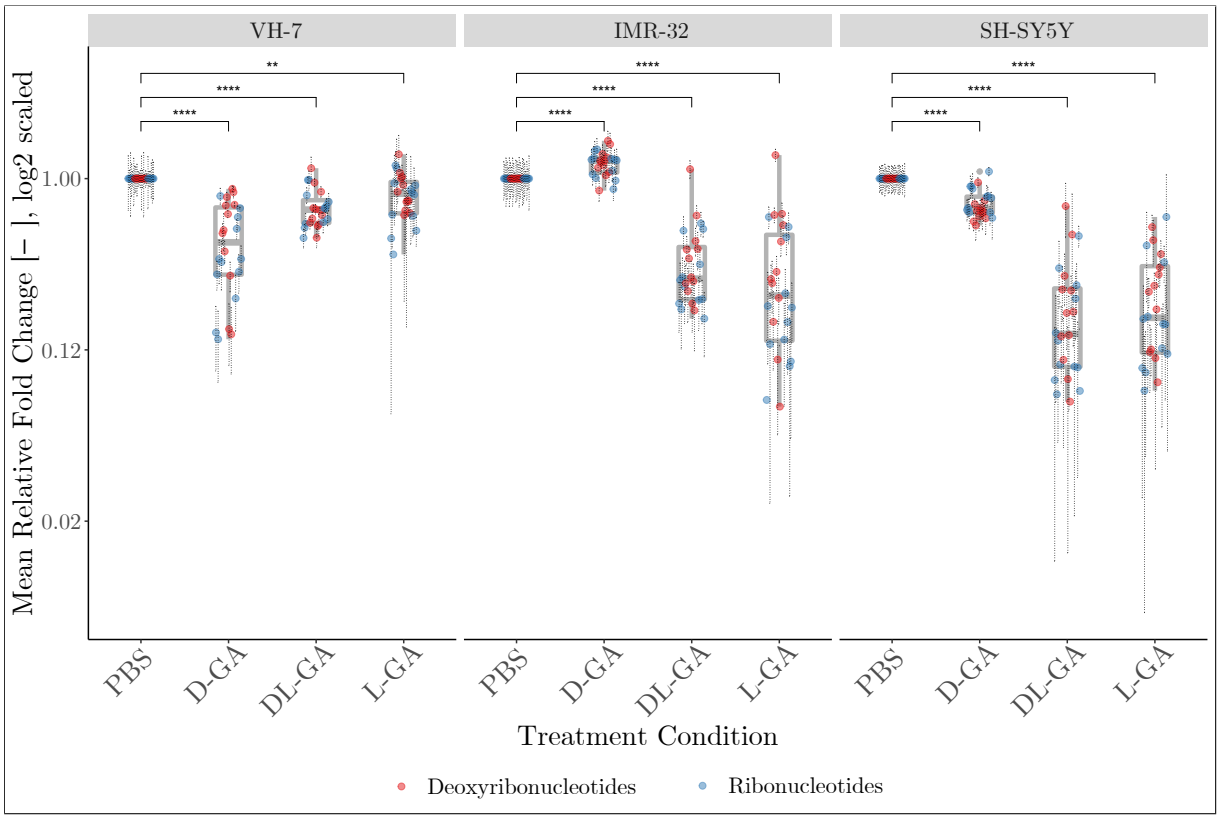

Figure 3.16: L-GA is a more potent inhibitor than D-GA or DL-GA. Cell lines VH-7, IMR-32 and SH-SY5Y were treated with 1 mM LGA, D-GA, DL-GA or PBS for 24 hrs. Nucleotides were extracted from cell lysates and measured by DI-MS/MS. Box plots present the mean fold change in intensity of deoxy-(red) and ribonucleotides (blue) relative to PBS. Data shown represents n=6 with 3 technical replicates. Error bars represent ± SEM. P-values were calculated using the Wilcoxon non-parametric test with PBS as the reference group and Holm post-hoc correction. Stars represent: ns $p \geq 0.05$; * $p \leq 0.05$; ** $p \leq 0.01$; *** $p \leq 0.001$; **** $p \leq 0.0001$.

In summary, we conclude that L-GA, or its presence in a racemic preparation, is more effective than D-GA at depleting nucleotide pools in neuroblastoma cells. The data presented a marginal difference in the median depletion of nucleotides following DL- and L-GA treatment. Intriguingly, D-GA caused a greater reduction in nucleotides compared to L-GA in fibroblasts, contrary to observations in neuroblastoma cells. This data complements findings in section 3.1.1, whereby L-GA inhibited growth more effectively than D-GA. This lead to the question as to whether glycolytic inhibition via glyceraldehyde is solely responsible for nucleotide depletion.

3.4.6 Alternate modes of glycolytic inhibition is not as effective as L-GA at depleting nucleotide pools

In the previous sections, the data presented significant decreases in all nucleotides upon L-GA treatment, however D-GA was not as effective. In order to delineate the metabolic mode of action of L-GA, it was examined whether the inhibition of glycolysis is the driving factor behind nucleotide depletion. In order to discern this, cell lines IMR-32 and SH-SY5Y were treated with the glycolytic inhibitor bromopyruvate (BrPyr) and subjected to glucose starvation (0 g/l). The synthesis of R5P relies upon the metabolites G6P, or F6P and GA3P from the oxidative and non-oxidative pentose phosphate pathway, respectively. It was hypothesised that starving the cells of glucose would result in a depletion of G6P, thereby depleting R5P pools. Bromopyruvate is

a strong inhibitor of GAPDH, as shown by (Pietzke, 2015). Given that bromopyruvate targets downstream of routes of R5P synthesis, it was expected that bromopyruvate would deplete ATP levels and the phosphorylation of nucleotide intermediates.

Cell lines IMR-32 and SH-SY5Y were seeded at 1.5e+6 and left to settle for 24 hrs in triplicate plates for each treatment condition. Media was exchanged with: 1X PBS, 1 mM L-GA, 100 µM BrPyr and glucose was removed from one treatment condition, concentrations were chosen based on (Pietzke, 2015). Cells were incubated with each treatment condition for 24 hrs. Following incubation with each treatment condition cells were harvested and nucleotides analysed as per the method in section 1.3.3. Figure 3.17 shows the fold change in 24 nucleotides relative to PBS. In IMR-32, L-GA and BrPyr caused the most significant decrease in nucleotide pools with a median fold change reduction of 0.68 ($p \leq 0.0001$) and 0.24 ($p \leq 0.0001$) respectively. Starvation of glucose induced a median reduction of 0.55, although not significant. SH-SY5Y showed no significant reduction in nucleotides, except with L-GA which caused a median reduction of 0.59 ($p \leq 0.0001$). From this data we may conclude that IMR-32 and SH-SY5Y have heterogeneous responses to glycolytic inhibition and nucleotide biosynthesis, with IMR-32 showing greater nucleotide depletion in response to glycolytic inhibition.

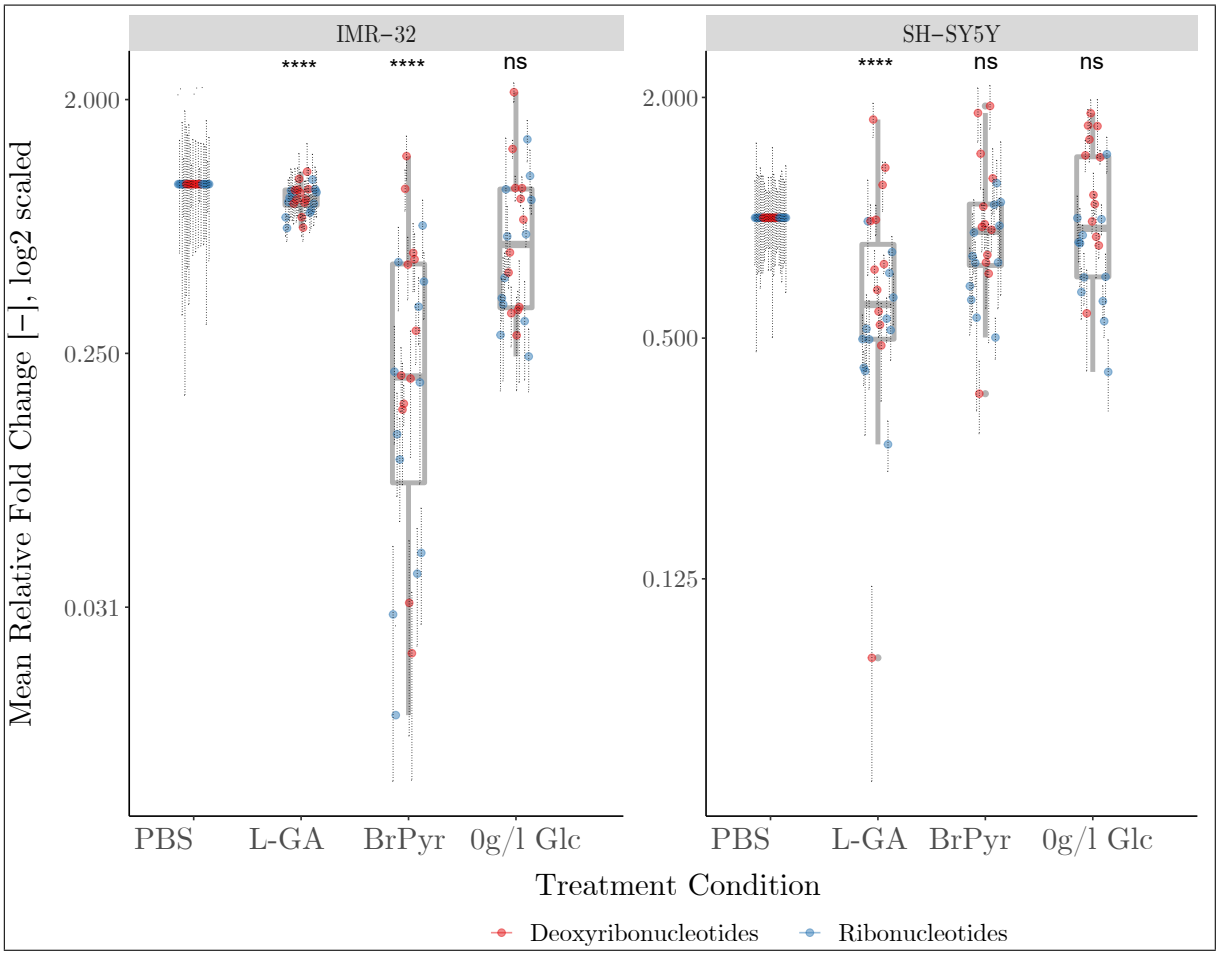

Figure 3.17: Glycolytic inhibition depletes nucleotide pools. Cell lines IMR-32 and SH-SY5Y were treated with 1 mM L-GA, 100 µM BrPyr and 0g/l glucose for 24 hrs. Nucleotides were extracted from cell lysates and measured by DI-MS/MS. Box plots present the mean fold change in intensity of deoxy-(red) and ribonucleotides (blue) relative to PBS. Data shown represents n=3 with 3 technical replicates. Error bars represent ± SEM. P-values were calculated using Wilcoxon non-parametric test with PBS as the reference group. Stars represent: ns $p \geq 0.05$; * $p \leq 0.05$; ** $p \leq 0.01$; *** $p \leq 0.001$; **** $p \leq 0.0001$.

3.5 Glyceraldehyde inhibits glycolysis and induces metabolic reprogramming in neuroblastoma cells

Previous work in the Kempa lab (Pietzke, 2015) showed that L-GA inhibited glycolysis of T98G and HEK293 cells. Specifically, L-GA treatment resulted in the inhibition of the flux of carbon from glucose into metabolites downstream of aldolase- which utilises GA3P as a substrate. Furthermore, L-GA was shown to be more effective at inhibiting glycolysis than D-GA. Given this, the aim was to show that neuroblastoma cells are also susceptible to glycolytic inhibition via L-GA. To measure the flux of carbon through metabolic pathways we measure the change in metabolite pool sizes in cooperation with pulsed stable isotope resolved metabolomics (pSIRM), as described in section 2.4.2. pSIRM requires U-^{13}C-glucose to resolve the flux of carbons through glycolysis and the TCA cycle as a function of time. The labelling of metabolites from carbon-13 induces a mass shift in the metabolites which is then detected via GC-MS.

3.5.1 L-GA and D-GA inhibit glycolysis downstream of aldolase

Initial experiments aimed to discern where in the glycolytic pathway L-GA targets. Pietzke (2015) had shown that L-GA treatment results in the accumulation of fructose-1,6-bisphosphate (F16BP) in T98G and HEK293 cells. This accumulation was hypothesised to be due to the inhibition of aldolase (ALDOA) via L-GA. It was aimed to show that this also occurs in neuroblastoma cells. Figure 3.18 shows the difference in metabolite pools between L-GA treated cells relative to PBS. It was found that F16BP indeed accumulates, however it was also found that pyruvate accumulates upon L-GA treatment. From this data it was hypothesised that L-GA acts between F16BP and pyruvate. To understand the mechanism by which this accumulation occurs pSIRM was employed to measure the flux of carbon through glycolysis.

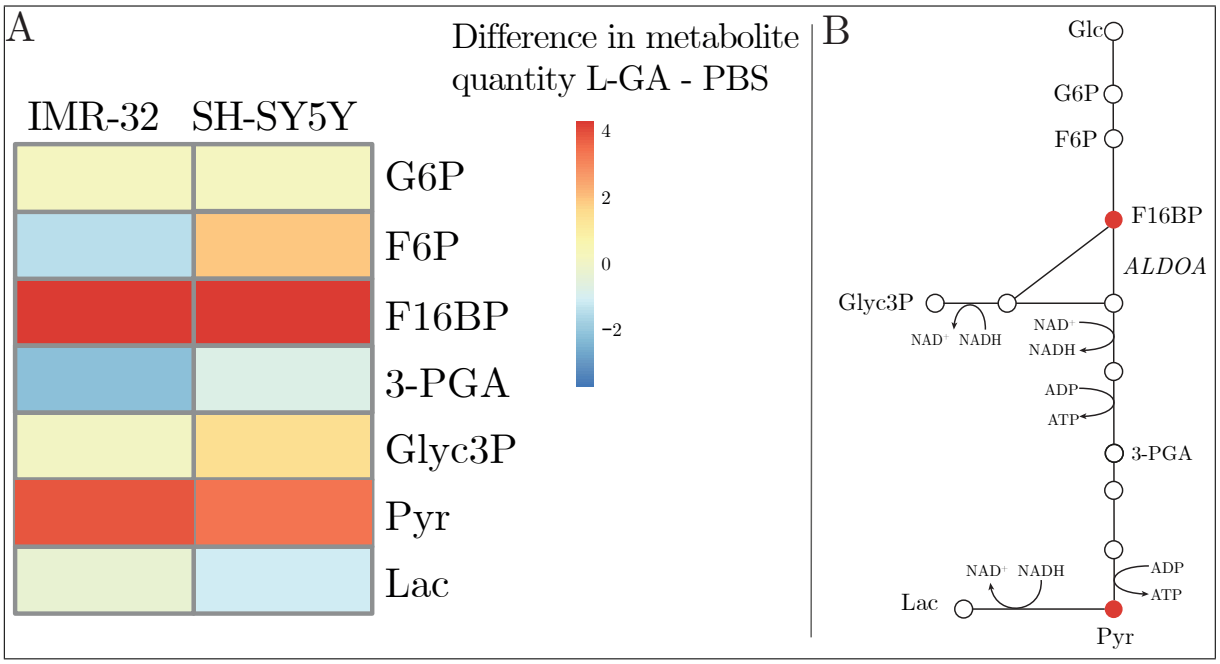

Figure 3.18: Effects of L-GA on glycolysis intermediates in IMR-32 and SH-SY5Y cells. A: Polar metabolites were extracted from IMR-32 and SH-SY5Y cell lines following treatment of 1 mM L-GA for 1 hr. Samples were processed via GC-MS and analysed to attain the abundance of metabolite pools of glycolysis intermediates. Heatmaps show the difference in metabolite quantities (L-GA - PBS) for the glycolysis intermediates: G6P - glucose-6-phosphate, F6P-fructose-6-phosphate, F16BP- fructose-1,6-bisphosphate, 3PGA- glyceric acid-3-phosphate, Glyc3P- glycerol-3-phosphate, Lac- lactic acid and Pyr- pyruvic acid in cell lines IMR-32 and SH-SY5Y. B: Schematic shows the locality of accumulated metabolites in the glycolytic pathway. F16BP and Pyr are labelled red to denoted their accumulation. Aldolase - ALDOA, is shown in italics.

Briefly, cell lines IMR-32 and SH-SY5Y were seeded at 2e+6 cells per plate in triplicate 10cm plates. Twenty four hours after seeding cells were treated for 1 hr with PBS or 1 mM L-, D-GA. Within the 1 hr treatment time cell culture media was exchanged supplemented with U-^{13}C-glucose to initiate metabolite labelling. Labelling was quenched at 2, 5, 10 and 15 mins, metabolites were extracted and subjected to GC-MS, the labelling strategy is exemplified in figure 3.19, A. Two metabolites in phase I glycolysis (G6P, F6P) and 3 metabolites (3-PGA, Lac, Pyr) in phase II glycolysis were measured. Glyc3P traverses the boundary between phase I and phase II glycolysis, as glyceraldehyde-3-phosphate (GA3P) is the fulcrum between the two phases. Cit was measured as a indication of flux of ^{13}C-label into the TCA cycle derived from U-^{13}C-glucose. Figure 3.19, B shows the relative metabolite abundance, ^{13}C-label incorporation and relative of ^{13}C-label quantity of measured metabolites after 10 mins of labelling in IMR-32 cells. All data were normalised to the cinnamic acid internal control and mean cell count for each condition. The labelling incorporation for all time points are found in supplementary material section 5.2.2, figure 5.3.

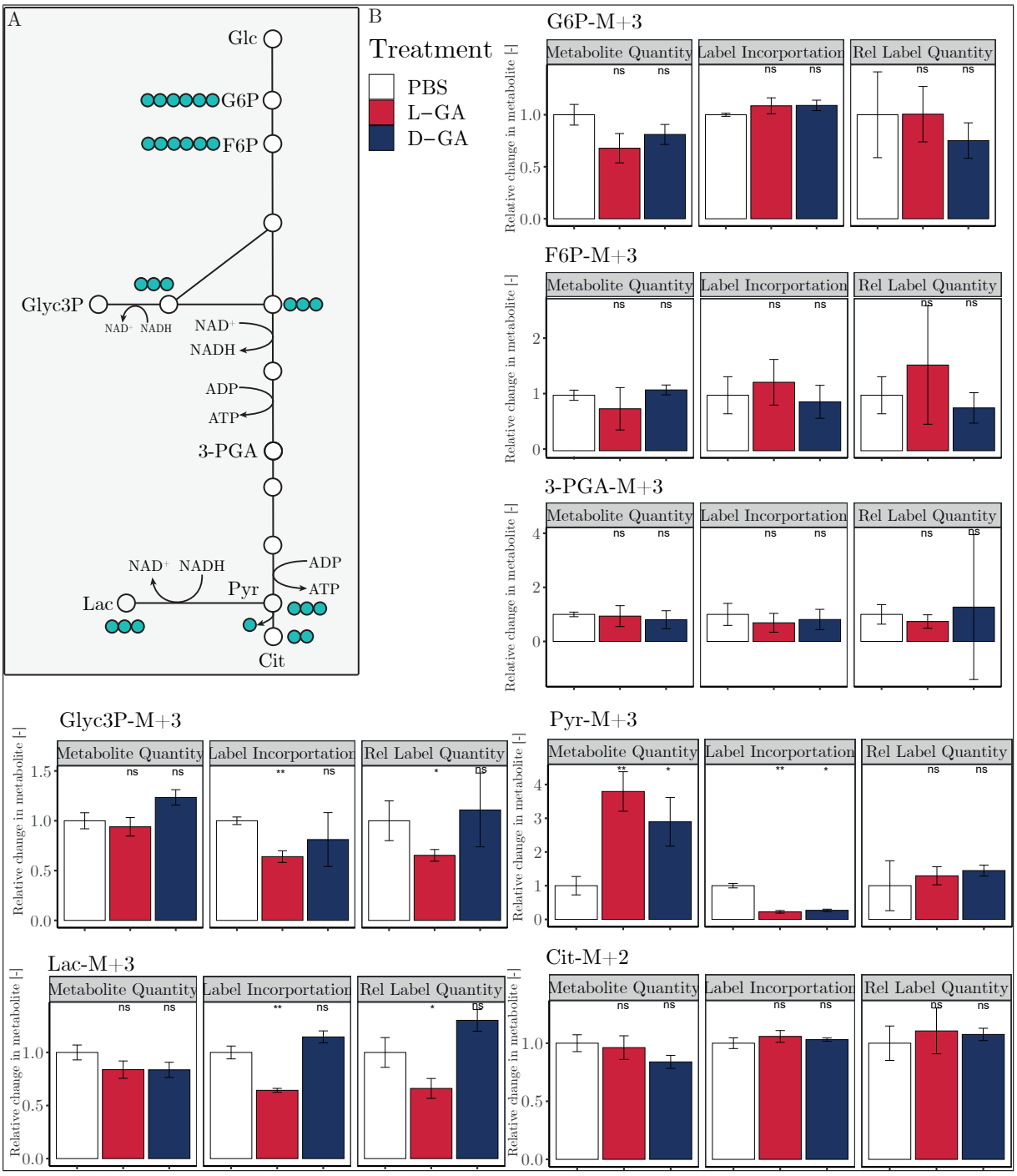

Figure 3.19: Effects of L- and D-GA on glycolysis intermediates in IMR-32 cells. A: Diagram depicts the metabolites of the glycolytic pathway and the flow of labelled carbons from U-^{13}C-Glucose. B: Polar metabolites were extracted from IMR-32 cell lines following treatment of L-GA and D-GA for 1 hr. Samples were processed via GC-MS and analysed to attain the abundance and label incorporation of U-^{13}C-glucose following 10 mins of labelling. Bar charts represent the fold change in relative metabolite abundance, relative ^{13}C-label incorporation and relative ^{13}C-label quantity, following 10 mins labelling; ± SE, n=3. P-values were calculated using two-tailed T-test with PBS as the reference and Holm post-hoc correction. Stars represent: ns $p \geq 0.05$; * $p \leq 0.05$; ** $p \leq 0.01$; *** $p \leq 0.001$; **** $p \leq 0.0001$. Abbreviations: Cit-Citrate; Glc6P_BP- Glucose-6-phosphate; Frc6P_MP- Fructose-6-phosphate; Glyc3P- Glycerol-3-phosphate; 3-PGA - Glyceric acid-3-phosphate; Lac - Lactate; Pyr - Pyruvate

In IMR-32 cells there was no significant changes in the metabolite abundance, label incorporation or relative label quantity in metabolites up to 3-PGA following treatment with L- or D-GA. When assessing Glyc3P no significant change in the relative abundance was observed.

Although, in L-GA treated cells there was a relative reduction of 0.7 ($p \leq 0.01$) to the control in the label incorporation. Similarly, the relative label quantity was reduced to 0.65 ($p \leq 0.05$). Following both D- and L-GA treatment the data presents a significant increase in the relative abundance of Pyr, L-GA induced a 3.7-fold ($p \leq 0.01$) and D-GA a 2.9-fold ($p \leq 0.05$) increase relative to PBS. Both treatments also show a significant decrease in the label incorporation. For L-GA and D-GA treated cells there was a reduction to 0.22 ($p \leq 0.01$) and 0.26 ($p \leq 0.05$) to that of the control, respectively. No significant changes were found in the relative labelled quantities. The label incorporation and relative label quantity was reduced in Lac, to 0.64 ($p \leq 0.01$) and 0.66 ($p \leq 0.05$) to that of the control, respectively. Although, the metabolite quantity was unaffected. D-GA induced no significant changes in the Lac metabolite profile. In summary, the flux of labelled carbons into Lac and Glyc3P decreased with L-GA treatment although no change in the metabolite pools. Both L-GA and D-GA result in increased metabolite pools and reduced label incorporation into Pyr, yet L-GA produced a more pronounced change in the metabolite's profile. This is curious given that Pyr to Lac metabolism is up-regulated in cancer cells, one would assume that the increase in Pyr pools would generate increased Lac pools. It is suggested that the flux of carbons from Pyr to Lac is impeded.

Figure 3.20, B shows the relative metabolite abundance, U-^{13}C-glucose incorporation and relative of U-^{13}C-glucose label quantity of measured metabolites after 10 mins of labelling in SH-SY5Y cells. The labelling incorporation for all time points are found in supplementary material section 5.2.2, figure 5.3. As found with IMR-32, there were no significant changes in the metabolite profiles of G6P or F6P. Although results were not significant, there is evidence for decreased label incorporation and relative metabolite quantity in 3-PGA following D- and L-GA treatment. Upon L-GA treatment there was decreased label incorporation and relative labelled quantity in Gly3P. However, only the 0.66 decrease in label incorporation showed significance ($p \leq 0.0001$). Curiously, there was a significant increase in the relative abundance and label quantity of Gly3P in D-GA treated cells. In a similar fashion, Lac showed significant decreases in label incorporation following L-GA treatment, but not D-GA. Pyr presented significant increases, approximately 2.5-fold, in the metabolite abundance in L-GA and D-GA treated cells. Label incorporation is decreased to 0.24 ($p \leq 0.05$) and 0.21 ($p \leq 0.05$) to that of the control for L-GA and D-GA, respectively. Although not significant, a slight increase in the Pyr relative labelled quantity for L-GA treated cells was found. It appeared that upon L-GA treatment carbons are routed into Cit. An approximately 2.1-fold ($p \leq 0.05$) increase in the Cit relative label incorporation, although this was not observed with D-GA.

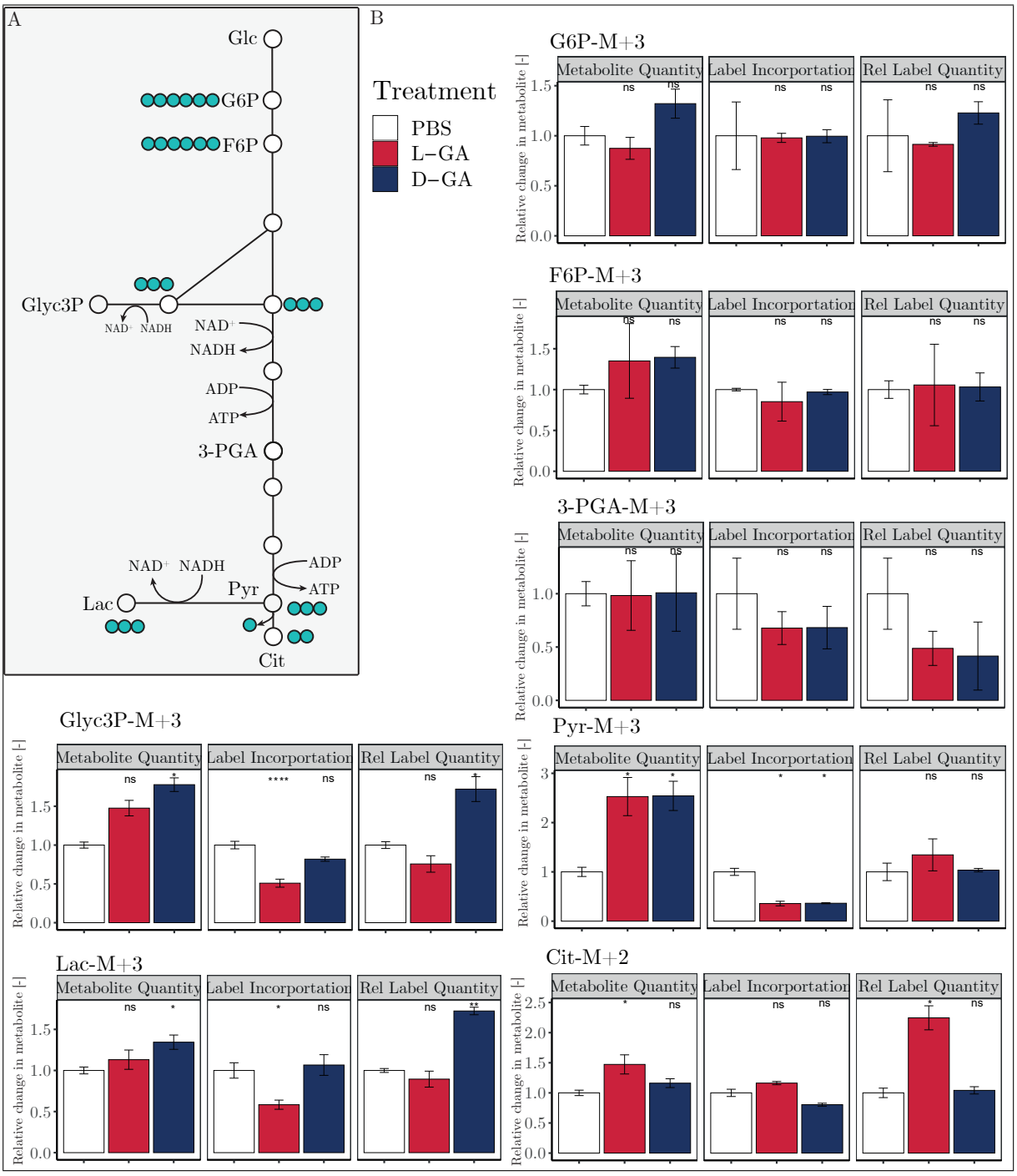

Figure 3.20: Effects of L- and D-GA on glycolysis intermediates in SH-SY5Y cells. A: Diagram depicts the metabolites of the glycolytic pathway and the flow of labelled carbons from U-^{13}C-Glucose. B: Polar metabolites were extracted from SH-SY5Y cell lines following treatment of L-GA and D-GA for 1 hr. Samples were processed via GC-MS and analysed to attain the abundance and label incorporation of U-^{13}C-glucose following 10 mins of labelling. Bar charts represent the fold change in relative metabolite abundance, relative ^{13}C-label incorporation and relative ^{13}C-label quantity, following 10 mins labelling; ± SE, n=3. P-values were calculated using two-tailed T-test with PBS as the reference and Holm post-hoc correction. Stars represent: ns $p \geq 0.05$; * $p \leq 0.05$; ** $p \leq 0.01$; *** $p \leq 0.001$; **** $p \leq 0.0001$. Abbreviations: Cit-Citrate; Glc6P_BP- Glucose-6-phosphate; Frc6P_MP- Fructose-6-phosphate; Glyc3P- Glycerol-3-phosphate; 3-PGA - Glyceric acid-3-phosphate; Lac - Lactate; Pyr - Pyruvate.

In summary, L-GA and D-GA present differing metabolic modes of action. L-GA is more efficient at inhibiting glycolytic flux of carbon-13 into Glyc3P and Lac. Both enantiomers act in a similar manner on Pyr and conversely on 3-PGA. Metabolites upstream of aldolase - the

putative target of L- and D-GA - show no to minimal response to glyceraldehyde treatment. One can conclude that L-GA indeed targets glycolysis phase II. The data presented a decrease in the the pools sizes and incorporation of labelled glucose into Lac, Glyc3P and Pyr. Gly3P and Lac also showed decreased labelled quantities, suggestive of both decreased flux and production of the metabolites. However, for SH-SY5Y the labelled quantity of Pyr upon L-GA treatment was marginally increased. This is not the case with IMR-32. It is assumed that this phenotype is the result of the accumulation of Pyr in SH-SY5Y cell lines. We may also conclude that lactate dehydrogenase (LDH) and glycerol-3-phosphate dehydrogenase (GPD1) show reduced function. Both of these enzymes require NADH as a co-factor. It is hypothesised that L-GA inhibits glyceraldehyde dehydrogenase (GAPDH) and the production of NADH resulting in the inhibition of LDH and GPD1. It is clear from the labelled quantities of Lac and Gly3P that, D-GA does not break the NAD+/NADH cycling as efficiently as L-GA. This hypothesis was recapitulated by measuring the NAD+ and NADH pools sizes after 1 hr and 8 hrs L-GA treatment. As shown in figure 3.21 A, there is a slight decrease in NADH in IMR-32 and an increase in NADH in SH-SY5Y following treatment. However, figure 3.21 B, shows increases in the NAD+/NADH ratio in both cell lines following treatment, suggesting NADH depletion relative to NAD+. This is more striking after 8 hrs L-GA treatment. In both cell lines we see an increase in the NAD+/NADH ratio, yet SH-SY5Y shows a greater increase. This data concurs with the hypothesis that NADH is not replenished following L-GA treatment.

The heterogeneous response of IMR-32 and SH-SY5Y at the Pyr position is indicative of accumulation of labelled Pyr in SH-SY5Y and a larger pool size of Pyr overall. Excess Pyr is metabolised to Cit, as shown by the increased labelled quantity of Cit in SH-SY5Y cells. Given this metabolic switch in SH-SY5Y cells, we were intrigued to know how the TCA cycle responds to L-GA treatment. Cells may also employ glutamine as a fuel source, in the event of glycolytic inhibition it was hypothesised that cells employ glutaminolysis to compensate for decreased glycolysis.

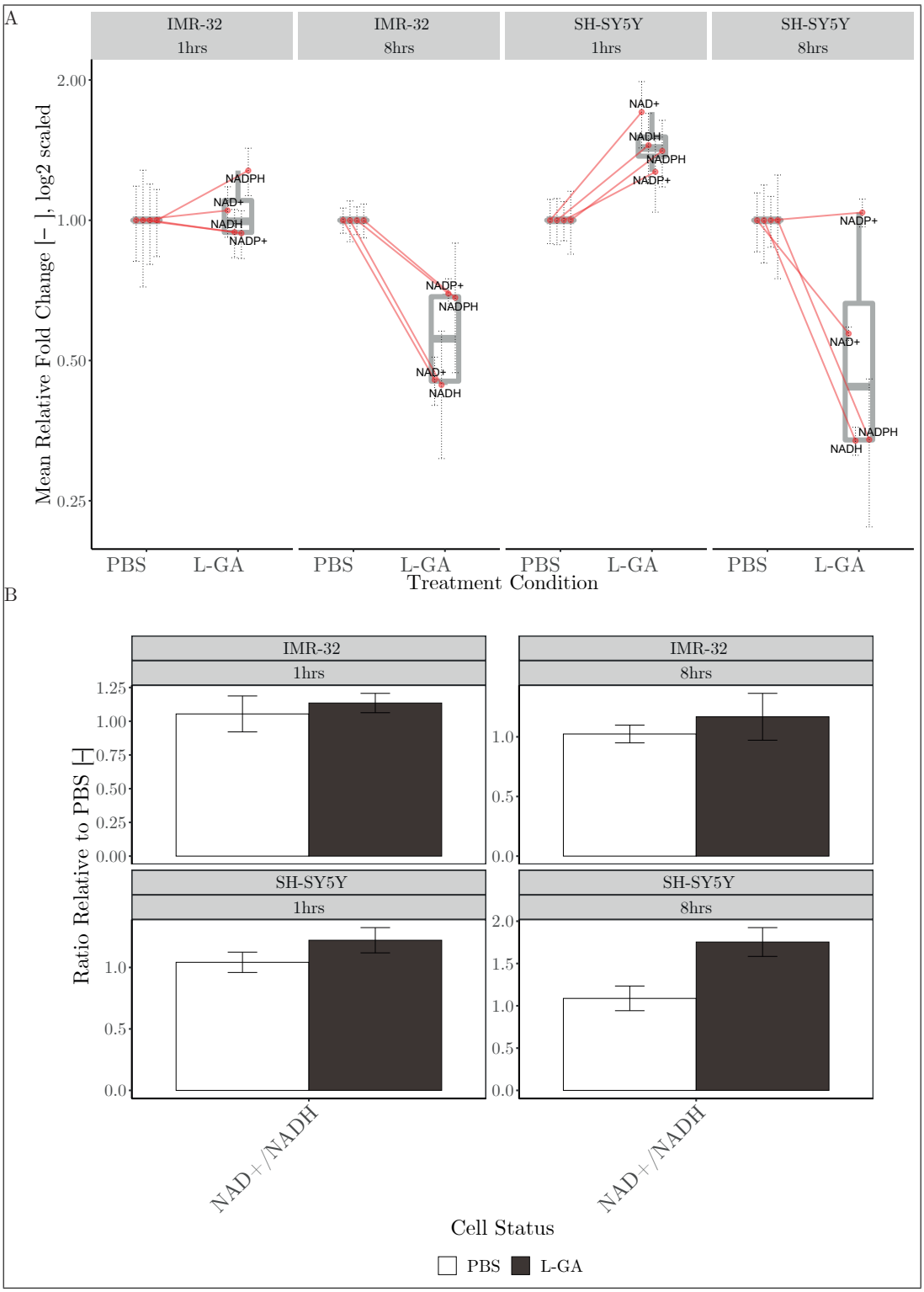

Figure 3.21: Effects of L-GA on the NAD+ and NADH pools. A. Cell lines IMR-32 and SH-SY5Y were treated with 1 mM L-GA or PBS for 1 hr and 8 hrs. Nucleotides were extracted from cell lysates and measured by DI-MS/MS. Box plots present the mean fold change in nucleotide intensity relative to PBS. B. Bar charts show the ratios of NAD+/NADH following 1 hr and 8 hrs. Error bars represent ± SEM, n=3.

3.5.2 L-GA causes a metabolic switch to glutaminolysis

The assessment of the effect of L-GA and D-GA on the TCA cycle, with U-^{13}C-glutamine was performed in the same manner as described in section 3.5.2. Twenty four hours after seeding cells were treated for 1 hr with PBS or 1 mM L-, D-GA. Within the 1 hr treatment time cell culture media was exchanged supplemented with U-^{13}C-glutamine to initiate metabolite labelling. Labelling was quenched at 5, 15, 30 and 45 mins, metabolites were extracted and subjected to GC-MS, the labelling strategy is exemplified in figure 3.22, A. Figure 3.22, B shows the relative metabolite abundance, ^{13}C-label incorporation and relative of ^{13}C-label quantity of measured metabolites after 30 mins of labelling in IMR-32 cells. All data were normalised to the cinnamic acid internal control and mean cell count for each condition. The labelling incorporation for all time points are found in supplementary material section 5.2.2, figure 5.4.

In IMR-32 cells, no significant change in the metabolite abundance of the TCA cycle, except for α-KG was found. Both L-GA and D-GA caused an approximately 6-fold increase in α-KG ($p \leq 0.01$). There was a significant decrease in the abundance of Glu following both L-GA and D-GA treatment. As the flow of labelled carbons proceeds from α-KG to Suc, Fum, Mal and Cit (M+4) there was a significant increase in the label incorporation and relative label quantity in L-GA treated cells. The data provided for Mal displayed an increase in label incorporation and label quantity although due to high variance no statistical significance was found for L-GA treated cells. Interestingly, L-GA and D-GA caused significant increases in the label incorporation and relative label quantity of Cit (M+5), originating from α-KG and not via Mal (M+4).

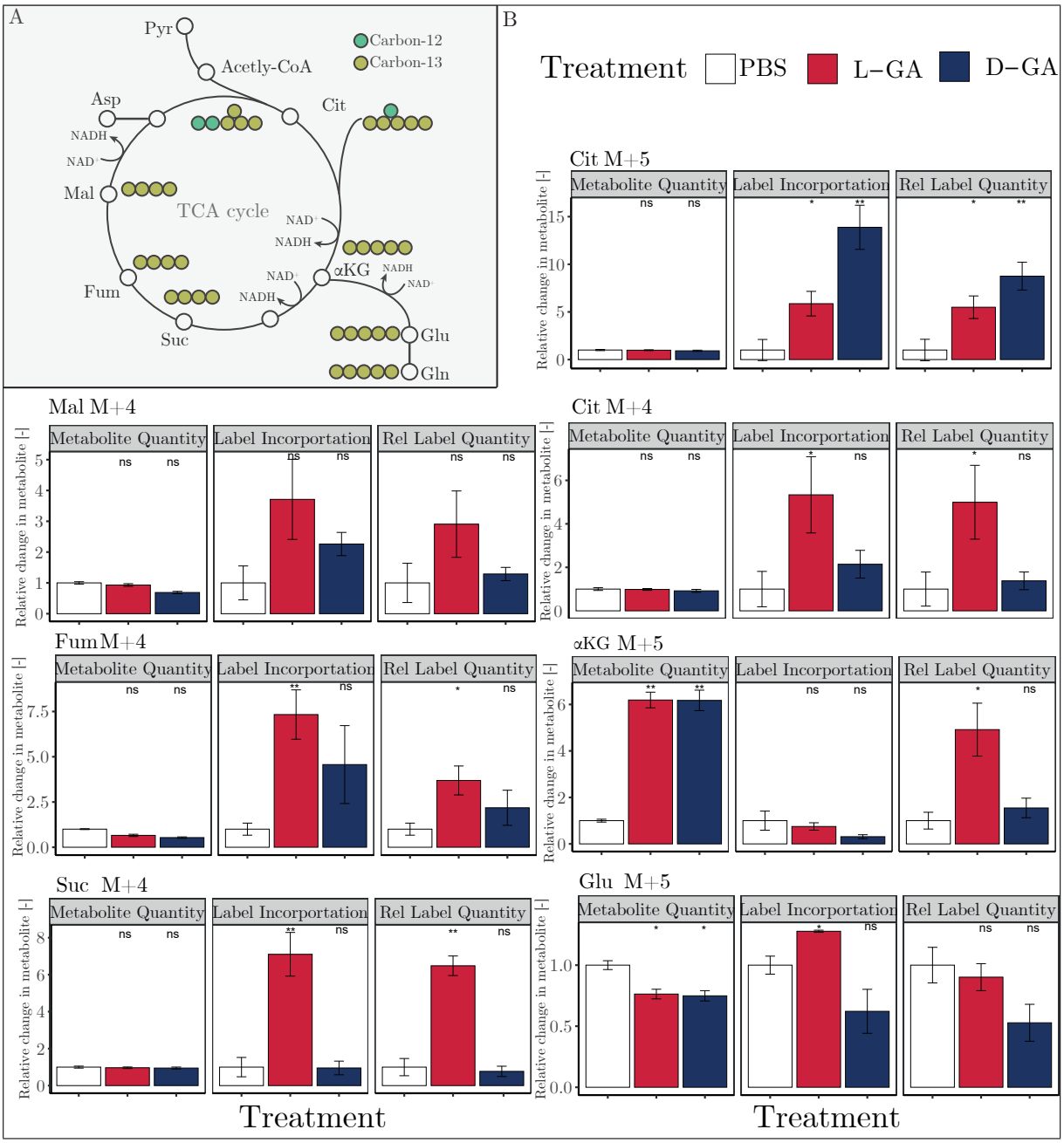

Figure 3.22: Effects of L- and D-GA on TCA cycle intermediates in IMR-32 cells. A: Diagram depicts the metabolites of the TCA cycle and the flow of labelled carbons from U-^{13}C-glutamine. B: Polar metabolites were extracted from IMR-32 cell lines following treatment of L-GA and D-GA for 1 hr and. Samples were processed via GC-MS and analysed to attain the abundance and label incorporation of U-^{13}C-glutamine.Bar charts represent the fold change in relative metabolite abundance, relative ^{13}C-label incorporation and relative ^{13}C-label quantity following 30 mins labelling; ± SE, n=3. P-values were calculated using two-tailed T-test with PBS as the reference and Holm post-hoc correction.. Stars represent: ns $p \geq 0.05$; * $p \leq 0.05$; ** $p \leq 0.01$; *** $p \leq 0.001$; **** $p \leq 0.0001$. Abbreviations: Gln- Glutamine; Glu-Glutamate; α -KG-α -keto-glutaric acid; Cit- Citrate; Suc-Succinate; Fum-Fumarate; Mal-Malate.

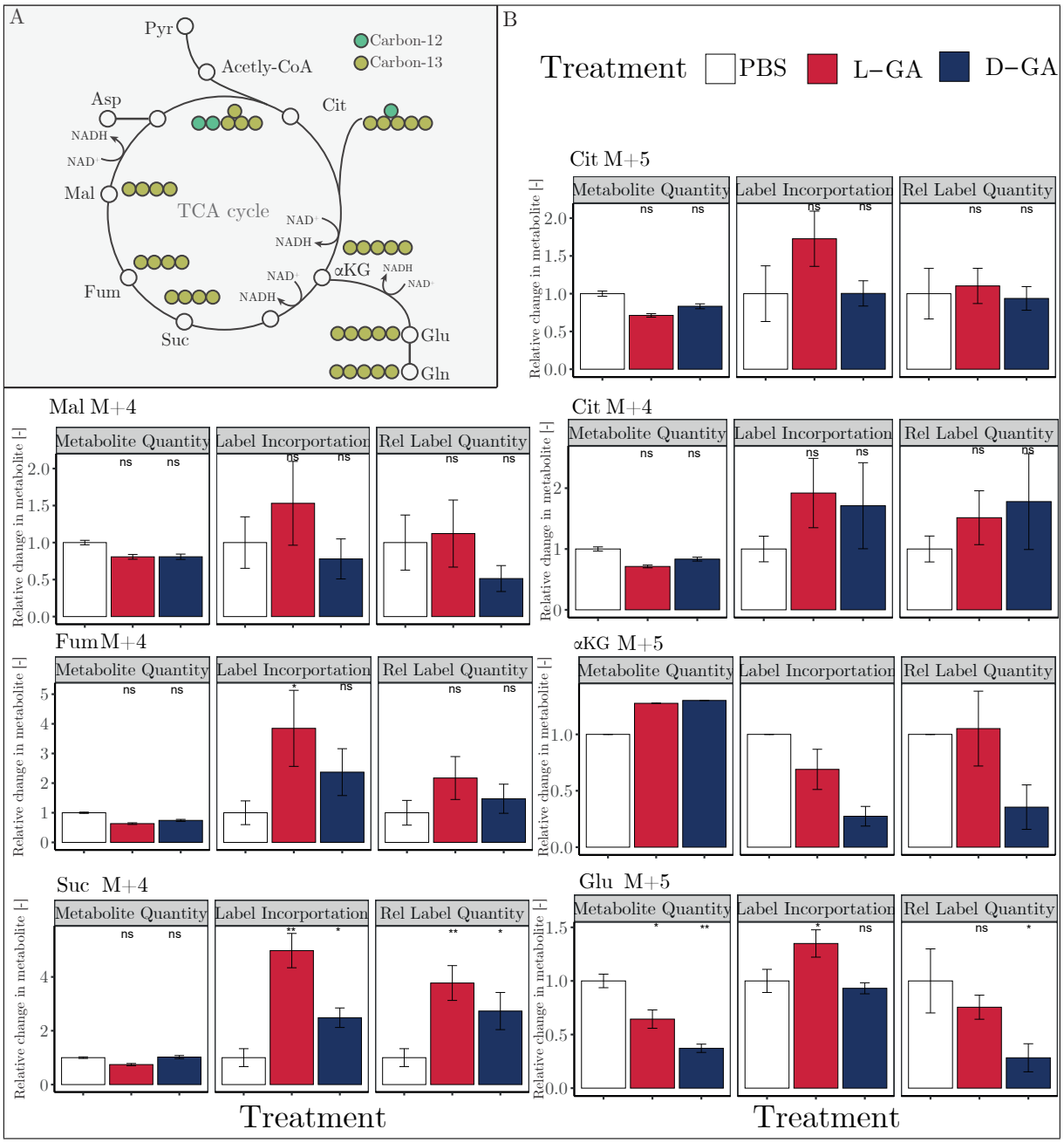

Figure 3.23: Effects of L- and D-GA on TCA cycle intermediates in SH-SY5Y cells. A: Diagram depicts the metabolites of the TCA cycle and the flow of labelled carbons from U-^{13}C-glutamine. B: Polar metabolites were extracted from SH-SY5Y cell lines following treatment of L-GA and D-GA for 1 hr. Samples were processed via GC-MS and analysed to attain the abundance and label incorporation of U-^{13}C-glutamine. Bar charts represent the fold change in relative metabolite abundance, relative ^{13}C-carbon label incorporation and relative ^{13}C-carbon label quantity,following 30 mins labelling; $\pm$ SE, n=3. P-values were calculated using two-tailed T-test with PBS as the reference and Holm post-hoc correction.. Stars represent: ns $p \geq 0.05$; * $p \leq 0.05$; ** $p \leq 0.01$; *** $p \leq 0.001$; **** $p \leq 0.0001$. Abbreviations: Gln- Glutamine; Glu-Glutamate; α-KG-α-keto-glutaric acid; Cit- Citrate; Suc-Succinate; Fum-Fumarate; Mal-Malate.

Figure 3.23, B, shows the relative metabolite abundance, ^{13}C-label incorporation and relative of ^{13}C-label quantity of measured metabolites after 30 mins of labelling in SH-SY5Y. The labelling incorporation for all time points are found in supplementary material section 5.2.2, figure 5.4. As with IMR-32, there was no significant change in the metabolite abundances of the TCA cycle intermediates. α-KG and Glu showed inverse metabolite abundances. It is to be noted that there was very low abundance of α-KG in the PBS treated cells. Therefore, no

statistical tests could be performed and the data quality is questionable. As we follow the label incorporation from Suc to Cit (M+4) displayed a significant increase in L-GA treated cells, although not in D-GA treated cells. The data presents no significant increase in Cit (M+5) label incorporation with treated cells, as found in IMR-32.

In summary, both cell lines presented increased TCA activity upon L-GA treatment but not D-GA treatment. Indeed, the label incorporation in Suc and Fum was increased by 4-fold in both cell lines. However, Mal and Cit (M+4) did not show the same extreme increase in label incorporation. It is curious that both cell lines increased the relative abundance of α-KG without increasing the label incorporation. This is suggestive of another mode of α-KG production, that is independent of the Gln to Glu labelling pathway. α-KG also plays a role in the defence against ROS. α-ketoglutarate dehydrogenase (α-KGDH) is a highly regulated enzyme, which could determine the metabolic flux through the TCA cycle. It catalyses the conversion of α-KG, succinyl-CoA (suc-CoA) which is metabolised to Suc and produces NADH providing electrons for the ETC. α-KGDH is sensitive to ROS and inhibition of this enzyme could give reasoning to the high levels of α-KG (Tretter and Adam-Vizi, 2005). However, the increase in label incorporation into Suc in L-GA treated cells shows a disconnect in this mechanism. Given that α-KG is compartmentalised in both the cytosol and mitochondria, it is difficult to discern the rate of conversion of α-KG to Suc.

3.6 Proteomic Analysis of L-GA treated Cells

A proteomic analysis was performed in an effort to elucidate which enzymes and their associated pathways are up- or down-regulated upon L-GA treatment. A panel of cell lines were chosen to give a broad view of the proteomic landscape between neuroblastoma cells. If indeed glycolysis is hindered and ROS sensitive enzymes show inhibition, it was hypothesised that an oxidative stress response is initiated and that it is a common phenotype between cell lines.

Cell lines SY-SY5Y, SK-N-AS, IMR-32, VH-7, GI-ME-N and BE(2)-C were subjected to shotgun proteomics in an effort to find metabolic pathways that are associated with L-GA treatment. All cell lines were seeded at 2e+6 cells per 10cm plate in triplicates. Following 24 hrs settling time, cells were treated with either 1 mM L-GA or PBS. Cells were harvested, proteins extracted and analysed by LC-MS according to section 2.3. Label free quantities (LFQ) of 5,340 proteins were measured, of which 244 were annotated to be associated with 17 pathways of interest.

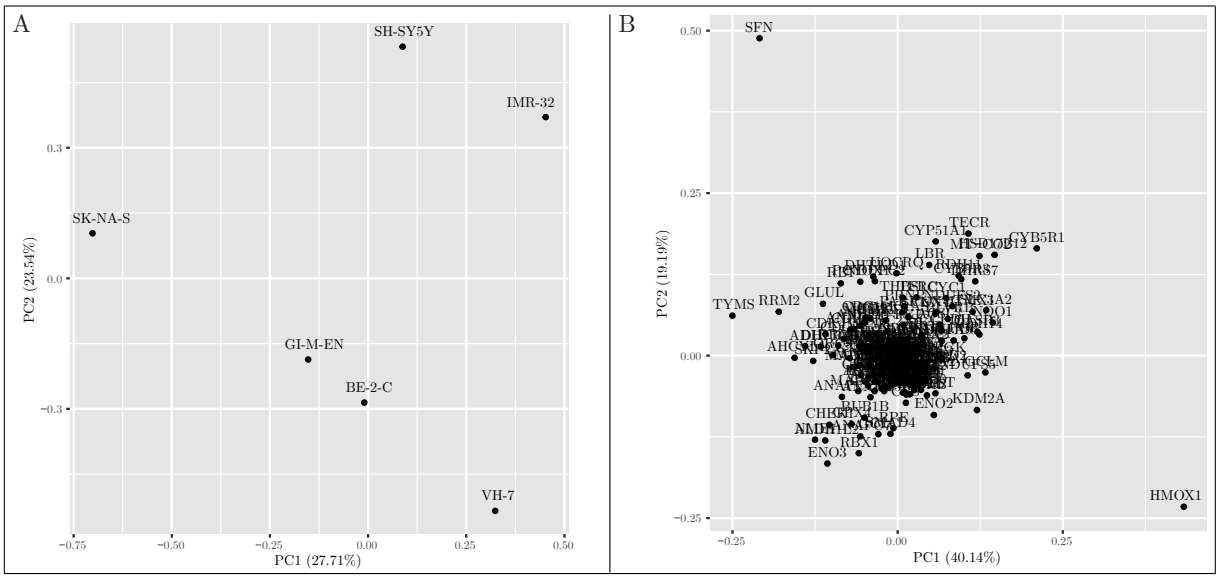

Figure 3.24: L-GA induces a change in the proteomic landscape. Proteomic analysis of cell lines: BE-2C, GI-ME-N, VH-7, SH-SY5Y, IMR-32 and SK-N-AS treated for 24 hrs. A: Principal component analysis (PCA) analysis was performed to show the variance of LFQ data between cell lines that were treated with L-GA. B: LFQ data from all each protein from cell lines in A elucidated proteins with high variance in the PCA.

Initial analysis aimed to describe the differences between cell lines in their response to L-GA treatment. Figure 3.24, A, shows the PCA analysis of all cell lines treated with L-GA. There was apparent clustering of SH-SY5Y and IMR-32, and the independent clustering of GI-M-EN and BE-2C. VH-7 and SK-N-AS showed the most extreme variance, suggesting that the response of these cell lines are significantly different. Following this, the aim was to see which proteins account for the most variance upon L-GA treatment within all cell lines. As displayed in figure 3.24, B, SFN, TYMS and RRM2 to be clear outliers. In order to discern the pathways in which these proteins reside, proteins were annotated by their associated pathways as detailed in section 5.2.3. Figure 3.25 shows a heatmap of the difference of the Log_2(LFQ) of L-GA-PBS of all annotated proteins. The data presents clustering of up-regulated proteins in the oxidoreductase pathway in IMR-32 and SH-SY5Y, although this is less pronounced in the other cell lines. Furthermore, there is clustering of cell cycle and apoptosis pathways in all cell lines, where cell cycle proteins are down-regulated. Interestingly, glycolysis and the TCA cycle do not show apparent levels of clustering.

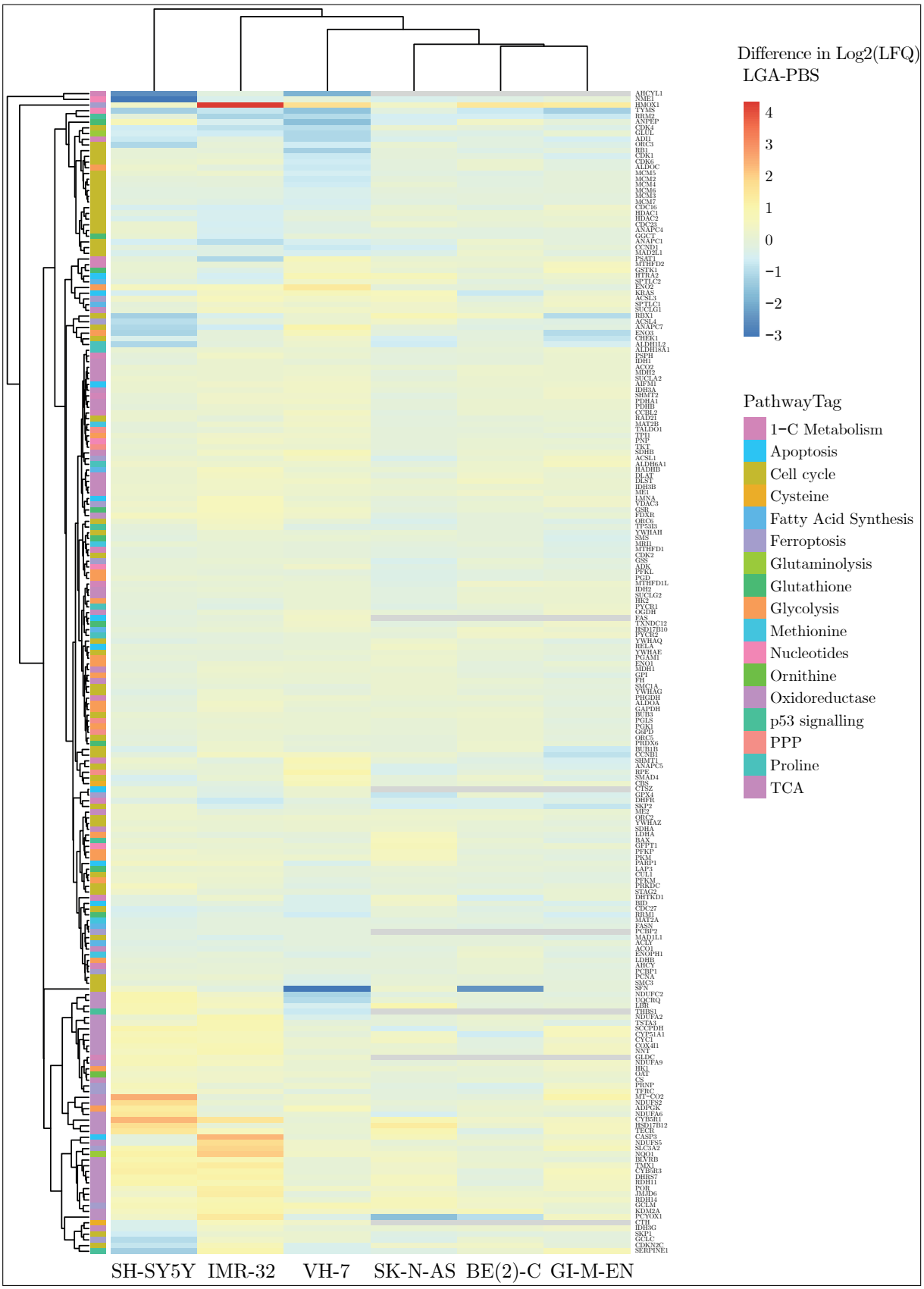

Figure 3.25: L-GA induces a change in the proteomic landscape. Proteomic analysis of cell lines: BE-2C, GI-M-EN, VH-7, SH-SY5Y, IMR-32 and SK-N-AS treated for 24 hrs with 1 mM L-GA or PBS and subjected to LC-MS proteomic analysis. Hierarchical clustering of annotated proteins show clustering of pathways between cell types. Data represents difference in label free quantity Log_2(LFQ) of L-GA treated cells relative to PBS treated cells, n= 3 for each cell line.

In an effort to precisely determine which proteins show the greatest difference relative to untreated cells, arbitrary boundaries of > 1 and < -1, were set for annotation. Figure 3.26 shows the Log_2(LFQ) ratio of proteins relative to PBS treated cells. Upon initial analysis, Haemeoxygenase (HMOX1) is the most common up-regulated protein in L-GA treated cells. HMOX1 was upregulated in BE(2)-C, IMR-32 and VH-7. Although HMOX1 was not up-regulated in SH-SY5Y, proteins of the same pathway - Oxidoreductase - are up-regulated upon L-GA treatment. GI-M-EN and SK-N-AS are apparently the least responsive to L-GA treatment with polo-like kinase 1 (PLK1) and Inositol 1,4,5-trisphosphate receptor, type 3 (ITPR3) being the only proteins captured by the set boundaries. VH-7 and BE(2)-C show similar profiles with HMOX1 observing an up-regulation and a down-regulation of Stratifin (SFN). In SH-SY5Y and VH-7 the data showed a down-regulation of nucleotide synthesis proteins, Nucleoside diphosphate kinase A (NME1) and Thymidylate synthase (TYMS), respectively. It is apparent that VH-7 is the only cell line to show a response from proteins of the glycolytic pathway, enolase 2 (ENO2) is up-regulated upon L-GA treatment. From the data provided, it is inferred that the oxidoreductase pathway is up-regulated in the majority of cell lines, with the exception of GI-M-EN and SK-N-AS. IMR-32 and SH-SY5Y present the most amount of up-regulated proteins in the oxidoreductase pathway. Oxidoreductase is an enzyme, or group of enzymes, that perform redox reactions. The redox reaction constitutes the transfer of electrons from an oxidant to reductant. This is exemplified by the NAD+/NADH and NADP+/NADPH co-factors which are essential to redox reactions and maintaining cellular oxidative homeostasis. Within this set of genes is the KEAP1 and NRF2 antioxidant pathway. This pathway includes HMOX1 and NQO1 and NDUF as downstream targets. NQO1 and HMOX1 were up-regulated in IMR-32. NQO1 and NDUF were found to be up-regulated in SH-SY5Y. It was hypothesised that the up-regulation of proteins related to the oxidoreductase pathway was a response to a redox imbalance or increase in oxidative stress caused by L-GA. Furthermore, the data suggests that the NRF2 pathway is activated upon L-GA treatment. Given this, we were interested to know if L-GA promotes an increase in reactive oxygen species.

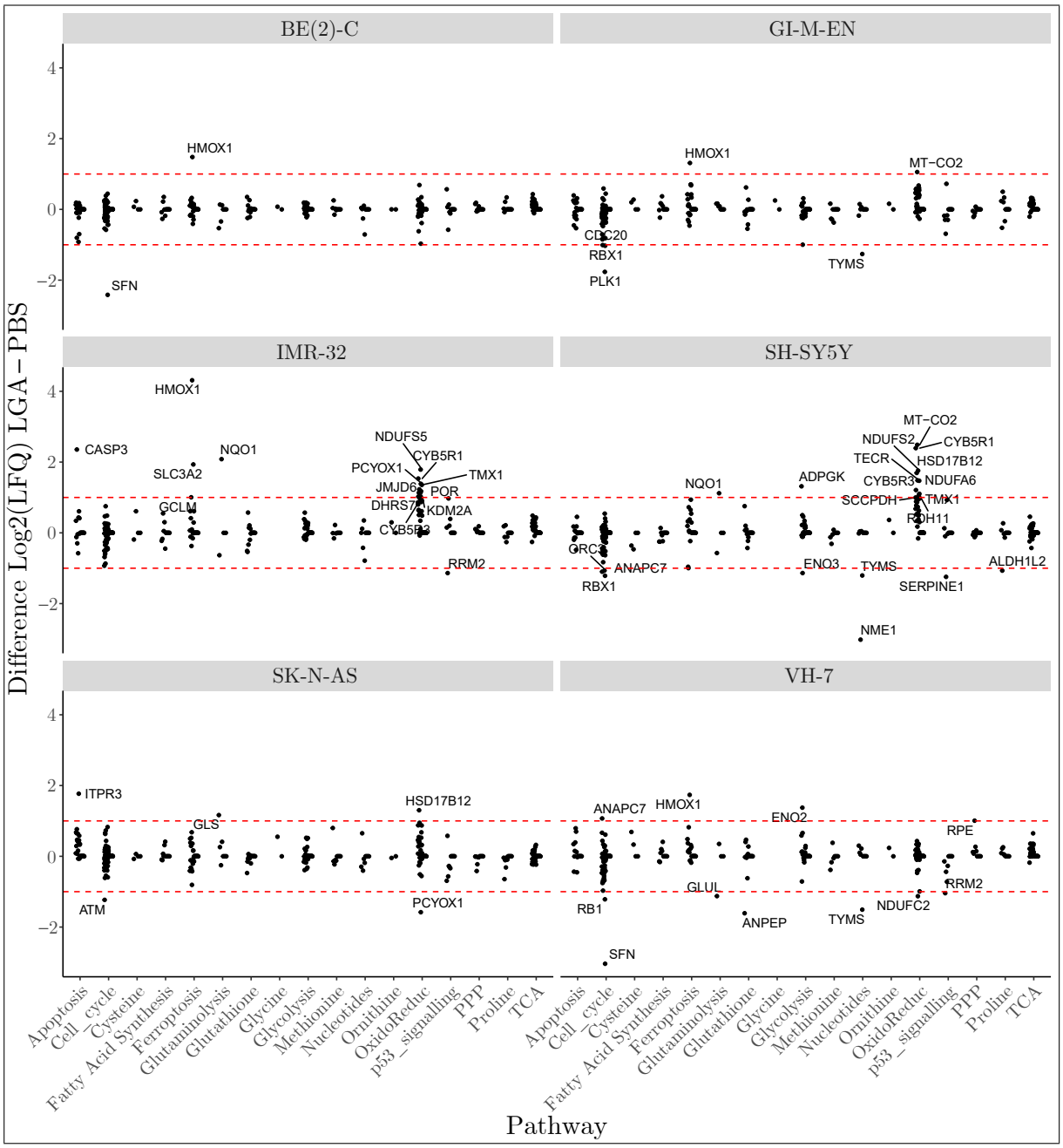

Figure 3.26: Elements of the oxidoreductase pathway is over-expressed in L-GA treated cells. Proteomic analysis of cell lines: BE(2)-C, GI-ME-N, VH-7, SH-SY5Y, IMR-32 and SK-N-AS treated for 24 hrs with 1 mM L-GA or PBS and subjected to LC-MS proteomic analysis. Analysed proteins were filtered by > 1 and < -1 difference in label free quantity Log_2(LFQ) of L-GA treated cells relative to PBS treated cells. Filtered proteins are highlighted by a red dotted line. Proteins that show differences outside of this line are labelled by text.

3.7 L-GA induces oxidative stress in neuroblastoma cells

We aimed to quantify the production of reactive oxygen species in L-GA treated cells. This was prompted by the observation of NAD+ and NADH depletion in section 3.4.2 and the increase in response of the oxidoreductase pathway in the proteomics data in section 3.6. Furthermore, the flux of carbon decreases into metabolites of glycolysis that require NADH as a co-factor (section 3.5.2).

ROS generation can be monitored by the fluorometric analysis of the oxidation of the cell

permeable compound, 2',7' –dichlorofluorescin diacetate (DCFDA) by ROS into 2', 7' –dichlorofluorescein (DCF). DCF is highly fluorescent which can be quantified by fluorescence spectroscopy (Keston and Brandt, 1965; Brandt and Keston, 1965). ROS generation can be quenched by the application of N-acetyl-Cysteine (NAC). NAC is a pro-drug to L-cysteine which is a precursor of the antioxidant glutathione. The thiol group of glutathione scavenges ROS, thereby reducing oxidative stress (Sansone and Sansone, 2011). The experimental aim was to assess whether L-GA induces ROS generation and if this can be rescued by NAC.

3.7.1 L-GA induces oxidative stress

Cell lines IMR-32 and SH-SY5Y were seeded at 2.5e+4 cells per well in a black walled 96-well plate (Corning). Following 24 hrs settling time media was exchanged and supplemented with: 1X PBS, 1 mM L-GA, 100 µM H_2O_2, 1 mM L-GA + 5 mM NAC, 100 µM H_2O_2+ 5 mM NAC and 1X PBS + 5 mM NAC. Cells were incubated for 4 hrs with each treatment condition before DCFDA staining and fluorescence reading as described in section 2.1.7. Figure 3.27 shows fluorescence intensity after treatment normalised to PBS treated cells. In both cell lines 100 µM H_2O_2, induces a 17- and 24-fold increase in fluorescence in IMR-32 and SH-SY5Y, respectively. L-GA induces a 1.9- and 2.1-fold increase in IMR-32 and SH-SY5Y. The data showed that the increase in IMR-32 is significant ($p \leq 0.05$), although not in SH-SY5Y. Upon treatment with 5 mM NAC, the fluorescence of 100 µM H_2O_2treated cells decreases significantly. IMR-32 fluorescence is reduced to 0.4 and SH-SY5Y is reduced to 0.8 to that of PBS treated cells. Similarly, there is a significant reduction ($p \leq 0.05$) in fluorescence of L-GA treated IMR-32 cells in the presence of NAC. In SH-SY5Y cells treated with L-GA and NAC there is a reduction to 0.8 of PBS treated cells, although this is not found to be significant. From this data, we can conclude that 1 mM L-GA does induce an increase in DCFDA fluorescence and indicates an increase in ROS. The application of 5 mM NAC reduces the fluorescence of L-GA and H_2O_2treated cells, indicating that NAC does indeed reduce ROS in these cell lines. In section 3.1.1 it was found that L-GA inhibits neuroblastoma cell growth, in light of this, the aim was to examine whether NAC can rescue cell growth in L-GA treated cells.

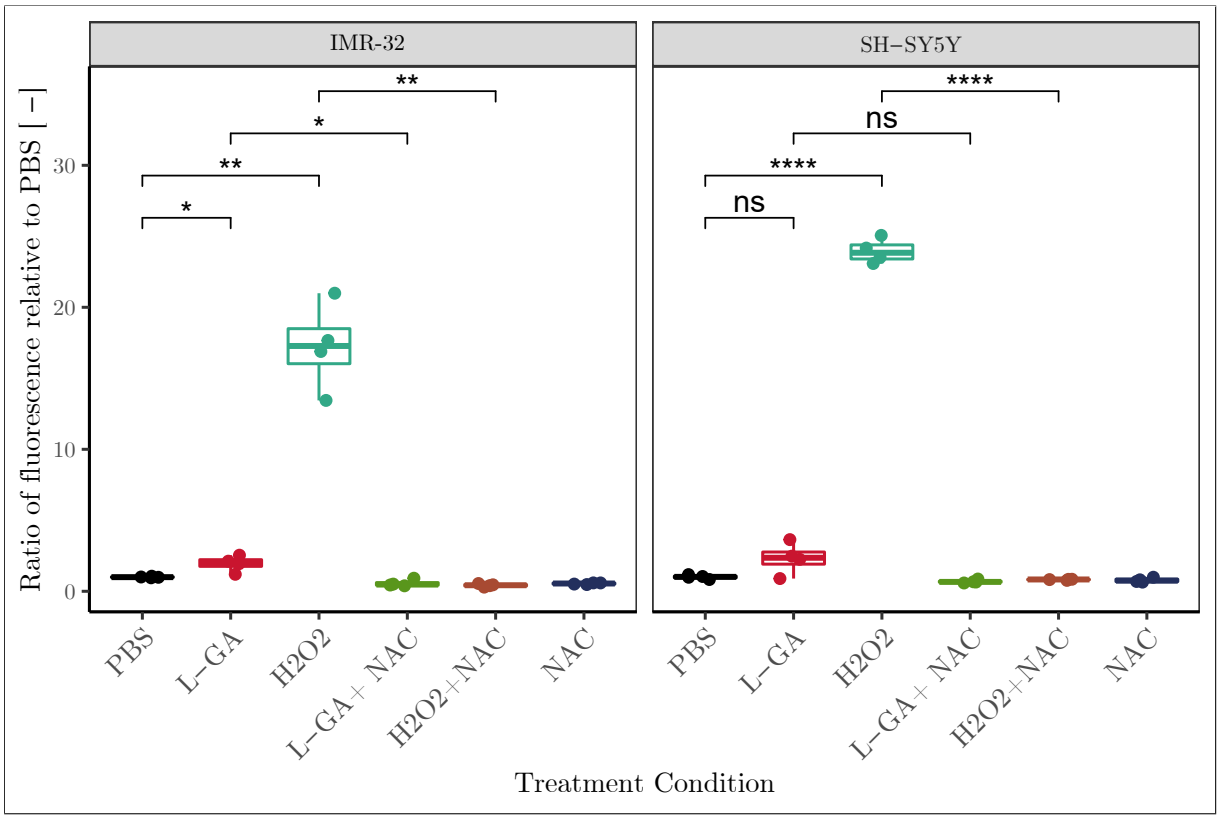

Figure 3.27: Quantification of reactive oxygen species following L-GA treatment. Cell lines IMR-32 and SH-SY5Y were treated for 6 hrs with 1 mM L-GA, 100 µM H_2O_2, 5 mM NAC and combinations as shown. ROS species were quantified using the Cellular ROS Assay Kit (ab113851), measuring the fluorescence from DCFDA signal at Ex/Em: 485/535 nm on a Spectramax iD microplate reader (Molecular Devices). Bar charts show the ratio of fluorescence relative to the PBS control. Error bars ± SEM, n=6. P-values were calculated using pairwise T-test with Holm post-hoc correction. Stars represent: ns $p \geq 0.05$; * $p \leq 0.05$; ** $p \leq 0.01$; *** $p \leq 0.001$; **** $p \leq 0.0001$.

3.7.2 L-GA induces the NRF2 pathway which is rescued by NAC

To confirm the findings from the proteomics data I performed a western blot to probe for KEAP1, NRF2, HMOX1, NQO1 and CASPIII. KEAP1 and NRF2 regulate the expression of HMOX1 and NQO1 as described in detail in section 1.5.2. Briefly, cells were seeded at 2e+6 cells and allowed to settle for 24 hrs before treatment with 1X PBS, 1 mM L-GA or 1 mM L-GA + 5 mM NAC. Cells were harvested following the protocol in section 2.2.1. Proteins were extracted and prepared for western blot via the protocol described in section 2.2.4.

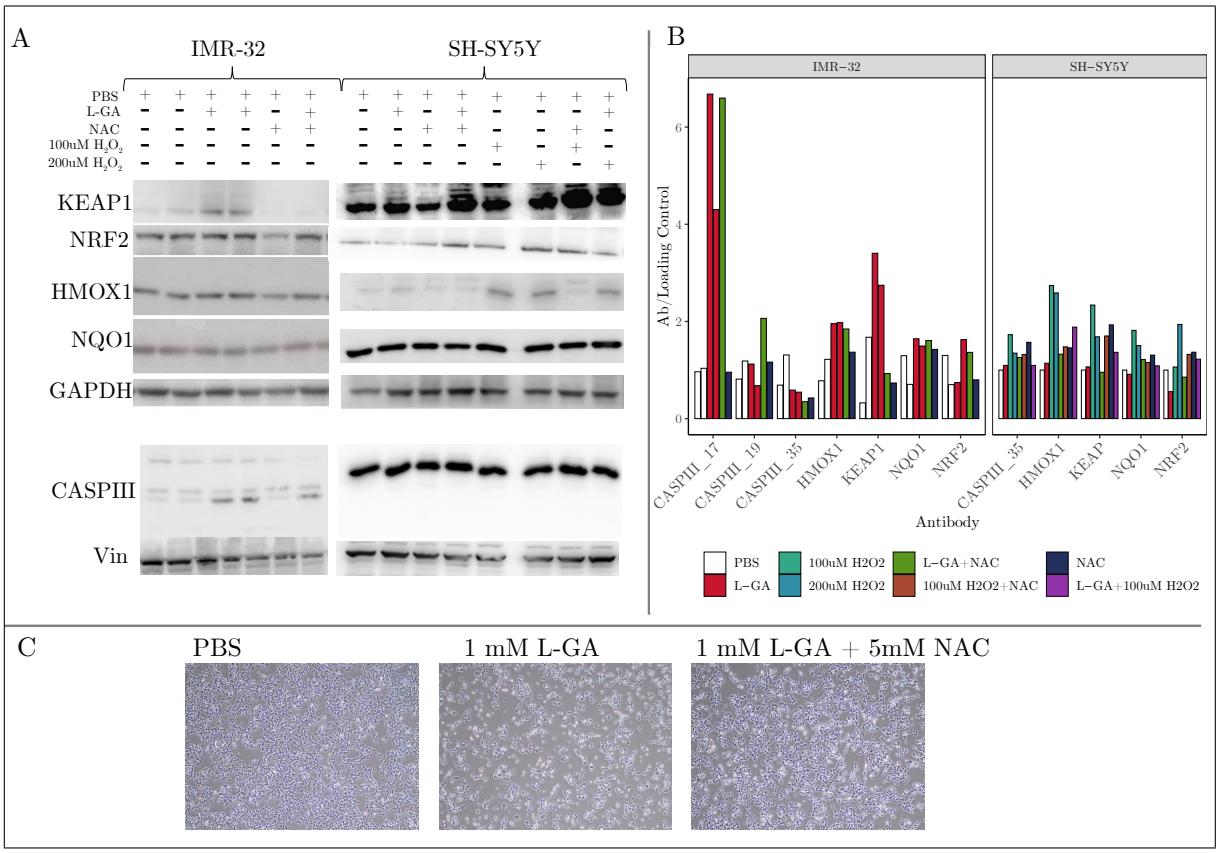

Figure 3.28: The KEAP1-NRF2 pathway is induced upon L-GA treatment in IMR-32 cells. A: IMR-32 was treated for 24 hrs with PBS, 1 mM L-GA, NAC and 1 mM L-GA + 5 mM NAC. SH-SH5Y was treated for 24 hrs with PBS, 1 mM L-GA, 1 mM L-GA + 5 mM NAC, 5 mM NAC, 100 µM H_2O_2, 200 µM H_2O_2, 100 µM H_2O_2 +NAC and 100 µM H_2O_2 + 1 mM LGA. Cell lysates were collected and subjected to SDS-PAGE probing for: KEAP1, NRF2, HMOX1, NQO1, CASPIII using Vinculin and GAPDH (For NRF2 only) as loading controls. B: Intensity of bands on exposed membranes were measured using ImageJ software and peak areas of each intensity were normalised to their respective loading control. All ratios were normalised to the PBS treatment for each protein of interest. C: IMR-32 cells were treated for 24 hrs with the treatments described, cells were imaged via phase contrast microscopy at 10X magnification on a Nikon Eclipse TS2 microscope.

Figure 3.28, A, shows western blots and quantification of the proteins described above. In IMR-32 cells KEAP1 was increased upon L-GA treated which was decreased in the presence of NAC. NRF2 was constitutively expressed in all conditions although there was a decrease in intensity in the presence of NAC. Similarly, there was a marginal decrease in the intensity of HMOX1 when NAC was present. L-GA induced a slight increase in HMOX1 expression. NQO1 did not appear to show any difference between treatments, it may be that its basal expression is high. The activity of CASPIII, the apoptosis marker, is inferred by its cleavage. Three cleavage markers in which samples treated with L-GA show the high intensity of cleaved products are observed. NAC caused a marginal reduction in the intensity of the cleaved products although it is not apparent if apoptosis was inhibited. SH-SY5Y cells showed less response of KEAP1-NRF2 targets than IMR-32 when treated with L-GA. When using 100 µM H_2O_2 as a positive control for NRF2 activation, there was an increase in HMOX1. Comparatively, L-GA does not produce a strong HMOX1 response. Application of NAC reduced HMOX1 expression in H_2O_2 treated cells. No significant differential in NRF2, KEAP1 or NQO1 regulation was found. Furthermore, no apoptotic markers were found from CASPIII cleavage. Figure 3.28, C, shows phase contrast images of IMR-32 cells following 24 hrs incubation with 1X PBS, 1 mM

L-GA and 1 mM L-GA + 5 mM NAC. Qualitatively, the data presented improved cell number, morphology and density in cells that were treated with L-GA+NAC. Following this data, the aim was to assess whether NAC has persistent effects on cell growth, and is able to negate the inhibitory effect of L-GA, particularly in IMR-32 cells.

3.7.3 Cell growth is partially restored by NAC in L-GA treated cells

Cell lines IMR-32 and SH-SY5Y were treated for 72 hrs, with sampling of the cell count every 24 hrs. Cells were treated with: 1X PBS, 1 mM L-GA, 50 µM H_2O_2, 1 mM L-GA + 5 mM NAC, 50 µM H_2O_2+ 5 mM NAC and 1X PBS + 5 mM NAC. For both cells lines, cell growth is inhibited with 1 mM L-GA. Upon supplementation with 5 mM NAC, L-GA treated IMR-32 cells show cell growth similar to L-GA with a slightly reduced log phase. After 72hrs treatment with 1 mM L-GA cell counts in IMR-32 were 25-fold and and 26-fold lower than counts treated with PBS and LGA+NAC, respectively. SH-SY5Y did not show the same level of recovery when NAC was applied with L-GA. Following 72 hrs incubation, L-GA treated cells showed a 5-fold reduction in cell count relative to PBS, whereas NAC generates a 1.67-fold increase in cell count when in combination with L-GA. 50 µM H_2O_2 does not show significant decreases in cell count following 72 hrs incubation in either cell line. However after 48 hrs the data presented a 1.2-fold and 1.3-fold reduction in cell counts upon 50 µM H_2O_2 treatment relative to PBS in IMR-32 and SH-SY5Y respectively. When supplementing H_2O_2treated cells with 5 mM NAC there was a 1.3-fold increase in cell counts for both IMR-32 and SH-SY5Y relative to H_2O_2treated cells.

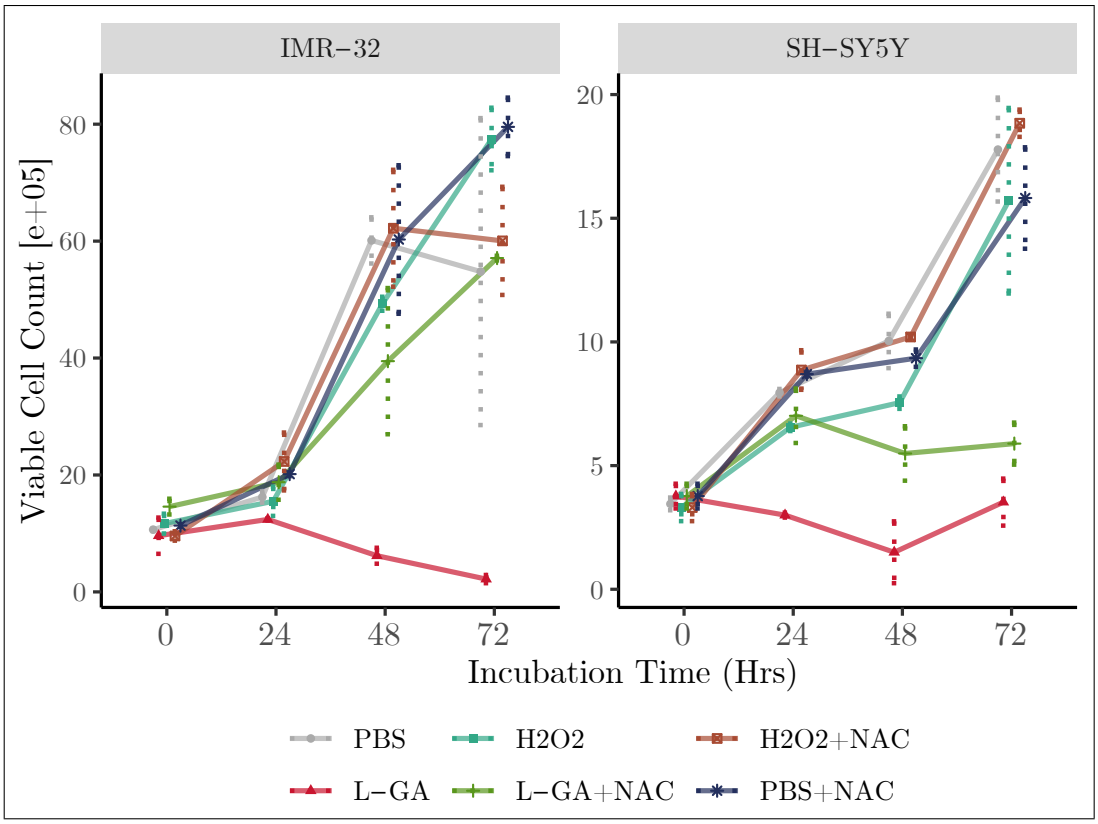

Figure 3.29: L-GA reduces cell growth which is recovered via NAC. Cell lines IMR-32 and SH-SY5Y were treated for 72 hrs with 1 mM L-GA, 50 µM H_2O_2 and 5 mM NAC and in the combinations shown. Cells were seeded at 2e+5 cells per well in a 6-well plate. Viable cell counts were taken every 24 hrs via the trypan exclusion method. Error bar representing the ± SD of the mean for three biological replicates. Experiments were carried out by Richard Kempa (Master student, Stefan Kempa Lab, BIMSB/ Berlin, Germany)

In summary, NAC acts to partially restore cell growth in L-GA treated cells, although SH-SY5Y appear to be less sensitive to NAC treatment. As L-GA has been shown to deplete nucleotide pools, the aim was to assess whether NAC restores nucleotide pools when in combination with L-GA treatment.

3.7.4 Oxidative stress reduces nucleotide pools which is rescued via NAC

It was hypothesised that the application of NAC would restore nucleotide pools in cells experiencing oxidative stress. Nucleotides were measured after 16 hrs treatment with 1 mM L-GA, 100 µM H_2O_2 and 5 mM NAC and in the combinations shown in figure 3.30. Briefly, cells were seeded at 2e+6 cells per 10cm plate in triplicate. Cells were allowed to settle for 24 hrs before treatment. Cells were harvested, nucleotides extracted and analysed DI-MS-MS following the protocol described in section 2.5. Figure 3.30 shows the fold change in 40 measured nucleotides relative to PBS. As found previously, there was a significant reduction mean fold change of nucleotides following L-GA treatment. The data presents a median of 0.61 ($p \leq 0.0001$) and 0.33 ($p \leq 0.0001$) for IMR-32 and SH-SY5Y respectively. Upon 100 µM H_2O_2 treatment, nucleotides were reduced by a median of 0.02 ($p \leq 0.0001$) and 0.2 ($p \leq 0.0001$) for IMR-32 and SH-SY5Y, respectively. At 200 µM H_2O_2 IMR-32 cells did not survive and no nucleotides were measured. However, SH-SY5Y cells presented a median reduction of 0.19 $p \leq 0.0001$). Upon application of 5 mM NAC to L-GA treated IMR-32 cells, the median of the mean fold change of nucleotides is 0.94 to that of the control, which is a 1.5-fold increase from L-GA treated cells. Similarly, SH-SY5Y presented a median of 0.62 for L-GA and NAC treated cells, which equates to a 1.88-fold increase from L-GA treated cells. The application of NAC to 100 µM H_2O_2 treated cells increased the median nucleotide pools in IMR-32 to 0.24, resulting in a 13-fold increase to 100 µM H_2O_2 treated nucleotides. SH-SY5Y presented a 2-fold increase in nucleotides treated with 100 µM H_2O_2 and NAC, relative to 100 µM H_2O_2 alone. Similarly, 200 µM H_2O_2 and NAC caused a 3-fold increase in nucleotide pools relative to 200 µM H_2O_2 alone.

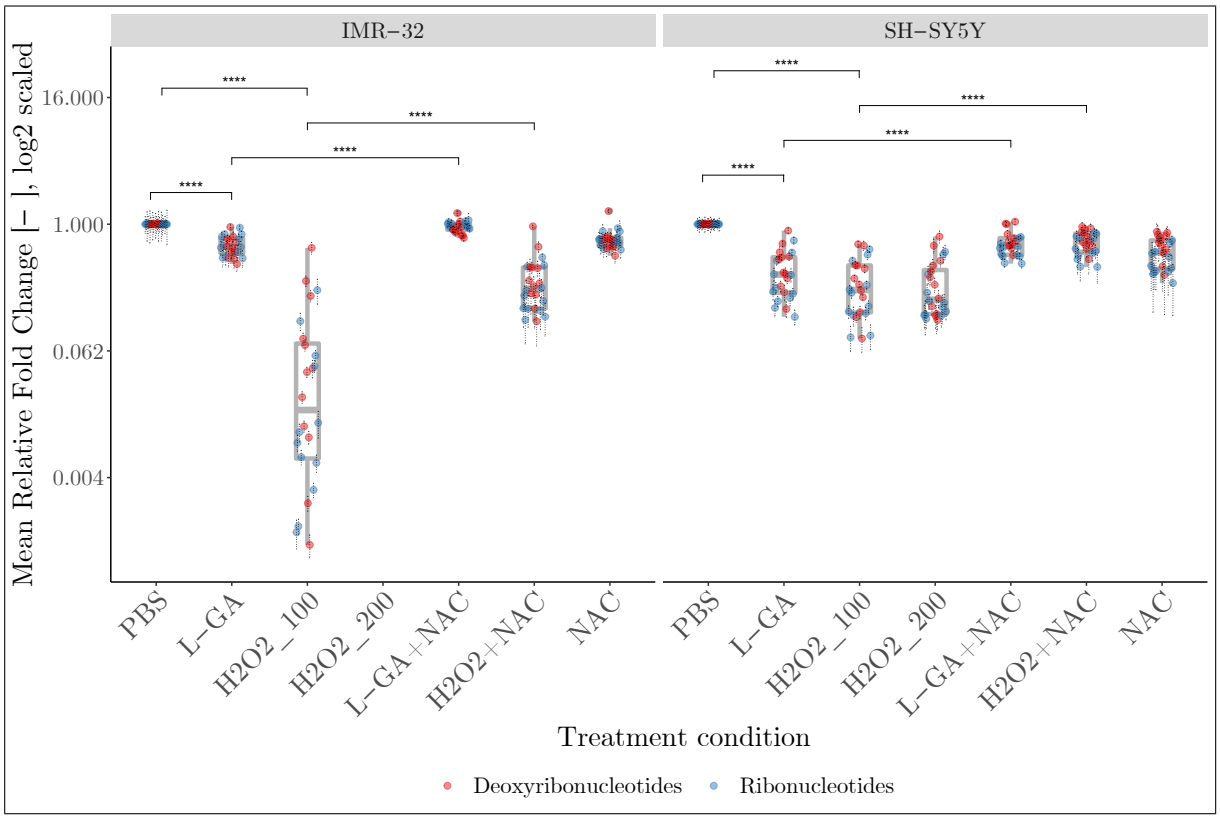

Figure 3.30: L-GA reduces nucleotide pools in a fashion similar to ROS. Cell lines IMR-32 and SH-SY5Y were treated for 16 hrs with 1 mM L-GA, 100 µM H_2O_2 and 5 mM NAC and in the combinations shown. 200 µM H_2O_2 resulted in complete cell death in IMR-32 therefore data is not shown. Nucleotides were extracted from cell lysates and measured by DI-MS/MS. Boxplots present the mean fold change in deoxy- and ribonucleotide intensities relative to PBS. Data shown represents n=4 with 3 technical replicates. P-values were calculated using pairwise Wilcoxon test with Holm post-hoc correction, stars represent: ns $p \geq 0.05$; * $p \leq 0.05$; ** $p \leq 0.01$; *** $p \leq 0.001$; **** $p \leq 0.0001$.

The data indicated that ROS induces a depletion in nucleotides. At 100 µM H_2O_2 there was a greater depletion in nucleotides than that observed with 1 mM L-GA. Therefore, at these concentrations H_2O_2 is a more potent oxidiser. Upon analysis of the cell status the NAD+/NADH ratio, the phosphorylation potential and the AMP/ATP ratio were the most significantly affected in both cell lines (figure 3.31). In IMR-32, the AMP/ATP ratio was significantly increased in both L-GA and 100 µM H_2O_2 treated cells. Upon addition of NAC, AMP/ATP levels returned almost to levels found with PBS treated cells. The NAD+/NADH ratio was significantly increased with L-GA treatment in IMR-32 cells, although not with 100 µM H_2O_2. When NAC was applied the NAD+/NADH ratio returns to PBS treatment levels. The phosphorylation potential of L-GA and 100 µM H_2O_2 treated cells was significantly reduced. SH-SY5Y appeared to be more resistant to oxidative stress. This is highlighted by a less extreme response in NAD+/NADH and NADP+/NADPH ratios following L-GA and H_2O_2 treatment. The data presented a similar profile for AMP/ATP and phosphorylation potential ratios as found with IMR-32.

In summary, oxidative stress induced by L-GA and H_2O_2 caused a redox imbalance and had a significant effect on the phosphorylation potential of the cell. This phenotype is remedied by the addition of the antioxidant NAC. It was hypothesised that NAC may restore metabolic

function by increasing NAD+/NADH cycling and ATP production for phosphorylation potential.

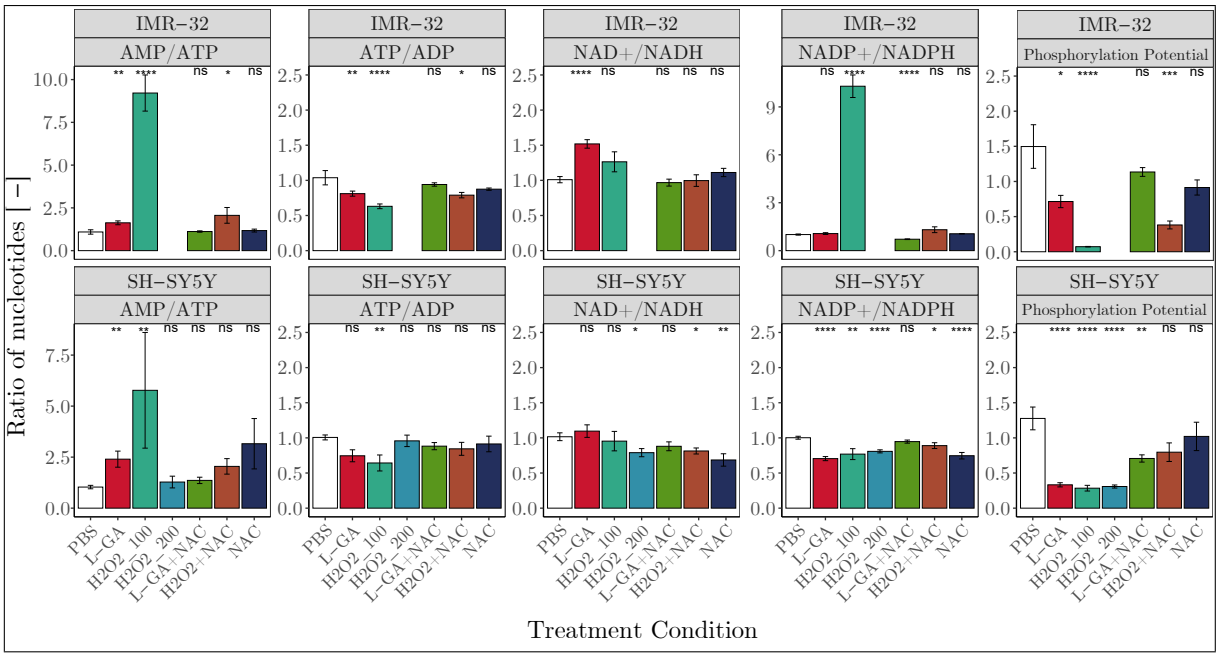

Figure 3.31: L-GA reduces nucleotide pools in a fashion similar to ROS. Cell lines IMR-32 and SH-SY5Y were treated for 16 hrs with 1 mM L-GA, 100 µM H_2O_2 and 5 mM NAC and in the combinations shown. 200 µM H_2O_2 resulted in complete cell death in IMR-32 therefore data is not shown. Nucleotides were extracted from cell lysates and measured by DI-MS/MS. Boxplots present the ratio of nucleotides from equations stated in 3.4.2. Data shown represents n=4 with 3 technical replicates. P-values were calculated using Wilcoxon non-parametric test with PBS as the reference group and Holm post-hoc correction, stars represent: ns $p \geq 0.05$; * $p \leq 0.05$; ** $p \leq 0.01$; *** $p \leq 0.001$; **** $p \leq 0.0001$.

3.7.5 NAC restores metabolic function of L-GA treated cells

In order to assess the effect of NAC and L-GA on the flux of carbon through glycolysis the pSIRM method was employed. Briefly, cell lines IMR-32 and SH-SY5Y were seeded at 2e+6 cells per plate in triplicate 10cm plates. Twenty four hours after seeding cells were treated for 16 hrs with 1X PBS, 1 mM L-GA or 1 mM L-GA + 5 mM NAC. Within the 16 hrs treatment time cell culture media was exchanged supplemented with U-^{13}C-glucose to initiate metabolite labelling. Labelling was quenched at 2, 5, 10 and 15 mins, metabolites were extracted and subjected to GC-MS, the labelling strategy is exemplified in figure 3.32, A. Figure 3.32, B shows the relative metabolite abundance, ^{13}C-label incorporation and relative of ^{13}C-label quantity of measured metabolites after 10 mins of labelling in IMR-32 and SH-SY5Y cells. All data were normalised to the cinnamic acid internal control and mean cell count for each condition and cell line. The labelling incorporation for all time points are found in supplementary material section 5.2.2, figure 5.5.

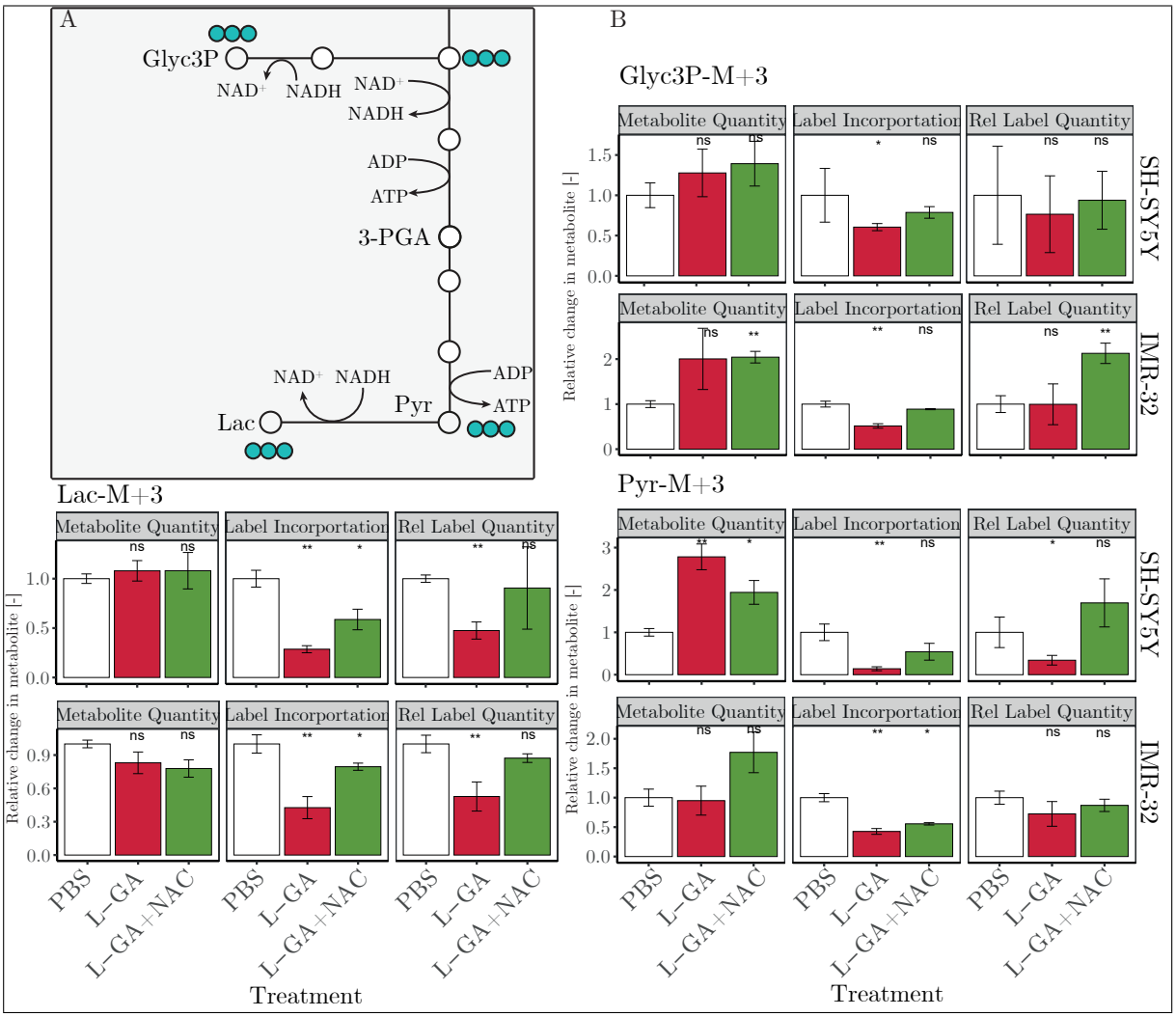

Figure 3.32: Effects of L-GA and NAC on glycolysis intermediates in IMR-32 and SH-SY5Y cells. A: Diagram depicts the metabolites of the glycolytic pathway and the flow of labelled carbons from U-^{13}C-Glucose. B: Polar metabolites were extracted from IMR-32 and SH-SY5Y cell lines following treatment of L-GA and L-GA + NAC for 16 hrs. Samples were processed via GC-MS and analysed to attain the abundance and label incorporation of U-^{13}C-glucose. Bar charts represent the fold change in absolute metabolite concentration, label incorporation and relative ^{13}C-label quantity, relative to PBS ± SE, n=3. P-values were calculated using a two-tailed T-test with PBS as the reference and Holm post-hoc correction. Stars represent: ns $p \geq 0.05$; * $p \leq 0.05$; ** $p \leq 0.01$; *** $p \leq 0.001$; **** $p \leq 0.0001$. Abbreviations: Glyc3P- Glycerol-3-phosphate; Lac - Lactate; Pyr - Pyruvate.

For SH-SY5Y cells, no significant change in the relative metabolite abundance of Lac or Glyc3P upon L-GA treatment was found. As seen with the 1 hr treatment in section 3.5.2, an accumulation of Pyr was observed. When assessing the relative ^{13}C-label incorporation there was a significant reduction in Glyc3P, Lac and Pyr ($p \leq 0.01$). This was also reflected in labelled quantity of Lac and Pyr however the labelled quantity of Glyc3P was ambiguous. Upon L-GA and NAC treatment there was no significant change in the metabolite abundances of Lac or Glyc3P, however Pyr abundance was decreased relative to L-GA treated cells. Although this was still significantly above PBS treated cells ($p \leq 0.05$). ^{13}C-label incorporation for Glyc3P increased 1.2-fold relative to L-GA treated cells when NAC was present. Lac incorporation increased 2.5-fold. For Pyr label incorporation increased 2.4-fold. Similar values were found for the relative label incorporation of Lac and Pyr, however Glyc3P was ambiguous.

For IMR-32 cells there was an increase in the metabolite abundance of Glyc3P upon L-GA

and L-GA+NAC treatment, although no significance was found with L-GA alone. No change in the metabolite abundance of Lac with L-GA treatment was found. Contrary to findings in section 3.5.2, the data presented no change in Pyr abundance with L-GA treatment but an increase in cells treated with both L-GA and NAC. When considering ^{13}C-label incorporation there was a significant decrease for Glyc3P, Lac and Pyr upon L-GA treatment which was recovered by the addition of NAC. Addition of NAC increased label incorporation into Glyc3P by 1.8-fold, Lac by 2-fold and Pyr by 1.25-fold. Similarly there was an increase in the labelled quantity for Lac and Glyc3P, although no increase in Pyr when considering cells treated with L-GA and NAC, relative to L-GA alone.

3.7.6 Serine and Glycine metabolism is not affected by L-GA

Serine and glycine metabolism is essential for the folate cycle which supplies nitrogen groups to N^{10}-formyltetrahydrofolate for the synthesis of the nucleotide intermediates, FAICAR from AICAR. We suspected that glycolytic inhibition after GAPDH would inhibit 3-phosphoglycerate, serine and glycine metabolism, thereby hindering nucleotide metabolism. Figure 3.33 shows the relative metabolite concentrations, ^{13}C-label incorporation and relative incorporation for serine, glycine and alanine following 10 mins of U-^{13}C-glucose labelling. For both cell lines no significant difference was found in the metabolite concentrations of Ser or Gly following L-GA treatment. Similarly, no change was found in the label incorporation, although the presence of L-GA slightly increased the relative label quantity, suggestive of a reduction in the usage of both amino acids. This is possibly explained by the depletion of nucleotides and less demand for Gly and Ser. Following L-GA treatment label incorporation into Ala decreased slightly however it is unknown how significant of a biological effect this had on the cells. It was found that L-GA had only a marginal effect on amino acid synthesis as shown by the heat maps in supplementary material figure 5.6. The data provided here suggests that Ser and Gly are not a source of nucleotide depletion upon L-GA treatment.

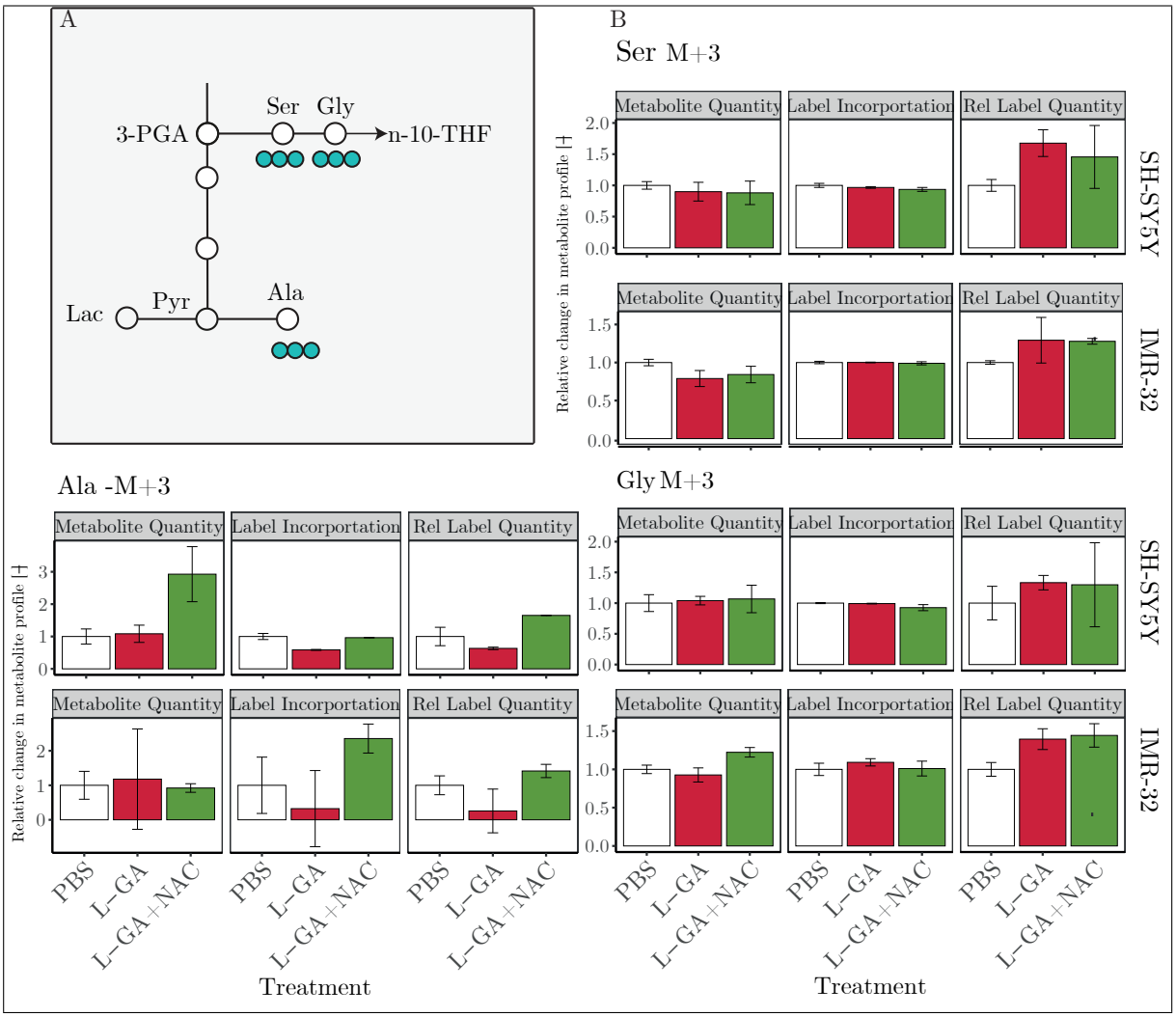

Figure 3.33: L-GA does not effect synthesis of serine and glycine. A: Diagram depicts the metabolites of the glycolytic pathway and the flow of labelled carbons from U-^{13}C-Glucose. B: Polar metabolites were extracted from IMR-32 and SH-SY5Y cell lines following treatment of L-GA and L-GA + NAC for 16 hrs. Samples were processed via GC-MS and analysed to attain the abundance and label incorporation of U-^{13}C-glucose. Bar charts represent the fold change in absolute metabolite concentration, label incorporation and relative ^{13}C-label quantity. Abbreviations: Ala- Alanine Gly- Glycine; Ser - Serine.

In summary, when applying NAC in the presence of L-GA, NAC restores the incorporation of ^{13}C-label into Glyc3P, Lac and Pyr. From the evidence provided in section 3.7.4, L-GA depletes NADH pools, as shown by an increase in the NAD+/NADH ratio. NADH is produced via GAPDH and utilised by LDH and GPDH to produce Lac and Glyc3P from Pyr and DHAP, respectively. It is that L-GA inhibits GAPDH, likely through oxidation of its cysteine rich active site, breaking NADH cycling. NAC acts to protect oxidation of GAPH thereby restoring NADH cycling. The fate of L-GA metabolism is shown in figure 3.34. In both cell lines L-GA was metabolised to glyceric acid and glycerol with no difference between NAC presence or without. In the presence of NAC, there were increased levels of 3-PGA in IMR-32 cells but not in SH-SY5Y. Glycerol-3-phosphate showed no difference in metabolite abundance with or without NAC. The metabolism of L-GA to glycolic and glyoxylic acid accumulated in both cell lines without the presence of NAC. This is of particular interest as the metabolism of glyoxylic acid via glyoxylate reductase is an NAD(P)+/NAD(P)H dependent reaction, which L-GA inhibits.

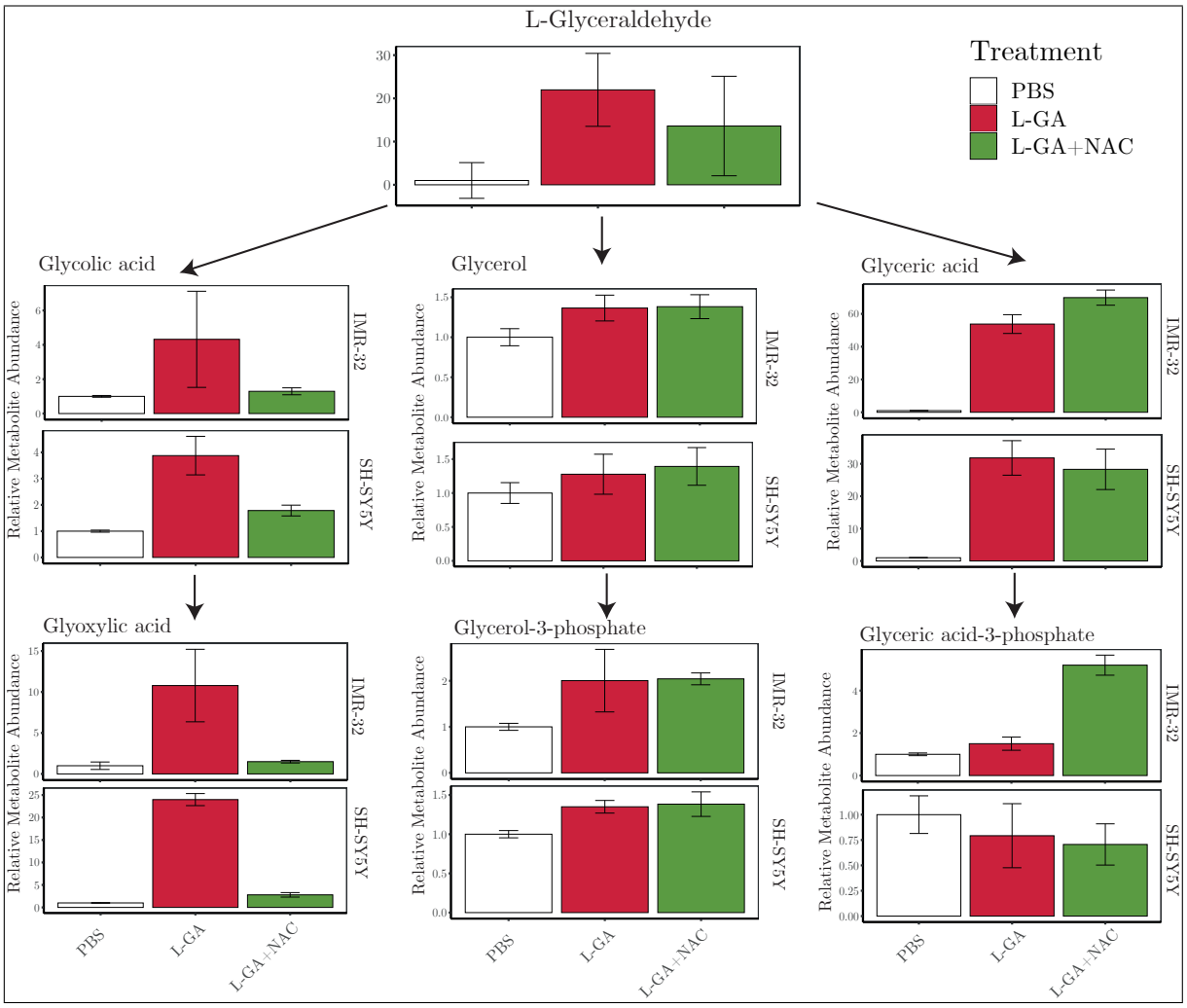

Figure 3.34: The fate of glyceraldehyde metabolism in the presence of NAC. Diagram depicts the metabolites of the glycolytic pathway and the flow of labelled carbons from U-^{13}C-glucose. B: Polar metabolites were extracted from IMR-32 and SH-SY5Y cell lines following treatment of L-GA and L-GA + NAC for 16 hrs. Samples were processed via GC-MS and analysed to attain the abundance and label incorporation of U-^{13}C-glucose. Bar charts represent the fold change in absolute metabolite concentration, label incorporation and relative ^{13}C-label quantity, relative to PBS $\pm$ SE, n=3. Abbreviations: Glyc3P- Glycerol-3-phosphate; Lac - Lactate; Pyr - Pyruvate.

Chapter 4

Discussion

It is expected that in excess of 50% of patients with high-risk neuroblastoma will relapse, despite intensive multi-modal therapeutic strategies (Morgenstern and Irwin, 2019). As high-risk neuroblastoma requires successive rounds of aggressive treatment, therapy often results in serious jeopardy to the health of the patient and may drive development of resistant clonality (Scatena et al., 2008; Pelicano et al., 2006). Current treatment strategies such as chemo- and radiotherapy typically have very low therapeutic index, therefore there is scope for novel therapeutic development.

The understanding of cancer cell metabolism is paramount in supporting the development of novel therapeutic avenues, or indeed reviving historical anti-tumoural compounds. As has been described, the cancer cell harbours a unique phenotype. In the context of this thesis, the metabolic phenotype defines the nature of the cancer cell and presents a viable therapeutic target. Cells utilise carbohydrates, amino acids and fatty acids for the production of ATP, and intermediates for the biosynthesis of macromolecules. In order to support high rates of anabolism for proliferative growth, tumour cells possess up-regulated metabolic pathways to produce abundant precursors and metabolite intermediates (De Berardinis and Chandel, 2016). Compounds that are able to perturb cancer cell metabolism, specifically glycolysis, may confer high therapeutic value. Glyceraldehyde has been shown to inhibit the growth of tumour cells, inhibit glycolysis and be well tolerated at high concentrations *in vivo* (Warburg et al., 1924; Stickland, 1941; Needham et al., 1951; Warburg et al., 1963). Furthermore, it has been shown to be effective at reducing growth in neuroblastoma cell lines *in vitro* (Prasad, 1972).

The work presented in this thesis describes how L-GA inhibits neuroblastoma cell growth. L-GA induces significant changes and the metabolic profile and hinders nucleotide biosynthesis. In addition, L-GA generates oxidative stress, likely through breaking of redox mechanisms. In response to this global effect on the cell, the regulation of the cell cycle is arrested and there is evidence for the initiation of apoptosis. We will discuss the results presented and the molecular mechanism by which L-GA presents its potential therapeutic efficacy.

4.1 Growth inhibition and cell cycle arrest

In figure 3.1 L-GA is shown to inhibit neuroblastoma cell growth at millimolar concentrations. This data is concordant with the findings presented by Prasad (1972), in which neuroblastoma

cell growth was inhibited by 100% after 24 hrs treatment with 1 mM DL-glyceraldehyde. In the same paper it was found that the non-cancerous control cell line CHO-K1 was not as profoundly inhibited as the neuroblastoma cells, despite having a higher growth rate. The findings in this thesis concur. The non-cancerous control cell line (VH-7) did not show the same level of inhibition of growth at equimolar L-GA concentrations as IMR-32 and SH-SY5Y. Interestingly, we also found that growth rate did not correlate with the EC_{50} of L-GA in IMR-32, IMR-32 presented a slightly higher EC_{50}, although the doubling time is more than half that of SH-SY5Y (Tumilowicz et al., 1970; Ross et al., 1983). In addition to the work presented by Prasad (1972) and competing data on the efficacy of the L- and D-glyceraldehyde isomers, we showed that L-GA is more effective at inhibiting neuroblastoma cell growth than D-GA. The work presented in this thesis is the first to use the pure L-glyceraldehyde isomer in neuroblastoma cells. The superiority of L-GA over DL- or D-GA correlates with results found in T98G and HEK293 cells (Pietzke, 2015). Prasad (1972) state that DL-glyceraldehyde caused an 88% neuroblastoma cell growth inhibition with 10 hrs. The RTCA iCelligence™ system permitted monitoring of cell growth in 15 minute intervals. It was shown that L-GA inhibits growth by 50% after approximately 11 hrs for IMR-32 and 22 hrs for SH-SY5Y.

4.1.1 Neuroblastoma cells produce a heterogeneous cell cycle response to L-GA

The progression of the cell cycle is maintained via the cross talk between metabolic feedback mechanisms and cell cycle regulators (Huber et al., 2020). The coordination of metabolic pathways ensure that sufficient abundances of metabolites, co-factors and macromolecules are present at specific cell cycle phases. The inhibition of these pathways result in cell cycle arrest. Cell lines SK-N-AS, IMR-32, IMR 5/75 and BE(2)-C were arrested in the G_2/M phase following L-GA treatment. In an example of neuroblastoma heterogeneity, SH-SY5Y, CLB-GA and GI-ME-N cell lines were arrested in the S-phase. The cell cycle is regulated via cyclins and their associated cell cycle dependent kinase (CDK). Cyclin A-CDK2 drives progression in S, cyclin A-CDK1 in G2 phase, and cyclin B-CDK1 regulates progression from through the G_2/M phase (Casimiro et al., 2014). The G_2/M checkpoint is significant as it is an indicator of DNA damage and cell stress. Under these conditions cells will not enter mitosis and initiate apoptosis. Furthermore, the requirement of ATP during the late G_2 phase is high and glycolytic enzymes are up-regulated to provide an 'ATP' boost (DiPaola, 2002). From the data provided in figure 3.6 we postulate that L-GA causes DNA damage which modulates the G_2/M checkpoint and apoptotic pathways in the cell lines described. The G_2M checkpoint receives information about the DNA integrity of the cell via the ATR-CHK1 and p53 pathway. Upon DNA damage CHK1 negatively regulates the mitotic activator, cdc2. Although there is no comparative research on the mechanism L-GA in relation to cell cycle arrest, glycolytic inhibitors have been shown to induce cell cycle arrest. The glycolytic inhibitor 2-DG induces G_O/G_1 arrest and apoptosis in SW60 colorectal cancer cells (Muley et al., 2015). 2-DG induces an in increase p53 expression, although this was found to be independent of its inhibitory function on glycolysis. BrPyr has been shown to induce cell cycle arrest in the S-phase in THP-1 leukaemia cells (Cal et al., 2020). The authors claim that BrPyr induces double stranded breaks in DNA through an increase in ROS, resulting in cell cycle arrest. Although, the mechanism is not described, it would not be gratuitous to assume that the p53/ATR pathway suppresses cell cycle progression.

In 3 out of the 7 neuroblastoma cell lines treated with L-GA, the cell cycle is arrested in the S-phase. During the S-phase cells synthesise DNA. The hallmark of S-phase arrest is the slowing of DNA replication, yet not the complete ablation (Rhind and Russell, 2000). This is in contrast to G_2/M arrest in which cells have completed DNA synthesis but contain damaged DNA. We therefore deduce that SH-SY5Y, GI-ME-N and CLB-GA halt DNA synthesis when exposed to L-GA. Despite this, a significant increase in the fraction of apoptotic cells was observed. Apoptosis is known to occur in S-phase arrest via PI3K/Akt/mTOR, p53, MAPK and E2F-1 mediated pathways (Pizarro et al., 2011; Segerström et al., 2011; Qiao et al., 2012). It is unclear which pathway, or pathways, L-GA activates in neuroblastoma cells. However, the chemotherapeutics resveratrol and doxorubicin are known to induce S-phase arrest in neuroblastoma cells via DNA damage and activation of ATR/ATM apoptotic pathways (Chen et al., 2004; Rahman et al., 2012). It is possible that L-GA acts in a similar manner.

In summary, we find a heterogeneous response in cell cycle arrest in the neuroblastoma cell lines tested with L-GA. The research shows that there is a common increase in the fraction of sub-G1 cells, synonymous with apoptosis. Cell lines SK-N-AS, IMR-32, IMR 5/75 and BE(2)-C appear to evade the S-phase arrest checkpoint and enter G_2/M phase in which they are arrested. When addressing the genetic profile, it is known that the *MYCN* status varies between neuroblastoma cell lines (Lodrini et al., 2017). Cell lines that exhibit G_2/M arrest harbour amplified *MYCN* copy numbers, whereas cell lines that exhibit S-phase arrest harbour *MYCN* gain or *MYCN* diploid status. Although, SK-N-AS is an exception as it harbours *MYCN* diploid, yet arrests in the G_2/M phase. MYCN drives the transition from G_1/S to G_2/M, the amplification of MYCN further forces this transition. It has been shown that application of anti-tumoural drugs to *MYCN* amplified cells causes the accumulation of cells in the G_2/M phase. Conversely, non-amplified *MYCN* cells accumulated in the G_1/S phase upon treatment (Paffhausen et al., 2007). High *MYCN* expression is also linked to increased cyclin D and E2F to drive G_1/S progression (Bell et al., 2007). MYCN is shown to cause the up-regulation of CHK1, an important regulator of S-phase and G_2/M checkpoints (Cole et al., 2011). It is suspected that cells with high *MYCN* expression evade S-phase arrest, via MYCN influence on G_1/S checkpoint associated regulators.

The fibroblast cell line, VH-7 presented G_2/M arrest, although no significant increase of the apoptotic fraction. It is reported that low concentrations of oxidants can induce cell cycle arrest in fibroblasts to a senescent like state (Dumont et al., 2000; Debacq-Chainiaux et al., 2005). Analysis of the cell growth, cell imaging and cell cycle upon L-GA treatment of VH-7 cells, suggests transition to a senescent state. L-GA did not causes detachment of VH-7 from plates but hindered growth rates. Upon cell imaging, the research shows that cellular morphology was altered yet this appeared non-toxic to the cell. As we have found L-GA to present oxidative stress, it is likely that L-GA inhibits VH-7 growth and induces senescence.

Dysregulation of the actin cytoskeleton

In correlation to cell cycle arrest and inhibited cell growth we found that L-GA causes dysregulation of the cytoskeleton (figure 3.5). The maintenance of the cytoskeleton is an ATP dependent reaction as the monomeric G-actin polymerises to F-actin utilising ATP. Currently, there

is a sparsity of research on the effect of glyceraldehyde and the cytoskeleton. However, we may look to research conducted by Huang et al. (2015) for a common mechanism. Glycolytic inhibition via 2-DG has been shown to dysregulate actin polymerisation. In concordance with our data, 2-DG was found to inhibit the formation of lamellipodia and filopodia and causes dysregulation of F-actin. Furthermore, it has been reported that the blocking of the glycolytic activator PFKFB3 also induces F-actin dysregulation (De Bock et al., 2013). Interestingly, the authors state that F-actin dysregulation is a result of a depletion of glycolysis derived ATP and mitochondrial ATP was not sufficient to maintain F-actin structure. Our data provides a novel insight. We find that not only is F-actin structure dysregulated but polymerisation is inhibited, as shown by the increase in the G-action fraction. As described by Galluzzi et al. (2014) the cytoskeleton responds to and can initiate apoptotic signals. Specifically, BIM and BMF sense damage of the cytoskeletal and translocate to the mitochondria to induce caspase activity and mitochondrial outer membrane permeabilisation (MOMP) (Schmelzle et al., 2007; Galluzzi et al., 2014). In further support of the data provided in this thesis, the cytoskeleton is sensitive to oxidative stress. The actin bound protein cofillin A (CFL) dissociates from actin under oxidative stress and translocates to the mitochondria to induce necrosis, apoptosis or anoikis (the process of detachment of cells from a substrate) (Dalle-Donne et al., 2001; Leadsham et al., 2010).

During the analysis of the cytoskeleton we found that multinucleation of cells was a hallmark of L-GA treated cells. Multinucleation has been reported to be induced in response to DNA damage, mitotic spindle damage and to cause apoptosis and cell cycle arrest (Hart et al., 2020). We found that with increasing concentrations of L-GA the percentage of multinucleation in neuroblastoma cells positively correlated. Interestingly, this was not observed in fibroblasts. Cytotoxic compounds such as paclitaxel, doxorubicin and cisplatin generate DNA damage, cell cycle arrest and multinucleation, mainly through the ATR-p53-p21 pathway (Eom et al., 2005; Murray and Mirzayans, 2020). Given this, L-GA may act in a similar way, by inducing replicative stress, inducing cell cycle arrest and inhibition of mitotic division.

In summary, cell cycle arrest, dysregulation and growth arrest are the hallmarks of L-GA treatment in neuroblastoma cells. Nevertheless, we find significant heterogeneity between the cell lines in response to treatment. Further work is required to disentangle the molecular and genetic variation between neuroblastoma cell lines. It is suggested that a phosphoproteomics approach would elucidate activation of specific cell line specific pathways. Although heterogeneity is evident, it is promising that L-GA is effective at inducing cell death and apoptosis in all neuroblastoma cells tested. Furthermore, fibroblast cells experience significantly less cytotoxicity in response to L-GA.

4.2 L-GA targets nucleotide biosynthesis causing severe depletion of pools

The work presented in this thesis provides a novel role of L-GA in inhibiting nucleotide biosynthesis. In order to apply reasoning for the effect of L-GA on cell cycle arrest in neuroblastoma cells, nucleotide pools were measured following L-GA treatment in a concentration and a time

dependent manner. In a similar manner to the results from the cell cycle analysis, we found a heterogeneous response of the depletion of nucleotides pools in response to L-GA between neuroblastoma cell lines. As described in figure 3.10, IMR-32 and SH-SY5Y experience minimal decrease in nucleotide pools below 1 mM L-GA. Curiously, at 0.2 mM L-GA increases nucleotide pools in IMR-32. As shown in the supplementary material figure 5.7 GI-M-EN displayed a step-wise decrease in nucleotide pools as L-GA concentration increased. SK-N-AS showed a resistance to L-GA treatment, even at high L-GA concentration. However, there is uncertainty about the relationship between cell growth and nucleotide metabolism in GI-M-EN and SK-N-AS as no growth curves were produced. VH-7 presented a significantly less severe response to L-GA treatment. As found with the rapid reduction in cell growth, nucleotides are depleted at a similar rate. In IMR-32 and SH-SY5Y L-GA depletes nucleotide pools within 8 hrs. The inhibition of nucleotide synthesis in cancer cells is achieved through a select few small molecules as described in table 4.1. The common denominator between the drugs presented, is that they inhibit downstream of ribose-5-phosphate (R5P). Boros et al. (1997) and Raïs et al. (1999) showed in two separate studies that oxythiamine and dehydroepiandrosterone inhibit R5P production via transketolase inhibition in the non-oxidative pentose phosphate pathway. Furthermore, both drugs caused cell cycle arrest in the S and G_2/M phases of Ehrlich Ascites tumour cells (Raïs et al., 1999), in a similar manner to L-GA. However, the authors found no apoptotic response. We performed cell growth analysis of IMR-32 and SH-SY5Y in the presence of oxythiamine at concentrations above that described by Raïs et al. (1999) and found no evidence for cell growth inhibition figure 4.1. For this reason, we did not perform analysis on nucleotide levels following oxythiamine treatment.

Drug	**Mode of action**
5-Fluorouracil (5-FU)	converted to 5-fluoro-2'-deoxyuridine monophosphate and inhibits thymidylate synthase.
Hydroxyurea (HU)	inhibits ribonucleoside diphosphate reductase, resulting in dNTP depletion
Methotrexate (MTX)	A folic acid analogue that inhibits dihydrofolate reductase and the one carbon transfer reactions required for *de novo* synthesis of purines.
Mycophenolic Acid (MPA)	Inhibits Inosine-5'-Monophosphate Dehydrogenase (IMPDH) reducing purine pools

Table 4.1: An example of therapeutic inhibitors of nucleotide metabolism (Thompson Coon, 2010; Siebert et al., 2020)

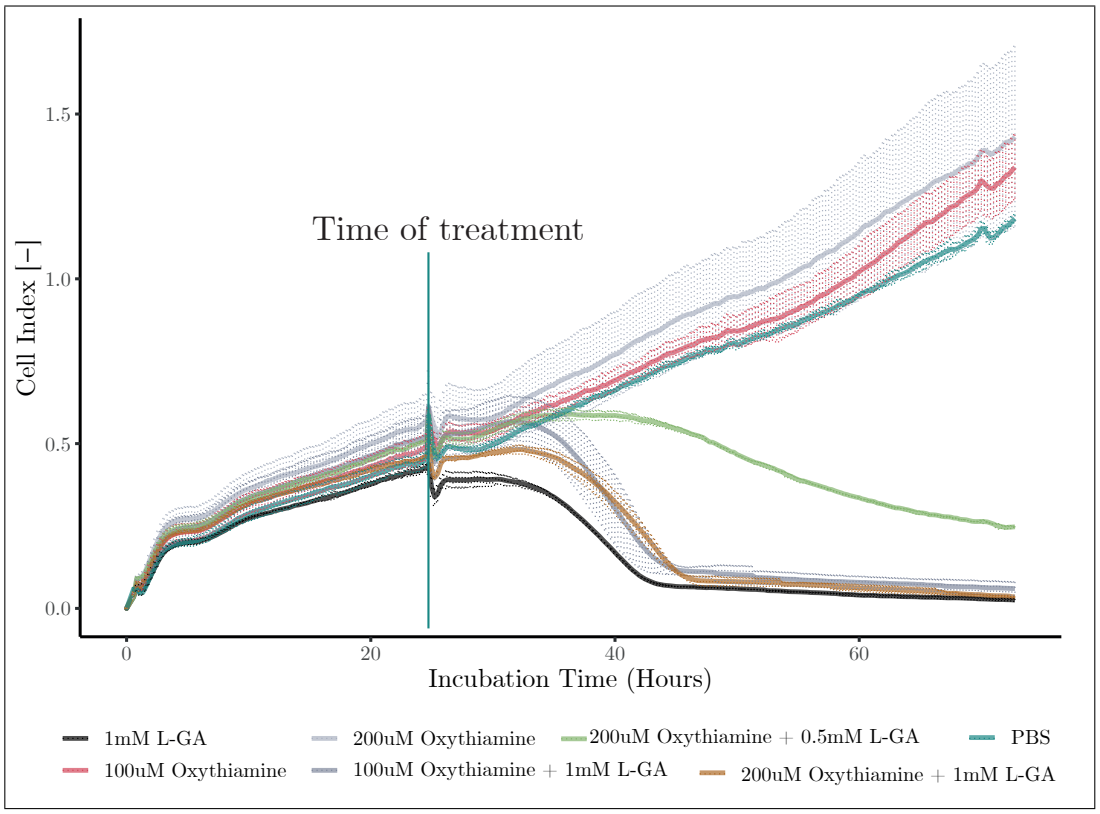

Figure 4.1: Oxythiamine does not affect cell growth of IMR-32 cells. IMR-32 was seeded at a density of 1.5e+4 cells per well in a 16-well RTCA iCelligence™ chip. Two wells were per treatment condition. Cells were treated with either PBS or 1 mM L-GA 0.5 mM LGA, 200 µM Oxythiamine, 100 µM Oxythiamine, 100 µM Oxythiamine + 1 mM LGA, 200 µM Oxythiamine + 1 mM LGA and 200 µM Oxythiamine + 0.5 mM LGA 24 hrs post seeding, as shown in the graph. Measurements were taken in triplicate every 15 minutes for 72 hrs. Error bars represent ± SD of the mean.

4.2.1 L-GA targets specific nucleotide intermediates

As stated, we did not find that inhibiting TKT via oxythiamine had an effect on neuroblastoma cell growth. The proposed action of L-GA is both an inhibition of glycolysis and on enzymes requiring GA3P as a substrate. The nucleotide intermediates utilised by enzymes of *de novo* purine and pyrimidine synthesis are depleted upon L-GA treatment (figure 3.11). As described in figure 1.2, R5P is the root metabolite required for nucleotide biosynthesis. The synthesis of R5P via the non-oxidative pathway requires GA3P as a substrate. The inhibition of glycolysis at the GA3P position via L-GA may have a profound effect on nucleotide biosynthesis. The data shows that the nucleotide intermediates which presented the largest depletion were IMP and UMP, the terminal nucleotide intermediates before pyrimidine and purine synthesis. Interestingly, AICAR and SAICAR are found to be the least affected intermediates in SH-SY5Y cells and SAICAR and PRPP in IMR-32 cells. This suggests that the co-factors that are required for the synthesis of nucleotides after SAICAR are depleted. Qian et al. (2018) provide a possible explanation for depletion of specific nucleotides. They state that glucose deprivation activates AMPK which in turn inhibits phosphoribosyl pyrophosphate synthetase 1 (PRPS1). PRPS1 catalyses the metabolism of PRPP from R5P. It is possible that glyceraldehyde acts in a similar manner to target PRPS1 via AMPK. Glycolysis supplies ATP needed for nucleotide phosphorylation. L-GA affects mono-, di- and tri- phoshorylated nucleotides in a step-wise fashion, suggestive of depleted available ATP. In support of this, a significant increase in the AMP/ATP

ratio as a function of L-GA concentration is observed. In order to delineate the effect of glycolytic inhibition on nucleotide biosynthesis and the role of L-GA in the pentose phosphate pathway IMR-32 and SH-SY5Y cells were treated with BrPyr and starved of glucose. L-GA treatment resulted in a more severe nucleotide depletion than alternate modes of glycolytic depletion. In agreement with Pietzke (2015) and Ihrlund et al. (2008) there is a severe depletion of ATP when neuroblastoma cells were treated with BrPyr. In addition, the D-isomer does not affect nucleotide depletion as significantly as the L-isomer. This data correlates with the relative level of growth inhibition observed in figure 3.16 and with the glycolytic inhibitory potential of L- over D-GA (Mendel et al., 1938).

To summarise, L-GA targets nucleotide biosynthesis via glycolytic inhibition and by possible reduction of co-factors required for nucleotide intermediates. Glycolytic inhibition alone does not result in the same severity of nucleotide depletion as L-GA presents. The relative efficacy of D- and DL-GA correlates with previous research. In line with cell cycle data, there is a heterogeneity between the response nucleotide depletion between neuroblastoma cell lines. However, the data does not provide sufficient evidence to explain this heterogeneity. As previously described, the cell lines tested harbour varying *MYCN* expression. IMR-32 presents the highest *MYCN* expression followed by SH-SY5Y, GI-M-EN and SK-N-AS. MYCN has been reported to target and up-regulate enzymes of pathways including: nucleotide biosynthesis, RNA metabolism, DNA replication and repair, amino acid and one-carbon metabolism (Huang et al., 2019). When considering nucleotide biosynthesis, Huang et al. (2019) found: guanine monophosphate synthase (GMPS), IMP cyclohydrolase (ATIC), phosphoribosyl pyrophosphate amidotransferase (PPAT) and thymidylate synthetase (TYMS) to be targets of MYCN. Curiously, GI-M-EN has the most sensitive nucleotide response to L-GA treatment, whereas SK-N-AS is the least sensitive. Therefore, it is unlikely that the *MYCN* status of the cell correlates with sensitivity to nucleotide depletion on L-GA treatment.

4.3 The impact of L-GA on the metabolic profile of neuroblastoma cells

The function of glyceraldehyde as a glycolytic inhibitor has dominated the focus of its previous research. In line with Lardy et al. (1950) and Pietzke (2015), the data presented in this thesis shows that L-GA causes a significantly greater inhibition of glycolysis than D-GA. Yet, the data elucidates a novel mechanism by which L-GA inhibits neuroblastoma metabolism. Employing the pSIRM strategy enabled the discovery that L-GA decreases the carbon flow into metabolites that require NADH as a co-factor. Through the integration of GC- and DI- mass spectrometry data sets, it was found that L-GA breaks the cycling of cytosolic NAD+/NADH. This breakage impacts the redox state of the cell thereby inhibiting cellular metabolism. The following sections describe the process by which L-GA targets neuroblastoma metabolism.

4.3.1 L-GA targets NAD+/NADH cycling

In order to measure the perturbations in the rapidly changing central carbon metabolism we employed an instationary heavy isotope labelling approach. The pSIRM method permitted

the measurement of metabolite concentration and incorporation of ^{13}-C labelled carbon into metabolites in a time-dependent manner. Cell lines, IMR-32 and SH-SY5Y showed significant inhibition of glycolysis within 1 hr of L-GA treatment (figures 3.19, 3.20).

The mode of L-GA action was found to target down stream of glucose-6-phosphate (G6P) and fructose-6-phosphate (F6P). This data contradicts Lardy et al. (1950) whereby they claim that L-GA, or its metabolite sorbose-1-phosphate, inhibits hexokinase and synthesis of G6P. Pietzke (2015) describes the inhibition of glycolysis by L-GA to be located between F6P and glyceric acid-3-phosphate (3-PGA). This observation is more fitting with the data presented in this thesis. In IMR-32 and SH-SY5Y ^{13}-C label incorporation was depleted in glycerol-3-phosphate (Glyc3P), lactate (Lac) and pyruvate (Pyr). Contrary to Pietzke (2015), 3-PGA was not significantly affected. However, the measurement of this metabolite proved to be low in sensitivity and reproducibility, therefore we cannot claim that 3PGA is unaffected by L-GA. Label incorporation into Glyc3P, Pyr, and Lac is reduced in both IMR-32 and SH-SY5Y, therefore L-GA acts down stream of F6P. The metabolite concentrations of Lac and Gly3P are unaffected by L-GA treated suggesting that L-GA does not affect the utilisation of these metabolites. The inhibition of label incorporation is suggestive of an inhibition in the enzymatic reaction fuelling Lac and Glyc3P synthesis. This data is supported by the accumulation of Pyr observed in both cell lines upon L-GA treatment. The decrease in label incorporation and increase in metabolite pool reflects the inability of lactate dehydrogenase (LDH) to metabolise Pyr. Although glycolysis is inhibited up-stream of Pyr, as denoted by the decrease in label incorporation, the metabolism of Pyr to Lac is also inhibited by L-GA. The accumulation of Pyr resulted in the re-routing of carbons to citrate (Cit) as shown in figure 3.19. Curiously, D-GA treatment resulted in the accumulation of Pyr and a decrease in the label incorporation, but did not affect the label incorporation into Lac and Gly3P. D-GA does indeed inhibit glycolysis upstream of Pyr but does not inhibit NADH dependent enzymes.

The principle producer of NADH is glyceraldehyde-3-phosphate dehydrogenase (GAPDH). The data presented indicates that L-GA inhibits GAPDH- or directly upstream at aldolase-thereby inhibiting NADH production. Maswoswe et al. (1986) showed that D-GA did not change cytoplasmic NAD+/NADH ratio, as indicated by the unchanged Lac/Pyr ratio in hepatocytes. The authors suggest that ATP depletion is a result of metabolism of D-GA to fructose and its subsequent phosphorylation to fructose-1-phosphate (F1P). Pietzke (2015) complements this data via the observation of increased F1P concentration upon D-GA treatment. Furthermore, F1P can be metabolised to glyceraldehyde-3-phosphate to maintain glycolysis, whereas sorbose-1-phosphate produced from L-GA is not a substrate for glycolysis (Baker, 1938; Lardy et al., 1950; Needham et al., 1951). Although fructose-1-phosphate was not measured in this thesis, the data agrees with Lardy et al. (1950), Maswoswe et al. (1986) and Pietzke (2015) that L-GA is a more effective inhibitor of the CCM. We postulate that L-GA targets the NADH dependent enzymes glycerol-3-phosphate dehydrogenase (GPD) and LDH via a mechanism outside of glycolytic inhibition alone. This will be discussed in section 4.5.

4.3.2 L-GA induces increased glutaminolysis

In addition to high rates of glycolysis, cancer cells up-regulate glutaminolysis to support the biosynthesis of amino acids and nutrients for biosynthesis of macromolecules (De Berardinis and Chandel, 2016; Ades et al., 2017). We measured the rate of glutaminolysis in neuroblastoma cells by employing the pSIRM method supplemented with U-^{13}C-glutamine. The data provided in this thesis shows that L-GA induces an increase in the utilisation of glutamine and the flow of labelled carbons within TCA cycle intermediates increases (figures 3.22, 3.23)). Curiously, D-GA did not increase label incorporation into intermediates of the TCA cycle.

In both IMR-32 and SH-SY5Y the U-^{13}C-glutamine derived label incorporation into TCA metabolites: succinate, fumarate, malate and citrate was increased upon L-GA treatment. The increase in glutaminolysis was confirmed by the increase in label incorporation in glutamate. However, in IMR-32 the label incorporation of α-ketoglutarate (α-KG) does not change relative to untreated cells, in SH-SY5Y it was apparently decreased. This would seem counter-intuitive as α-KG is the initial metabolite that drives the TCA cycle derived from glutamine. Furthermore, α-KG metabolite concentrations were significantly increased upon L- and D-GA treatment, which is strikingly similar to the results from U-^{13}C-glucose derived Pyruvate. Two possible explanation for this phenotype exist. Firstly, the rate of oxidative deamination of glutamate to α-KG is significantly up-regulated upon glyceraldehyde treatment resulting in an accumulation of α-KG due to production out-weighing its consumption - or more precisely its conversion to succinate. This theory would be supported by the reduction in metabolite concentration of glutamate in glyceraldehyde treated cells. It is also to be noted that the oxidative deamination of glutamate to α-KG is an NAD+ dependent reaction, indeed if glyceraldehyde favours the production of NAD+ thereby generating an oxidising environment; oxidising reactions will be favoured. This is supported by the significant increase in labelled quantity of α-KG in L-GA treated IMR-32 cells. Secondly, we may state that unlabelled α-KG is produced through routes independent of glutamine, which are up-regulated upon L-GA treatment. Isocitrate dehydrogenase (IDH) catalyses the conversion of isocitrate to α-KG. We observed the accumulation of pyruvate and citrate upon L-GA treatment during U-^{13}C-glucose labelling. Therefore, the accumulation of pyruvate and citrate would favour the forward reaction of citrate-isocitrate-α-KG via IDH (Kaminska et al., 2019). As we will discuss in more detail, L-GA induces a redox imbalance and an increase in oxidative stress. α-ketoglutarate dehydrogenase (α-KGDH) converts α-KG to succinyl-CoA (suc-CoA). We suggest that the increase in oxidative stress, particularly in IMR-32 cells, inhibits α-KGDH and leads to α-KG accumulation. In addition, NAD+/NADH ratio is a key regulator of ROS production by α-KGDH, as α-KGDH produces H_2O_2 during α-KG metabolism. Tretter and Adam-Vizi (2004) postulated that α-KGDH is not only a target of ROS but could significantly contribute to generation of oxidative stress in the mitochondria. Therefore, it is possible there is a strong positive feedback loop between L-GA, NAD+/NADH cycling and the production of ROS. As L-GA causes redox stress via breakage of NAD+/NADH cycling, ROS increases and ROS-sensitive enzymes are inhibited.

In summary, the data provided in the thesis addresses the role of glyceraldehyde within the CCM in a novel light. To date, the effect of glyceraldehyde on glutaminolysis is unreported.

L-GA and D-GA show significantly different modes of action on both glycolysis and the TCA cycle when intermediates are labelled with U-^{13}C-glucose and U-^{13}C-glutamine, respectively. We have elucidated a mechanism by which NADH-dependent enzymes are inhibited by L-GA although not D-GA in a 1 hr treatment window. Further work is required to extend this treatment window in the context of the apparent increase in TCA activity upon L-GA treatment and glutaminolysis. As stated by Tretter and Adam-Vizi (2004), glutaminolysis induces ROS production via α-KGDH. Given that L-GA increases TCA activity we may assume that mitochondrial ROS levels continue to rise as a function of L-GA exposure time. It would be of significant interest to test this hypothesis in relation to mitochondrial activity given the extensive research on the cytosolic effect of L-GA. As stated by Wang et al. (2018), *MYCN*-amplified neuroblastoma cell lines increase glutaminolysis. We may account for the apparently reduced levels of α-KG levels in SH-SY5Y relative to IMR-32 by their *MYCN* status. Enzymes catalysing reactions within the TCA cycle (CS, IDH2, α-KGDH) show enhanced mRNA and protein expression in MYCN amplified neuroblastoma cells (Otte et al., 2021). Therefore we suggest that IMR-32 is more sensitive to ROS agents such as L-GA due to its up-regulation of ROS producing pathways.

4.4 L-GA induces perturbations in the proteome

We employed a shotgun proteomics approach to address the effect of L-GA on the proteome and discern perturbations in metabolic pathways. The proteomic landscape of L-GA treated neuroblastoma cells supported previous evidence that significant heterogeneity exists. Through PCA analysis of identified proteins we identified SK-N-AS to be significantly unique, IMR-32 and SH-SY5Y showed similarity as did BE(2)-C and GI-M-EN. In line with the metabolic profile, the main pathway identified in L-GA treated cells was associated with redox and ROS pathways. Here we discuss the identities of the statistically significant proteins identified after L-GA treatment (list of significant proteins given in supplementary material table 5.12).

4.4.1 Up-regulation of the oxidoreductase enzyme class

An oxidoreductase is an enzyme that utilises the co-factors NADP+ or NAD+ to transfer electrons from a reductant to an oxidant. For example, haemeoxygenase (HMOX1) is oxidised by O_2 to mitigate oxidative stress in the cell. As shown in figures (3.24, 3.26) we found the up-regulation of enzymes of the oxidoreductase class in 4 out 5 neuroblastoma cell lines and VH7. SK-N-AS did not show increased oxidoreductase activity. Upon pathway annotation of the up-regulated oxidoreductases, the KEAP1-NRF2 pathway was elucidated. The KEAP1-NRF2 pathway is initiated upon increase of ROS (Mitsuishi et al., 2012). Chemotherapeutics such as doxorubicin and cisplatin induce ROS and DNA damage in cancer cells (Conklin, 2004; Marullo et al., 2013). Furthermore, glycolytic inhibitors 2-deoxyglucose and bromopyruvate also induce elevated ROS (Ihrlund et al., 2008; Wang et al., 2011). Although these studies do not address NRF2, we show that targets of NRF2-mediated ROS response are up-regulated in L-GA treated cells in a similar manner to other therapeutics. NRF2 induces metabolic reprogramming in cancer cells. Mitsuishi et al. (2012) show that NRF2 redirects glucose and glutamine into anabolic pathways, particularly under the sustained activation of PI3K-AKT signaling. We found that

the NRF2 targets of antioxidant response were up-regulated (NQO1 and HMOX1) but G6PD was not, nor did we find evidence for increased glycolytic or TCA cycle targets. The data presented in figure 3.31 showed that NADPH production was not increased in neuroblastoma cells. This complements the observation that glycolytic enzymes were not increased by NRF2 activation.

The KEAP1-NRF2 pathway initiates a cryoprotective response therefore it seems counter-intuitive that we observe antioxidant mechanisms in cell lines that also show cell death upon L-GA treatment. We suggest that this method of proteomic analysis is in fact selection. When treating the cells for 24 hrs with 1 mM L-GA the cells that remain on the plate are of a population of 'surviving' cells. Therefore, we understand only that in response to L-GA cells may attenuate oxidative stress by antioxidant mechanisms. Although, it is clear not every cell line acts with this response.

4.4.2 Apoptotic signalling pathways are initiated in response to L-GA

Cell cycle analysis showed that after 72 hrs incubation of L-GA the sub-G1 population of all neuroblastoma cell lines tested increased. Sub-G1 is indicative of apoptotic cells. Across cell lines we observed an increase in apoptotic related proteins such as: BAD, MCL1, CYCS, CASP3 (sup. material, table 5.12). Interestingly, in SH-SY5Y cells we observed an increase in the NFκB protein, suggestive of PI3K activation upon L-GA treatment. Apoptosis is also induced via 2-DG and BrPyr in cancer cells. Xu et al. (2005) showed that the AKT-BAD mediated apoptotic pathway is induced following 18 hrs treatment with 100 µM with BrPyr in HL-60 liver cancer cells, furthermore increased caspase 3 cleavage occurs. Although we have not discerned the exact pathway which initiates apoptosis we may suggest from the up-regulated protein profile that L-GA modulates, or in part, the PI3K-AKT-mTOR mediated apoptosis and autophagy. However, further work is required to define this hypothesis. Given the broad spectrum of L-GA action, we postulate that many energy sensing pathways are modulated.

4.4.3 Cell cycle specific proteins correlate to cell cycle analysis

Cell cycle arrest can be defined not only by measuring the DNA content and deriving the specific cell cycle phases, but also by the expression of cell cycle specific proteins. As described in figure 3.6 SH-SY5Y and GI-M-EN experienced S-phase arrest following L-GA treatment, whereas IMR-32, SK-N-AS and BE(2)-C arrest in G_2/M. Thymidylate synthase (TYMS) is an S-phase specific enzyme which catalyzes the conversion of dUMP to dTMP, its inhibition leads is known to induce S-phase arrest (Sakoff and Ackland, 2000). In line with our data, Zhang et al. (2020) describe that the knockdown of TYMS in retroperitoneal liposarcoma cells induces significant S-phase arrest and apoptosis. The mechanism by which L-GA down-regulates TYMS in SH-SY5Y and GI-M-EN is not understood from the data provided in this thesis, as we cannot dicepher whether L-GA induces TYMS down-regulation or whether TYMS down-regulation is a facet of S-phase arrest. Interestingly, ribonucleotide reductase subunit 2 (RRM2), which responsible for the ribonucleotide to deoxyribonucleotide conversion during the S phase, is down-regulated in all cell lines except SY-SY5Y and GI-M-EN. We suggest that TYMS and RRM2 are markers of S-phase arrest and depletion of deoxyribonucleotides in SH-SY5Y and

GI-M-EN. IMR-32, SK-N-AS and BE(2)-C displayed markers of G_2/M arrest. Stratifin (SFN) is a master regulator of G_2/M transition (Laronga et al., 2000). SFN prevents mitosis by sequestering cdc2/cyclin B1 and stalling the cell cycle to allow for p53-mediated DNA damage repair (Yang et al., 2003). In the data provided in this thesis SFN showed an extreme response to L-GA, therefore it is suggested that the regulation of this protein be investigated in further work. In addition we found SRC to be significantly down-regulated on L-GA treatment. As shown by Park et al. (2009) and Hishiki et al. (2011), SRC inactivation leads to cell cycle arrest in breast cancer cells and apoptosis in neuroblastoma cells. The authors describe that down-regulation of SRC modulates the PI3K/AKT/mTOR pathway to induce cell death. This may give credence to the investigation of the effect of L-GA on the PI3K/AKT/mTOR pathway.

In summary, the proteomic profile of L-GA treated cells significantly changed. In concurrence with anti-tumoural drugs, L-GA induces an anti-oxidant response. Although, this response is heterogeneous between neuroblastoma cell lines, evidence is presented towards the modulation of the PI3K/AKT/mTOR signalling pathway by L-GA. Furthermore, enzymes of the nucleotide biosynthesis pathway show significant response to L-GA treatment. However, the mechanism by which L-GA modulates enzymes such as TYMS, RRM2 and NME1 is unclear. As previously discussed, it is apparent that L-GA may modulate a number of pathways which are glycolysis dependent. Deciphering the relative importance and impact of these pathways requires a highly integrated approach which is outside the scope of this thesis. We suggest that a time framed phospho-proteomic method be the most appropriate way to untangle L-GA action as a function of time.

4.5 Oxidative stress is a hallmark of L-GA treatment

The data presented in this thesis clearly shows that the oxidative stress induced by L-GA is a factor in its anti-cancer action. Analysis of metabolites, nucleotides, proteomics and cell growth showed that oxidative stress is induced. The application of the anti-oxidant, N-acetyl cysteine (NAC), remedied the action of L-GA in IMR-32 and SH-SY5Y cells. The mitigation of oxidative stress restored metabolic function and nucleotide synthesis.

Takahashi et al. (2004) reported that 2 mM D-glyceraldehyde induces ROS in Wistar rat islets. The application of NAC reduced D-glyceraldehyde induced ROS . The data in this thesis complements Takahashi et al. (2004) findings, although D-GA was not tested for ROS production in neuroblastoma cells. The data provided shows that L-GA inhibits metabolism at NAD+/NADH cycling bottlenecks and induces a redox crisis. We postulate that the increase in ROS species generated L-GA inhibits ROS sensitive enzymes. Here we discuss the mechanism by which L-GA induced ROS is remedied by NAC.

4.5.1 Nucleotide biosynthesis is a ROS sensitive process

Nucleotide biosynthesis has been shown to be significantly inhibited by ROS. The application of H_2O_2 in IMR-32 and SH-SY5Y neuroblastoma cells induced a depletion of nucleotide pools (figure 3.30). Through the measurement of the ratios of nucleotide intermediates it was evident that SH-SY5Y and IMR-32 respond differently to oxidative stress. IMR-32 proved to be

much more sensitive to H_2O_2 with early intermediates such as PRPP depleting significantly. Curiously, in both cell lines SAICAR was displayed accumulation upon ROS exposure (figure 4.2). This is of particular mechanistic significance as accumulation of SAICAR induces increased PKM2 activity. Keller et al. (2014) showed that SAICAR induces the phosporylation of PKM2, driving the metabolism of phosphoenol pyruvate to pyruvate promoting cancer cell growth. This mechanism may be additive to the accumulation of pyruvate via lactate dehydrogenase inhibition. The addition of NAC restores nucleotide depletion of L-GA treated neuroblastoma cells and reduces SAICAR accumulation. This evidence supports the fact that nucleotide biosynthesis is a ROS sensitive pathway. Adenylsuccinate lyase (ADSL) catalyses the metabolism of SAICAR to AICAR, given that SAICAR is accumulated upon both L-GA and H_2O_2 treatment. It is likely that ADSL is highly ROS sensitive.

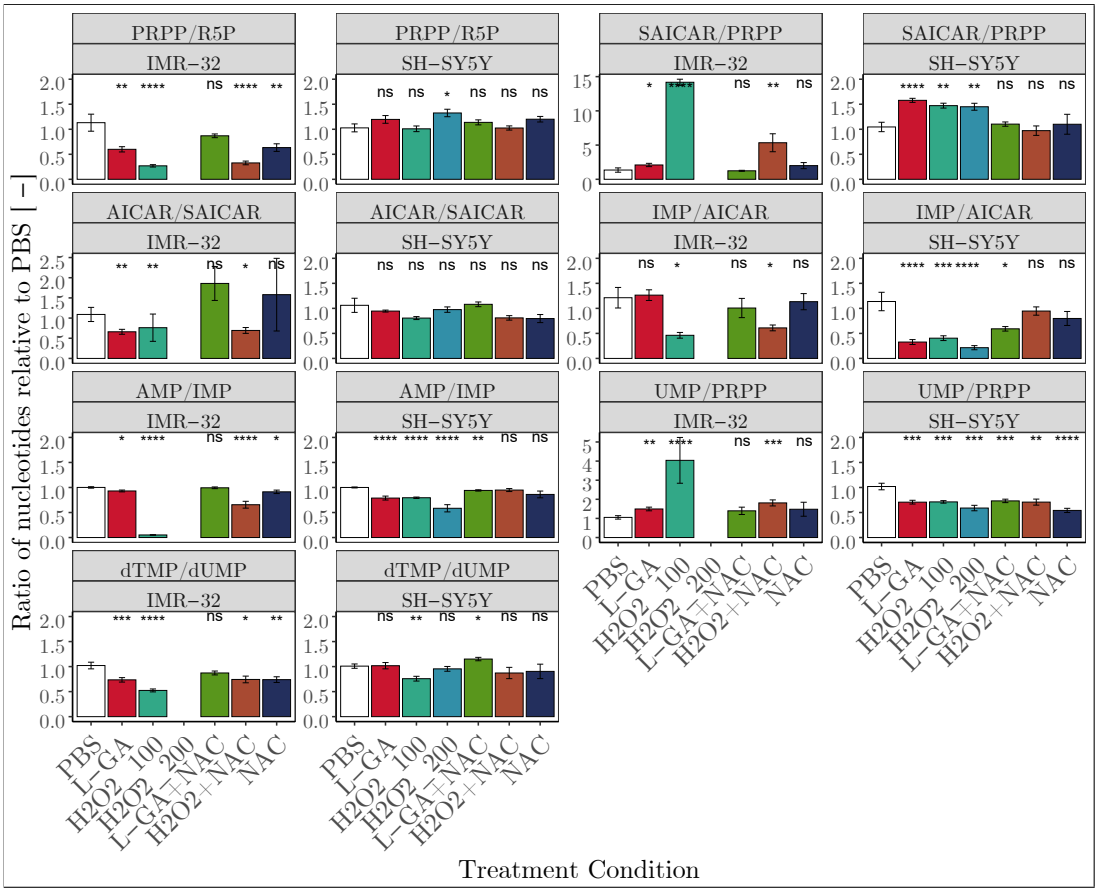

Figure 4.2: Ratio of nucleotide intermediates following ROS exposure. Cell lines IMR-32, SH-SY5Y were treated with treated with a range of L-GA concentrations (0-1.5 mM) or PBS for 24 hrs. Nucleotides were extracted from cell lysates and measured by DI-MS/MS. Boxplots present the ratio of intermediates as product/substrate. Data shown represents n=4 with 3 technical replicates. Error bars represent ± SEM. P-values were calculated using the Wilcox test. Stars represent: ns $p \geq 0.05$; * $p \leq 0.05$; ** $p \leq 0.01$; *** $p \leq 0.001$; **** $p \leq 0.0001$.

Research into the effect of ROS on the nucleotide intermediate metabolism is sparse. Although much is known about the effect of ROS on depletion of ATP production and DNA damage, the research in this thesis provides novel insights to how ROS affects nucleotide intermediates. We show that L-GA has a similar action to H_2O_2 in depleting nucleotides and which intermediates are most affected. The application of NAC confirms that nucleotide synthesis is indeed ROS sensitive. Further work is required to identify the specific enzymes which are most

susceptible to ROS. It is unclear whether it is a direct action of ROS on nucleotide metabolising enzymes or whether it is a result of signalling pathway perturbation.

4.5.2 Application of NAC restores NAD+/NADH cycling inhibited by L-GA

In order to discern whether the metabolic inhibition of neuroblastoma cells was a result of an increase in reactive oxygen species, we supplemented L-GA treated cells with the antioxidant NAC. Through the employment of the pSIRM method it was discovered that NAC restores the metabolic function of NADH-dependent enzymes. Specifically, it was found that the incorporation of labelled carbon from U-^{13}C-glucose was restored with NAC treatment into lactate, pyruvate and glycerol-3-phosphate. Figure 3.31 showed that the phosphorylation potential of L-GA treated cells was recovered upon NAC treatment, suggesting that glycolytic function and ATP production was restored. Furthermore the NAD+/NADH ratio returned to untreated levels upon NAC treatment. Together these results complement the hypothesis that L-GA induces oxidative stress that inhibits NADH-dependent enzymes which serve to maintain adequate glycolytic production of ATP. The results presented in this thesis are supported by the findings of Uetaki et al. (2015), they showed that Vitamin C induces strikingly similar effects in MCF7 human breast adenocarcinoma and HT29 human colon cancer cells as L-GA does in liver cancer or neuroblastoma cells. At 1 mM Vitamin C (notice that this concentration is equivalent to the molarity of L-GA used in this thesis) HMOX1 is up-regulated. The addition of 10 mM NAC reduced HMOX1 to untreated levels. The authors find that there is a depletion in reduced glutathione (a major ROS scavenger) as a function of vitamin C concentration. It is unfortunate that we, as yet, have not measured glutathione levels in L-GA treated neuroblastoma cells. Upon metabolic analysis the authors found that the glycolytic flux between glyceraldehyde 3-phosphate (GA3P) and D-glycerate 1,3-bisphosphate (1,3-BPG) mediated by glyceraldehyde 3-phosphate dehydrogenase (GAPDH) was suppressed by vitamin C in the MCF7 and HT29 cells. Furthermore, vitamin C depleted NAD+ levels and inhibited dNTP synthesis. However, and probably most crucially, vitamin C did not show global depletion of nucleotides and their intermediates (Uetaki et al., 2015). The authors fall short in explaining the mechanism by which vitamin C induces apoptosis through NAD+ and glycolytic depletion. We suggest that L-GA acts in a similar way on glycolysis as vitamin C, however L-GA exhibits a more pronounced effect on nucleotide biosynthesis and depletes NADH levels via GAPDH inhibition.

In summary, it is clear that the effects of L-GA are mitigated by the application of the antioxidant NAC. The metabolic profile and NADH-dependent enzyme functions are restored. As shown in figure 3.34 we found that L-GA was not inactivated by the presence of NAC, as similar intracellular L-GA quantities were present in the cells. Therefore, we conclude that NAC acts to reduce L-GA induced reactive oxygen species inhibit levels. ROS inhibit multiple glycolytic enzymes, including glyceraldehyde 3-phosphate dehydrogenase, pyruvate kinase M2, and phosphofructokinase-1 (Mullarky and Cantley, 2015). It is proposed that NAC restores metabolic function in L-GA treated cells through the reduction in ROS that inhibit the catalytic site of GAPDH, thereby restoring NADH production. In support of the data in this thesis, Le et al. (2010) showed that the inhibition of LDH contributes to oxidative stress and the application of NAC mitigated ROS induced cell death. The data in this thesis links oxidative stress to nucleotide biosynthesis. It is shown that depletion of nucleotides via L-GA is reversible

by NAC application, this is also reflected with the the strong oxidant H_2O_2. However, the data only shows the effect of H_2O_2 on nucleotide pools, for completion it is suggested the metabolite pools are also measured.

4.5.3 The fate of glyceraldehyde

It is in the interest of due diligence that we address the metabolites of L-GA. Pietzke (2015) showed that the metabolite of L-GA, sorbose, does not inhibit cancer cell growth when applied to cell culture medium. In figure 3.34 three main metabolites of L-GA were found in neuroblastoma cells. In line with Pietzke (2015), we found that L-GA is metabolised to glyceric acid, glycerol and glycolic acid. Remarkably, we found that NAC did not affect the metabolism of L-GA to glycerol or glyceric acid. However, the metabolite quantities of glycolic and glyoxylic acid are significantly reduced in both IMR-32 and SH-SY5Y cells when NAC is present. To further support the narrative that NADH availability is central to the mechanism L-GA action, the NADH-dependent glyoxylate reductase enzyme metabolises glycolic acid and glyoxylic acid (Booth et al., 2006). Accumulation of both of these metabolites is indicative of insufficient NADH pools and both present toxicity at elevated concentrations (Baker et al., 2004).

4.6 Conclusions and limitations

The data presented provides significant reasoning for the importance of homeostasis to the neuroblastoma cells. It is shown that L-GA causes disastrous metabolic inhibition which either consequently, or concurrently leads to: inhibited cell growth, cell cycle arrest, depleted nucleotides and dysregulation of the cytoskeletal structure. This multifaceted cell response initiates redox defence mechanisms. However, at the concentration of L-GA used, the metabolic system is overwhelmed and cell death ensues. The application of the anti-oxidant NAC results in an almost complete reversal of the L-GA treated phenotype. Figure 4.3 postulates a mechanism whereby L-GA generates ROS to deplete NADH and ATP in a positive feedback mechanism. ROS inhibits GAPDH and initiates NRF2. The increase in AMP/ATP ratio by deleption of ATP activates AMPK leading to cell cycle arrest and apoptosis. This section of the mechanism needs resolving through further signalling pathway analysis. Upon application of NAC the NAD+/NADH cycle is restored through lowering ROS and metabolic function proceeds.

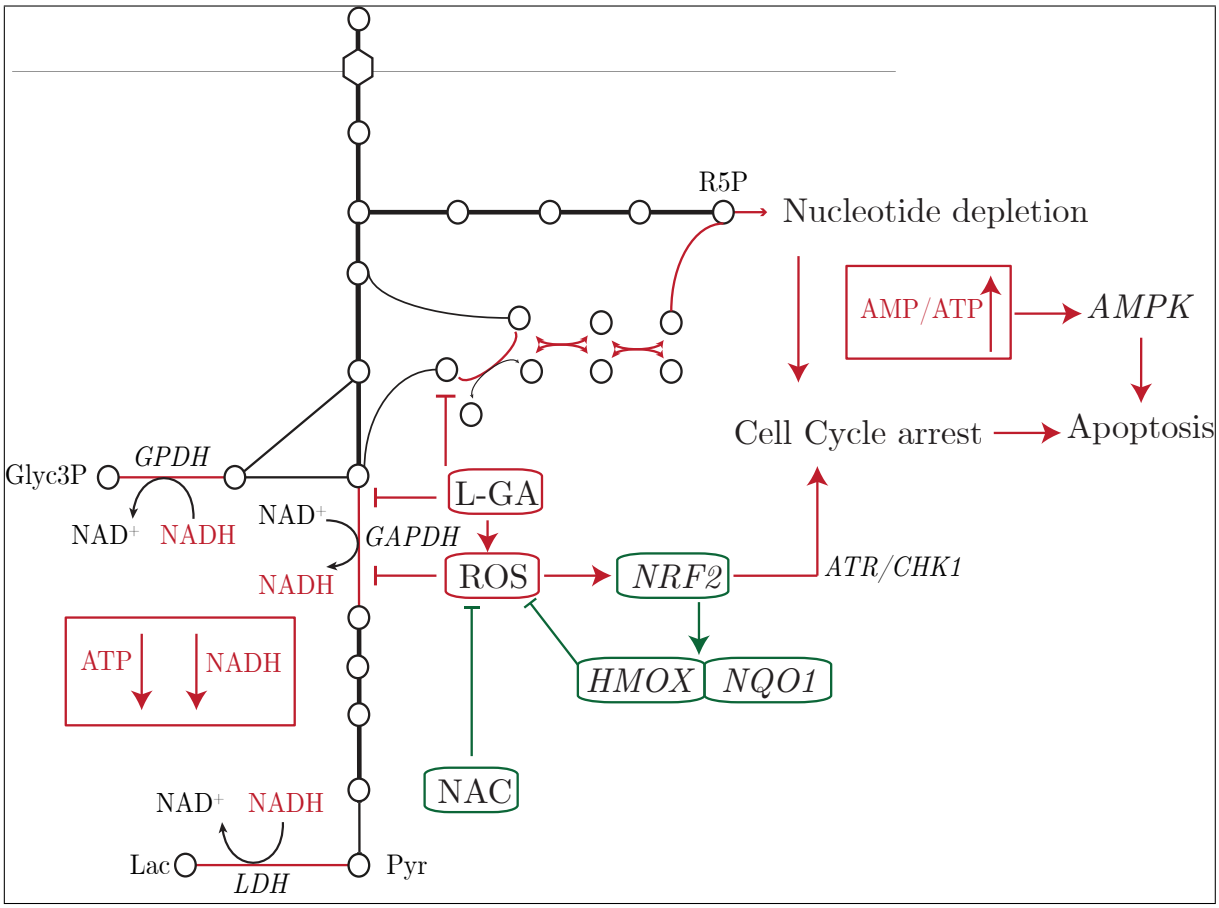

Figure 4.3: Proposed mechanism of the action of L-GA. At adequate concentrations of L-GA, the NAD+/NADH cycle is inhibited leading to depleted NADH and ATP pools. Depletion of NADH creates a redox crisis in the cell leading to increased ROS levels which further inhibit NADH production at GAPDH. Phosphorylation of nucleotides from mono- to di- to tri- is inhibited via glycolytic inhibition resulting in increased AMP levels and activation of AMPK. Increased ROS levels stimulate NRF2 activation and an anti-oxidant response to cope with L-GA treatment. As ROS levels exceed homeostatic levels NRF2 coordinates cell cycle arrest via ATR/CHK1 pathway (Márton et al., 2018). L-GA may also act to reduce the activity of the non-oxidative pentose phosphate pathway. The application of NAC reduces ROS levels restoring metabolic function, nucleotide biosynthesis and avoidance of apoptosis. Enzymes are presented in italics, metabolites and cellular responses are in Roman serif. Pathways and metabolites that negatively effect the cell are depicted in red. Arrows indicate positive regulation and barred ends indicate inhibition.

The work presented in this thesis has drawbacks specific to the protocol and technology employed. Here we address the relative limitations to the project. The GC-MS pipeline requires thermally stable compounds for both the process of derivitisation and for measurement. The central carbon metabolic pathway is populated by hexose and triose phosphates and their isomers. GC-MS has the benefit of distinguishing isomers such as fructose-6-phosphate and glucose-6-phosphate with relative ease, given their unique retention times in the GC column (Halket et al., 2005). However, due to the hydrolysis of the sugar-phosphate bond, low abundant phosphate metabolites, such as glyceraldehyde-3-phosphate, present difficulty in measuring. Furthermore, molecules must evaporate during the injection process into the machine. High heat is inconducive to the integrity of thermolabile phosphate bonds, such as di- and triphosphates (F1,6BP, ATP and NADPH) (Lu et al., 2017). In the context of this thesis, metabolites of the oxidative and non-oxidative pentose phosphate pathway (PPP) were in most cases unquantifiable or not reproducible. To gain better coverage over the PPP - which is integral

to understanding the link of the action of L-GA to nucleotide biosynthesis - we suggest an alternative method of analysis. The method used for nucleotide extraction and subsequent ESI DI-MS/MS enriches for phosphorylated molecules. Although it was untested in this thesis, it is not unlikely that PPP intermediates will be enriched along with nucleotide. However, a drawback to this method would be the quantity of work required to select the specific MS/MS transitions for each molecule. This is further complicated when selecting unique transitions in a ^{13}C-labelling protocol.

The nucleotide analysis in this thesis takes a relative concentration approach. This is effective at comparing treated to untreated samples, but does not account for the differences in total nucleotide pools between cell types. It was chosen to take a relative approach to normalise each nucleotide to its relative treatment condition. In the event that a researcher wishes to compare nucleotide abundance between cell types, absolute concentration must be employed. In addition, the hydrolysis of tri- di- to mono phosphorylated nucleotides during extraction is difficult to account for. Future experiments may account for this by spiking in a labelled triphosphorylated nucleotide and measuring the relative degradation to subsequent phosphorylation states.

The limitations of nucleotide and metabolite analysis links to signalling pathway analysis. To further the research presented, it is suggested that key metabolites are investigated as modulators of signalling pathways. Sid et al. (2014) showed that the nucleotide intermediate AICAR induces NRF2 activation in hepatocarcinoma cells. Given that we observed significant effects on both SAICAR and AICAR, elucidating their role in redox would be recommended. Preliminary results, with unsuccessful reproducibility, showed activation of AMPK and AMPK phosphorylation upon L-GA treatment (supplementary material section 5.2, figure 5.2). However, this is supported by the evidence of high AMP levels in nucleotide analysis (figure 3.31). The quantification of AMPK phosphorylation by western blot is, by conjecture, notoriously difficult. We suggest that AMPK activity is inferred by the activity of S6K and the mTOR target-ACC, which have proved successful in recent studies (Orozco et al., 2020).

The experiments carried out in this thesis are, and can only be, interpreted as the effect of a compound under *in vitro* conditions. *In vitro* testing has the advantage of relatively large sample size, which can be sampled at short intervals. In the context of pSIRM, this is essential to understanding the kinetics of a metabolic system. However, to extrapolate *in vitro* kinetics to *in vivo* kinetics is a fallacy. Under *in vitro* conditions, a synthetic environment is created in which nutrient and oxygen availability does not reflect the system in a tumoural environment. As described in the introduction, the tumour micro-environment (TME) varies spatially, with oxygen availability depleting towards the centre of a tumour mass. In addition, nutrient availability is not uniform within the TME, therefore metabolism would not be uniform in cells of a tumour mass. This caveat is linked to the choice of a non-cancerous control cell line when performing *in vitro* experiments. It must be stressed that using a fibroblast cell line as a reference to a neuroblastoma cell line is not an optimal comparison. It is a generally accepted issue that there is a lack of appropriate *in vitro* control cell lines for neuroblastoma research. This is, in part, due to the heterogeneous lineage of neuroblastoma cells. It is suggested that the use of spheroid cell cultures and organoids would be an improvement on *in vitro* model systems.

4.6.1 Outlook

Despite 80 years of research L-GA has yet to take hold as a viable therapeutic. When bracketed in a manner similar to BrPyr and 2-DG, the therapeutic concentration required is relatively high. For comparison, in the context of neuroblastoma the conventional regimen of vincristine [O], cisplatin [P], etoposide [E], and cyclophosphamide [C], OPEC, dosages are in the micromolar range. However, the therapy lasts up to 126 days. Patients experience severe side effects ranging from hair loss, appetite suppression, nausea and increased chance of resistance (Pearson et al., 2008). Due to the the high molarity of L-GA required for potential therapy it is unlikely to translate into a mono-therapy. However, L-GA has scope to be used as an adjunct to provide more efficacy to OPEC regimens, reducing the concentrations and time for chemotherapy treatment. Indeed, BrPyr and 2-DG have been explored as chemopotentiators for platinum derived therapeutics showing promising results (Ihrlund et al., 2008). The synergistic effect of L-GA with current neuroblastoma therapeutics needs to be explored. Indeed, it has been shown as recently as 2014 that, 2-DG and DL-GA act in synergy to reduce tumour growth of ehrlich ascites carcinoma (Kapoor et al., 2014). It is hoped that this research is continued in partnership with the clinic and the laboratory, to achieve the translational potential of L-GA and the work described in this thesis.

Bibliography

F. Ades, K. Tryfonidis, and D. Zardavas. The past and future of breast cancer treatment - From the papyrus to individualised treatment approaches, jun 2017. ISSN 17546605.

G. Antony, L. W. White, and B. H. Landaljo. Metabolism of D-and L-glyceraldehyde in adipose tissue: a stereochemical probe for glycerokinase activity. Technical report. URL `www.jlr.org`.

P. Armitage and R. Doll. The age distribution of cancer and a multi-stage theory of carcinogenesis. *British Journal of Cancer*, 8(1):1–12, 1954. ISSN 15321827. doi: 10.1038/bjc.1954.1.

D. E. Atkinson and G. M. Walton. Adenosine triphosphate conservation in metabolic regulation. Rat liver citrate cleavage enzyme. *Journal of Biological Chemistry*, 1967. ISSN 00219258. doi: 10.1016/S0021-9258(18)95956-9.

D. L. Baker, M. L. Schmidt, S. L. Cohn, J. M. Maris, W. B. London, A. Buxton, D. Stram, R. P. Castleberry, H. Shimada, A. Sandler, R. C. Shamberger, A. T. Look, C. P. Reynolds, R. C. Seeger, and K. K. Matthay. Outcome after Reduced Chemotherapy for Intermediate-Risk Neuroblastoma. *New England Journal of Medicine*, 2010. ISSN 0028-4793. doi: 10.1056/nejmoa1001527.

P. R. Baker, S. D. Cramer, M. Kennedy, D. G. Assimos, and R. P. Holmes. Glycolate and glyoxylate metabolism in HepG2 cells. *American Journal of Physiology - Cell Physiology*, 2004. ISSN 03636143. doi: 10.1152/ajpcell.00238.2004.

Z. Baker. Studies on the inhibition of glycolysis by glyceraldehyde. *Biochemical Journal*, 1938. ISSN 0306-3283. doi: 10.1042/bj0320332.

J. H. Banoub and P. A. Limbach. Mass spectrometry of nucleosides and nucleic acids. *Mass Spectrometry of Nucleosides and Nucleic Acids*, 2009. doi: 10.1201/9781420044034.

E. Bell, J. Lunec, and D. A. Tweddle. Cell cycle regulation targets of MYCN identified by gene expression microarrays. *Cell Cycle*, 2007. ISSN 15514005. doi: 10.4161/cc.6.10.4222.

L. R. Bennett and F. E. Connon. Comparative effects of DL-glyceraldehyde, 6-mercaptopurine, methotrexate and 5-fluorouracil on the ehrlich ascites carcinoma in vivo. *International Journal of Cancer*, 1966. ISSN 10970215. doi: 10.1002/ijc.2910010308.

M. Berg, Jeremy, J. L. Tymoczko, G. J. Gatto, and L. Stryer. *Biochemistry 8th Edition*. 2015. ISBN 978-1-4641-2610-9.

M. P. Booth, R. Conners, G. Rumsby, and R. L. Brady. Structural Basis of Substrate Specificity in Human Glyoxylate Reductase/Hydroxypyruvate Reductase. *Journal of Molecular Biology*, 2006. ISSN 00222836. doi: 10.1016/j.jmb.2006.05.018.

L. G. Boros, J. Puigjaner, M. Cascante, W. N. P. Lee, J. L. Brandes, S. Bassilian, F. I. Yusuf, R. D. Williams, P. Muscarella, W. S. Melvin, and W. J. Schirmer. Oxythiamine and dehydroepiandrosterone inhibit the nonoxidative synthesis of ribose and tumor cell proliferation. *Cancer Research*, 1997. ISSN 00085472.

L. K. Boroughs and R. J. Deberardinis. Metabolic pathways promoting cancer cell survival and growth. *Nature Cell Biology*, 17(4):351–359, apr 2015. ISSN 14764679. doi: 10.1038/ncb3124.

R. Brandt and A. S. Keston. Synthesis of diacetyldichlorofluorescin: A stable reagent for fluorometric analysis. *Analytical Biochemistry*, 1965. ISSN 10960309. doi: 10.1016/0003-2697(65)90035-7.

N. Brock and T. Niekamp. Zur Frage der cytostatischen Wirksamkeit von D-Glycerinaldehyd. *Zeitschrift für Krebsforschung*, 1965. ISSN 01715216. doi: 10.1007/BF00524151.

M. R. Buchakjian and S. Kornbluth. The engine driving the ship: Metabolic steering of cell proliferation and death. *Nature Reviews Molecular Cell Biology*, 11(10):715–727, 2010. ISSN 14710080. doi: 10.1038/nrm2972. URL `https://pubmed.ncbi.nlm.nih.gov/20861880/`.

E. Cadenas and A. Boveris. Mitochondrial Free Radical Production , Antioxidant Defenses and Cell Signaling. *Environmental Chemistry*, 2005.

M. Cal, I. Matyjaszczyk, I. Litwin, D. Augustyniak, R. Ogórek, Y. Ko, and S. Ułaszewski. The Anticancer Drug 3-Bromopyruvate Induces DNA Damage Potentially Through Reactive Oxygen Species in Yeast and in Human Cancer Cells. *Cells*, 2020. ISSN 20734409. doi: 10.3390/cells9051161.

M. Camici, M. Garcia-Gil, R. Pesi, S. Allegrini, and M. G. Tozzi. Purine-metabolising enzymes and apoptosis in cancer. *Cancers*, 2019. ISSN 20726694. doi: 10.3390/cancers11091354.

J. R. Cantor and D. M. Sabatini. Cancer cell metabolism: One hallmark, many faces. *Cancer Discovery*, 2012. ISSN 21598274. doi: 10.1158/2159-8290.CD-12-0345.

S. Carujo, J. M. Estanyol, A. Ejarque, N. Agell, O. Bachs, and M. J. Pujol. Glyceraldehyde 3-phosphate dehydrogenase is a SET-binding protein and regulates cyclin B-cdk1 activity. *Oncogene*, 2006. ISSN 09509232. doi: 10.1038/sj.onc.1209433.

M. C. Casimiro, M. Velasco-Velázquez, C. Aguirre-Alvarado, and R. G. Pestell. Overview of cyclins D1 function in cancer and the CDK inhibitor landscape: Past and present. *Expert Opinion on Investigational Drugs*, 2014. ISSN 13543784. doi: 10.1517/13543784.2014.867017.

Y. Chen, S. H. Tseng, H. S. Lai, and W. J. Chen. Resveratrol-induced cellular apoptosis and cell cycle arrest in neuroblastoma cells and antitumor effects on neuroblastoma in mice. *Surgery*, 2004. ISSN 00396060. doi: 10.1016/j.surg.2004.01.017.

N. K. V. Cheung, J. Zhang, C. Lu, M. Parker, A. Bahrami, S. K. Tickoo, A. Heguy, A. S. Pappo, S. Federico, J. Dalton, I. Y. Cheung, L. Ding, R. Fulton, J. Wang, X. Chen, J. Becksfort, J. Wu, C. A. Billups, D. Ellison, E. R. Mardis, R. K. Wilson, J. R. Downing, and M. A. Dyer. Association of age at diagnosis and genetic mutations in patients with neuroblastoma. *JAMA - Journal of the American Medical Association*, 2012. ISSN 00987484. doi: 10.1001/jama.2012.228.

F. Ciccarese and V. Ciminale. Escaping death: Mitochondrial redox homeostasis in cancer cells. *Frontiers in Oncology*, 2017. ISSN 2234943X. doi: 10.3389/fonc.2017.00117.

M. L. Circu and T. Y. Aw. Reactive oxygen species, cellular redox systems, and apoptosis. *Free Radical Biology and Medicine*, 2010. ISSN 08915849. doi: 10.1016/j.freeradbiomed.2009.12.022.

S. L. Cohn, A. D. Pearson, W. B. London, T. Monclair, P. F. Ambros, G. M. Brodeur, A. Faldum, B. Hero, T. Iehara, D. Machin, V. Mosseri, T. Simon, A. Garaventa, V. Castel, and K. K. Matthay. The International Neuroblastoma Risk Group (INRG) classification system: An INRG task force report. *Journal of Clinical Oncology*, 2009. ISSN 0732183X. doi: 10.1200/JCO.2008.16.6785.

K. A. Cole, J. Huggins, M. Laquaglia, C. E. Hulderman, M. R. Russell, K. Bosse, S. J. Diskin, E. F. Attiyeh, R. Sennett, G. Norris, M. Laudenslager, A. C. Wood, P. A. Mayes, J. Jagannathan, C. Winter, Y. P. Mosse, and J. M. Maris. RNAi screen of the protein kinome identifies checkpoint kinase 1 (CHK1) as a therapeutic target in neuroblastoma. *Proceedings of the National Academy of Sciences of the United*

States of America, 2011. ISSN 00278424. doi: 10.1073/pnas.1012351108.

M. C. Coleman, C. R. Asbury, D. Daniels, J. Du, N. Aykin-Burns, B. J. Smith, L. Li, D. R. Spitz, and J. J. Cullen. 2-Deoxy-d-glucose causes cytotoxicity, oxidative stress, and radiosensitization in pancreatic cancer. *Free Radical Biology and Medicine*, 2008. ISSN 08915849. doi: 10.1016/j.freeradbiomed.2007.08.032.

K. A. Conklin. Chemotherapy-associated oxidative stress: Impact on chemotherapeutic effectiveness. *Integrative Cancer Therapies*, 2004. ISSN 15347354. doi: 10.1177/1534735404270335.

I. Dalle-Donne, R. Rossi, A. Milzani, P. Di Simplicio, and R. Colombo. The actin cytoskeleton response to oxidants: From small heat shock protein phosphorylation to changes in the redox state of actin itself. *Free Radical Biology and Medicine*, 2001. ISSN 08915849. doi: 10.1016/S0891-5849(01)00749-3.

I. Dando, M. Cordani, and M. Donadelli. Mutant p53 and mTOR/PKM2 regulation in cancer cells. *IUBMB Life*, 2016. ISSN 15216551. doi: 10.1002/iub.1534.

C. V. Dang. MYC, metabolism, cell growth, and tumorigenesis. *Cold Spring Harbor Perspectives in Medicine*, 2013. ISSN 21571422. doi: 10.1101/cshperspect.a014217.

R. J. De Berardinis and N. S. Chandel. Fundamentals of cancer metabolism, may 2016. ISSN 23752548.

K. De Bock, M. Georgiadou, S. Schoors, A. Kuchnio, B. W. Wong, A. R. Cantelmo, A. Quaegebeur, B. Ghesquière, S. Cauwenberghs, G. Eelen, L. K. Phng, I. Betz, B. Tembuyser, K. Brepoels, J. Welti, I. Geudens, I. Segura, B. Cruys, F. Bifari, I. Decimo, R. Blanco, S. Wyns, J. Vangindertael, S. Rocha, R. T. Collins, S. Munck, D. Daelemans, H. Imamura, R. Devlieger, M. Rider, P. P. Van Veldhoven, F. Schuit, R. Bartrons, J. Hofkens, P. Fraisl, S. Telang, R. J. Deberardinis, L. Schoonjans, S. Vinckier, J. Chesney, H. Gerhardt, M. Dewerchin, and P. Carmeliet. Role of PFKFB3-driven glycolysis in vessel sprouting. *Cell*, 2013. ISSN 00928674. doi: 10.1016/j.cell.2013.06.037.

F. Debacq-Chainiaux, C. Borlon, T. Pascal, V. Royer, F. Eliaers, N. Ninane, G. Carrard, B. Friguet, F. de Longueville, S. Boffe, J. Remacle, and O. Toussaint. Repeated exposure of human skin fibroblasts to UVB at subcytotoxic level triggers premature senescence through the TGF-β1 signaling pathway. *Journal of Cell Science*, 2005. ISSN 00219533. doi: 10.1242/jcs.01651.

R. J. DeBerardinis, J. M. Mates, E. S. Jin, C. Yang, A. R. Mullen, J. Sudderth, and T. Cheng. Pyruvate carboxylase is required for glutamine-independent growth of tumor cells. *Proceedings of the National Academy of Sciences*, 108(21):8674–8679, may 2011. ISSN 0027-8424. doi: 10.1073/pnas.1016627108. URL `https://www.pnas.org/content/108/21/8674.long`.

G. M. Denicola, F. A. Karreth, T. J. Humpton, A. Gopinathan, C. Wei, K. Frese, D. Mangal, K. H. Yu, C. J. Yeo, E. S. Calhoun, F. Scrimieri, J. M. Winter, R. H. Hruban, C. Iacobuzio-Donahue, S. E. Kern, I. A. Blair, and D. A. Tuveson. Oncogene-induced Nrf2 transcription promotes ROS detoxification and tumorigenesis. *Nature*, 2011. ISSN 00280836. doi: 10.1038/nature10189.

R. S. DiPaola. To arrest or not to G2-M cell-cycle arrest. *Clinical Cancer Research*, 2002. ISSN 10780432.

M. R. Doe, J. M. Ascano, M. Kaur, and M. D. Cole. Myc posttranscriptionally induces HIF1 protein and target gene expression in normal and cancer cells. *Cancer Research*, 2012. ISSN 00085472. doi: 10.1158/0008-5472.CAN-11-2371.

P. Dumont, M. Burton, Q. M. Chen, E. S. Gonos, C. Frippiat, J. B. Mazarati, F. Eliaers, J. Remacle, and O. Toussaint. Induction of replicative senescence biomarkers by sublethal oxidative stresses in normal

human fibroblast. *Free Radical Biology and Medicine*, 2000. ISSN 08915849. doi: 10.1016/S0891-5849(99)00249-X.

E. Ehrke, C. Arend, and R. Dringen. 3-bromopyruvate inhibits glycolysis, depletes cellular glutathione, and compromises the viability of cultured primary rat astrocytes. *Journal of Neuroscience Research*, 2015. ISSN 10974547. doi: 10.1002/jnr.23474.

J. O. Ely. 2-deoxy-d-glucose as an inhibitor of cancerous growth in animals. *Journal of the Franklin Institute*, 1954. ISSN 00160032. doi: 10.1016/0016-0032(54)90946-1.

Y. W. Eom, M. A. Kim, S. S. Park, M. J. Goo, H. J. Kwon, S. Sohn, W. H. Kim, G. Yoon, and K. S. Choi. Two distinct modes of cell death induced by doxorubicin: Apoptosis and cell death through mitotic catastrophe accompanied by senescence-like phenotype. *Oncogene*, 2005. ISSN 09509232. doi: 10.1038/sj.onc.1208627.

R. Fritsche-Guenther, C. Zasada, G. Mastrobuoni, N. Royla, R. Rainer, F. Roßner, M. Pietzke, E. Klipp, C. Sers, and S. Kempa. Alterations of mTOR signaling impact metabolic stress resistance in colorectal carcinomas with BRAF and KRAS mutations. *Scientific Reports*, 2018. ISSN 20452322. doi: 10.1038/s41598-018-27394-1.

S. Galadari, A. Rahman, S. Pallichankandy, and F. Thayyullathil. Reactive oxygen species and cancer paradox: To promote or to suppress? *Free Radical Biology and Medicine*, 2017. ISSN 18734596. doi: 10.1016/j.freeradbiomed.2017.01.004.

L. Galluzzi, J. M. Bravo-San Pedro, and G. Kroemer. Organelle-specific initiation of cell death. *Nature Cell Biology*, 2014. ISSN 14764679. doi: 10.1038/ncb3005.

J. F. H. Geschwind, Y. H. Ko, M. S. Torbenson, C. Magee, and P. L. Pedersen. Novel therapy for liver cancer: Direct intraarterial injection of a potent inhibitor of ATP production. *Cancer Research*, 2002. ISSN 00085472.

L. Gong, Y. Wei, X. Yu, J. Peng, and X. Leng. 3-Bromopyruvic Acid, A Hexokinase II Inhibitor, is an Effective Antitumor Agent on the Hepatoma Cells : in vitro and in vivo Findings. *Anti-Cancer Agents in Medicinal Chemistry*, 2014. ISSN 18715206. doi: 10.2174/1871520614666140416105309.

C. Granchi and F. Minutolo. Anticancer Agents That Counteract Tumor Glycolysis. *ChemMedChem*, 2012. ISSN 18607179. doi: 10.1002/cmdc.201200176.

F. Grimm, L. Fets, and D. Anastasiou. Gas chromatography coupled to mass spectrometry (GC–MS) to study metabolism in cultured cells. In *Advances in Experimental Medicine and Biology*. 2016. doi: 10.1007/978-3-319-26666-4_5.

G. G. Guidotti, A. Fonnesu, and E. Ciaranfi. Inhibition of Amino Acid Incorporation into Protein of Yoshida Ascites Hepatoma Cells by Glyceraldehyde. *Cancer Research*, 24(5), 1964.

K. Hagopian, J. J. Ramsey, and R. Weindruch. Enzymes of glycerol and glyceraldehyde,metabolismin mouse liver: Effects of caloric restriction and age on activities. *Bioscience Reports*, 2008. ISSN 01448463. doi: 10.1042/BSR20080015.

J. M. Halket, D. Waterman, A. M. Przyborowska, R. K. Patel, P. D. Fraser, and P. M. Bramley. Chemical derivatization and mass spectral libraries in metabolic profiling by GC/MS and LC/MS/MS. In *Journal of Experimental Botany*, 2005. doi: 10.1093/jxb/eri069.

D. Hanahan and R. A. Weinberg. Hallmarks of cancer: The next generation. *Cell*, 144(5):646–674, mar 2011. ISSN 00928674. doi: 10.1016/j.cell.2011.02.013.

I. S. Harris, A. E. Treloar, S. Inoue, M. Sasaki, C. Gorrini, K. C. Lee, K. Y. Yung, D. Brenner, C. B. Knobbe-Thomsen, M. A. Cox, A. Elia, T. Berger, D. W. Cescon, A. Adeoye, A. Brüstle, S. D. Molyneux, J. M. Mason, W. Y. Li, K. Yamamoto, A. Wakeham, H. K. Berman, R. Khokha, S. J. Done, T. J. Kavanagh, C. W. Lam, and T. W. Mak. Glutathione and Thioredoxin Antioxidant Pathways Synergize to Drive Cancer Initiation and Progression. *Cancer Cell*, 2015. ISSN 18783686. doi: 10.1016/j.ccell.2014.11.019.

M. Hart, S. D. Adams, and V. M. Draviam. Multinucleation Associated DNA Damage causes quiescence despite compromised p53. *bioRxiv*, page 2020.12.22.424035, jan 2020. doi: 10.1101/2020.12.22.424035. URL `http://biorxiv.org/content/early/2020/12/22/2020.12.22.424035.abstract`.

N. Hay. Reprogramming glucose metabolism in cancer: Can it be exploited for cancer therapy? *Nature Reviews Cancer*, 2016. ISSN 14741768. doi: 10.1038/nrc.2016.77.

T. Hishiki, T. Saito, Y. Sato, T. Mitsunaga, E. Terui, G. Matsuura, E. Saito, R. Shibata, N. Mise, Y. Yokoyama, and H. Yoshida. Src kinase family inhibitor PP2 induces aggregation and detachment of neuroblastoma cells and inhibits cell growth in a PI3 kinase/Akt pathway-independent manner. *Pediatric Surgery International*, 27(2):225–230, feb 2011. ISSN 01790358. doi: 10.1007/s00383-010-2775-2. URL `https://pubmed.ncbi.nlm.nih.gov/21046121/`.

M. C. Hsu and W. C. Hung. Pyruvate kinase M2 fuels multiple aspects of cancer cells: From cellular metabolism, transcriptional regulation to extracellular signaling. *Molecular Cancer*, 2018. ISSN 14764598. doi: 10.1186/s12943-018-0791-3.

H. Hu, A. Juvekar, C. A. Lyssiotis, E. C. Lien, J. G. Albeck, D. Oh, G. Varma, Y. P. Hung, S. Ullas, J. Lauring, P. Seth, M. R. Lundquist, D. R. Tolan, A. K. Grant, D. J. Needleman, J. M. Asara, L. C. Cantley, and G. M. Wulf. Phosphoinositide 3-Kinase Regulates Glycolysis through Mobilization of Aldolase from the Actin Cytoskeleton. *Cell*, 2016. ISSN 10974172. doi: 10.1016/j.cell.2015.12.042.

C. C. Huang, S. Y. Wang, L. L. Lin, P. W. Wang, T. Y. Chen, W. M. Hsu, T. K. Lin, C. W. Liou, and J. H. Chuang. Glycolytic inhibitor 2-deoxyglucose simultaneously targets cancer and endothelial cells to suppress neuroblastoma growth in mice. *DMM Disease Models and Mechanisms*, 2015. ISSN 17548411. doi: 10.1242/dmm.021667.

C. T. Huang, C. H. Hsieh, W. C. Lee, Y. L. Liu, T. S. Yang, W. M. Hsu, Y. J. Oyang, H. C. Huang, and H. F. Juan. Therapeutic targeting of non-oncogene dependencies in high-risk neuroblastoma. *Clinical Cancer Research*, 2019. ISSN 15573265. doi: 10.1158/1078-0432.CCR-18-4117.

K. Huber, A. Mestres-Arenas, L. Fajas, and L. C. Leal-Esteban. The multifaceted role of cell cycle regulators in the coordination of growth and metabolism. *FEBS Journal*, 2020. ISSN 17424658. doi: 10.1111/febs.15586.

L. S. Ihrlund, E. Hernlund, O. Khan, and M. C. Shoshan. 3-Bromopyruvate as inhibitor of tumour cell energy metabolism and chemopotentiator of platinum drugs. *Molecular Oncology*, 2008. ISSN 15747891. doi: 10.1016/j.molonc.2008.01.003.

J. Kalucka, R. Missiaen, M. Georgiadou, S. Schoors, C. Lange, K. De Bock, M. Dewerchin, and P. Carmeliet. Metabolic control of the cell cycle. *Cell Cycle*, 14(21):3379–3388, 2015. ISSN 15514005. doi: 10.1080/15384101.2015.1090068. URL `/pmc/articles/PMC4825590/?report=abstracthttps://www.ncbi.nlm.nih.gov/pmc/articles/PMC4825590/`.

H. Kamata and H. Hirata. Redox regulation of cellular signalling. *Cellular Signalling*, 1999. ISSN 08986568. doi: 10.1016/S0898-6568(98)00037-0.

B. Kaminska, B. Czapski, R. Guzik, S. K. Król, and B. Gielniewski. Consequences of IDH1/2 mutations in gliomas and an assessment of inhibitors targeting mutated IDH proteins. *Molecules*, 2019. ISSN 14203049. doi: 10.3390/molecules24050968.

E. Kansanen, S. M. Kuosmanen, H. Leinonen, and A. L. Levonenn. The Keap1-Nrf2 pathway: Mechanisms of activation and dysregulation in cancer. *Redox Biology*, 2013. ISSN 22132317. doi: 10.1016/j.redox.2012.10.001.

R. Kapoor, D. B. Gundpatil, B. L. Somani, T. K. Saha, S. Bandyopadhyay, and P. Misra. Anticancer effect of DL-glyceraldehyde and 2-deoxyglucose in Ehrlich ascites carcinoma bearing mice and their effect on liver, kidney and haematological parameters. *Indian Journal of Clinical Biochemistry*, 2014. ISSN 09740422. doi: 10.1007/s12291-013-0343-y.

S. Kardeh, S. Ashkani-Esfahani, and A. M. Alizadeh. Paradoxical action of reactive oxygen species in creation and therapy of cancer. *European Journal of Pharmacology*, 2014. ISSN 18790712. doi: 10.1016/j.ejphar.2014.04.023.

K. E. Keller, Z. M. Doctor, Z. W. Dwyer, and Y. S. Lee. SAICAR induces protein kinase activity of PKM2 that is necessary for sustained proliferative signaling of cancer cells. *Molecular Cell*, 2014. ISSN 10972765. doi: 10.1016/j.molcel.2014.02.015.

S. Kempa, J. Hummel, T. Schwemmer, M. Pietzke, N. Strehmel, S. Wienkoop, J. Kopka, and W. Weckwerth. An automated GCxGC-TOF-MS protocol for batch-wise extraction and alignment of mass isotopomer matrixes from differential13C-labelling experiments: A case study for photoautotrophic-mixotrophic grown Chlamydomonas reinhardtii cells. *Journal of Basic Microbiology*, 2009. ISSN 0233111X. doi: 10.1002/jobm.200800337.

A. S. Keston and R. Brandt. The fluorometric analysis of ultramicro quantities of hydrogen peroxide. *Analytical Biochemistry*, 1965. ISSN 10960309. doi: 10.1016/0003-2697(65)90034-5.

E. Kováts. Gas-chromatographische Charakterisierung organischer Verbindungen. Teil 1: Retentionsindices aliphatischer Halogenide, Alkohole, Aldehyde und Ketone. *Helvetica Chimica Acta*, 1958. ISSN 15222675. doi: 10.1002/hlca.19580410703.

G. Kroemer and J. Pouyssegur. Tumor Cell Metabolism: Cancer's Achilles' Heel. *Cancer Cell*, 13 (6):472–482, jun 2008. ISSN 15356108. doi: 10.1016/j.ccr.2008.05.005. URL `http://www.cell.com/article/S1535610808001608/fulltexthttp://www.cell.com/article/S1535610808001608/abstracthttps://www.cell.com/cancer-cell/abstract/S1535-6108(08)00160-8`.

P. H. J. L. Kuich, N. Hoffmann, and S. Kempa. Maui-VIA: A User-Friendly Software for Visual Identification, Alignment, Correction, and Quantification of Gas Chromatographyâ€"Mass Spectrometry Data. *Frontiers in Bioengineering and Biotechnology*, 2015. ISSN 2296-4185. doi: 10.3389/fbioe.2014.00084.

U. K. Laemmli. Cleavage of structural proteins during the assembly of the head of bacteriophage T4. *Nature*, 1970. ISSN 00280836. doi: 10.1038/227680a0.

A. N. Lane and T. W. Fan. Regulation of mammalian nucleotide metabolism and biosynthesis. *Nucleic Acids Research*, 2015. ISSN 13624962. doi: 10.1093/nar/gkv047.

H. A. Lardy, V. D. Wiebelhaus, and K. M. Mann. The mechanism by which glyceraldehyde inhibits glycolysis. *The Journal of biological chemistry*, 1950. ISSN 00219258. doi: 10.1016/s0021-9258(19)50957-7.

C. Laronga, H. Y. Yang, C. Neal, and M. H. Lee. Association of the cyclin-dependent kinases and 14-3-3 sigma negatively regulates cell cycle progression. *Journal of Biological Chemistry*, 2000. ISSN 00219258. doi: 10.1074/jbc.M905616199.

A. Le, C. R. Cooper, A. M. Gouw, R. Dinavahi, A. Maitra, L. M. Deck, R. E. Royer, D. L. Vander Jagt, G. L. Semenza, and C. V. Dang. Inhibition of lactate dehydrogenase A induces oxidative stress and inhibits tumor progression. *Proceedings of the National Academy of Sciences of the United States of America*, 2010. ISSN 00278424. doi: 10.1073/pnas.0914433107.

J. E. Leadsham, V. N. Kotiadis, D. J. Tarrant, and C. W. Gourlay. Apoptosis and the yeast actin cytoskeleton. *Cell Death and Differentiation*, 2010. ISSN 13509047. doi: 10.1038/cdd.2009.196.

G. Y. Liou and P. Storz. Reactive oxygen species in cancer. *Free Radical Research*, 2010. ISSN 10715762. doi: 10.3109/10715761003667554.

M. Lo, Y. Z. Wang, and P. W. Gout. The xc- cystine/glutamate antiporter: A potential target for therapy of cancer and other diseases. *Journal of Cellular Physiology*, 215(3):593–602, jun 2008. ISSN 00219541. doi: 10.1002/jcp.21366. URL `https://pubmed.ncbi.nlm.nih.gov/18181196/https://pubmed.ncbi.nlm.nih.gov/18181196/?dopt=Abstract`.

M. Lodrini, A. Sprüssel, K. Astrahantseff, D. Tiburtius, R. Konschak, H. N. Lode, M. Fischer, U. Keilholz, A. Eggert, and H. E. Deubzer. Using droplet digital PCR to analyze MYCN and ALK copy number in plasma from patients with neuroblastoma. *Oncotarget*, 2017. ISSN 19492553. doi: 10.18632/oncotarget.19076.

P. Lorkiewicz, R. M. Higashi, A. N. Lane, and T. W. Fan. High information throughput analysis of nucleotides and their isotopically enriched isotopologues by direct-infusion FTICR-MS. *Metabolomics*, 2012. ISSN 15733882. doi: 10.1007/s11306-011-0388-y.

W. Lu, X. Su, M. S. Klein, I. A. Lewis, O. Fiehn, and J. D. Rabinowitz. Metabolite measurement: Pitfalls to avoid and practices to follow. *Annual Review of Biochemistry*, 2017. ISSN 15454509. doi: 10.1146/annurev-biochem-061516-044952.

M. J. MacDonald, F. W. Chaplen, C. K. Triplett, Q. Gong, and H. Drought. Stimulation of insulin release by glyceraldehyde may not be similar to glucose. *Archives of Biochemistry and Biophysics*, 2006. ISSN 00039861. doi: 10.1016/j.abb.2006.01.019.

J. C. Maher, A. Krishan, and T. J. Lampidis. Greater cell cycle inhibition and cytotoxicity induced by 2-deoxy-D-glucose in tumor cells treated under hypoxic vs aerobic conditions. *Cancer Chemotherapy and Pharmacology*, 2004. ISSN 03445704. doi: 10.1007/s00280-003-0724-7.

S. Mandal, W. A. Freije, P. Guptan, and U. Banerjee. Metabolic control of G1-S transition: Cyclin E degradation by p53-induced activation of the ubiquitin-proteasome system. *Journal of Cell Biology*, 2010. ISSN 00219525. doi: 10.1083/jcb.200912024.

R. Mariadasse, J. Biswal, P. Jayaprakash, G. R. Rao, S. K. Choubey, S. Rajendran, and J. Jeyakanthan. Mechanical insights of oxythiamine compound as potent inhibitor for human transketolase-like protein 1 (TKTL1 protein). *Journal of Receptors and Signal Transduction*, 2016. ISSN 15324281. doi: 10.3109/10799893.2015.1080272.

M. Márton, N. Tihanyi, P. Gyulavári, G. Bánhegyi, and O. Kapuy. NRF2-regulated cell cycle arrest at early stage of oxidative stress response mechanism. *PLoS ONE*, 2018. ISSN 19326203. doi: 10.1371/journal.pone.0207949.

R. Marullo, E. Werner, N. Degtyareva, B. Moore, G. Altavilla, S. S. Ramalingam, and P. W. Doetsch. Cisplatin induces a mitochondrial-ros response that contributes to cytotoxicity depending on mitochondrial redox status and bioenergetic functions. *PLoS ONE*, 2013. ISSN 19326203. doi: 10.1371/journal.pone.0081162.

G. Maschek, N. Savaraj, W. Priebe, P. Braunschweiger, K. Hamilton, G. F. Tidmarsh, L. R. De Young, and T. J. Lampidis. 2-Deoxy-D-glucose Increases the Efficacy of Adriamycin and Paclitaxel in Human Osteosarcoma and Non-Small Cell Lung Cancers in Vivo. *Cancer Research*, 2004. ISSN 00085472. doi: 10.1158/0008-5472.CAN-03-3294.

S. M. Maswoswe, F. Daneshmand, and D. R. Davies. Metabolic effects of D-glyceraldehyde in isolated hepatocytes. *Biochemical Journal*, 240(3):771–776, 1986. ISSN 02646021. doi: 10.1042/bj2400771.

K. K. Matthay, J. M. Maris, G. Schleiermacher, A. Nakagawara, C. L. Mackall, L. Diller, and W. A. Weiss. Neuroblastoma. *Nature Reviews Disease Primers*, 2016. ISSN 2056676X. doi: 10.1038/nrdp.2016.78.

I. Meijerman, J. H. Beijnen, and J. H. Schellens. Combined action and regulation of phase II enzymes and multidrug resistance proteins in multidrug resistance in cancer. *Cancer Treatment Reviews*, 2008. ISSN 03057372. doi: 10.1016/j.ctrv.2008.03.002.

B. Mendel. Krebszelle und Glycerinaldehyd. *Klinische Wochenschrift*, 1929. ISSN 00232173. doi: 10.1007/BF01748597.

B. Mendel, F. Strelitz, and D. Mundell. 1-Glyceric aldehyde and tumor metabolism. *Science*, 1938. ISSN 00368075. doi: 10.1126/science.88.2276.149.

E. Messina, P. Gazzaniga, V. Micheli, M. R. Guaglianone, S. Barbato, S. Morrone, L. Frati, A. M. Aglianó, and A. Giacomello. Guanine nucleotide depletion triggers cell cycle arrest and apoptosis in human neuroblastoma cell lines. *International Journal of Cancer*, 2004. ISSN 00207136. doi: 10.1002/ijc.11642.

Y. Mitsuishi, K. Taguchi, Y. Kawatani, T. Shibata, T. Nukiwa, H. Aburatani, M. Yamamoto, and H. Motohashi. Nrf2 Redirects Glucose and Glutamine into Anabolic Pathways in Metabolic Reprogramming. *Cancer Cell*, 22(1):66–79, jul 2012. ISSN 15356108. doi: 10.1016/j.ccr.2012.05.016.

D. A. Morgenstern and M. S. Irwin. Current and future strategies for treatment of relapsed neuroblastoma. In *Neuroblastoma: Molecular Mechanisms and Therapeutic Interventions*. 2019. ISBN 9780128120057. doi: 10.1016/B978-0-12-812005-7.00015-1.

P. Muley, A. Olinger, and H. Tummala. 2-Deoxyglucose induces cell cycle arrest and apoptosisin colorectal cancer cells independent of its glycolysis inhibition. *Nutrition and Cancer*, 2015. ISSN 15327914. doi: 10.1080/01635581.2015.1002626.

E. Mullarky and L. C. Cantley. Diverting Glycolysis to Combat Oxidative Stress. *Innovative Medicine*, 2015. doi: 10.1007/978-4-431-55651-0_1.

D. Murray and R. Mirzayans. Cellular responses to platinum-based anticancer drugs and UVC: Role of P53 and implications for cancer therapy. *International Journal of Molecular Sciences*, 2020. ISSN 14220067. doi: 10.3390/ijms21165766.

D. M. Needham, L. Siminovitch, and S. M. Rapkine. On the mechanism of the inhibition of glycolysis by glyceraldehyde. *The Biochemical journal*, 49(1):113–124, 1951. ISSN 14708728. doi: 10.1042/bj0490113. URL https://www.ncbi.nlm.nih.gov/pmc/articles/PMC1197464/.

J. Needham and H. Lehmann. Intermediary carbohydrate metabolism in embryonic life. *Biochemical Journal*, 1937. ISSN 0306-3283. doi: 10.1042/bj0311913.

K. M. Nieman, H. A. Kenny, C. V. Penicka, A. Ladanyi, R. Buell-Gutbrod, M. R. Zillhardt, I. L. Romero, M. S. Carey, G. B. Mills, G. S. Hotamisligil, S. D. Yamada, M. E. Peter, K. Gwin, and E. Lengyel. Adipocytes promote ovarian cancer metastasis and provide energy for rapid tumor growth. *Nature Medicine*, 2011. ISSN 10788956. doi: 10.1038/nm.2492.

P. C. Nowell. The clonal evolution of tumor cell populations. *Science*, 194(4260):23–28, oct 1976. ISSN 00368075. doi: 10.1126/science.959840.

J. M. Orozco, P. A. Krawczyk, S. M. Scaria, A. L. Cangelosi, S. H. Chan, T. Kunchok, C. A. Lewis, and D. M. Sabatini. Dihydroxyacetone phosphate signals glucose availability to mTORC1. *Nature Metabolism*, 2(9):893–901, sep 2020. ISSN 25225812. doi: 10.1038/s42255-020-0250-5. URL https://pubmed.ncbi.nlm.nih.gov/32719541/.

J. Otte, C. Dyberg, A. Pepich, and J. I. Johnsen. MYCN Function in Neuroblastoma Development. *Frontiers in Oncology*, 10:3210, 2021. URL https://www.frontiersin.org/article/10.3389/fonc.2020.624079.

T. Paffhausen, M. Schwab, and F. Westermann. Targeted MYCN expression affects cytotoxic potential of chemotherapeutic drugs in neuroblastoma cells. *Cancer Letters*, 2007. ISSN 03043835. doi: 10.1016/j.canlet.2006.09.010.

N. Papavramidou, T. Papavramidis, and T. Demetriou. Ancient greek and greco-Roman methods in modern surgical treatment of cancer. *Annals of Surgical Oncology*, 17(3):665–667, mar 2010. ISSN 10689265. doi: 10.1245/s10434-009-0886-6.

E. J. Park, H. Y. Min, H. J. Chung, J. Y. Hong, Y. J. Kang, T. M. Hung, U. J. Youn, Y. S. Kim, K. H. Bae, S. S. Kang, and S. K. Lee. Down-regulation of c-Src/EGFR-mediated signaling activation is involved in the honokiol-induced cell cycle arrest and apoptosis in MDA-MB-231 human breast cancer cells. *Cancer Letters*, 2009. ISSN 03043835. doi: 10.1016/j.canlet.2008.11.029.

J. R. Park, R. Bagatell, W. B. London, J. M. Maris, S. L. Cohn, K. M. Mattay, and M. Hogarty. Children's Oncology Group's 2013 blueprint for research: Neuroblastoma. *Pediatric Blood and Cancer*, 2013. ISSN 15455009. doi: 10.1002/pbc.24433.

A. D. Pearson, C. R. Pinkerton, I. J. Lewis, J. Imeson, C. Ellershaw, and D. Machin. High-dose rapid and standard induction chemotherapy for patients aged over 1 year with stage 4 neuroblastoma: a randomised trial. *The Lancet Oncology*, 2008. ISSN 14702045. doi: 10.1016/S1470-2045(08)70069-X.

H. Pelicano, D. S. Martin, R. H. Xu, and P. Huang. Glycolysis inhibition for anticancer treatment, 2006. ISSN 09509232.

B. Perillo, M. Di Donato, A. Pezone, E. Di Zazzo, P. Giovannelli, G. Galasso, G. Castoria, and A. Migliaccio. ROS in cancer therapy: the bright side of the moon. *Experimental and Molecular Medicine*, 2020. ISSN 20926413. doi: 10.1038/s12276-020-0384-2.

G. Petrosillo, F. M. Ruggiero, and G. Paradies. Role of reactive oxygen species and cardiolipin in the

release of cytochrome c from mitochondria. *The FASEB Journal*, 2003. ISSN 0892-6638. doi: 10.1096/fj.03-0012com.

I. Philippe, Z. Xiao-Dong, L. Edwige, L. Marie-Hélène, A. Stéphane, L. Hubert, and P. Laurent. Experimental results using 3-bromopyruvate in mesothelioma: In vitro and in vivo studies. *Journal of Bioenergetics and Biomembranes*, 2012. ISSN 15736881. doi: 10.1007/s10863-012-9415-6.

M. Pietzke. *Analysis of the metabolic control of cell growth using stable isotope resolved metabolomics*. PhD thesis, Freie Universitaet Berlin, 2015. URL `http://dx.doi.org/10.17169/refubium-4786`.

M. Pietzke, C. Zasada, S. Mudrich, and S. Kempa. Decoding the dynamics of cellular metabolism and the action of 3-bromopyruvate and 2-deoxyglucose using pulsed stable isotope-resolved metabolomics. *Cancer & Metabolism*, 2(1):9, 2014. doi: 10.1186/2049-3002-2-9.

J. G. Pizarro, E. Verdaguer, V. Ancrenaz, F. Junyent, F. Sureda, M. Pallàs, J. Folch, and A. Camins. Resveratrol inhibits proliferation and promotes apoptosis of neuroblastoma cells: Role of sirtuin 1. *Neurochemical Research*, 2011. ISSN 03643190. doi: 10.1007/s11064-010-0296-y.

K. N. Prasad. Effect of DL-Glyceraldehyde on Mouse Neuroblastoma Cells in Culture. *Cancer Research*, 1972. ISSN 15387445.

X. Qian, X. Li, L. Tan, J. H. Lee, Y. Xia, Q. Cai, Y. Zheng, H. Wang, P. L. Lorenzi, and Z. Lu. Conversion of prps hexamer to monomer by AMPK-mediated phosphorylation inhibits nucleotide synthesis in response to energy stress. *Cancer Discovery*, 8(1):94–107, jan 2018. ISSN 21598290. doi: 10.1158/2159-8290.CD-17-0712. URL `www.aacrjournals.org`.

J. Qiao, P. Paul, S. Lee, L. Qiao, E. Josifi, J. R. Tiao, and D. H. Chung. PI3K/AKT and ERK regulate retinoic acid-induced neuroblastoma cellular differentiation. *Biochemical and Biophysical Research Communications*, 2012. ISSN 0006291X. doi: 10.1016/j.bbrc.2012.06.125.

G. Qing, N. Skuli, P. A. Mayes, B. Pawel, D. Martinez, J. M. Maris, and M. C. Simon. Combinatorial regulation of neuroblastoma tumor progression by N-Myc and hypoxia inducible factor HIF-1α. *Cancer Research*, 2010. ISSN 00085472. doi: 10.1158/0008-5472.CAN-10-0740.

R. Quinn, M. Basanta-Sanchez, R. E. Rose, and D. Fabris. Direct infusion analysis of nucleotide mixtures of very similar or identical elemental composition. *Journal of Mass Spectrometry*, 2013. ISSN 10765174. doi: 10.1002/jms.3207.

M. A. Rahman, N. H. Kim, S. H. Kim, S. M. Oh, and S. O. Huh. Antiproliferative and cytotoxic effects of resveratrol in mitochondria-mediated apoptosis in rat B103 neuroblastoma cells. *Korean Journal of Physiology and Pharmacology*, 2012. ISSN 12264512. doi: 10.4196/kjpp.2012.16.5.321.

B. Raïs, B. Comin, J. Puigjaner, J. L. Brandes, E. Creppy, D. Saboureau, R. Ennamany, W. N. Paul Lee, L. G. Boros, and M. Cascante. Oxythiamine and dehydroepiandrosterone induce a G1 phase cycle arrest in Ehrlich's tumor cells through inhibition of the pentose cycle. *FEBS Letters*, 1999. ISSN 00145793. doi: 10.1016/S0014-5793(99)00924-2.

N. Rhind and P. Russell. Checkpoints: It takes more than time to heal some wounds. *Current Biology*, 2000. ISSN 09609822. doi: 10.1016/S0960-9822(00)00849-6.

R. A. Ross, B. A. Spengler, and J. L. Biedler. Coordinate Morphological and Biochemical Interconversion of Human Neuroblastoma Cells. *Journal of the National Cancer Institute*, 1983. ISSN 14602105. doi: 10.1093/jnci/71.4.741.

J. A. Sakoff and S. P. Ackland. Thymidylate synthase inhibition induces S-phase arrest, biphasic mitochondrial alterations and caspase-dependent apoptosis in leukaemia cells. *Cancer Chemotherapy and Pharmacology*, 2000. ISSN 03445704. doi: 10.1007/s002800000164.

M. Salazar-Roa and M. Malumbres. Fueling the Cell Division Cycle. *Trends in Cell Biology*, 2017. ISSN 18793088. doi: 10.1016/j.tcb.2016.08.009.

R. A. Sansone and L. A. Sansone. Getting a knack for nac: N-acetyl-cysteine. *Innovations in Clinical Neuroscience*, 2011. ISSN 21588333.

R. Scatena, P. Bottoni, A. Pontoglio, L. Mastrototaro, and B. Giardina. Glycolytic enzyme inhibitors in cancer treatment. *Expert Opinion on Investigational Drugs*, 2008. ISSN 13543784. doi: 10.1517/13543784.17.10.1533.

P. Schauder, C. McIntosh, J. Arends, R. Arnold, H. Frerichs, and W. Creutzfeldt. Somatostatin and insulin release from isolated rat pancreatic islets in response to D-glucose, L-leucine, α-ketoisocaproic acid or D-glyceraldehyde: Evidence for a regulatory role of adenosine-3,5-cyclic monophosphate. *Biochemical and Biophysical Research Communications*, 1977. ISSN 10902104. doi: 10.1016/0006-291X(77)91519-4.

T. Schmelzle, A. A. Mailleux, M. Overholtzer, J. S. Carroll, N. L. Solimini, E. S. Lightcap, O. P. Veiby, and J. S. Brugge. Functional role and oncogene-regulated expression of the BH3-only factor Bmf in mammary epithelial anoikis and morphogenesis. *Proceedings of the National Academy of Sciences of the United States of America*, 2007. ISSN 00278424. doi: 10.1073/pnas.0700115104.

P. T. Schumacker. Reactive Oxygen Species in Cancer: A Dance with the Devil. *Cancer Cell*, 27(2):156–157, feb 2015. ISSN 18783686. doi: 10.1016/j.ccell.2015.01.007. URL `http://dx.doi.org/10.1016/j.ccell.2015.01.007`.

L. Segerström, N. Baryawno, B. Sveinbjörnsson, M. Wickström, L. Elfman, P. Kogner, and J. I. Johnsen. Effects of small molecule inhibitors of PI3K/Akt/mTOR signaling on neuroblastoma growth in vitro and in vivo. *International Journal of Cancer*, 2011. ISSN 00207136. doi: 10.1002/ijc.26268.

L. A. Sena and N. S. Chandel. Physiological roles of mitochondrial reactive oxygen species. *Molecular Cell*, 2012. ISSN 10974164. doi: 10.1016/j.molcel.2012.09.025.

T. N. Seyfried and L. M. Shelton. Cancer as a metabolic disease, 2010. ISSN 17437075.

T. Shibata, T. Ohta, K. I. Tong, A. Kokubu, R. Odogawa, K. Tsuta, H. Asamura, M. Yamamoto, and S. Hirohashi. Cancer related mutations in NRF2 impair its recognition by Keap1-Cul3 E3 ligase and promote malignancy. *Proceedings of the National Academy of Sciences of the United States of America*, 2008. ISSN 10916490. doi: 10.1073/pnas.0806268105.

B. Sid, C. Glorieux, M. Valenzuela, G. Rommelaere, M. Najimi, N. Dejeans, P. Renard, J. Verrax, and P. B. Calderon. AICAR induces Nrf2 activation by an AMPK-independent mechanism in hepatocarcinoma cells. *Biochemical Pharmacology*, 2014. ISSN 18732968. doi: 10.1016/j.bcp.2014.07.010.

A. Siebert, M. Deptuła, M. Cichorek, A. Ronowska, G. Cholewiński, and J. Rachon. Anticancer Properties of Amino Acid and Peptide Derivatives of Mycophenolic Acid. *Anti-Cancer Agents in Medicinal Chemistry*, 2020. ISSN 18715206. doi: 10.2174/1871520620666200516151456.

D. Singh, A. K. Banerji, B. S. Dwarakanath, R. P. Tripathi, J. P. Gupta, T. L. Mathew, T. Ravindranath, and V. Jain. Optimizing cancer radiotherapy with 2-deoxy-D-glucose: Dose escalation studies in patients with glioblastoma multiforme. *Strahlentherapie und Onkologie*, 2005. ISSN 01797158. doi:

10.1007/s00066-005-1320-z.

A. Sobhakumari, L. Love-Homan, E. V. Fletcher, S. M. Martin, A. D. Parsons, D. R. Spitz, C. M. Knudson, and A. L. Simons. Susceptibility of Human Head and Neck Cancer Cells to Combined Inhibition of Glutathione and Thioredoxin Metabolism. *PLoS ONE*, 2012. ISSN 19326203. doi: 10.1371/journal.pone.0048175.

P. Som, H. L. Atkins, D. Bandoypadhyay, J. S. Fowler, R. R. MacGregor, K. Matsui, Z. H. Oster, D. F. Sacker, C. Y. Shiue, H. Turner, C. N. Wan, A. P. Wolf, and S. V. Zabinski. A fluorinated glucose analog, 2-fluoro-2-deoxy-D-glucose (F-18): Nontoxic tracer for rapid tumor detection. *Journal of Nuclear Medicine*, 1980. ISSN 01615505. doi: 10.1097/00004728-198012000-00045.

C. Sonnenschein and A. M. Soto. The aging of the 2000 and 2011 Hallmarks of Cancer reviews: A critique. *Journal of Biosciences*, 38(3):651–663, sep 2013. ISSN 02505991. doi: 10.1007/s12038-013-9335-6.

C. Sonnenschein and A. M. Soto. An Integrative Approach Toward Biology, Organisms, and Cancer. *Methods in molecular biology (Clifton, N.J.)*, 1702:15–26, 2018. ISSN 1940-6029. doi: 10.1007/978-1-4939-7456-6_2. URL `http://www.ncbi.nlm.nih.gov/pubmed/29119499http://www.pubmedcentral.nih.gov/articlerender.fcgi?artid=PMC6176718`.

P. Sonveaux, F. Végran, T. Schroeder, M. C. Wergin, J. Verrax, Z. N. Rabbani, C. J. De Saedeleer, K. M. Kennedy, C. Diepart, B. F. Jordan, M. J. Kelley, B. Gallez, M. L. Wahl, O. Feron, and M. W. Dewhirst. Targeting lactate-fueled respiration selectively kills hypoxic tumor cells in mice. *Journal of Clinical Investigation*, 2008. ISSN 00219738. doi: 10.1172/JCI36843.

M. B. Sporn and K. T. Liby. NRF2 and cancer: The Good, the bad and the importance of context. *Nature Reviews Cancer*, 2012. ISSN 1474175X. doi: 10.1038/nrc3278.

L. H. Stickland. The inhibition of glucolysis by glyceraldehyde. *Biochemical Journal*, 35(8-9):859–871, sep 1941. ISSN 0306-3283. doi: 10.1042/bj0350859. URL `https://www.ncbi.nlm.nih.gov/pmc/articles/PMC1265578/`.

Z. E. Stine, Z. E. Walton, B. J. Altman, A. L. Hsieh, and C. V. Dang. MYC, metabolism, and cancer. *Cancer Discovery*, 2015. ISSN 21598290. doi: 10.1158/2159-8290.CD-15-0507.

Q. Sun, X. Chen, J. Ma, H. Peng, F. Wang, X. Zha, Y. Wang, Y. Jing, H. Yang, R. Chen, L. Chang, Y. Zhang, J. Goto, H. Onda, T. Chen, M. R. Wang, Y. Lu, H. You, D. Kwiatkowski, and H. Zhang. Mammalian target of rapamycin up-regulation of pyruvate kinase isoenzyme type M2 is critical for aerobic glycolysis and tumor growth. *Proceedings of the National Academy of Sciences of the United States of America*, 2011. ISSN 00278424. doi: 10.1073/pnas.1014769108.

H. Takahashi, P. Oanh, T. Tran, E. Leroy, J. S. Harmon, Y. Tanaka, and R. P. Robertson. D-Glyceraldehyde Causes Production of Intracellular Peroxide in Pancreatic Islets, Oxidative Stress, and Defective Beta Cell Function via Non-mitochondrial Pathways* Downloaded from. *THE JOURNAL OF BIOLOGICAL CHEMISTRY*, 279(36):2020, 2004. doi: 10.1074/jbc.M403070200. URL `http://www.jbc.org/`.

S. Taniguchi, M. Okinaka, K. Tanigawa, and I. Miwa. Difference in mechanism between glyceraldehyde- and glucose-induced insulin secretion from isolated rat pancreatic islets. *Journal of Biochemistry*, 2000. ISSN 0021924X. doi: 10.1093/oxfordjournals.jbchem.a022606.

I. F. Tannock, I. F. Tannock, P. Guttman, A. M. Rauth, I. F. Tannock, and A. M. Rauth. Failure of 2-Deoxy-D-glucose and 5-Thio-D-glucose to Kill Hypoxic Cells of two Murine Tumors. *Cancer Research*, 1983.

ISSN 15387445.

D. A. Tennant, R. V. Durán, H. Boulahbel, and E. Gottlieb. Metabolic transformation in cancer. *Carcinogenesis*, 2009. ISSN 01433334. doi: 10.1093/carcin/bgp070.

J. Thompson Coon. Goodman and Gilman's the Pharmacological Basis of Therapeutics. *Focus on Alternative and Complementary Therapies*, 2010. ISSN 1551-4056. doi: 10.1111/j.2042-7166.2002.tb05480.x.

D. M. Townsend, L. He, S. Hutchens, T. E. Garrett, C. J. Pazoles, and K. D. Tew. NOV-002, a glutathione disulfide mimetic, as a modulator of cellular redox balance. *Cancer Research*, 2008. ISSN 00085472. doi: 10.1158/0008-5472.CAN-07-5957.

L. Tretter and V. Adam-Vizi. Generation of reactive oxygen species in the reaction catalyzed by α-ketoglutarate dehydrogenase. *Journal of Neuroscience*, 2004. ISSN 02706474. doi: 10.1523/JNEUROSCI.1842-04.2004.

L. Tretter and V. Adam-Vizi. Alpha-ketoglutarate dehydrogenase: A target and generator of oxidative stress. *Philosophical Transactions of the Royal Society B: Biological Sciences*, 2005. ISSN 09628436. doi: 10.1098/rstb.2005.1764.

C. W. Tseng, W. H. Kuo, S. H. Chan, H. L. Chan, K. J. Chang, and L. H. Wang. Transketolase Regulates the Metabolic Switch to Control Breast Cancer Cell Metastasis via the a-Ketoglutarate Signaling Pathway. *Cancer Research*, 2018. ISSN 15387445. doi: 10.1158/0008-5472.CAN-17-2906.

J. J. Tumilowicz, W. W. Nichols, J. J. Cholon, and A. E. Greene. Definition of a continuous human cell line derived from neuroblastoma. *Cancer Research*, 1970. ISSN 00085472.

S. Tyanova, T. Temu, P. Sinitcyn, A. Carlson, M. Y. Hein, T. Geiger, M. Mann, and J. Cox. The Perseus computational platform for comprehensive analysis of (prote)omics data. *Nature Methods*, 2016. ISSN 15487105. doi: 10.1038/nmeth.3901.

M. Uetaki, S. Tabata, F. Nakasuka, T. Soga, and M. Tomita. Metabolomic alterations in human cancer cells by Vitamin C-induced oxidative stress. *Scientific Reports*, 2015. ISSN 20452322. doi: 10.1038/srep13896.

A. Vazquez, E. K. Markert, and Z. N. Oltvai. Serine biosynthesis with one carbon catabolism and the glycine cleavage system represents a novel pathway for ATP generation. *PLoS ONE*, 2011. ISSN 19326203. doi: 10.1371/journal.pone.0025881.

M. Vučetić, Y. Cormerais, S. K. Parks, and J. Pouysségur. The central role of amino acids in cancer redox homeostasis: Vulnerability points of the cancer redox code. *Frontiers in Oncology*, 2017. ISSN 2234943X. doi: 10.3389/fonc.2017.00319.

J. Wang, X. Zhang, D. Ma, W.-N. P. Lee, J. Xiao, Y. Zhao, V. L. Go, Q. Wang, Y. Yen, R. Recker, and G. G. Xiao. Inhibition of transketolase by oxythiamine altered dynamics of protein signals in pancreatic cancer cells. *Experimental Hematology & Oncology*, 2013. ISSN 2162-3619. doi: 10.1186/2162-3619-2-18.

Q. Wang, B. Liang, N. A. Shirwany, and M. H. Zou. 2-deoxy-D-glucose treatment of endothelial cells induces autophagy by reactive oxygen species-mediated activation of the AMP-activated protein kinase. *PLoS ONE*, 2011. ISSN 19326203. doi: 10.1371/journal.pone.0017234.

T. Wang, L. Liu, X. Chen, Y. Shen, G. Lian, N. Shah, A. M. Davidoff, J. Yang, and R. Wang. MYCN drives glutaminolysis in neuroblastoma and confers sensitivity to an ROS augmenting agent article. *Cell*

Death and Disease, 2018. ISSN 20414889. doi: 10.1038/s41419-018-0295-5.

O. Warburg. Über die Entstehung der Krebszellen. *Die Naturwissenschaften*, 42(14):401–406, 1955.

O. Warburg, K. Posener, and E. Negelein. The metabolism of cancer cells. *Biochem Z*, 1924.

O. Warburg, F. Wind, and N. Negelein. The metabolism of tumors in the body. *J Gen Physiol.*, 8(6): 519–530, 1926. URL `https://www.ncbi.nlm.nih.gov/pmc/articles/PMC2140820/pdf/519.pdf`.

O. Warburg, K. Gawehn, A. W. Geissler, and S. Lorenz. Über Heilung von Mäuse-Ascites-Krebs durch D-und L-Glycerinaldehyd. *Z. Klin. Chem*, 1963.

P. S. Ward and C. B. Thompson. Metabolic Reprogramming: A Cancer Hallmark Even Warburg Did Not Anticipate. *Cancer Cell*, 2012. ISSN 15356108. doi: 10.1016/j.ccr.2012.02.014.

R. Weindruch, K. P. Keenan, J. M. Carney, G. Fernandes, R. J. Feuers, R. A. Floyd, J. B. Halter, J. J. Ramsey, A. Richardson, G. S. Roth, and S. R. Spindler. Caloric restriction mimetics: metabolic interventions. *The journals of gerontology. Series A, Biological sciences and medical sciences*, 2001. ISSN 10795006. doi: 10.1093/gerona/56.suppl_1.20.

S. Weinhouse. Studies on the Fate of Isotopically Labeled Metabolites in the Oxidative Metabolism of Tumors. *Cancer Research*, 11(8):585–591, 1951. ISSN 0008-5472. URL `https://cancerres.aacrjournals.org/content/11/8/585`.

S. Weinhouse. The Warburg Hypothesis Fifty Years Later. *Z. Krebsforsch*, 87:115–126, 1976.

S. Weinhouse, O. Warburg, and D. Burk. On respiratory impairment in cancer cells. *Science*, 1956. URL `https://www.jstor.org/stable/1751794`.

S. B. Whittle, V. Smith, E. Doherty, S. Zhao, S. McCarty, and P. E. Zage. Overview and recent advances in the treatment of neuroblastoma, 2017. ISSN 17448328.

R. H. Xu, H. Pelicano, Y. Zhou, J. S. Carew, L. Feng, K. N. Bhalla, M. J. Keating, and P. Huang. Inhibition of glycolysis in cancer cells: A novel strategy to overcome drug resistance associated with mitochondrial respiratory defect and hypoxia. *Cancer Research*, 2005. ISSN 00085472.

H. Yang, R. M. Villani, H. Wang, M. J. Simpson, M. S. Roberts, M. Tang, and X. Liang. The role of cellular reactive oxygen species in cancer chemotherapy. *Journal of Experimental and Clinical Cancer Research*, 2018. ISSN 17569966. doi: 10.1186/s13046-018-0909-x.

H.-Y. Yang, Y.-Y. Wen, C.-H. Chen, G. Lozano, and M.-H. Lee. 14-3-3σ Positively Regulates p53 and Suppresses Tumor Growth. *Molecular and Cellular Biology*, 2003. ISSN 0270-7306. doi: 10.1128/mcb.23.20.7096-7107.2003.

J. R. Yates. The revolution and evolution of shotgun proteomics for large-scale proteome analysis. *Journal of the American Chemical Society*, 2013. ISSN 00027863. doi: 10.1021/ja3094313.

C. Zasada and S. Kempa. Quantitative analysis of cancer metabolism: From pSIRM to MFA. In *Metabolism in Cancer*, pages 207–220. Springer, 2016.

D. W. Zhang, J. Shao, J. Lin, N. Zhang, B. J. Lu, S. C. Lin, M. Q. Dong, and J. Han. RIP3, an energy metabolism regulator that switches TNF-induced cell death from apoptosis to necrosis. *Science*, 2009. ISSN 00368075. doi: 10.1126/science.1172308.

S. Zhang, L. Yan, C. Cui, Z. Wang, J. Wu, M. Zhao, B. Dong, X. Guan, X. Tian, and C. Hao. Identification of TYMS as a promoting factor of retroperitoneal liposarcoma progression: Bioinformatics analysis and biological evidence. *Oncology Reports*, 2020. ISSN 17912431. doi: 10.3892/or.2020.7635.

X. L. Zu and M. Guppy. Cancer metabolism: Facts, fantasy, and fiction. *Biochemical and Biophysical Research Communications*, 313(3):459–465, jan 2004. ISSN 0006291X. doi: 10.1016/j.bbrc.2003.11.136.

Publications

B. Arlt, C. Zasada, K. Baum, J. Wuenschel, G. Mastrobuoni, M. Lodrini, K. Astrahantseff, A. Winkler, J.H. Schulte, S. Finkler, **M. Forbes**, P. Hundsdoerfer, D. Guergen, J. Hoffmann, J. Wolf, A. Eggert, S. Kempa, H.E. Deubzer (2021). Inhibiting phosphoglycerate dehydrogenase counteracts chemotherapeutic efficacy against MYCN-amplified neuroblastoma.
International Journal of Cancer. https://doi.org/10.1002/ijc.33423

S. Bayram, S. Fürst, **M. Forbes**, S. Kempa (2020). Analysing central metabolism in ultra-high resolution: At the crossroads of carbon and nitrogen.
Molecular Metabolism. https://doi.org/10.1016/j.molmet.2019.12.002

M. Alikian, P. Ellery. **M. Forbes**, G. Gerrard, D. Kasperaviciute, A. Sosinsky, A.G. Reid (2016). Next-Generation Sequencing-Assisted DNA-Based Digital PCR for a Personalized Approach to the Detection and Quantification of Residual Disease in Chronic Myeloid Leukemia Patients.
Journal of Molecular Diagnostics. https://doi.org/10.1016/j.jmoldx.2015.09.005

Chapter 5

Supplementary Data

5.1 Materials

Table 5.1: Cell culture reagents and supplements

Name	Supplier
2-Deoxyglucose	Sigma-Aldrich, D - Darmstadt
3-Bromopyruvate	Sigma-Aldrich, D - Darmstadt
Dimethyl sulfoxide	Sigma-Aldrich, D - Darmstadt
D-Glyceraldehyde	Sigma-Aldrich, D - Darmstadt
D,L-Glyceraldehyde	Sigma-Aldrich, D - Darmstadt
DMEM, no glucose, glutamine, phenol red	Gibco, USA - Waltham
Fetal bovine serum	Gibco, USA - Waltham
Glucose	Sigma-Aldrich, D - Darmstadt
L-Glutamine	Gibco, USA - Waltham
L-Glyceraldehyde	Sigma-Aldrich, D - Darmstadt
N-acetyl-L-cysteine	Sigma-Aldrich, D - Darmstadt
Phosphate-buffered saline	Gibco, USA - Waltham
Trypan Blue Solution (0.4%)	Gibco, USA - Waltham
TrypLE Express	Gibco, USA - Waltham
U-^{13}C-Glucose	Campro-Scientific, D - Berlin
U-^{13}C-Glutamine	Campro-Scientific, D - Berlin

Table 5.2: Chemicals

Compound	Supplier
Acetic acid	Fluka, D - Darmstadt
Acetonitrile	VWR, USA - Radnor
Acrylamide	Carl Roth, D - Karlsruhe
Ammonium bicarbonate	Fluka, D - Darmstadt
Ammonium persulfate	Sigma-Aldrich, D - Darmstadt
Bromphenol blue	AppliChem GmbH, D - Darmstadt
BSA	SERVA, D - Heidelberg
$CaCl_2$ (1 M), nuclease-free	Sigma-Aldrich, D - Darmstadt
Chloroform	Sigma-Aldrich, D - Darmstadt
Chloroform-isoamyl alcohol (24:1)	Carl Roth, D - Karlsruhe
Cinnamic acid	Sigma-Aldrich, D - Darmstadt
DAPI	Sigma-Aldrich, D - Darmstadt
DNA loading dye (6x)	Thermo Fisher, USA - Waltham

Continued on next page

Table 5.2: Continued from previous page

Compound	Supplier
DTT	Sigma-Aldrich, D - Darmstadt
EDTA	Carl Roth, D - Karlsruhe
Ethanol (EtOH)	LiChrosolv, D - Darmstadt
Formaldehyde (16%)	Polysciences, USA - Warrington
Formamide	AppliChem GmbH, D - Darmstadt
Formic acid	Fluka, D - Darmstadt
Glucose	Sigma-Aldrich, D - Darmstadt
Glycerol	Carl Roth, D - Karlsruhe
Glycine	Carl Roth, D - Karlsruhe
HEPES	Sigma-Aldrich, D - Darmstadt
Hexylamine	Sigma-Aldrich, D - Darmstadt
IAA	Sigma-Aldrich, D - Darmstadt
Isopropanol	Carl Roth, D - Karlsruhe
$MgCl_2$	Sigma-Aldrich, D - Darmstadt
MeOH	Merck, D - Darmstadt
MeOx	Sigma-Aldrich, D - Darmstadt
Skim milk powder	Sigma-Aldrich, D - Darmstadt
MSTFA	VWR, USA - Radnor
NaCl	Sigma-Aldrich, D - Darmstadt
Na-deoxycholate	Sigma-Aldrich, D - Darmstadt
NaOAc	Thermo Fisher, USA - Waltham
NH_4Ac	Carl Roth, D - Karlsruhe
NH_4OH	Sigma-Aldrich, D - Darmstadt
NP-40	Sigma-Aldrich, D - Darmstadt
Page ruler prestained protein ladder	Bio-Rad, D - München
PBS (10x)	Biochrom, D - Darmstadt
Phophatase inhibitor cocktail	Sigma-Aldrich, D - Darmstadt
PMSF	Sigma-Aldrich, D - Darmstadt
Protease Inhibitor Cocktail, EDTA-free	Roche, D - Darmstadt
Pyridine	Sigma-Aldrich, D - Darmstadt
Sodium acetate (3 M), pH 5.5, nuclease free	Invitrogen, USA - Waltham
SDS (20%)	Carl Roth, D - Karlsruhe
TEMED	Carl Roth, D - Karlsruhe
Triflouracetic acid	Merck, D - Darmstadt
TrisBase	Carl Roth, D - Karlsruhe
TrisHCl	Carl Roth, D - Karlsruhe
Triton x-100	Carl Roth, D - Karlsruhe
Trypsin Beads	Aplied Biosystems, USA - Waltham
Tween-20	Carl Roth, D - Karlsruhe
Urea	Carl Roth, D - Karlsruhe

Table 5.3: SDS-PAGE gel preparation

Component	4%	8%	10%	12%
H_2O	6.1 mL	4.6 mL	4.0 mL	3.3 mL
Acrylamide 30%	1.33 mL	2.7 mL	3.3 mL	4.0 mL
0.5 M Tris (pH 6.8)	2.5 mL	-	-	-
1.5 M Tris (pH 8.8)	-	2.5 mL	2.5 mL	2.5 mL
SDS 10%	100 µL	50 µL	50 µL	50 µL
Ammonium persulfate 10%	50 µL	50 µL	50 µL	50 µL
TEMED	10 µL	6 µL	4 µL	4 µL

Table 5.4: Commercial kits

Kit	Supplier
DCFDA / H2DCFDA - Cellular ROS Assay Kit	abcam, UK-Cambridge
ECL Prime Western Blotting Detection Reagent	GE Healthcare, UK - Little Chalfont
MycoAlert Mycoplasma Detection Kit	Lonza, CH - Basel
Pierce BCA Protein Assay Kit	Thermo Fisher, USA - Waltham

Table 5.5: Antibodies

Antibody	Cat.-No	Manufacturer
Anti-AMPK	2793	Cell Signaling
Anti-AMPK-phospho(Thr172)	2531	Cell Signaling
Anti-Caspase III	ab13847	abcam, UK-Cambridge
Anti-GAPDH	ab9485	abcam, UK-Cambridge
Anti-Heme Oxygenase 1	ab137749	abcam, UK-Cambridge
Anti-Keap1	ab196346	abcam, UK-Cambridge
Anti-Nrf2	ab137550	abcam, UK-Cambridge
Anti-NQO1 antibody	ab34173	abcam, UK-Cambridge
Mouse, horseradish peroxidase-linked	7075	Cell Signaling
Goat, horseradish peroxidase-linked	7074	Cell Signaling
Rabbit, horseradish peroxidase-linked	7076	NEB, DE, Frankfurt am Main
Vinculin	V9131	Sigma-Aldrich, D - Darmstadt

Table 5.6: Consumables

Name	Supplier
Cell lifter	Sigma-Aldrich, D - Darmstadt
Counting slides	Biorad, D - München
Gas liner, CI34	Gerstel, D - Mühlheim an der Ruhr
Glass vials	Th.Geyer, D - Berlin
Nytran N Blotting Membrane	GE Healthcare, UK - Little Chalfont
PVDF membrane	GE Healthcare, UK - Little Chalfont
Whatman Blotting paper	Biorad, D - München

Table 5.7: Equipment

Name	Manufacturer
Autosampler - MPS2XL-Twister	Gerstel, DE - Mühlheim an der Ruhr
Autosampler, ESI ion source - TriVersa NanoMate	Advion, DE - Ithaca
Blotting device - TransBlot Turbo	Biorad, DE - München
Cell counter - TC20	Biorad, DE - München
Centrifuge - 5417R	Eppendorf, DE - Hamburg
Centrifuge - 5430	Eppendorf, DE - Hamburg
Electrophoresis system - ReadySub-Cell	Biorad, DE - München
Electrophoresis system - Protean Tetra cell	Biorad, DE - München
Gas chromatograph - Agilent 78903	LECO, USA - St. Joseph

Continued on next page

Table 5.7: Continued from previous page

Name	Manufacturer
Imager - Vilber fusion	GE Healthcare, UK - Little Chalfont
Mass Spectrometer - Q Exactive Plus	Thermo Fisher, USA - Waltham
Mass Spectrometer - TSQ Quantiva	Thermo Fisher, USA - Waltham
Mass Spectrometer-TOF - Pegasus IV	LECO, USA - St. Joseph
Microplate reader-Infinite M200	Tecan, CH - Männedorf
Microplate reader- Spectramax iD microplate reader	Molecular Devices, USA, California
Microscope- Keyence Bz-x700	Keyence
Japan, Osaka	
Microscope-Eclipse TS2 microscope	Nikon, DE- Düsseldorf
Nano Liquid Chromatograph 400	Eksigent, DE - Darmstadt
pH meter - VMS C7	VWR, USA - Radnor
Power supply - PowerPac Universal	Biorad, DE - München
Vacuum concentrator - 2-33 CD plus	Christ, DE - Osterode
Sonicator - Sonorex Digitech DT 100	Bandelin, DE - Berlin
Tube roller - SRT6D	Stuart, UK - Staffordshire

Table 5.8: Software

Name
ChromaToF (Version 4.51.6.0)
FlowJo (Version.10)
Fuji
Adobe Illustrator (Version 5.6)
ImageJ
MAUI-SILVIA (Version 1.0.5)
MaxQuant (Version 1.5.3.30)
MetMax
Perseus (Version 1.5.6.0)
RStudio Desktop (Version 1.1.383

5.1.1 Nucleotides

Table 5.9: Direct infusion MS transition parameters

Compound	Precursor [m/z]	Product [m/z]	Collision Energy [V]	RF lens [V]
ADP	426.02	134.06	24	92
ADP	426.02	158.92	27	92
AICAR	337.00	79.00	29	93
AICAR	337.00	97.00	20	93
AMP	346.06	107.08	47	80
AMP	346.06	134.06	31	80
ATP	505.99	158.96	29	92
ATP	505.99	408.04	20	92
cAMP	328.02	107.08	44	78
cAMP	328.02	134.07	25	78
CDP	402.01	159.03	25	94
CDP	402.01	272.94	23	94

Continued on next page

Table 5.9: Continued from previous page

Compound	Precursor [m/z]	Product [m/z]	Collision Energy [V]	RF lens [V]
CMP	322.04	79.03	26	72
CMP	322.04	97.01	22	72
CTP	481.98	159.05	29	85
CTP	481.98	383.93	20	85
dADP	410.09	158.94	25	94
dADP	410.09	256.96	24	94
dAMP	330.09	134.12	27	68
dAMP	330.09	194.94	27	68
dATP	490.05	158.94	26	136
dATP	490.05	256.96	29	136
dCDP	86.05	158.96	23	78
dCDP	86.05	177.01	22	78
dCMP	306.08	97.00	23	80
dCMP	306.08	110.11	23	80
dCTP	66.01	158.94	26	111
dCTP	466.01	256.80	28	111
dGDP	426.05	158.96	24	99
dGDP	426.05	176.94	24	99
dGMP	346.09	79.00	22	73
dGMP	346.09	150.07	25	73
dGTP	506.11	159.03	28	120
dGTP	506.11	238.97	26	120
dTDP	401.05	158.94	24	82
dTDP	401.05	256.96	23	82
dTMP	321.11	125.05	22	69
dTMP	321.11	194.95	16	69
dTTP	480.98	158.94	30	90
dTTP	480.98	256.84	15	90
GDP	442.00	158.93	26	105
GDP	442.00	343.96	16	105
GMP	362.05	133.05	40	83
GMP	362.05	150.06	29	83
GTP	522.03	240.96	29	163
GTP	522.03	320.90	26	163
IMP	347.00	97.07	22	80
IMP	347.00	135.05	27	80
NAD+	622.09	272.91	34	68
NAD+	622.09	539.94	15	68
NADH	664.07	396.94	31	231
NADH	664.07	407.94	31	231
NADP+	742.05	272.92	40	80
NADP+	742.05	619.88	16	80
NADPH	744.06	272.92	33	97
NADPH	744.06	407.94	16	97
PRPP	389.00	621.66	16	75
PRPP	389.00	177.00	18	75
SAICAR	453.00	294.00	21	124
SAICAR	453.00	355.00	17	124
UDP	402.99	158.91	22	95

Continued on next page

Table 5.9: Continued from previous page

Compound	Precursor [m/z]	Product [m/z]	Collision Energy [V]	RF lens [V]
UDP	402.99	272.89	22	95
UMP	323.03	79.04	28	70
UMP	323.03	97.02	23	70
UTP	482.98	158.93	28	118
UTP	482.98	403.01	24	118

5.1.2 Metabolomics

Table 5.10: GC-MS masses used for quantification. Peak areas under the indicated masses, were summed and normalised to Cinnamic acid and cell counts.

Metabolite	Derivate	RI	Quantification masses [m/z]
Alanine	(2TMS)	1106	110;133;114;100;188;190
Aspartic acid	(2TMS)	1442	160
Cinnamic acid, trans-	(1TMS)	1555	205
Citric acid	(4TMS)	1848	149.0;273.0;183.0;133.0;211.0;275.0;277.0;278.0
Cysteine	(3TMS)	1574	116;100;132;218;220
Dihydroxyacetone-phosphate	(1MEOX)(3TMS)	1773	133;103;142;89;315;400;403
Fructose-1,6-diphosphate	(1MEOX)(7TMS)	2795	217;299;387;315;129;220
Fructose-6-phosphate	(1MEOX)(6TMS)	2385	129;217;299;315;103;220
Fumaric acid	(2TMS)	1369	143;246;133;115;245;247;249
Gluconic acid	(6TMS)	2060	292
Gluconic acid-6-phosphate	(7TMS)	2512	129;299;133;387;101;220
Glucose-6-phosphate	(1MEOX)(6TMS)	2420	160;299;129;387;133;220;162;132
Glutamic acid	(3TMS)	1640	246
Glutaric acid, 2-hydroxy-	(3TMS)	1596	129
Glutaric acid, 2-oxo-	(1MEOX)(2TMS)	1596	156;112;170;89;198;200;203
Glyceric acid	(3TMS)	1362	189
Glyceric acid-3-phosphate	(4TMS)	1840	211;227;299;101;133;357;359
Glycerol	(3TMS)	1303	205
Glycerol-3-phosphate	(4TMS)	1794	101;299;133;357;103;359
Glycine	(2TMS)	1124	86.0;133.0;175.0;100.0;174.0
Glycine	(3TMS)	1330	86.0;133.0;175.0;100.0;174.0
Isoleucine	(1TMS)	1179	86
Lactic acid	(2TMS)	1065	118.0; 190.0; 191.0; 117.0; 133.0;119.0; 193.0; 219.0; 222.0
Leucine	(1TMS)	1158	86
Lysine	(3TMS)	1867	174
Malic acid	(3TMS)	1507	101;133;117;149;233;245;247;249
Methionine	(2TMS)	1532	176
Phenylalanine	(2TMS)	1642	192
Proline	(2TMS)	1318	142
Putrescine	(4TMS)	1754	174
Pyroglutamic acid	(2TMS)	1534	157
Pyruvic acid	(1MEOX)(1TMS)	1053	100.0 ;99.0 ;89.0; 174.0; 115.0 ;177.0
Ribose-5-phosphate	(1MEOX)(5TMS)	2161	299.0;315.0;217.0;133.0;129.0;220.0
Serine	(3TMS)	1391	116;218;133;204;100;206
Succinic acid	(2TMS)	1336	149;247;129;133;172;249;251
Threonine	(3TMS)	1417	218
Uracil	(2TMS)	1363	241

Urea	(2TMS)	1253	171
Uridine	(3TMS)	2506	217
Valine	(2TMS)	1230	144

Table 5.11: GC-MS fragment ranges used for determination of stable isotope incorporation

Metabolite	Derivate	Fragment Min	Fragment Max
Alanine	(2TMS)	116	120
Aspartic acid	(2TMS)	245	251
Citric acid	(4TMS)	273	279
Fructose-1,6-diphosphate	(1MEOX)(7TMS)	217	222
Fructose-6-phosphate	(1MEOX) (6TMS)	217	222
Fumaric acid	(2TMS)	245	251
Gluconic acid-6-phosphate	(7TMS)	217	220
Glucose-6-phosphate	(1MEOX) (6TMS)	217	220
Glutamic acid	(3TMS)	246	250
Glutamine, DL-	(3TMS)	156	163
Glutaric acid, 2-hydroxy-	(3TMS)	247	252
Glutaric acid, 2-oxo-	(1MEOX) (2TMS)	198	205
Glutaric acid, 2-oxo-	(1MEOX)(2TMS)	288	295
Glyceric acid	(3TMS)	357	361
Glyceric acid-3-phosphate	(4TMS)	357	361
Glycerol	(3TMS)	218	222
Glycerol-3-phosphate	(4TMS)	357	361
Glycine	(3TMS)	276	279
Lactic acid	(2TMS)	219	224
Malic acid	(3TMS)	245	251
Pyruvic acid	(1MEOX)(1TMS)	174	179
Serine	(3TMS)	204	208
Serine	(2TMS)	116	120
Succinic acid	(2TMS)	247	252

5.2 Additional results

5.2.1 Cell biology and Western blotting

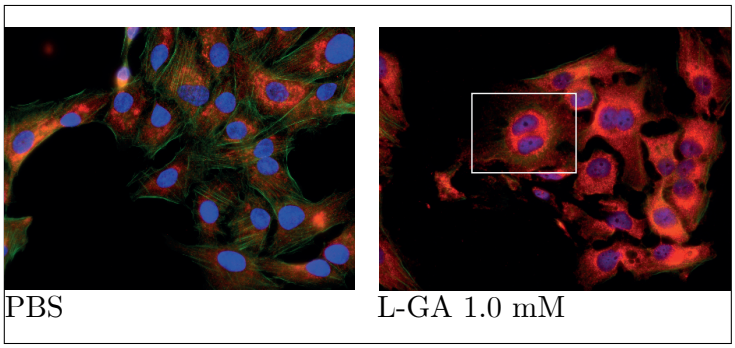

Figure 5.1:
L-GA causes multi nucleation of neuroblastoma cells. Cell nuclei were stained with DAPI (blue) and anti-aldolase (red) to count cells with multiple nuclei following L-GA treatment, exemplary images of nuclei counting is shown with multinucleation displayed in the white window. Images acquired using Keyence Bz-x700 microscope.

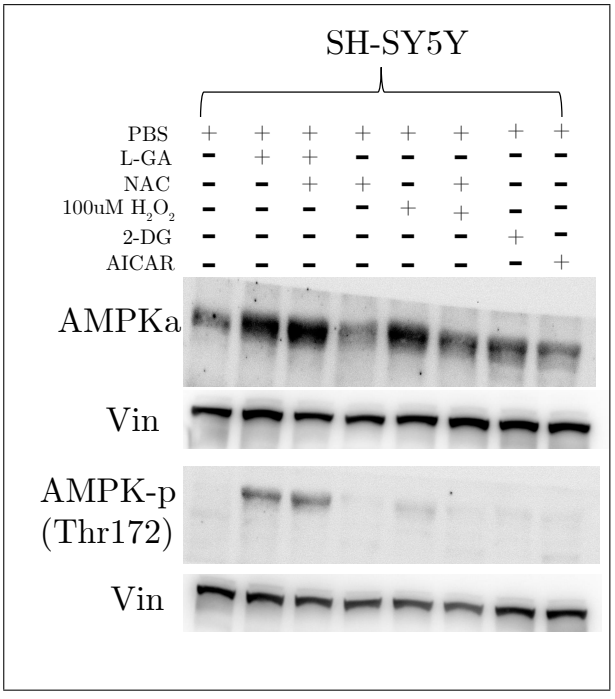

Figure 5.2: AMPK phosphorylation in L-GA, H_2O_2, 2-DG, AICAR and NAC treated SH-SY5Y cells. SH-SH5Y cells were treated for 16 hrs with PBS, 1 mM L-GA, 1 mM L-GA + 5 mM NAC, 5 mM NAC, 100 µM H_2O_2, 100 µM H_2O_2 +NAC, 100 µM H_2O_2 + 1 mM LGA, 2 mM 2-DG and 100 µM AICAR. Cell lysates were collected and subjected to SDS-PAGE probing for:using AMPK-α and AMPK-phospho(Thr172) with Vinculin loading controls.

5.2.2 Metabolomics

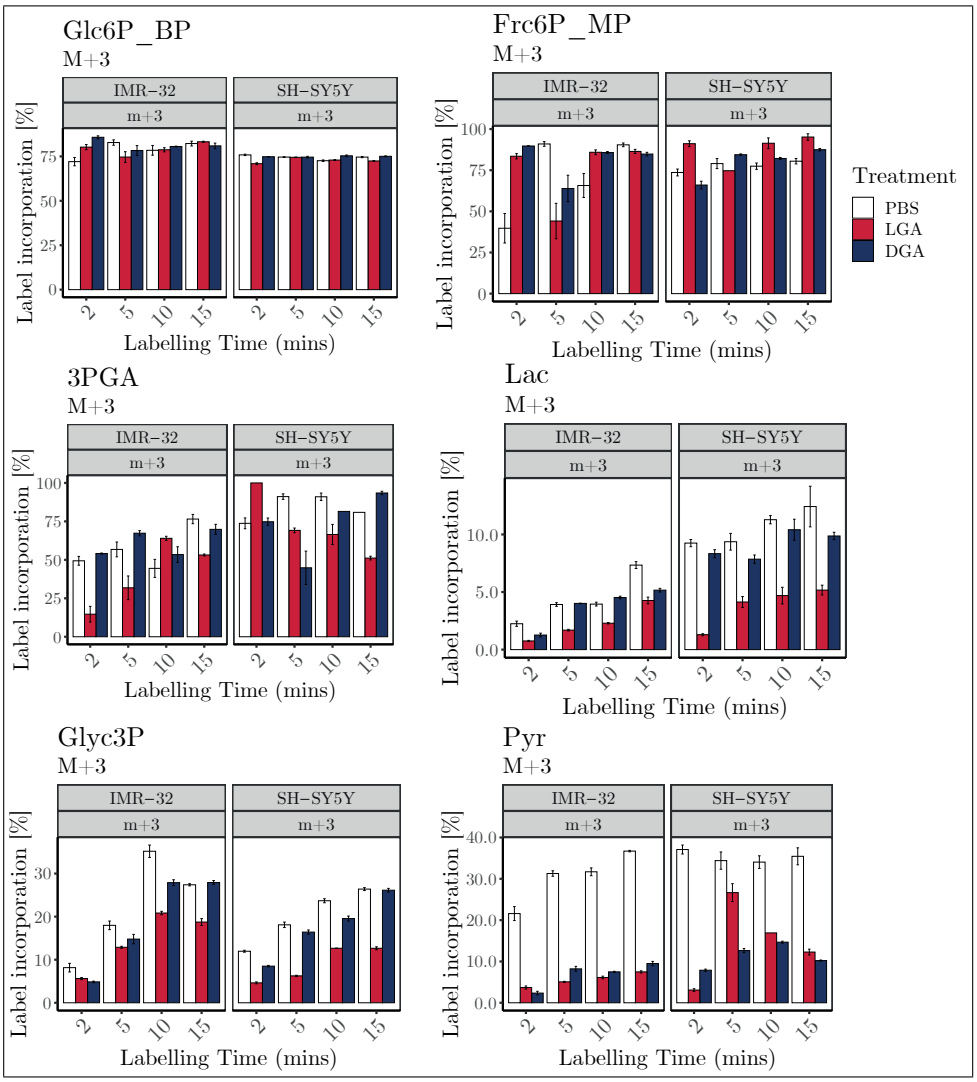

Figure 5.3:
pSIRM analysis of L-GA and D-GA treated cells. Incorporation of ^{13}C-label derived from U-^{13}C-glucose during pSIRM experiment into metabolites of interest. Polar metabolites were extracted from IMR-32 and SH-SY5Y cell lines following treatment of 1 mM L-GA and D-GA for 1 hr. Samples were processed via GC-MS and analysed to attain the percentage incorporation of ^{13}C-label at each labelling time point for the metabolites shown.

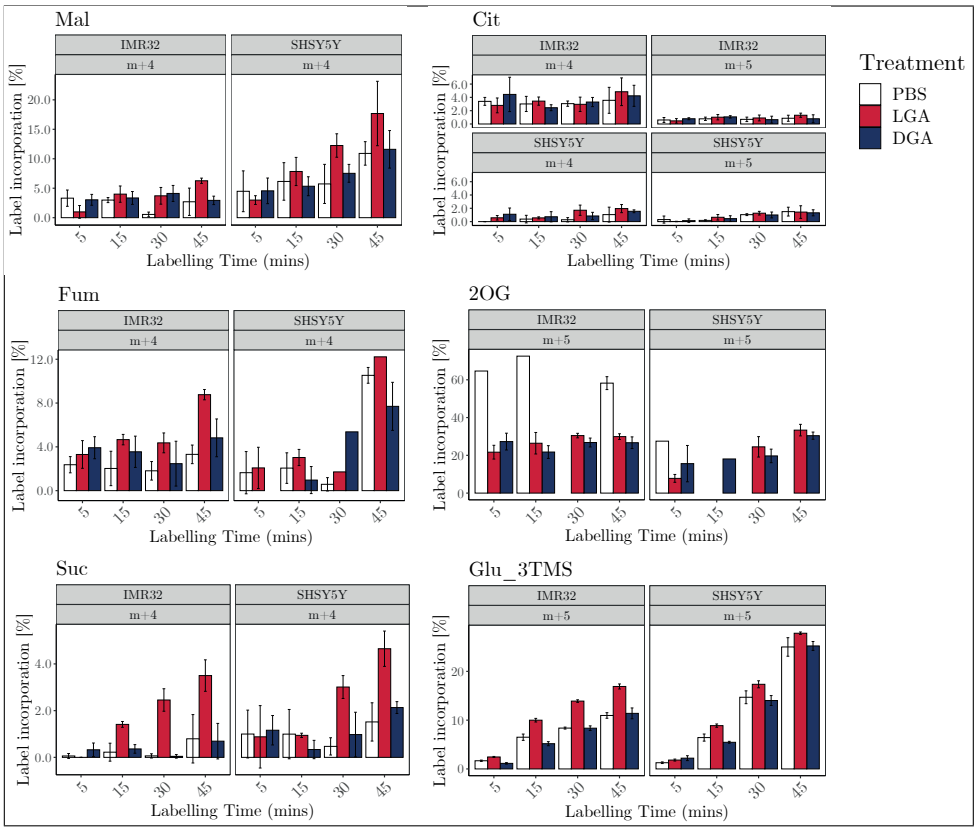

Figure 5.4: pSIRM analysis of L-GA and D-GA treated cells. Incorporation of ^{13}C-label derived from U-^{13}C-glutamine during pSIRM experiment into metabolites of interest. Polar metabolites were extracted from IMR-32 and SH-SY5Y cell lines following treatment of L-GA and D-GA for 1 hr. Samples were processed via GC-MS and analysed to attain the percentage incorporation of ^{13}C-label at each labelling time point for the metabolites shown.

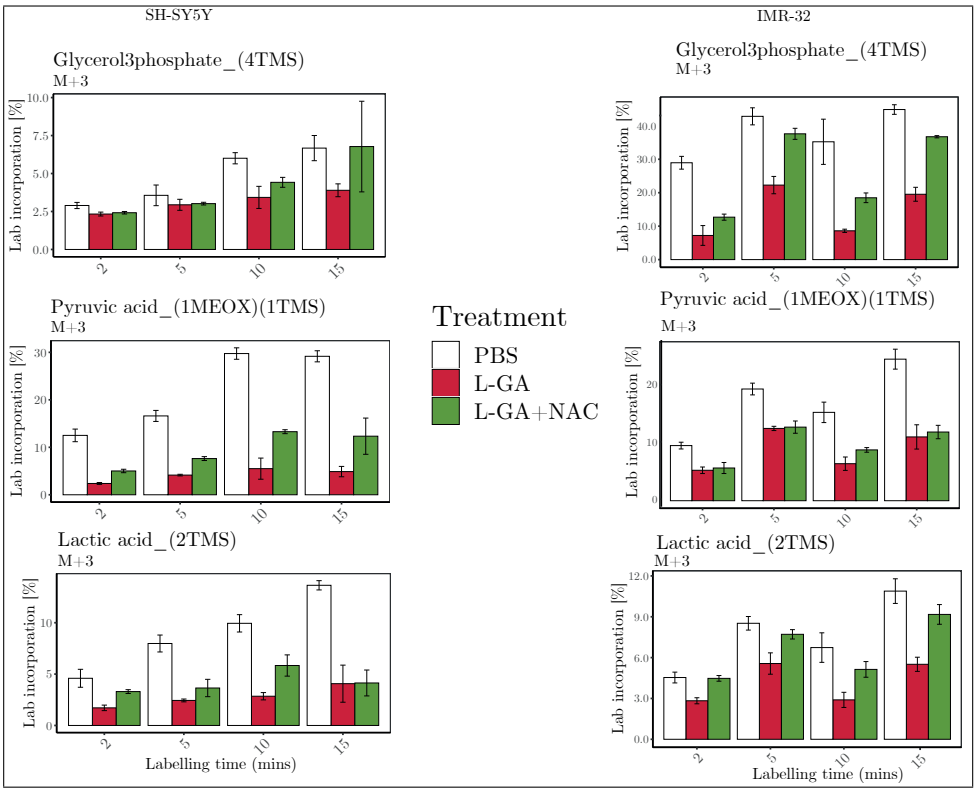

Figure 5.5: pSIRM analysis of L-GA and NAC treated cells. Incorporation of ^{13}C-label derived from U-^{13}C-glucose during pSIRM experiment into metabolites of interest. Polar metabolites were extracted from IMR-32 cell and SH-SY5Y cell lines following treatment of 1 mM L-GA and L-GA+NAC (5 mM) for 16 hrs. Samples were processed via GC-MS and analysed to attain the percentage incorporation of ^{13}C-label at each labelling time point for the metabolites shown.

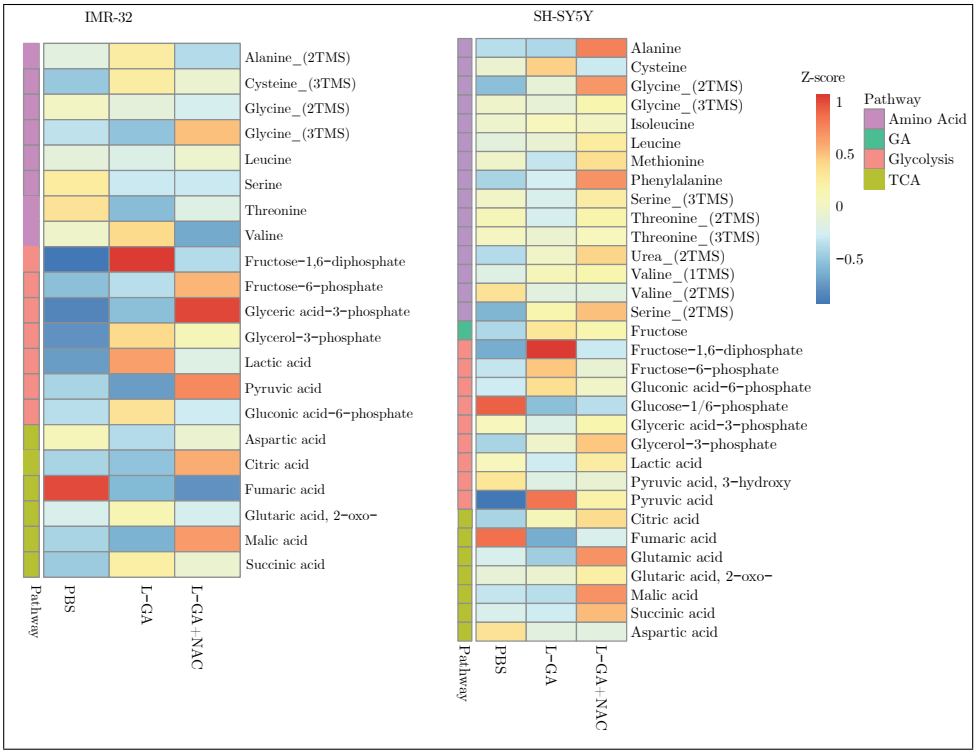

Figure 5.6: Clustering of metabolomics data for L-GA and NAC treated cells. Z scores of metabolite quantities for IMR-32 and SH-SY5Y and hierarchical clustering of annotated metabolites show clustering of pathways.

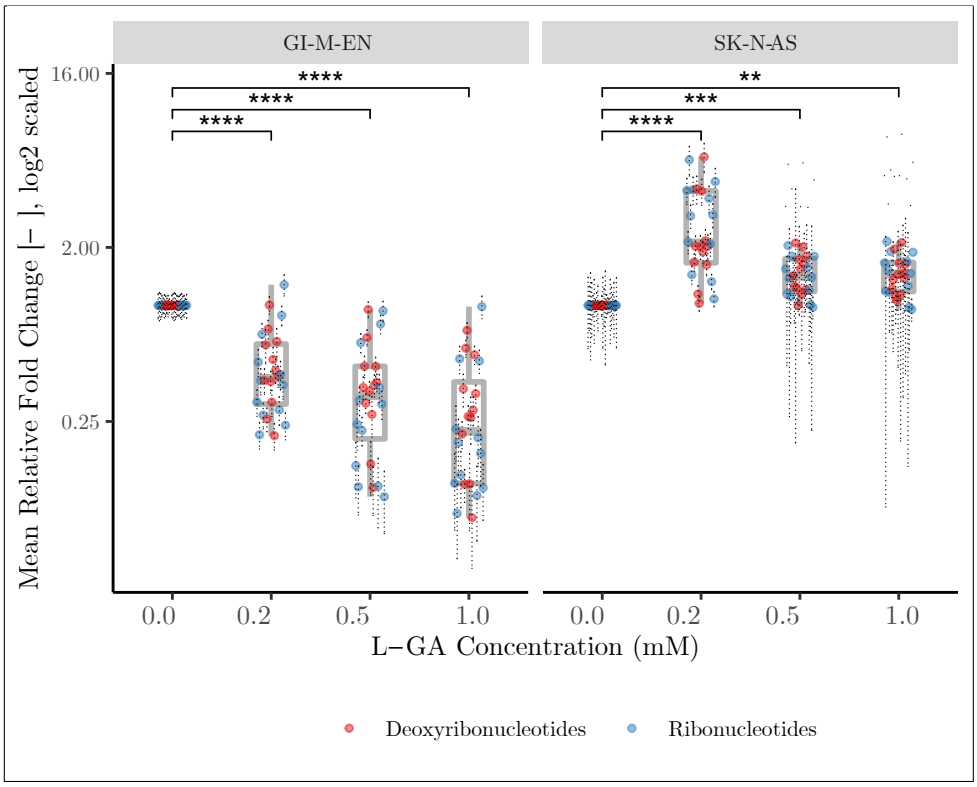

Figure 5.7: Nucleotide depletion in neuroblastoma cells is dependent on the concentration of L-GA. Cell lines GI-M-EN and SK-N-AS were treated with a range of L-GA concentrations (0-1.5 mM) for 24 hrs. Nucleotides were extracted from cell lysates and measured by DI-MS/MS. Boxplots present the mean fold change of nucleotide intensities relative to 0.0 mM L-GA for 24 nucleotides intensities measured in 4 biological and 3 technical replicates. Error bars represent ± SEM. P-values were calculated using Wilcoxon non-parametric test between concentrations of L-GA with 0.0 mM L-GA as the reference group with Holm correction. Stars represent ns $p \geq 0.05$; * $p \leq 0.05$; ** $p \leq 0.01$; *** $p \leq 0.001$; **** $p \leq 0.0001$.

5.2.3 Proteomics

Table 5.12: Proteins of interest with -log)pvalue >1.3 and difference between PBS/LGA >1 and <-1

Cell Line	-LogPvalue	PBS/LGA difference	Gene Name	Pathway
IMR-32	2.551	-4.31	HMOX1	Oxidoreductase
VH-7	1.835	-3.463	TAF15	Autophagy
IMR-32	2.139	-3.331	ZFAND5	FOXO signalling
SH-SY5Y	1.833	-3.28	HIST2H3A	Oxidative Stress Induced Senescence
VH-7	2.573	-2.996	FBLL1	Ribosome biogenesis
SK-N-AS	1.8451	-2.26679	BAD	Apoptosis/PI3K/AKT signaling
IMR-32	2.982	-2.255	MSN	Oxidative Stress induced senescence
SH-SY5Y	2.039	-1.91	PRKAA1	MTOR/AMPK signalling
SK-N-AS	1.51667	-1.87567	MTCL1	Apoptosis
VH-7	3.148	-1.813	EXOSC8	Exosome synthesis
VH-7	2.443	-1.786	ZC3H13	NA
VH-7	1.596	-1.737	HMOX1	Oxidoreductase
VH-7	2.422	-1.697	SQSTM1	Mitophagy
BE(2)- C	1.32802	-1.47563	HMOX1	Oxidoreductase
IMR-32	1.815	-1.464	SQSTM1	Mitophagy

Continued on next page

Table 5.12: Continued from previous page

Cell Line	-LogPvalue	PBS/LGA difference	Gene Name	Pathway
GI-M-EN	2.62345	-1.31112	HMOX1	Oxidoreductase
VH-7	1.935	-1.282	CKAP2	Cytoskeleton assembly
SK-N-AS	1.75666	-1.28042	ITGA2	Integrin synthesis
VH-7	1.349	-1.279	CTSC	NA
IMR-32	2.059	-1.279	SCNM1	NA
SK-N-AS	1.52469	-1.27109	RPL36AL	NA
GI-M-EN	2.09455	-1.2553	CYCS	Cytochrome C
VH-7	2.348	-1.253	LRWD1	NA
IMR-32	1.399	-1.223	PCYT1A	NA
GI-M-EN	1.54591	-1.19121	ATP2B1	Reduction of cytosolic Ca++ levels
BE(2)- C	2.39709	-1.18558	MBD1	NA
IMR-32	2.009	-1.138	MAP1A	NA
SH-SY5Y	1.864	-1.13	USP15	NA
SH-SY5Y	1.384	-1.09	NFKB2	NFKB signalling
SH-SY5Y	3.132	-1.088	ATP1B3	Ion homeostasis
VH-7	1.446	-1.087	ATP2B4	Reduction of cytosolic Ca++ levels
SH-SY5Y	1.523	-1.071	MYO1D	NA
IMR-32	1.946	-1.065	WDR45B	NA
SH-SY5Y	1.754	-1.063	TNC	NA
SH-SY5Y	1.376	-1.054	NAGA	NA
IMR-32	1.401	-1.05	KDM2A	OxidoReduc
SH-SY5Y	1.702	-1.043	BRD2	NA
IMR-32	1.801	-1.021	RAB30	NA
IMR-32	1.902	-1.016	ZNF622	NA
IMR-32	1.665	-1.013	DNAJB4	NA
IMR-32	1.823	-1.005	GCLM	Ferroptosis
GI-M-EN	3.39336	1.00844	CDC20	Cell_cycle
VH-7	2.713	1.016	P4HA2	NA
VH-7	1.59	1.016	TELO2	NA
BE(2)- C	1.92145	1.01715	S100A2	NA
GI-M-EN	1.30588	1.01739	RPGRIP1	NA
SH-SY5Y	1.456	1.018	KNSTRN	NA
SH-SY5Y	1.403	1.023	LRP1	NA
IMR-32	1.699	1.04	PHOX2A	NA
VH-7	1.775	1.041	YARS2	NA
VH-7	2.745	1.042	RRM2	p53_signalling
IMR-32	2.324	1.044	DFNA5	NA
BE(2)- C	1.33369	1.05963	PDE6D	NA
SH-SY5Y	2.049	1.075	HMGCS1	NA
VH-7	2.148	1.079	COL18A1	Collagen
VH-7	1.536	1.083	ELN	NA
GI-M-EN	2.1731	1.09056	HELLS	NA
IMR-32	2.28	1.102	NCOR2	NA
SK-N-AS	2.21834	1.10614	MRC2	NA
VH-7	1.583	1.119	SDF4	NA
IMR-32	1.611	1.138	RRM2	p53_signalling
VH-7	2.719	1.139	GTF2I	NA

Continued on next page

Table 5.12: Continued from previous page

Cell Line	-LogPvalue	PBS/LGA difference	Gene Name	Pathway
SK-N-AS	1.78336	1.14934	PDCL	NA
VH-7	1.87	1.154	CENPF	NA
SH-SY5Y	1.914	1.156	MVP	NA
GI-M-EN	2.19167	1.15608	DPH5	NA
SH-SY5Y	2.538	1.183	TIMM8B	NA
VH-7	1.969	1.194	RPL22L1	NA
GI-M-EN	2.31194	1.19471	GSDMD	NA
BE(2)- C	1.91508	1.19542	COL1A1	Collagen
SH-SY5Y	1.405	1.198	USP11	NA
SH-SY5Y	1.761	1.204	TYMS	Nucleotides
GI-M-EN	1.43935	1.20662	NUDT16L1	NA
BE(2)- C	1.6022	1.20666	COL5A1	NA
VH-7	1.884	1.238	WDHD1	NA
GI-M-EN	2.76915	1.26097	TYMS	Nucleotides
IMR-32	1.98	1.309	CTHRC1	NA
VH-7	1.717	1.31	SMC4	NA
IMR-32	1.331	1.357	ARNT	NA
IMR-32	1.302	1.374	PCBP4	NA
SH-SY5Y	2.079	1.379	LGALS3BP	NA
IMR-32	2.489	1.383	SDF4	NA
SH-SY5Y	1.591	1.396	PCOLCE	NA
IMR-32	2.025	1.41	MFGE8	NA
VH-7	2.313	1.437	DNMT1	Nucleotides
IMR-32	1.82	1.466	NBAS	NA
VH-7	2.641	1.466	TPM1	NA
VH-7	1.395	1.487	PCOLCE	NA
VH-7	2.122	1.494	ANKRD17	NA
VH-7	1.89	1.508	TYMS	Nucleotides
VH-7	1.41	1.515	GTF3C1	NA
VH-7	1.635	1.539	PQBP1	NA
IMR-32	2.015	1.55	CHGA	NA
VH-7	2.21	1.564	COL5A1	NA
VH-7	2.476	1.576	CEMIP	NA
SK-N-AS	1.71052	1.57724	PCYOX1	OxidoReductase
SK-N-AS	1.69886	1.59297	PDLIM1	NA
VH-7	1.342	1.61	URI1	NA
SK-N-AS	1.47504	1.61953	ELOVL1	NA
VH-7	2.23	1.636	COL12A1	NA
SH-SY5Y	1.675	1.679	NRCAM	NA
SH-SY5Y	1.523	1.708	PKD2	NA
SH-SY5Y	1.415	1.731	CTHRC1	NA
VH-7	1.537	1.733	UNC119B	NA
SH-SY5Y	2.056	1.79	LAMC1	NA
IMR-32	1.924	1.808	LRP1	NA
VH-7	1.801	1.815	MKI67	NA
SH-SY5Y	2.032	1.989	GNB4	G-protein effector
VH-7	1.626	2.011	IVNS1ABP	NA
VH-7	1.514	2.041	UHRF1	NA
IMR-32	3.47	2.135	TCF3	Notch signalling

Continued on next page

Table 5.12: Continued from previous page

Cell Line	-LogPvalue	PBS/LGA difference	Gene Name	Pathway
IMR-32	1.873	2.324	P4HA2	Collagen synthesis
VH-7	1.541	2.485	COL1A2	Collagen synthesis
SH-SY5Y	1.547	2.544	AHCYL1	1-C Metabolism
SH-SY5Y	1.586	3.025	COL1A1	Collagen
IMR-32	2.991	3.24	SRC	PI3K/AKT pathway
IMR-32	1.458	3.782	RNF213	Wnt signalling
VH-7	1.862	3.916	COL1A1	Collagen
SH-SY5Y	1.408	4.346	H3F3A	Chromatin remodelling

Declaration

Herewith, I declare

Ich erkläre hiermit, dass ich

- to have completed this Dissertation autonomously and without any ilegitimate means,

  die eingereichte Dissertation selbständig und ohne unerlaubte Hilfsmittel angefertigt habe,

- to have given due acknowledgement to material obtained from references, designating the version (edition and year of publication), and to have not used any other references or means besides the ones indicated in the bibliography,

  außer den im Schrifttumsverzeichnis angegebenen Quellen und Hilfsmitteln keine weiteren benutzt und alle Stellen, die aus dem Schrifttum ganz oder annähernd entnommen sind, als solche kenntlich gemacht und einzeln nach ihrer Herkunft unter Bezeichnung der Ausgabe (Auflage und Jahr des Erscheinens) des benützten Werkes nachgewiesen habe,

- to have not submitted this Dissertation elsewhere and that it has not served - neither entirely nor partially - any other functions.

  die Dissertation noch keiner anderen Stelle zur Prüfung vorgelegt habe und dass dieselbe noch nicht anderen Zwecken - auch nicht teilweise - gedient hat.

Berlin, ...